UNIVERSITY OF CALIFORNIA, SAN DIEGO

Structural and Functional Study of RI alpha – nucleated PKA Signaling Complexes

A dissertation submitted in partial satisfaction of the requirements for the degree
Doctor of Philosophy

in

Chemistry

by

Jessica Gundi Helga Bruystens

Committee in charge:

Professor Susan S. Taylor, Chair
Professor Thomas Hermann
Professor Patricia A. Jennings
Professor Alexandra C. Newton
Professor Elizabeth Villa Rodriguez

2014

The Dissertation of Jessica Gundi Helga Bruystens is approved, and it is acceptable in quality and form for publication on microfilm and electronically:

Chair

University of California, San Diego

2014

DEDICATION

For Justin

EPIGRAPH

Science is a means to an end
Where we try not to condescend
But to produce the new
And prove wrong the few

Justin Bruystens

TABLE OF CONTENTS

LIST OF ABBREVIATIONS

Å. Angstrom

ACRDYS. Acrodysostosis

AKAP. A-kinase anchoring protein

AKB. A-kinase binding domain

AMP-PNP. Adenylyl-imidophosphate

ATP. Adenosine triphosphate

cAMP. Adenosine 3',5'-cyclic monophosphate

cGMP. Guanosine 3',5'-cyclic monophosphate

C-subunit. The Catalytic Subunit of PKA

C-terminus. Caboxy-terminus

CNB. Cyclic nucleotide binding

CNC. Carney complex

CREB. cAMP response element-binding protein

DAG. Diacylglycerol

D/D. Dimerization/Docking domain

DNA. Deoxyribonucleic acid

DTT. Dithiothreitol

E. coli.. *Escherichia coli*

EDTA. Ethylenediaminetetraacetic acid

EGTA. [ethylenebis(oxyethylenenitrilo)] tetraacedic acid

ePK. Eukaryotic Protein Kinase

GFP. Green fluorescent protein

IP_3. inositol triphosphate

IP20. Residues 5-24 of PKI

IS. Inhibitor site

kDa. Kilodaltons.

MES. 2-(*N*-morpholino)ethanesulfonic acid.

$MgCl_2$. Magnesium chloride

mKO2. Monomeric Kusabira-Orange 2 fluorescent protein

mM. millimoles/liter

mg. milligram

µl. Microliter

NaCl. Sodium Chloride

N-terminus. Amino-terminus

PBC. Phosphate binding cassette

PEG. Polyethylene glycol

PKA. Protein Kinase A

PKC. Protein Kinae C

PKI. Protein Kinase Inhibitor

R-subunit. Regulatory Subunit of PKA

SANS. Small-angle neutron scattering

SAXS. Small-angle X-ray scattering

SDS. Sodium dodecyl sulfate

LIST OF FIGURES

LIST OF TABLES

ACKNOWLEDGEMENTS

I would like thank my advisor, Dr. Susan Taylor for allowing me to do my Ph.D. research in her group and I am grateful for all the support. She allowed me to become an independent, skilled, and critical scientist. She provided me with opportunities to collaborate, learn techniques outside of the lab, and let me present my work at conferences worldwide. From the rocky start to the intense finish she had my back during times of research frustrations as well as personal crisis. I also would like to thank my thesis committee, Dr. Thomas Hermann, Dr. Alexandra Newton, Dr. Patricia Jennings, Dr. Elizabeth Villa, and my previous committee member Dr. Hector Viadiu for all the helpful advice during committee meetings and talks.

I would like to thank Professor Friedrich Herberg for allowing me to visit his lab in Kassel, Germany to conduct experiments and for teaching me about surface plasmon resonance. In addition, I am grateful for all the assistance and guidance that was given by Dr. Daniela Bertinetti during my stay in Germany. I also would like to thank Professor Donald Blumenthal for teaching me about small-angle X-ray scattering and assisting in data collection and analysis as well for helpful advice for manuscript preparations. Thanks to Dr. Hartmut Luecke for allowing me to start research in his lab during my undergraduate studies and particular thanks goes to Dr. Jason Stagno, who got me excited about X-ray crystallography and taught me his great techniques, allowing me to be productive from the beginning of my Ph.D. work.

I would like to acknowledge all members of the Taylor lab that have made my graduate work environment not only stimulating and supportive but also fun. Mike Deal, Jie Yang, and Sarma helped during the challenging start in the Taylor lab. I am thankful for the help and interesting discussions with Adam Bastidas, Jian Wu, Pepijn Burgers, Lalima Ahuja, Frank Ma, Jeffrey Copps, Issa Moody, Nina Haste, Ping Zhang and Alexandr Kornev. Constant and reliable help, inside and outside the lab was provided by Mira Sastri, Eric Smith-Nguyen, Angela Chen, and Sventja von Daake. I am forever grateful for all their support and words of wisdom that got me through grad school.

Without my family, I would not have reached my goals. Only through their uncompromising love and support was I able to overcome obstacles throughout my academic path. As much as this was my dream, my husband, mother, sisters, and brothers kept pushing me to achieve my dreams. Pursuing my goals required much sacrifice from them. While not being able to see me achieve my goals, I would like thank my father for teaching me the importance of passion and dedication. Finally, I would like to acknowledge my incredibly talented and wise son, Justin for giving me the motivation and strength to never give up. I am humbly submitting and dedicating this doctoral dissertation to my son, with the hope to inspire him to follow his dreams.

Chapter 2, in part, was published as PKA RI alpha homodimer structure reveals an intermolecular interface with implications for cooperative cAMP binding and Carney complex disease. Bruystens, J.G., Wu, J., Fortezzo, A., Kornev, A.P.,

Blumenthal, D.K., and Taylor, S.S. (2014). Structure *22*, 59-69. The dissertation author was the primary investigator and author of this work.

Chapter 3, in part, has been submitted for publication as PKA-induced phosphorylation inhibits its association to A-kinase anchoring proteins. Burgers, P.P.; Bruystens, J.G.; Rose, R.J.; Keshwani, M.M.; Wu, J.; Janssen, B.; Taylor, S.S.; Heck, A.J., and Scholten, A. The dissertation author was a secondary investigator and author of this work.

Chapter 4, in its entirety, has been published as Realizing the allosteric potential of the tetrameric protein kinase A RIalpha holoenzyme. Boettcher, A.J., Wu, J., Kim, C., Yang, J., Bruystens, J., Cheung, N., Pennypacker, J.K., Blumenthal, D.A., Kornev, A.P., and Taylor, S.S. (2011). Structure *19*, 265-276. The dissertation author was a secondary investigator and author of this work.

Chapter 5, in part, will be submitted for publication as Structural and functional implications of RIα acrodysostosis-1 mutations. Bruystens, J.G.; Wu, J.; and Taylor, S.S. The dissertation author was the primary investigator and author of this work.

Chapter 6, in part, will be submitted for publication as Non-canonical PKA scaffolding interaction of RI subunits with P-Rex1. Bruystens, J.H.; Moody, I.; Ma, Y.; Sastri, M; Kornev, A; and Taylor, S.S. The dissertation author was the primary investigator and author of this work.

VITA

Education

2014	Ph.D., Chemistry University of California, San Diego
2011	M.S., Chemistry University of California, San Diego
2008	B.S., Biochemistry and Molecular Biology University of California, Irvine

Publications

Bruystens, J.G., Wu, J., and Taylor, S.S. Structural and functional implications of RI alpha acrodysostosis-1 mutations. *Manuscript in preparation.*

Bruystens, J.G., Moody, I.S., Ma, Y., Sastri, M., Kornev, A.P., and Taylor, S.S. Non-canonical PKA scaffolding interaction of RI subunits with P-Rex1. *Manuscript in preparation.*

Burgers, P.P., **Bruystens, J.G.**, Rose, R.J., Keshwani, M.M., Wu, J., Janssen, B., Taylor, S.S., Heck, A.J., and Scholten, A. PKA-induced phosphorylation inhibits its association to A-kinase anchoring proteins. *Manuscript submitted.*

Bruystens, J.G., Wu, J., Fortezzo, A., Kornev, A.P., Blumenthal, D.K., and Taylor, S.S. (2014). PKA RIalpha homodimer structure reveals an intermolecular interface with implications for cooperative cAMP binding and Carney complex disease. Structure *22*, 59-69.

Boettcher, A.J., Wu, J., Kim, C., Yang, J., **Bruystens, J.**, Cheung, N., Pennypacker, J.K., Blumenthal, D.A., Kornev, A.P., and Taylor, S.S. (2011). Realizing the allosteric potential of the tetrameric protein kinase A RIalpha holoenzyme. Structure *19*, 265-276.

Stagno, J., Aphasizheva, I., **Bruystens, J.**, Luecke, H., and Aphasizhev, R. (2010). Structure of the mitochondrial editosome-like complex associated TUTase 1 reveals divergent mechanisms of UTP selection and domain organization. J Mol Biol *399*, 464-475.

ABSTRACT OF THE DISSERTATION

Structural and Functional Study of RI alpha-nucleated PKA Signaling Complexes

by

Jessica Helga Gundi Bruystens

Doctor of Philosophy in Chemistry

University of California, San Diego, 2014

Professor Susan S. Taylor, Chair

cAMP-dependent protein kinase (PKA) is one of the most ubiquitous kinases in cells that relies on four functionally non-redundant cAMP sensing Regulatory (R). Largely influenced by the signaling state of the cell, the catalytic subunits of PKA exist in either the unbound active state or as part of phosphorylation-silent R-subunit nucleated macromolecular assemblies. The guiding theme of this thesis was to gain insights into RIα-mediated PKA signaling complexes utilizing X-ray crystallography, small-angle X-ray scattering (SAXS), as well as complementary biochemical

techniques. Specifically, this study targeted the elucidation of the RIα homodimer complex structure, a small membrane A-kinase anchoring protein (smAKAP) -bound RIα dimerization domain (D/D) structure, the RIα holoenzyme $(RI\alpha:C)_2$ complex, and the RI-mediated interaction with P-Rex1.

At the start of this project, only monomeric R structures where known, which fell short in explaining cAMP binding for the full-length protein as compared to the truncated R subunits. With X-ray crystallography, the full-length RIα homodimer structure was solved and revealed a novel, isoform-specific interface between the protomers. Next, the crystal structure of smAKAP's A-kinase binding domain (smAKAP-AKB) in complex with the dimerization/docking domain of PKA-RIα (PKA-RIαD/D) was solved, which revealed a unique interaction surface with a large number of contact residues to drive smAKAP's high specificity.

Furthermore, we present insights that have been gained for the assembly and function of the RIα holoenzyme with the description of an intriguing model and a low-resolution structure. Additionally, a focus on disease mutations of the RIα gene uncovers explanations for the downstream molecular effects that result in the severe clinical outcomes of Carney Complex disease and acrodysostosis-1. Finally, the RI-subunits' C-termini potential as a scaffolding module was tested. Based on our experiments we propose a binding model for the PDZ domains of P-Rex1 to the RIα/β CNB-B domain. In summary, this thesis emphasizes RIα as an essential regulator and partner for PKA cell signaling assemblies.

Chapter 1

Introduction

1.1 Cellular Signal Transduction

Living organisms must efficiently regulate and coordinate biological processes for survival. One of the main systems utilized for this purpose in animals is the endocrine system. The chemical messengers enabling the relay of information throughout the body are the hormones. Production of hormones at one place in the body and their targeting at other sites is a highly regulated process. While hormones can travel long-distance through the circulatory system, they are accepted by a sub-set of cells, which carry out a specific biological response. A diverse repertoire of differentiated cells are used as building blocks to create the tissues and organs of an animal.

Stress, glucose level changes, and developmental cues can stimulate the secretion of hormones by endocrine glands such as the pancreas, gonads, and adrenal glands. The chemical makeup of hormones includes peptides, proteins, glycoproteins and steroids. Examples are the proteins glucagon and insulin; pivotal hormones for the regulation of glucose levels in the blood that are excreted by the pancreas. When glucose levels exceed a homeostatic concentration, released insulin effectively lowers glucose levels by communicating with cells to take up the excess glucose. Glucagon carries out an opposing function by causing cells to release glucose and thus allow for the precise control of glucose homeostasis. The high blood pressure characteristic of one of the most prevalent endocrine disorders, Diabetes mellitus, is a result of deficient signaling in the blood glucose regulation.

Initiated from a long distance, the cell is responsible for receiving the extracellular signals and converting them into a biological response by putting in motion intracellular signaling cascades. Cells sense their environment with their membrane embedded receptors, the only molecules able to accept, translate, and transmit signals such as hormones to the inside of the cell. Examples include the G-protein-coupled receptors, receptor tyrosine kinases, and ion channel receptors, which are major targets of pharmacological agents. Binding of signaling molecules to the cell surface receptors can lead to the channeling and amplification of the signal to the inside of the cell.

Signaling progresses inside the cell with selective transmission and processing of messages by proteins. Often and through the action of the membrane receptors, the extracellular signal ("first-message") is converted to an intracellular second messenger molecule. These small ions or molecules can be generated quickly, readily diffuse, bind specifically to their targets, and can be degraded efficiently. They thus represent one of the main mechanisms to coordinate communication inside the cell. Some prominent examples are the cyclic nucleotides cAMP and cGMP, Ca^{2+}, inositol triphosphate (IP_3), and diacylglycerol (DAG). Part of the G-protein coupled receptor and tyrosine kinase receptor pathways is the widely used second messenger Ca^{2+} that modulates cell responses such as muscle cell contraction, secretion of substances, and cell division. Several hormones, neurotransmitters, and other substances cause the cell to produce the second messenger cAMP, an important molecule in the signaling cascade of heart rate regulation, cortisol secretion, and glycogen breakdown.

Epinephrine is a crucial hormone for the regulation of cellular energy metabolism. Research carried out by the Nobel Price Laureate Earl Sutherland demonstrated that the hormone epinephrine binds to the cell surface of liver cells and causes an intracellular elevation of cAMP. It turns out that this happens indirectly, through a signaling pathway where the activated G-protein coupled receptor (GPCR) leads to the activation and dissociation of a specific G protein. This G protein can in turn interact with and switch on another enzyme embedded in the plasma membrane called adenylyl cyclase, which finally converts ATP to cAMP and quickly increases the intracellular cAMP concentration. Diffused cAMP molecules bind to and thereby change the activity of downstream enzymes (**Fig. 1.1**).

In the epinephrine pathway, cAMP targets protein kinase A (PKA), which is followed by a cascade of enzyme activations (**Fig. 1.1**) and requires a conformational change upon cAMP binding. Only then does PKA become catalytically active and initiates the successive activation of phosphorylase kinase and glycogen phosphorylase. The signaling cascade involves direct interactions between the progressive enzymes and the chemical modification by each enzyme of its' downstream signaling partner. cAMP binds to PKA and activates it. In the active state PKA can now interact with and chemically modify phosphorylase kinase to switch on its' catalytic activity, which entails the activation of the downstream enzyme glycogen phosphorylase. Breakdown of glycogen and production of glucose-1-phosphate now commences through the active glycogen phosphorylase.

The extracellular stimulation by epinephrine causes a sharp increase in cAMP levels and through the utilization of a multistep signaling pathway allows amplification of the hormone message into the interior of the cell. Beginning with the reception of the signal, followed by relay and transduction within the cell, the result is a controlled and specific cellular response important for functional multicellular organisms. As crucial as the launch of a particular signaling pathway, is the termination of the signaling cascade. Compromised signaling can lead to uncontrolled proliferation of cells and cancer, as well as diseases due to endocrine disorders. Thus, negative control and feedback occurs at almost every step of a pathway: reversion of enzymes to their inactive states, receptor internalization to resist further hormone stimulation, and break down of second messengers by additional enzymes. For example, cAMP is converted to AMP by phosphodiesterases to control the cAMP concentraion and thereby terminating the downstream signaling.

1.2 Protein Phosphorylation

For the most part, the primary amino acid sequence synthesized from the DNA sequence through transcription and translation, determines the structure and principal composition of a protein or enzyme. The polypeptide chain starts folding while being synthesized on the ribosome and proteins called chaperones aid in the process of obtaining the correct conformation. The primary structure originated from the gene and directs the secondary structure of the folded protein. However, full functionality and regulation of a protein's activity is oftentimes accomplished through

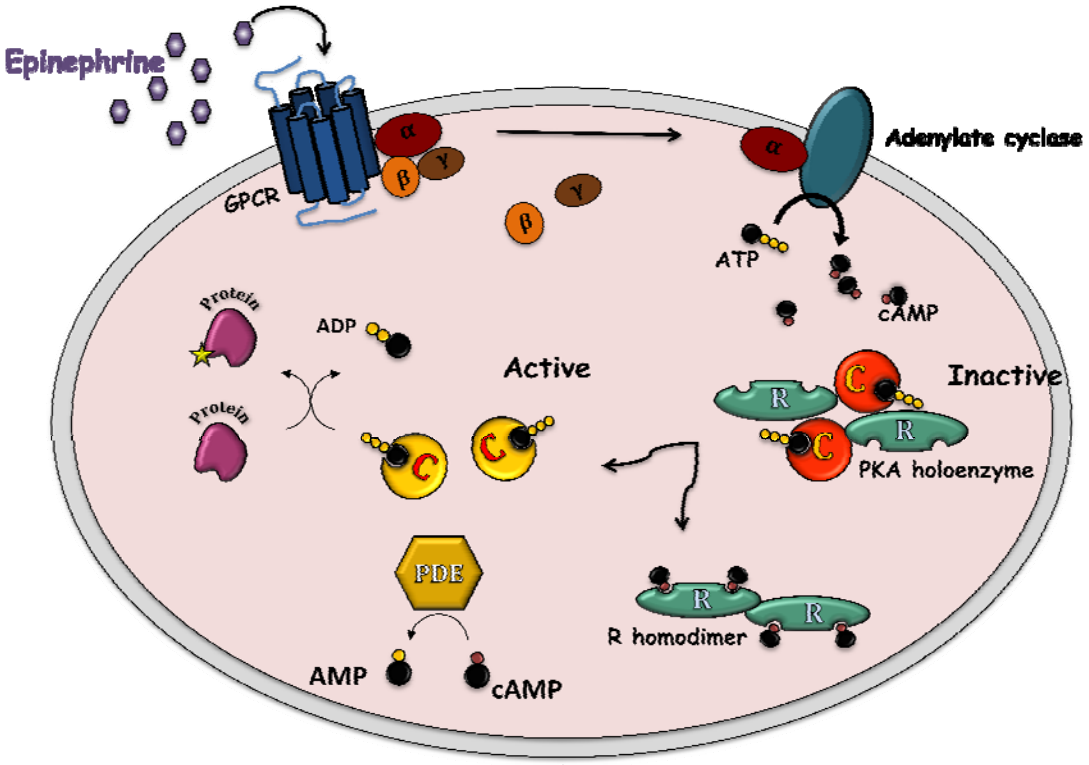

Figure 1.1. The epinephrine-induced PKA pathway in cells. The hormone epinephrine initiates a signaling cascade inside a cell by binding to GPCRs, which leads to production of the second messenger cAMP. In the resting cell PKA exists in the inhibited holoenzyme state. cAMP can bind to and activate PKA for signal transduction and downstream cellular effects.

post-translational modifications. This covalent chemical attachment of lipids, sugars, or phosphate groups further regulates cellular communication and responsiveness to the environment. Phosphorylation, myristylation, ubiquination, palmytylation, sumoylation and acetylation are some examples of modifactions proteins undergo to influence their behavior in cellular processes.

The phosporylation potential of a cell has been recognized as an important mechanism to control signaling cascades with Fischer and Krebs receiving the Nobel prize in physiology for their early work in the 1950s. Reversible phosporylation provides regulation with a variety of effects on the target enzymes such as changing their activity, binding properties, localization and stability. Phosporyalation is accomplished by protein kinases that carry out the attachment of a phospate (PO_4^{3-}) group to their protein targets, while protein phosphatases are responsible for the desphosphorylation by removal of the phosphate group (Krebs and Beavo, 1979). 30-50% of a cell's proteins are phosphorylated and the cellular outcomes are diverse (Manning, 2005). With over 500 putative kinases identified in humans, they are essential in metabolism, apoptosis, transcription, and countless other signaling paths and are evolutionarily conserved across many species (Manning et al., 2002).

The importance of kinases can be recognized by the fact that approximately 2% of our genes code for kinases making this one of the largest gene families in humans, termed the human kinome (Manning et al., 2002). Furthermore, approximately 150 phosphatases regulate phosphorylation in time and extent (Papin et al., 2005). Most kinases carry out the enzymatic addtion of the gamma phosphate from

ATP to the amino acids Ser, Thr, and Tyr within the recognition sequence of specific substrate proteins and thus require ATP as a co-factor (Pawson and Scott, 2005). Many kinases are involved in phosphorylation cascades where one kinase phosphorylates and thereby manipulates the downstream kinase to enable the propagation of a signal. Kinases play an important role in a plethora of biochemical pathways and thus the human kinome has been categorized into seven main groups, each containing several families and sub-families, according to sequence, evolutionary and functional similarities (**Fig. 1.2**) (Manning et al., 2002).

A large group of kinases are the tyrosine kinases, which phosphorylate tyrosine residues of substrates. Notably so the insulin receptor that upon binding of insulin on the extracellular chains first dimerizes and then goes through a series of autophosphorylations of the dimer-partner. This activates further the Tyr kinase activity of the intracellular domains and allows for the phosporylation of other target proteins to propagate the hormone signal to the cytosol and the nucleus. The CAMK group contains families that are related to the calcium/calmodulin-regulated kinases, even though not all have been shown to be dependent on calcium/calmodulin. The death associated protein kinases (DAPK) make up one family of this group and play various roles in apoptosis (Temmerman et al., 2000). Another family in this group, the MLCK family, contains the giant protein of muscle sarcomeres titin kinase, the largest gene product in humans (Bang et al., 2001).

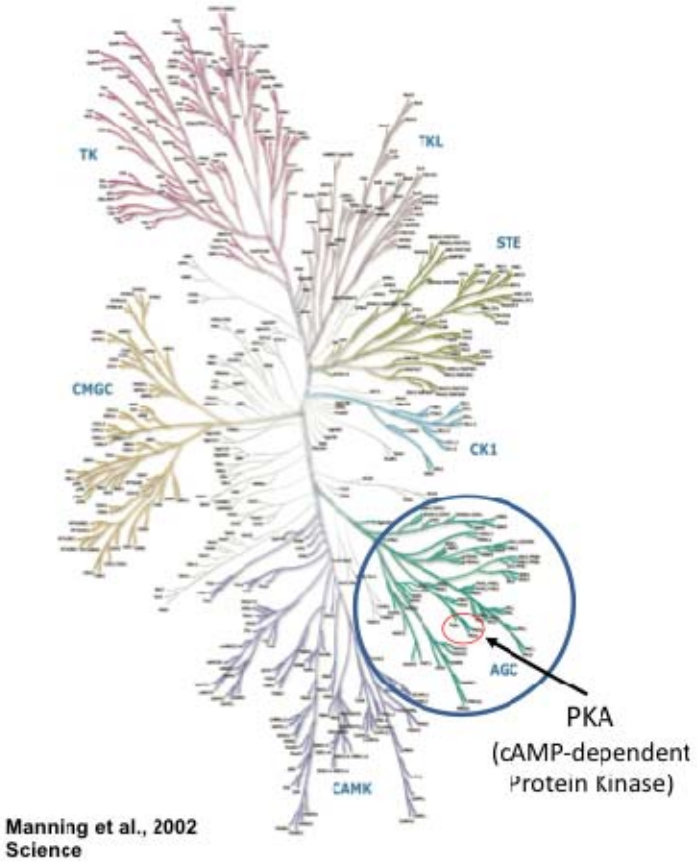

Figure 1.2. The human kinome. Protein kinases from the human genome have been organized into 7 major groups based on evolution and function by Manning et al. (2002) *Science* 298:1912. PKA (red circle) is part of the AGC branch (blue circle), which contains Ser/Thr kinases responsive to cyclic nucleotides.

CDK, MAPK, GSK3, and CLK kinases are part of the group termed CMCG. The tyrosine-kinase like group has most similarty to the tyrosine kinases but has activity on Ser/Thr residues of targets. The STE group is made up of the yeast homologous protein kinases in humans. The smallest group is abbreviated CK1, which stands for Cell Kinase 1.

Responsive to the cyclic nucleotide second messengers are the families of the AGC kinase group with members such as protein kinase A, G, and C. The catalytic region of these kinases have high sequence similarity, yet their activation mechanisms differ, and activation is achieved by different messenger molecules such as cyclic nucleotides for PKA and PKG, or Ca^{2+} and diacylglycerol (DAG) for PKC. While regulatory domains represent another common theme for these kinsaes, they differ in their mechanisms. PKA utilizes separate amino acid chains as regulatory subunits whereas PKC and PKG contains the regulatory subunit and catalytic subunit sequences as a fused protein complex.

cAMP dependent kinase A (PKA) is an AGC kinase and one of the most studied of the kinases. As such it has served as a prototype for analyzing and realizing the concept of a general kinase core for eukaryotic kinases (ePKs). PKA's phosphorylation activity is unleashed by a rise of the intracellular cAMP concentration and allows for the transcytosolic transmission of a signal with substrates in the cytosol as well as the nucleus. In the cytosol a prominent example is the phosphorylation of inactive phosporylase kinase discussed in the previous section. Another is lipid mobilization initiated by the drop in the glucose concentration in the blood. The

following glucagon stimulation on adipocytes triggers the downstream and intracellular phosphorylation of hormone-sensitive lipase allowing the release of fatty acids for fueling the oxidative energy machinery of animals (Horowitz, 2003). The catalytic activity can also be targeted to the nucleus, where PKA phosphorylates cAMP response element binding protein (CREB) for the control of gene expression (Meinkoth et al., 1990).

1.3 PKA Mediated Catalysis

A functional PKA core complex contains catalytic (C) and regulatory (R) subunit proteins. In the cell the inactive state conatins two C subunits bound by an R dimer. In the test tube however, a non-physiological truncation construct of the R monomer is sufficient to bind and inhibit one C subunit. The C subunit is a Ser/Thr protein kinase and contains the calatytic machinery of PKA able to carry out the Serine or Threonine side chain phosphorylation of substrates that contain the recognition sequence R-R-X-Ser/Thr-Hyd. There are five human C subunit isoform genes, which code for Cα, Cβ, Cγ, and PrKX and PrKY, which differ in sequence and have tissue-specific expression patterns. Cα1 and Cβ1 are the predominantly studied isoforms as they are ubiquitously expressed and play important biological roles in humans but multiple other expressed splice variants of the C subunit have been discovered. Limited expression has been found for Cγ in the testis as well as for Cα2, which is transcribed through the use of another promoter than Cα1 and is expressed in male germ cells (Beebe et al., 1990; Beebe et al., 1992; Desseyn et al., 2000; Reinton

et al., 1998). Most of the splice variants originate from the Cβ gene including the ubiquitously expressed protein Cβ1 and the brain specific proteins Cβ2 and Cβ3 (Guthrie et al., 1997). The main sequence differences exist at the N-terminus and Cβ2 is a peculiar isoform where the 15 N-terminal residues of Cβ1 are swapped for a 62 residue long domain of unknown function (Thullner et al., 2000).

A leap in kinase understanding was achieved when the PKA Cα subunit structure was solved in 1991 and while it was the first kinase structure it has to this day served as a prototype for many kinase studies. The 360 residues of this C subunit fold into an overall globular bilolobal enzyme. Residues 40 through 300 constitute the conserved eukaryotic kinase (EPK) core (**Fig. 1.3**), which is made up of a C- (**Fig. 1.3B**) and N-terminal lobe (**Fig. 1.3A**) (Taylor et al., 2008; Taylor et al., 2004). The secondary structure of the N-lobe contains 5 anti-parallel β-sheets and two α-helices and largely mediates ATP binding. The N-lobe mediates ATP binding by utilitizing crucial elements such as a glycine-rich loop for γ-phosphate positioning (**Fig. 1.3C**). Furthermore aiding in phospate positioning is the conserved Lys 72, which interacts with Glu 91 and Asp 164 (**Fig. 1.3D**) (Taylor et al., 2012).

Connected to the N-lobe by a linker is the C-lobe, which is solely composed of α helices and directs substrate binding. The C-lobe also contains several kinase conserved residues that are important for implementing phosporyl group transfer as well as a hydrophobic core created by the E and F helices. Crucial for aiding in the γ-phospate tranfer is the catalytic loop, which is located between β-strands 6 and 7 (**Fig. 1.3E**).

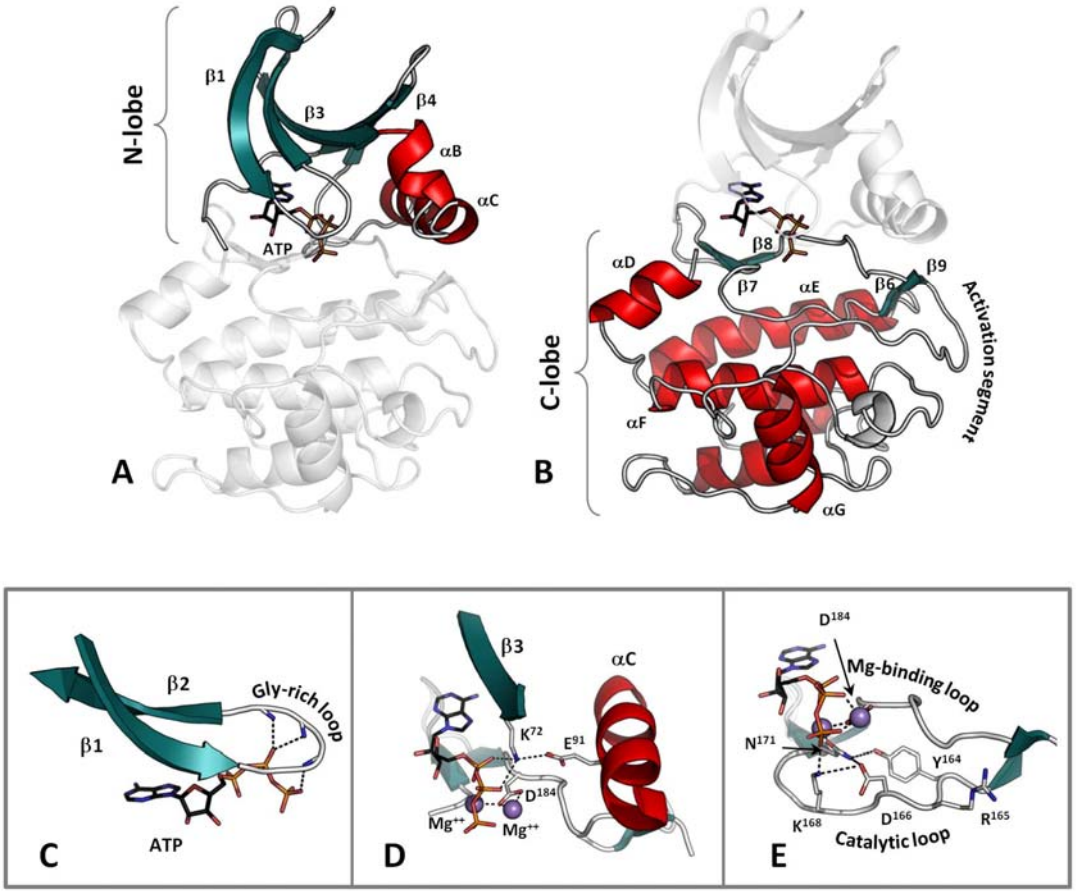

Figure 1.3. The eukaryotic kinase core. The N-lobe (A) and C-lobe (B) of the eukaryotic kinase core form an active site crevice between them that contains crucial conserved catalytic motifs (C-D). Taken from Taylor et al. (2012) *Philosophical Transactions B*. 367:2517.

The catalytic loop also contains Asp 166, which prepares and coordinates the substrate serine for accepting the phospate group (Taylor et al., 2012; Taylor et al., 2008; Taylor et al., 2004). The loop located between β-strands 8 and 9 of the C-lobe acts to further mediate coordination of the catalytic magnesium ions (**Fig. 1.3E**) (Taylor et al., 2012; Taylor et al., 2008).

Located in the crevice between the two lobes is the active site, where the catalytically essential magnesium ions, ATP, and the substrate can bind. Dynamic movements of the lobes enable the catalytic cycle through conformational changes that mediate opening and closing of the active site to allow binding of ligands, transfer of a phosphate to the substrate, and finally release of the products. Various crystal structures representing intermediate states of the PKA catalytic cycle have been solved and together with molecular dynamics simulations have provided a detailed understanding of the phosphorylation reaction progression (Taylor et al., 2004).

Spanning both lobes of the EPK core are groups of highly conserved hydrophobic residues as revealed by local spatial pattern (LSP) alignment that were termed the regulatory (R) and catalytic (C) spines (**Fig. 1.4**) (Taylor et al., 2012). The involved residues are non-consecutive in the primary amino acid sequence and assemble in the folded kinase into contiguous hydrophobic clusters. The R spine is intact in active kinases and is completed by the phosphorylation of the activation loop.

The C spine, which is positioned in parallel orientation to the R spine, is complete upon ATP binding and adenine ring insertion to connect hydrophobic

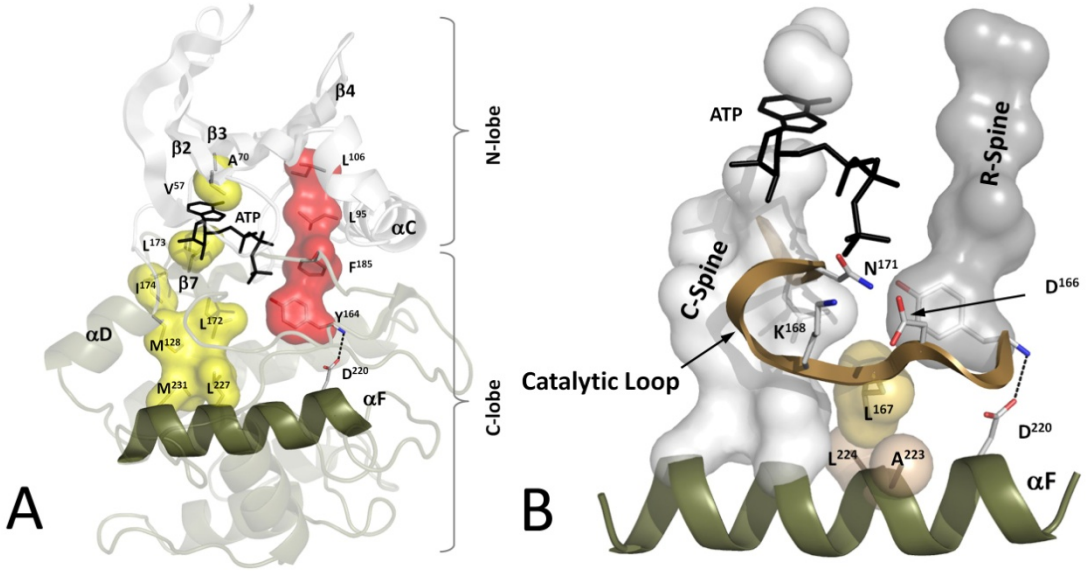

Figure 1.4. Hydrophobic spines of PKA. LSP revealed the internal architecture of EPKs to contain a hydrophobic C-spine (yellow) and hydrophobic R-spine (red) which span both the C- and N-lobe (A). The C-spine is completed by ATP and the R-spine is anchored by Asp220. Taken from Kornev et al (2008) *PNAS* 105:14377.

residues from the N and C lobe to enable the proper alignment of crucial catalytic residues (Taylor et al., 2012; Taylor and Kornev, 2011).

1.4 PKA Regulation

PKA is involved in a plethora of signaling cascades and it has emerged as the most ubiquitous cAMP-responsive enzyme in mammalian tissues (Kuo and Greengard, 1969). To prevent uncontrolled PKA activity and the corresponding detrimental consequences such as cancer, cardiovascular disease and endocrine disorders, mechanisms to control and regulate PKA in addition to the cAMP-coupled activity have been put in place. This includes not only tightly regulated and cell type specific expression but also C subunit inhibitors, regulation of localization to subcellular sites, and optimization of activity by cofactors and phosphorylation. The heat stable protein kinase inhibitor PKI, which is itself expressed in a cell-cycle dependant manner, is a potent physiologic inhibitor with a K_i of 0.5 to 2 nM. It binds to the C subunit active site with its pseudosubstrate sequence segment and thereby prevents PKA activity. A 20 residue peptide of PKI is a highly specific tight binder and has been used to obtain substrate bound crystal structures of the C subunit (Knighton et al., 1991b) and to monitor C subunit regulation with fluorescence polarization (Saldanha et al., 2006). PKI adds another layer of PKA control as it contains a nuclear export signal and when bound will translocate the C subunit from the nucleus to the cytoplasm (Fantozzi et al., 1994).

The N-terminus is the most variable among the PKA C subunit isoforms and for Cα there is a stable 30-residue α-helix called the A-helix. This is the docking site for A kinase interacting protein which can target the C subunit to the nucleus (Sastri et al., 2005). AKIP was found to bind the N-terminal helix of the C subunit in a yeast two-hybrid screen and has since been shown to play an important role in the regulation of cardiac stress (Sastri et al., 2005) (Sastri et al.). Recently the role of myristylation at the N-terminus of the C subunit has been dissected structurally and functionally. Thus, in addition to allowing PKA targeting and anchoring to the plasma membrane, myristoylation affects the activity of the C subunit and the myristyl binding pocket was proposed to be a site for allosteric regulation of PKA (Bastidas et al., 2012).

An intact kinase core is essential but fully functional PKA requires the assembly and interactions with the C-terminal tail, which wraps around the kinase core and contains three, among AGC kinases conserved, tethering motifs: the C-lobe tether (CLT), the active site tether (AST), and the N-lobe tether (NLT) (Kannan et al., 2007). Each tether comprises crucial interactions with the kinase core and provide intramolecular kinase regulation. The phosphorylation state of kinases themselves plays a major role in regulation and the Cα subunit of PKA contains 4 putative phosphorylation sites. Known autophosporylation sites are Thr 197 and Ser 338. Ser 10 phosporylation on the A-helix is important for stability and activity, and pivotal for activity in almost all eukaryotic kinases is activation loop phosphorylation, Thr 197 in PKA. Ser 338 represents the TM site of the C-tail serves to regulate activity and was

shown to occur cotranslationally before activation loop phosphorylation (Keshwani et al.).

An integral control of the physiologic PKA system is the regulatory (R) subunits and a functional PKA complex contains catalytic (C) and regulatory (R) subunit proteins. In the cell the inactive complex contains two C-subunits bound by an R-homodimer and there are four potential isoforms that can bind and inhibit C-subunit activity. The R subunits are encoded by separate genes and provide the main mode of inhibition for PKA and keep its phosphorylation activity under cAMP control since the R subunits contain the actual cAMP binding domains. This highlights the importance of the R subunits and explains why dysfunctional R subunits can cause disease.

1.5 PKA Complexes

The four regulatory subunit isoforms of PKA found in mammalian cells are dimers that contain the same basic functional domain organinzation and are responsible for translating the second messanger cAMP into a PKA response. Limited proteolysis first identified the basic functional domains of the R-subunits to be an N-terminal dimerization/docking domain (D/D), followed by a linker with an inhibitor site and the C-terminal tandem cAMP binding domains (CNB) (**Fig. 1.5**). It is however the key differences between the R isoforms that allow PKA to operate with specificity to provide the necessary intricacies of healthy signal transduction in a cell. Thus, the R isoforms are localized differently and their functions are non-redundant.

While secondary interactions between the monomers have been suggested, the D/D domain is the main mechanism for structurally maintaining the R-dimer. Each R monomer contributes at least 2 alpha-helices, α1 and α2, for hydrophobic interactions to create a stable antiparallel four-helix bundle as revealed by D/D domain crystal structures solved thus far for RIα, RIβ, and RIIα (Kinderman et al., 2006; Sarma et al., 2010), which is also consistent with earlier NMR studies. The RI D/D structures (pdb 3IM3 for RIα and 4F9K for RIβ) revealed a short third N-terminal helix from each monomer that provides additional interactions and has been termed α0. Cys16 from α0 makes a disulfide bond with the Cys37 at the end of α1 and maintains the helix bundle covalently in solution and oxidizing conditions (Sarma et al., 2010). While this is one distinguishing element as it is missing in the RII D/D domains, the biological significance and role of the D/D disulfide bonds in RI subunits are still unclear and under ongoing investigation.

Of equal importance to D/D domain function is its role for binding A-kinase anchoring proteins (AKAPs) and thus allowing spatiotemporal regulation of R-subunit and PKA complexes in the cell. AKAPs are large multidomain scaffolding proteins responsible for targeting PKA subcellularly in a cell type-specific manner. This interaction is accomplished by the A-kinase binding domain (AKB) of the AKAP, which forms an amphipathic α helix and binds to the D/D helix-bundle surface of the R-subunits (Banky et al., 1998; Gold et al., 2006; Kinderman et al., 2006; Sarma et al., 2010). Differential binding affinities to RI and RII subunits by the AKAPs provide another layer of specificity for signal transduction involving PKA.

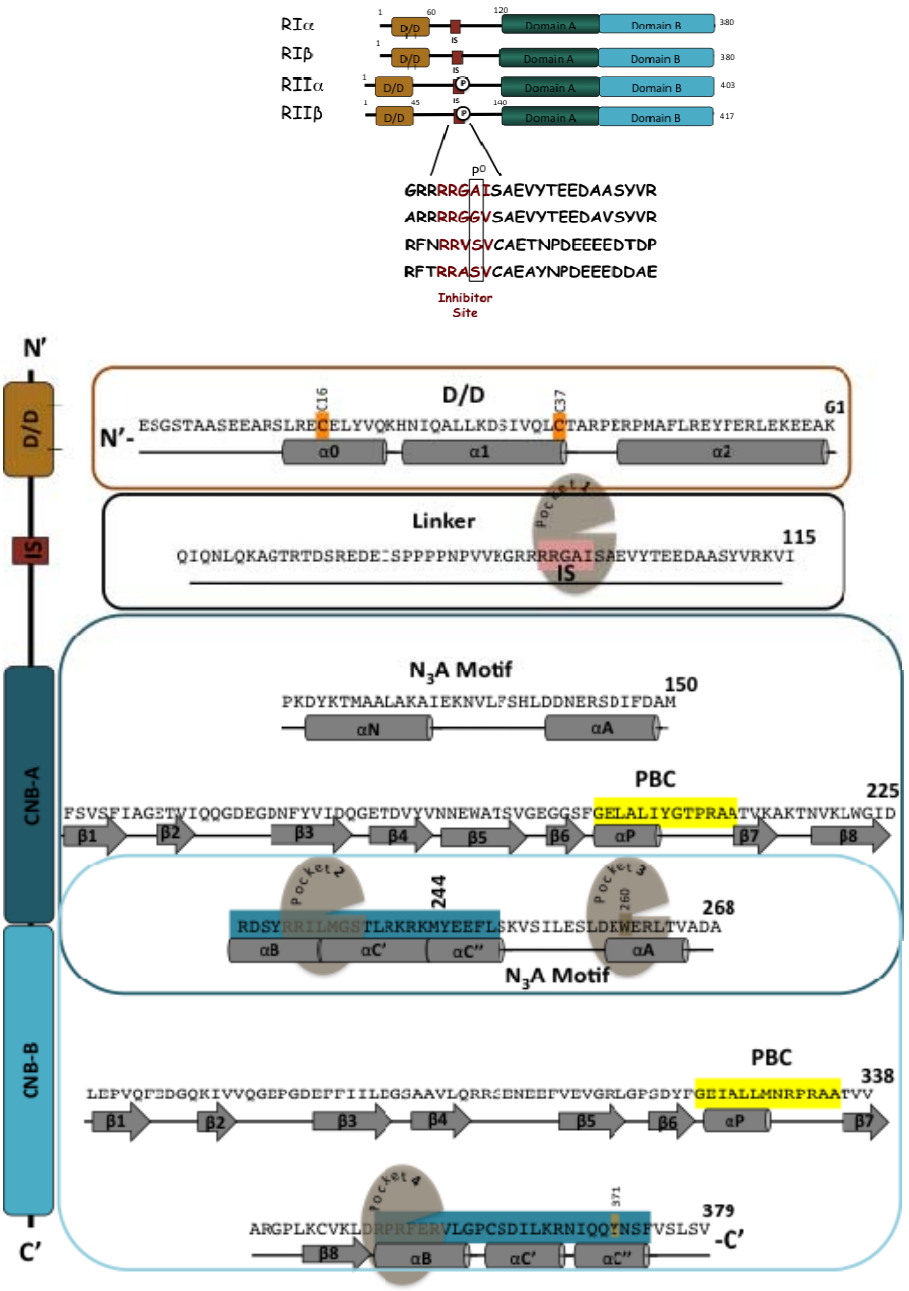

Figure 1.5. Domain organization of R subunits. The R-subunits of PKA contain an N-terminal D/D domain, a flexible linker, inhibotor site (IS), and two tandem CNB domains. (Top) The type II R-subunits have longer linkers and contain a phosphorylatable Ser. (Bottom) The human RIα sequence is shown with secondary structural elements under the sequence. Solid grey arrows represent β sheets and solid grey cylinders represent α helices. D/D domain disulfide bond residues are highlighted in orange, the inhibitor site is highlighted in pink, the PBCs are highlighted in yellow and the αBαC helices are highlighted in teal. C-subunit interaction site pockets 1-4 ((Kim et al., 2007; Kim et al., 2005)are shown with labeled grey ovals.

While most AKAPs are either RII or dual (RI and RII) specific binders, recently the RI-specific smAKAP was discovered (Burgers et al.). Crystal structures of AKAPs in complex with D/D domains have directed the effort to discern isoform-specific binding capabilities of AKAPs. Thus, the dual-specific AKAP 2 (D-AKAP2) in complex with the RIα D/D and RIIα D/D crystal structures revealed an isoform-specific shift in the AKB docking register (Sarma et al., 2010) that allows the AKAP to bind in a novel mode to RIα compared to RIIα. AKAPs and PKA serve critical roles in mammalian signal transduction. Characterizing AKAP-specificity has also provided crucial information to design isoform-specific peptide disruptors of PKA localization for their potential therapeutic applications (Burns-Hamuro et al., 2003; Wang et al.).

Another difference between the type II and I R-subunits lies in the sequence and nature of the linker and the inhibitor site located within (**Fig. 1.5**). While for all four isoforms this region starts after the D/D domain and ends with the beginning of the first CNB domain, the RII isoforms contain an extended version compared to the RI isoforms. The linker begins where the D/D domain of RIα and RIβ ends with the, which based on the published RIα structure is Lys61 and Asn72 for the RIβ structure (pdb 4F9K) and goes to Tyr120 making it a 50 to 60-residue linker.

Presumably and currently under investigation, the RIα D/D will also have a longer α2 helix when additional residues are included in the crystallization experiments as suggested by secondary structure predictions for this region. For the RII subunits however the linker is much longer with ~100 residues from amino acid

45 to 140 and this is the main cause for the different shapes observed with small angle X-ray studies for the R-subunits (**Fig. 1.6**) (Vigil et al., 2004).

Furthermore, significant differences in the linker regions' inhibitor site make the RII subunits substrates and the RI subunits pseudosubstrates of PKA (**Fig. 1.5**). While the recognition sequence of substrates contain Arg-Arg/Lys-X-Ser/Thr-Hyd with the P^0 site representing the phosporylatable amino acid. This recognition sequence is present in all four R-subunits, but the P^0 site in the RII subunits is a Ser in contrast to the Ala in RIα and the Gly in RIβ. Thus the RII-subunits are actual substrates and inhibitors of the C-subunit, whereas the RI-subunits are pseudosubstrate inhibitors. Even though the Ala and Gly P^0 site is non-phosphorylatable, nevertheless the RI subunits can bind to the C-subunit with high affinity. The structure of the RIIβ holoenzyme complex in the apo and phosphorylated form shows that they are possible physiologically relevant states and RII subunits in the heart is autophosporylated at the P^0 Ser (Zhang et al., 2012). AKAPs are responsible for keeping the R-subunits located within a signaling hub and thereby in close proximity to phophatases and substrates. The RII holoenzymes can thus be further regulated by its autophosphorylation in the C-subunit bound complex and following activation with cAMP can be dephosphorylated (Zhang et al., 2012).

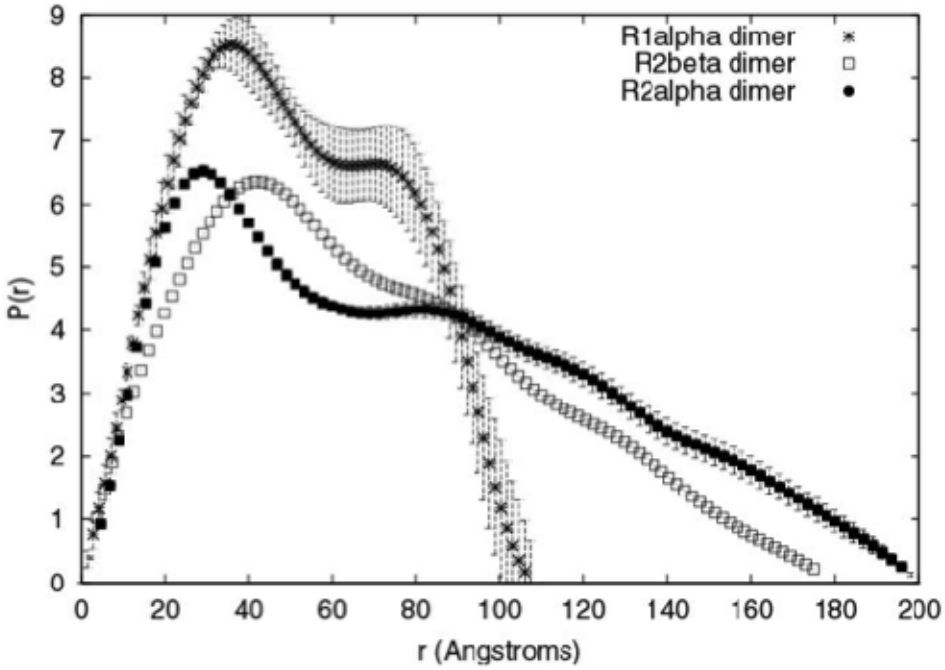

Figure 1.6. SAXS of PKA R-dimers. Small angle X-ray experiments show the overall shape differences between the regulatory subunits. The RIα dimer (crosses) is the most compact shaped with a D_{max} of ~100 Å. The extended shapes of RIIα (black circles) and RIIβ (squares) are evident and caused mostly by the longer linker regions.

The R subunits are the major cAMP-receptors in PKA where cAMP binding is mediated by highly conserved CNB domains. Each physiological PKA holoenzyme complex boasts four CNB domains with two tandem CNB domains contributed from each of the two monomer R chains. The two tandem CNB domains are connected to each other by the αB/C helix. A first structure of RIα was obtained with a deletion construct (91-379) (**Fig. 1.7**). This construct retains its ability to bind and inhibit the C-subunit since it contains the inhibitor site and crucial interaction surfaces for binding to the C-subunit (Kim et al., 2007; Kim et al., 2005). This deletion mutant of RIα displays equal cAMP binding affinities of 50 nM for the two tandem CNB domains and lacks cooperative binding (Herberg et al., 1994). In contrast, the full-length dimer binds cAMP with a cooperative profile and a Hill Slope of 1.62 (Herberg et al., 1994).

Each CNB contains a beta sandwich, which is followed by a helical α-subdomain (**Fig 1.8**). The 14 amino acid long docking module for cAMP, conserved in all cAMP-binding proteins, is the phosphate-binding cassette (PBC), which is found within the β-sandwich (Su et al., 1995). Also conserved among the R-subunits is the α-subdomains architecture with an αN helix, a short 3_{10} -loop and an αA helix, together termed the N3A-motif. The N3a-motif preceding the β-subdomain is also conserved in other cAMP-binding proteins such as exchange protein directly activated by cAMP (EPAC) and Potassium/sodium hyperpolarization-activated cyclic nucleotide-gated channel (Kornev et al., 2008).

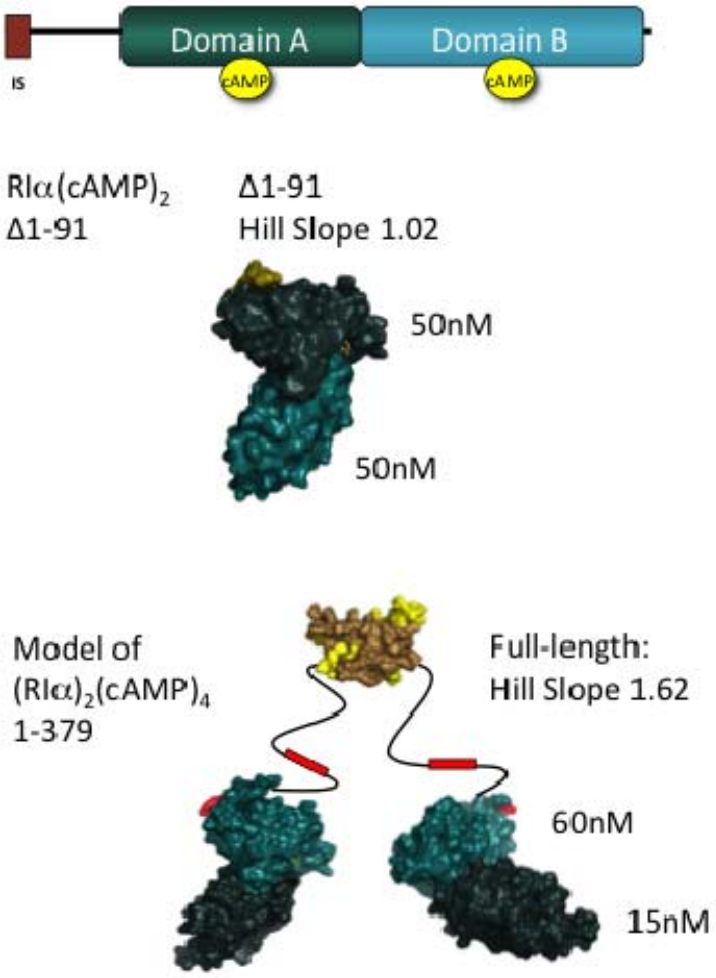

Figure 1.7. Structure and cAMP binding of RIα. A deletion construct of RIα (91-379) with cAMP bound revealed the structural makeup of CNB-A and CNB-B. cAMP-binding characteristics are different for the monomer compared to the physiologically relevant R-dimer.

The CNB domains toggle between the cAMP-bound B-form and its C-subunit bound H-form (**Fig. 1.8**) (Kim et al., 2007; Kim et al., 2005). The N3A-motif and αB/C helix movements are correlated; while one moves in towards the PBC, the other moves out away from the PBC. When cAMP is bound, the kinked αB/C helix puts it in close to the PBC. In the C-subunit bound state the αB/C helix is straight and positioned "out" away from the PBC allowing the N3A motif position to be "in" to interact with the PBC, which is different from the cAMP-bound state, where the N3A is in the "out" position and is moved up and away from the PBC. While crystal structures have captured and defined the B- and H-form, an equilibrium of these conformational states within the CNB domains has been observed by NMR and shows how the addition of ligand, C-subunit or cAMP, to the apo CNB domain pushes the equilibrium to accommodate the favored conformational state (Akimoto et al., 2013).

Not only are the R-subunits structurally similar but also the basic three-dimensional assembly of the different isoform heterodimer R:C complexes is similar (**Fig. 1.9**) (Boettcher et al., 2011; Diller et al., 2001; Ilouz et al., 2012; Kim et al., 2007; Kim et al., 2005; Su et al., 1995; Wu et al., 2007; Zhang et al., 2012). The first R:C complex contained the minimal binding fragment of RIα (91-244) which included the IS and only the first CNB-A domain and the C-subunit (Kim et al., 2005). This structure revealed how RIα's linker and IS becomes ordered by binding in the active site cleft of the C-subunit together with two Mn ions and AMP-PNP (a nonhydrolyzable ATP-

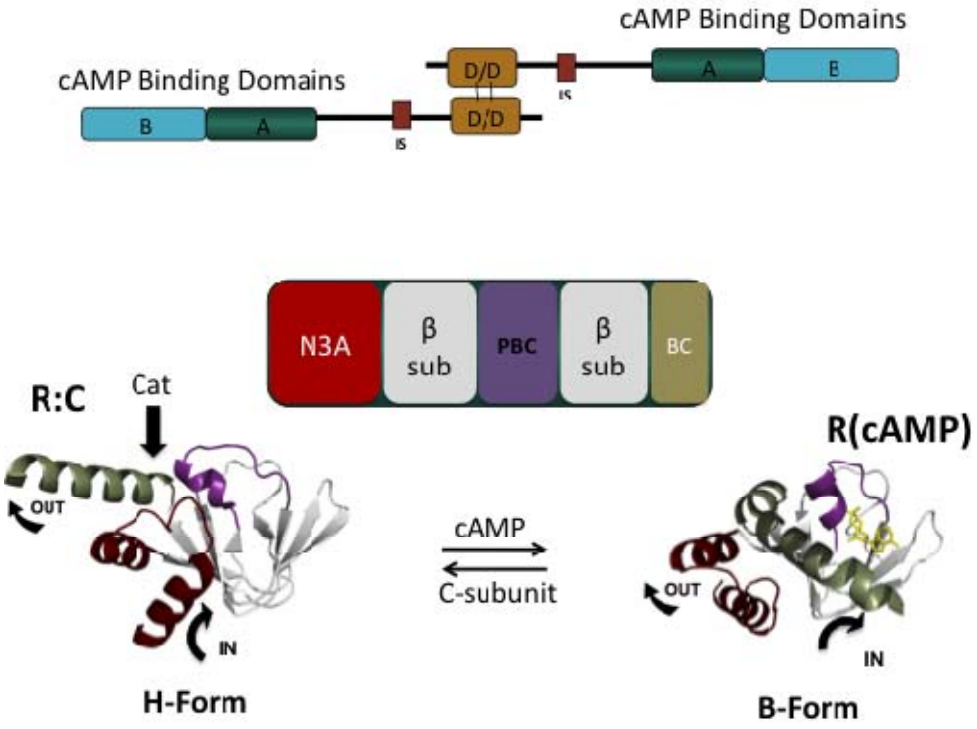

Figure 1.8. R subunit's CNB domain structural motif. The CNB domains are composed of the N_3A motif (red), β subdomain (grey), PBC (purple), and B-helix (green). Structural reorganization occurs upon ligand-binding.

analog). A large 3000 $Å^2$ interface between the CNB-A of RIα and the C-subunit forces structural rearrangements of RIα's α-helical segments compared to the cAMP-bound conformations. Here, the C-subunit is in its closed conformation and acts as a scaffold mostly utilizing its large lobe with site one defined as the active site cleft, site two the G helix, and site three the activation loop (**Fig. 1.10**). A larger complex containing both CNB domains A and B (91-379) confirmed and extended the previously seen surface (Kim et al., 2007). The additional site four is composed of the αH-αI loop of the C-subunit (residues 276-286) and the αB helix of CNB-B of RIα (**Fig. 1.10)**. This structure finally revealed the full extent of the conformational change the R-subunit must undergo when PKA is activated from the R:C complex to the cAMP-bound form (**Fig. 1.8**).

While the tertiary R:C heterodimer arrangements are alike, the architecture of how two R:C heterodimers come together in the holoenzyme structures is strikingly different. Early on studies targeted the tetrameric holoenzymes because it represents the physiologic state of PKA in cells. Due to the challenges of obtaining atomic resolution crystal strcutures of these large complexes, SAXS gave the first clues as to how different the isoform holoenzyme are (Heller et al., 2004; Ilouz et al., 2012; Vigil et al., 2006. More recently the crystal structures of the RIβ and RIIβ holoenzymes were solved and confirmed the SAXS data (Zhang, 2012). The RIIβ holoenzyme structure shows the compact architecture of two C-subunits and the RIIβ dimer complex. This doughnut-shaped, 2.3 Å structure revealed the holoenzyme-specific

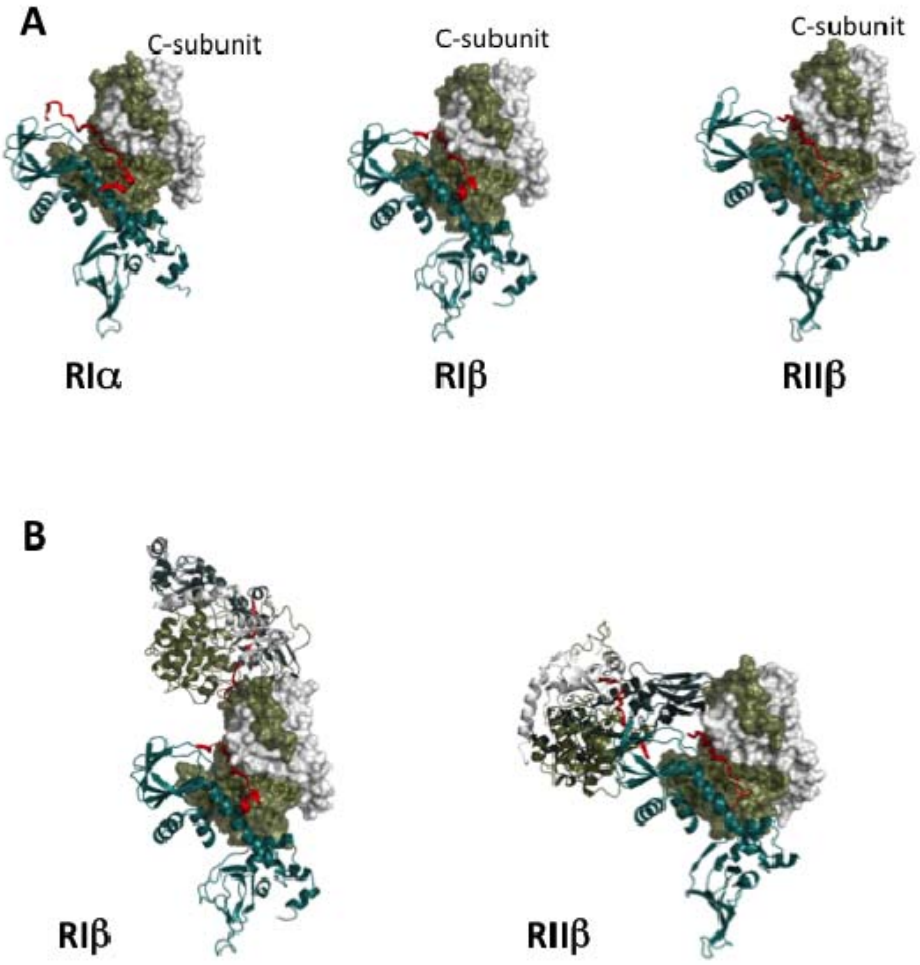

Figure 1.9. R:C complex structures. C-subunits are colered white and olive. R-subunits are colored teal with the linkers in red. **(**A) The three R-subunit isoforms assemble into a similar heterodimer with the C-subunit. (B) RIβ and RIIβ have different holoenzyme architectures.

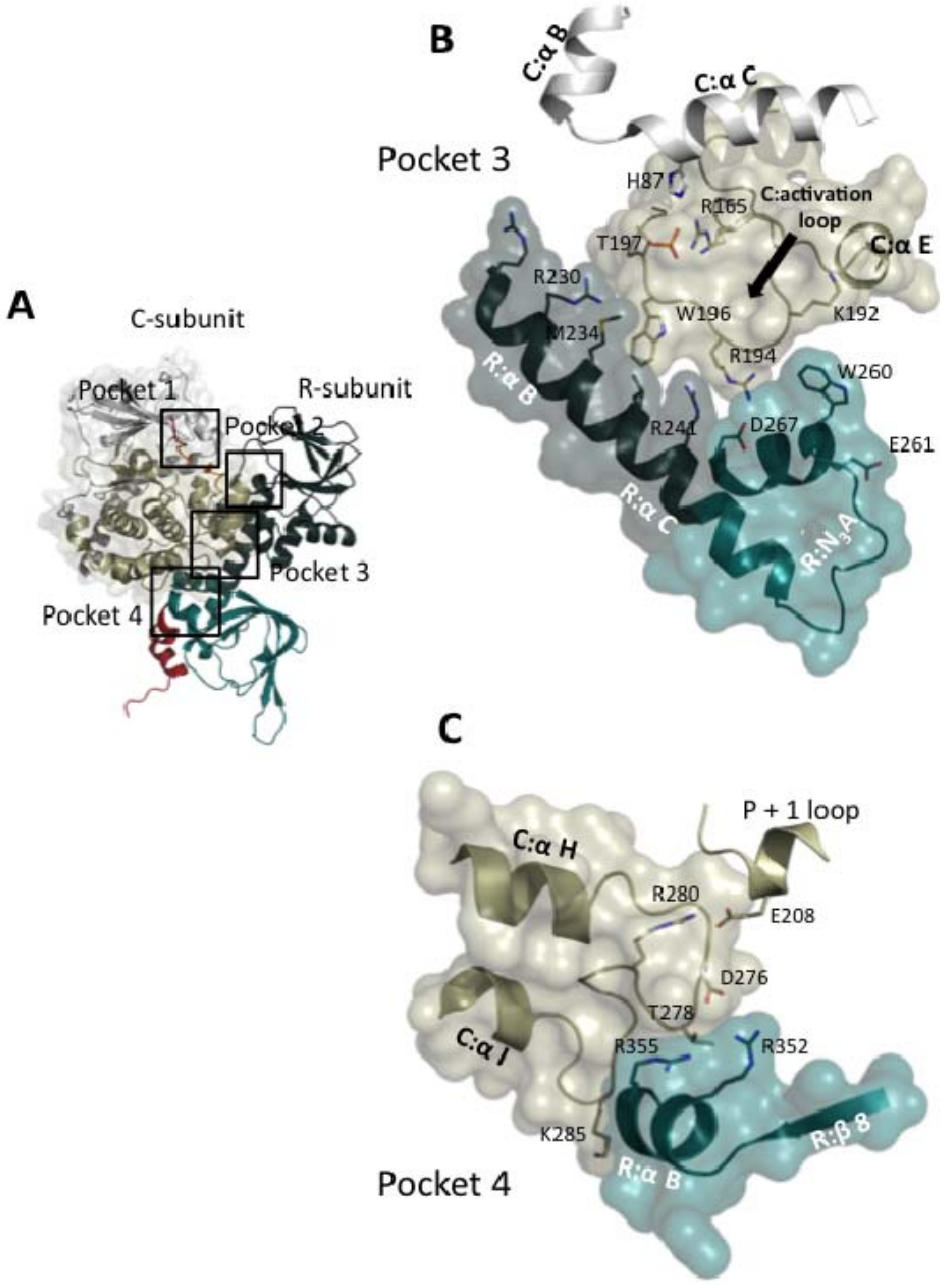

Figure 1.10. RIα:C crystal structure. Most contacts to the C-subunit are made with the CNB-A domain of R and the IS of the linker. Specific interaction pockets 1-4 between the R- and C-subunit are highlighted in the RIα:C heterodimer structure.

packing interaction of the R-subunits' CNB-A β4-β5 loop with the opposite C-subunit's C-terminal tail (residues 320-339). In contrast, in the RIβ holoenzyme the R-subunits are far apart and the RIβ heterodimer interface involves the two C-subunits' C-tails (**Fig. 1.9B**).

1.6 PKA and Disease

Kinases have emerged as major players in tumor cell proliferation and targeting catalytic activity with small molecule inhibitors has become an intense focus within the oncology drug discovery field (Zhang et al., 2009). With an incidence of 48% an L206 to R mutation in Cα was recently proposed to cause overactive PKA in adrenal adenomas (Kirschner; Kirschner et al., 2000) and this is likely due to interference with R-subunit binding. Disruption of the regulatory subunits' control of function in PKA activity also has detrimental consequences and can lead to memory defects, cancer, and endocrine disorders. While there are four regulatory subunit isoforms (RIα, RIβ, RIIα, and RIIβ) of PKA that are expressed in mammals, their tissue distribution und functions are non-redundant. These isoforms share a general domain organization, yet their cAMP response profiles as well as their knock-out effects in mice differ. Uniquely, knock-out mice of RIα are embryonically lethal, thus indicating RIα is pivotal and essential for survival (Boshart et al., 1991; Jones et al., 1991).

RIα has been directly linked as a cause of human disease and one example is CNC disease - an autosomal-dominant syndrome associated with mutations in the

PRKAR1A gene, effectively disrupting RIα inhibition and leading to overactive catalytic subunit. A majority of the approximately 120 mutations discovered so far to cause CNC disease are subject to nonsense mediated mRNA decay (NMD), which leads to haploinsufficiency of RIα protein levels in cells. The C subunits of PKA thus phosphorylate substrates in a cAMP-uncoupled signaling manner. Furthermore, RIα mutant proteins that escape NMD and are expressed, yet dysfunctional in their regulatory roles. The molecular causes for dysfunction of RIα are diverse and mutations have been found all along the gene. Some are located in the cAMP binding domains and others are involved in the binding interactions with the C subunit, but residues with less understood roles have also been documented (**Fig. 1.11**).

The importance of RIα expression levels has been studied and linked to disease. When RIα expression is lowered it can cause systemic lupus erythematosus (SLE) (Kammer et al., 2004) and Carney complex (CNC) (Veugelers et al., 2004), while RIα overexpression can also have negative consequences and is associated with breast cancer (Miller, 2002). Contrary to CNC disease, hormone resistance and lowered PKA activity was observed in acrodysostosis patients and subsequently mutations in the PRKAR1A gene were found (Linglart et al., 2011; Nagasaki et al., 2012). Acrodysostosis is a rare syndrome characterized by severe physical malformations due to skeletal dysplasia (Ablow et al., 1977). In addition, developmental delay and intellectual disability accompanies the effected patients (Linglart et al., 2011; Nagasaki et al., 2012). It has been shown to be an autosomal dominant genetic syndrome in some families.

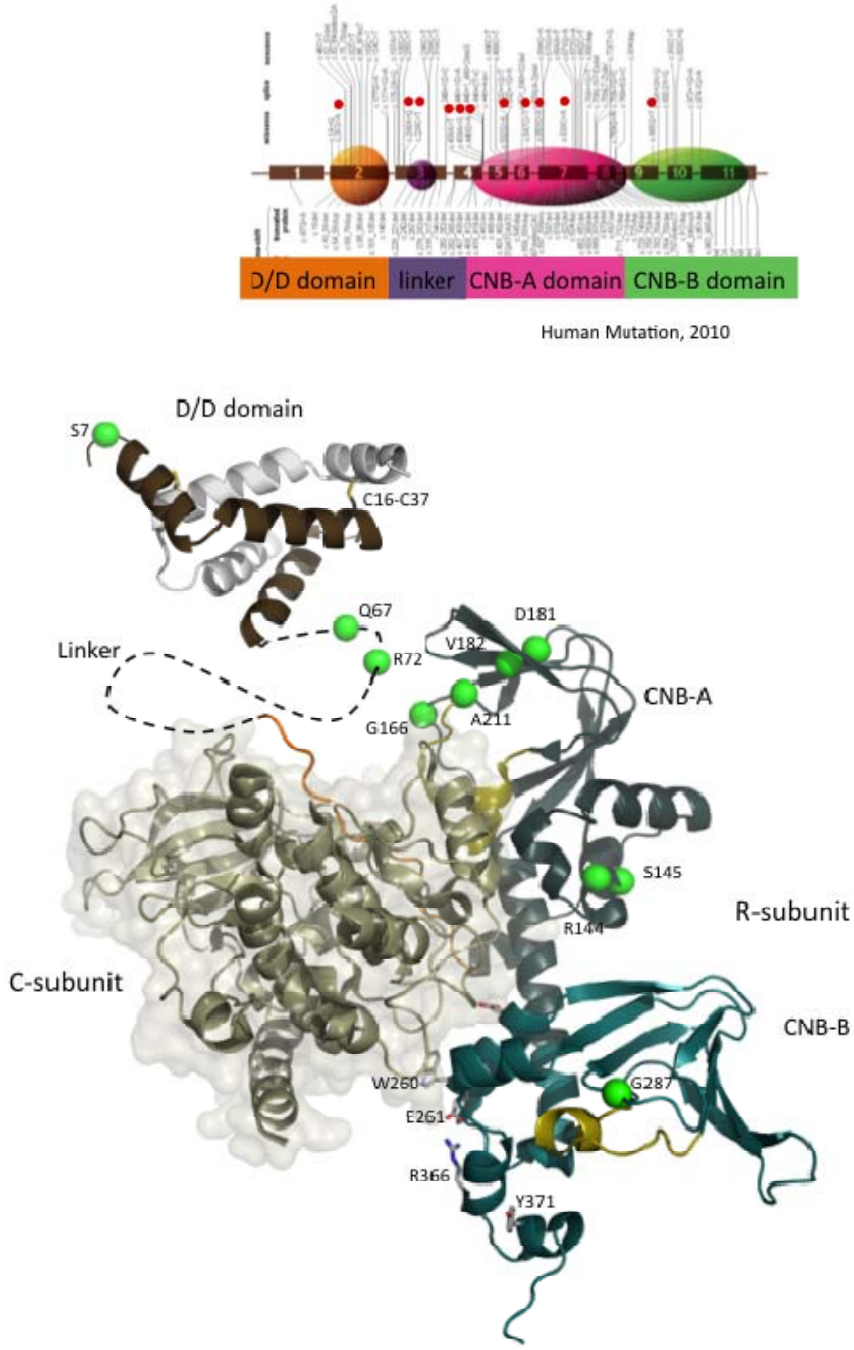

Figure 1.11. RIα mapping of CNC disease mutations. (Top) CNC disease mutations occur at various locations within the RIα gene and resulting domains. Most of the mutations are subject to NMD. **(Bottom)** Expressed CNC mutations (green spheres) are mapped onto the RIα:C structure (pdb id: 2qcs). The C-subunit is colored olive, the R-subunit is colored dark teal (CNB-A) and light teal (CNB-B) with the PBCs in yellow. The N-terminal part of linker (dashed black line) has been modeled. The D/D domain is colored brown and white.

The expressed mutant RIα associated with the acrodysostosis-1 patients is likely the culprit of the disease symptoms (Linglart et al., 2011; Nagasaki et al., 2012). Deletion of the C-terminus of RIα is one of ACRDYS1 mutations and was found in three unrelated patients but several point mutations have now also been uncovered (Nagasaki et al., 2012).

1.7 Thesis Guiding Questions

The PKA signaling system relies on four functionally non-redundant isoforms that enable the intricate and tight regulation of C-subunit phosphorylation and its associated biological outcomes. The structural characterization of isolated PKA components has provided a solid foundation for understanding this enzyme's basic functions. PKA exists as part of macromolecular signaling complexes in mammalian cells in the active state as regulatory and catalytic subunits and as the phosphorylation-silent holoenzyme complex. The guiding theme of this thesis was thus to approach an extended understanding of PKA with the RIα nucleated signaling complexes assembly into functional signaling complexes.

The RIα isoform homodimer is composed of two cAMP-bound regulatory subunits that are linked by their N-terminal dimerization/docking (D/D) domains. Though several structures of isolated domains of RIα have revealed the structural basis for their cAMP binding domains, a full-length RIα homodimer structure is essential for deciphering PKA regulation and molecular characteristics of the biological signaling protein. This formulates aim 1: to determine the dynamics and

structure of the PKA regulatory subunit 1 alpha homodimer complex. Can the differential cAMP-binding characteristics of the full-length versus the truncated RIα subunit be explained? In addition to the D/D domain are there other interactions between the protomers in the dimer? Is the D/D domain structurally integrated with contacts to the CNB domains?

PKA heterotetramer holoenzyme complexes have been probed to extract isoform-specific functional characteristics and posed many new questions. One still unanswered question is how the allosterically activated phosphorylation potential gets realized by binding of four cAMP molecules to the holoenzyme architecture. Comparisons of full-length and deletion mutant forms of RIα have shown significant differences in their cAMP sensitivity profile of activation and revealed that true allostery is achieved only by the holoenzyme (Hill coeffient of 1.2 versus 1.8). Several crystal structures of RIα monomoers and heterodimers have provided insights for PKA signaling, but the full-length structures of the RIα holotetramer $(R:C)_2$ remains elusive. This leads to Aim 2 of my thesis: to elucidate and characterize the subunit interactions that lead to full allostery within the RIα holoenzyme complex.

Aim 3 of this thesis is to study RIα-specific scaffolding functions. The main binding potential for the assembly of signaling complexes in the cell by the R-subunits is nucleated by the AKAP-D/D domain interaction. While most AKAPs are either RII or dual (RI and RII) specific binders, recently the RI-specific smAKAP was discovered (Burgers et al., 2012) and we set out to elucidate the molecular origin and function of this interaction with crystallography. Finally, the discovery of PRex1 as a

non-canonical binder with RIα's C-terminal PDZ motif spurred an investigation and characterization of this interaction.

The full-length proteins contain the full allosteric potential as a result of wide-ranging cooperative communication between the functional sites. The aims of my thesis are geared toward providing a more complete, biologically relevant picture of RIα isoform-specific architecture and complex assembly. In the short-term, this study was to provide RIα complex structures while aiming to contribute to a more comprehensive understanding of the type 1 alpha PKA signaling range.

Chapter 2

PKA RIα Homodimer Structure

2.1 Introduction

Since PKA was discovered in 1968 (Walsh et al., 1968), it has emerged as the most ubiquitous cAMP-responsive enzyme in mammalian tissues (Kuo and Greengard, 1969). As such it confers a myriad of cellular responses including cell differentiation, regulation of metabolism, and cell growth {Cho-Chung, 1995 #35}. In the absence of cAMP, PKA exists in an inhibited state composed of a regulatory (R) dimer bound to two catalytic (C) subunits. Compromised regulation of PKA activity has detrimental consequences. This is exemplified by RIα haploinsufficiency causing Carney complex disease (CNC), which is a familial multiple neoplasia syndrome characterized by cardiac and extra-cardiac myxomas (Veugelers et al., 2004). In mice, RIα knockout result in embryonic lethality (Amieux and McKnight, 2002), and it was identified as the tissue specific extinguisher of cAMP-mediated gene expression (Boshart et al., 1991). Although RIα is ubiquitously expressed in every cell, it is especially abundant in the central nervous system and the heart (Cadd and McKnight, 1989). Not only is expression of the four R isoforms RIα, RIβ, RIIα, and RIIβ tissue specific, but their functional roles are non-redundant.

Elucidating monomeric regulatory subunit structures has provided basic understanding for PKA-mediated signaling, yet each full-length R subunit exists in cells as a stable dimer (Potter and Taylor, 1979; Rubin, 1979). The full-length R subunits are composed of an N-terminal dimerization/docking (D/D) domain, a flexible linker, and the C-terminally positioned tandem cyclic nucleotide binding

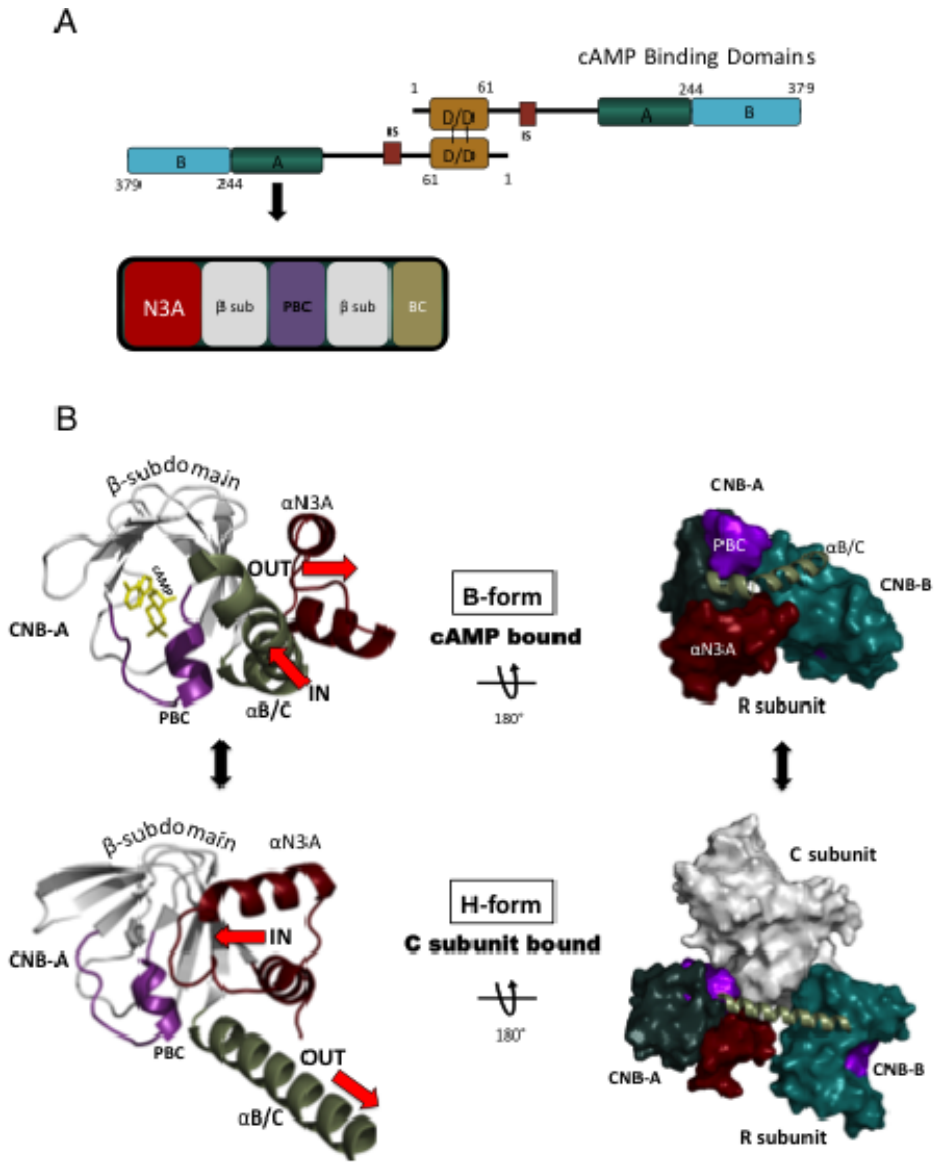

Figure 2.1. CNB-A structural motif organization. (A) Shown is the overall functional domain organization of the full-length RIα construct used in this study. This included the D/D domain, the linker with the inhibitor site that can bind to the C subunit in the holoenzyme, and the two tandem CNB domains. The bottom figure highlights the CNB-A structural motif makeup containing the N3A motif, the β sandwich, the PBC, and the αB/C helix. **(B)** Current understanding of the structural motif conformational changes within the CNB-A are demonstrated as they differ in the cAMP bound (B-Form, top) and the C subunit bound form (H-Form, bottom). The N3A is colored red, the αB/C helix green, the PBC purple, the β-sandwich white, and cAMP yellow. Top left figure is the CNB-A in the cAMP bound (B-Form) and bottom left is the CNB-A in the C subunit bound (H-Form). Top right shows the overall R monomer conformation in the B-Form. Bottom right shows the overall R conformation of the heterodimer R_1:C_1 (R is in the H-Form).

(CNB) A and B domains, which are connected to each other by the αB/C helix (**Fig. 2.1A**). Each CNB has a β-subdomain that forms a beta sandwich, which is flanked by a helical α-subdomain. Embedded within the beta sandwich is the phosphate-binding cassette (PBC) that serves as the docking site for cAMP in all cAMP binding proteins (Su et al., 1995). The α-subdomains are in turn composed of two motifs. Preceding the β-sandwich is an αN helix, a short 3_{10} -loop and an αA helix, together termed the N3A-motif (**Fig. 2.1.A**), which is conserved in other cAMP-binding proteins such as Exchange protein directly activated by cAMP (EPAC) and Potassium/sodium hyperpolarization-activated cyclic nucleotide-gated channel (Kornev et al., 2008). Following the β-sandwich is the αB-αC helix.

Structural studies of R monomers have uncovered some of the conformational changes as it toggles between its cAMP bound B-form and its C-subunit bound H-form (**Fig. 2.1.B**) (Kim et al., 2007; Kim et al., 2005). The N3A-motif and the αB/C helix were revealed to be pivotal and correlated; while one moves in towards the PBC, the other moves out. In the cAMP-bound form the kinked conformation of the αB/C helix positions it close to the PBC. In the C-subunit bound state the αB/C helix is contiguous and positioned "out" from the PBC. Conversely, the N3A motif slides to the "in" position when C is bound to R, which allows the N3A-motif to interact with the PBC. In the cAMP-bound state, on the other hand, the N3A is in the "out" position where it is moved up and away from the PBC, which as this study reveals is crucial for the cAMP-bound RIα dimer conformation.

While truncated structures of the R subunits provided fundamental knowledge for our understanding of PKA, a full-length dimer structure has not been elucidated even though there are significant biochemical differences compared to the monomeric form. A deletion mutant of RIα, that is missing most of the linker and the D/D domain and has typically been utilized for crystallography studies, displays equal cAMP binding affinities of 50 nM for the two tandem CNB domains. This monomeric protein also lacks cooperative cAMP activation (Herberg et al., 1994). In contrast, the full-length dimer binds cAMP with a cooperative profile with a Hill Slope of 1.62. Additionally, differential affinities for cAMP of the tandem CNB sites were noted: CNB-A has a K_a of 60nM and CNB-B has a higher affinity of 15nM (Herberg et al., 1994).

Hence, we hypothesized that there may be communication as a result of additional interaction sites between the dimer protomers in the full-length protein that could explain the cAMP binding differences as compared to the monomeric deletion mutant protein. This crystallographic study of the RIα homodimer uncovered a novel interaction surface between the protomers that allows communication in the dimer protein. The docking of two CNB-A domains within the dimer create a helical-helical bundle by utilizing their N3A structural motifs. The structure is consistent with small-angle scattering (SAXS) data and reveals a biologically relevant conformation. In addition, mutations within this interface result in structural and biochemical changes. Strong evidence for the biological relevance of the discovered interface is further established by the presence of Carney Complex disease mutations within this region,

which thus far lacked a structural rationale for altered RIα function. While present in the crystals, the D/D domain and most of the linkers do not give rise to electron density, which is due to the linker region's intrinsic flexibility. However, our structure reveals that, in addition to the D/D domain preventing long-distance dissociation by functioning as an N-terminal tether for the two protomer chains, it also enables formation of an intermolecular interface by the protomers' CNB domains. This interface, in turn, allows cross communication between the two CNB-A domains, which results in cooperative cAMP binding across the dimer molecule. Thus, this study presents the first R homodimer structure that can explain the cooperative cAMP binding by RIα and reveals an interface with implications for Carney Complex mutations.

2.2 Experimental Procedures

Protein Expression and Purification - Bovine full-length (1-379) wild type and mutant RIα proteins were purified as described previously (Su et al., 1995; Wu et al., 2004b). Mutations to analyze the interface biochemically were generated by QuickChange® site-directed mutagenesis. Expression was carried at out 16C for 16-20 hours in *E.coli* BL21 (DE3) from Novagen® suspended in YT Media. In summary, a combination of ammonium sulfate precipitation, affinity chromatography with cAMP-resin and size-exclusion chromatography were utilized to achieve >94% pure protein. Briefly, following expression cells were lysed with a Microfluidizer® processor at 18,000 psi, centrifuged at 16,000 rpm, and the soluble fraction was then ammonium

sulfate precipitated. The ammonium sulfate pellet was resuspended and batch bound over night to cAMP resin. After elution from the resin with 40mM cAMP the elution was applied to a Superdex™ 200 gel filtration column utilizing a buffer containing 50mM MES (pH 5.8), 200mM NaCl, 2mM EGTA, 2mM EDTA and 5mM DTT.

Crystallization of the RIα Homodimer - Purified RIα(1-379) was concentrated from 8 to 12 mg/ml with a 30K MWCO concentrator and cAMP was added to 3-fold molar exess of RIα. Protein was then centrifuged at 14,000 rpm for 10 minutes to remove particulate contamination and was set up by hanging-drop vapor diffusion with various commercially available screens at 50% protein plus 50% screen buffer at 4°C and 22°C. Several crystal hits with a similar tetragonal bipyramid shape were obtained but the optimized condition that yielded the best diffracting crystals was composed of 0.125 M sodium acetate (pH 5), 2M sodium formate with the protein at a final concentration of 4 mg/ml grown in a 2µl drop. SDS gel analysis of the crystals confirmed the full-length RIα and not a proteolyzed monomer form.

Structure determination and refinement - Crystals were flash frozen in liquid nitrogen after soaking in a cryoprotectant composed of mother liquor supplemented with 20% PEG 400. X-ray diffraction data sets were collected from one crystal at the Advanced Light Source, Berkeley California beamline 8.2.1 and processed with HKL2000 (Otwinowski and Minor, 1997). This resulted in a tetragonal $P4_12_12$ space group and cell dimensions of a=b=104.7 Å and c=218.3 (Table 1). The

best dataset resulted in a structure solution with final resolution of 3.88 Å. The full-length homodimer crystals contain a unique morphology and space group as compared to previous structures of the deletion mutant monomers, which have a hexagonal space group of P6 (Badireddy et al., 2011; Su et al., 1995; Wu et al., 2004a; Wu et al., 2004b). While in the previous monomer structures each asymmetric unit contained one monomer, this structure now contains the dimer in the asymmetric unit. The structure was solved using the RIα monomer structure with pdb access code 1rgs as a molecular replacement probe with the resulting LLG score of 1634 and TFZ score of 37.9 for using two copies of 1rgs as the search model (Su et al., 1995). Model building was carried out in Coot (Emsley and Cowtan, 2004). Initially, CNS with DEN restraints-assisted refinement was carried out (Schroder et al., 2010). This was followed by Refmac refinement with non-crystallographic symmetry (NCS) restraints applied (Murshudov et al., 1999). The positive F_o-F_c density at 3-σ level is visible for each of the four cAMP molecules in their binding pockets. The final model includes residues 105-376 for one chain (R), where the first 3 residues are displayed as alanines due to lack of side chain density. Residues 108-376 are included for the other monomer chain (R'). The R and R-free are 0.26 and 0.28, respectively, and the structure model has a good geometry as evaluated with PROCHECK (Laskowski R A, 1993)(Table 2.1).

Table 2.1. Data collection and refinement statistics of RIα dimer.

	$RI\alpha_2$
Data collection	
Space Group	$P4_12_12$
Cell dimensions (Å)	
a=b	104.7
c	218.3
No. of molecules per asymmetric unit	2
Resolution (Å)	3.88
R_{merge}	0.088 (0.575)[a]
Completeness (%)	99.9 (100.0)
I/sigma	35.9 (6.2)
No. reflections	11,860
Multiplicity	9 (9.4)
Refinement	
Resolution (Å)	50-3.88
R_{work} / R_{free} (%)	26.0/28.7
R.m.s. deviations	
Bond lengths (Å)	0.017
Bond angles (°)	2.0
Ramachandran angles (%)	
Most favored	71.5
Disallowed	None

[a]Values in parantheses are for highest-resolution shell (3.88 - 4.02 Å)

Small Angle X-ray Scattering - RIα full-length mutant proteins were purified as described above and the final buffer composition was 50mM MES (pH 5.8), 200mM NaCl, 2mM EGTA, 2mM EDTA and 5mM DTT. The protein concentrations for the SAXS experiments were in the range of 2-5 mg/ml. The SAXS data were collected for 90 min for the Y120A experiments sample and 240 min for the K121A sample. SAXS data were acquired at 12 °C using the SAXSess (Anton Paar) line collimation (10 mm) instrument at the University of Utah. Data were collected using an image plate detector, and reduced to I(q) versus q ($q = (4\pi\sin\theta)/\lambda$; 2θ is the scattering angle; $\lambda = 1.54$ Å CuK_α) using the program SAXSquant 2.0. X-ray scattering from the protein was obtained by subtracting the scattering of the normalized buffer blank. The theoretical scattering profile for the RIα homodimer crystal structure was calculated using the FoXS server (Schneidman-Duhovny et al., 2010; Schneidman-Duhovny et al., 2013). P(r) functions for the experimental and theoretical scattering were calculated using GNOM (as implemented in ATSAS 2.5.0; (Svergun, 1992)). The experimental scattering data were corrected for smearing effects in GNOM using beam length profiles parameters.

PKA Activation / IP-20 - The activation of wild-type and mutants of RIα holoenzymes was investigated by a fluorescence polarization assay (Saldanha et al., 2006). Holoenzyme was formed with molar ratio of 1.2 mol RIα to 1 mol C subunit and diluted in buffer containing 20 mM Hepes (pH 7), 75 mM KCl, 0.005% Triton X-100, 1 mM ATP, 1 mM DTT, and 10 mM $MgCl_2$. A 20-residue long PKA inhibitor

peptide (IP-20) labeled with succinimidyl activated carboxyfluorescein (FAM-IP20) was added to RIα holoenzymes, followed by addition of cAMP to activate PKA. The working concentration of C subunit was 12nM, FAM-IP20 was 2nM, and 2-fold serial dilutions from 2000 - 0 nM cAMP were added to initiate holoenzyme dissociation and FAM-IP20 binding to the C subunit. Fluorescence polarization readings with excitation at 485 nm and emission at 535 nm were carried out with a GENios Pro micro-plate reader (Tecan) using black flat-bottom Costar® assay plates. Each protein was tested in quadruplicate and the data were analyzed with Prism 4.

2.3 Results

The Dimer Structure Reflects the Biologically Relevant Conformation - To crystallize the full-length RIα homodimer, excess cAMP was added to the purified protein before setting up crystallization screens. Excess cAMP improves the stability of the protein in solution while preventing early degradation. Crystals were obtained in this way and resulted in a unique morphology and space group of $P4_12_12$ (Table 2.1), compared to previous structures of the deletion mutant monomers, which had hexagonal space groups of P6 (Badireddy et al., 2011; Su et al., 1995; Wu et al., 2004a; Wu et al., 2004b). While in the previous structures each asymmetric unit contained one monomer, the present structure now contains the homodimer in the asymmetric unit with an inverted U-shaped architecture and a rotational NCS two-fold symmetry (**Fig. 2.4A).** While the tandem CNB-A and CNB-B domains for each of the two chains (denoted R and R') are resolved with cAMP bound, the D/D domain and

N-terminal part of the linkers are not visible in the electron density maps. However, the crystal arrangement contains enough space above the CNB-A domains in the crystal lattice for the D/D domain. To establish if the D/D domain is indeed present in our crystals and verify that the crystals are not composed of degraded protein we washed and ran the crystals on a SDS gel. According to the SDS gel analysis, the protein runs at the full-length molecular weight and shows that the crystals are composed of full-length RIα (**Fig. 2.2**). The lack of electron density can thus be explained by the linker region's flexibility that may prevent the D/D domain from being captured in a consistent position. Previously, site-directed labeling experiments showed that these linkers are highly flexible (Li et al., 2000). In fact, the flexibility of the linker region and its resulting inherent instability was observed already at the early stages of studying PKA (Erlichman et al., 1973; Rannels and Corbin, 1980). Moreover, the linkers are predicted to be intrinsically disordered regions (**Fig. 2.3**) (Romero et al., 2001) and together with the above-mentioned studies can explain the absence of electron density for the D/D domain in our structure.

The overall shape, as revealed by our crystal structure, also agrees with early studies investigating the structural characteristics of RIα (Zoller et al., 1979). We thus compared our crystal structure to the solution structure of the protein, previously determined by SAXS analysis (Vigil et al., 2004). The small-angle scattering function

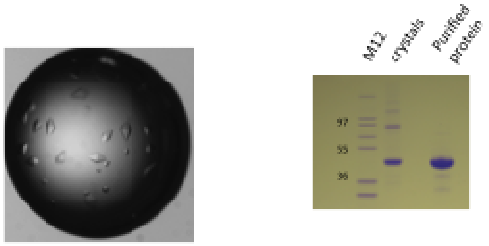

Figure 2.2. SDS gel of RIα dimer crystals. The crystals grown in the condition that resulted in the diffraction data set (left), which was used to solve the homodimer structure, were run on a reducing SDS gel (right) to test if the protein had not degraded. As compared to the purified protein the crystals do contain the full-length protein.

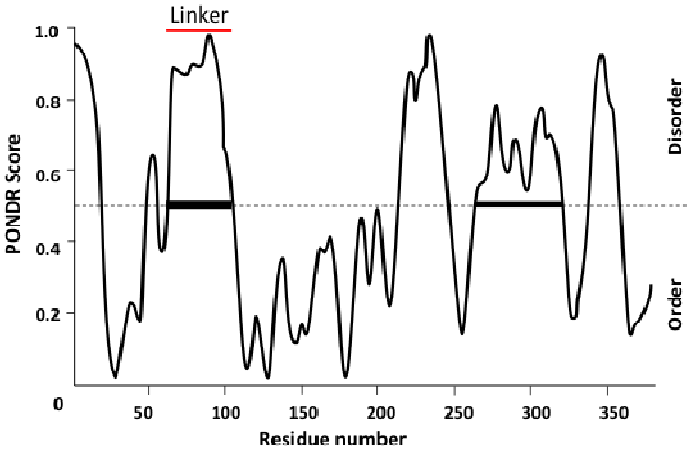

Figure 2.3. PONDR analysis of RIα sequence. Using PONDR to investigate the RIα sequence reveals that the residue region following the D/D domain around residue 60 up to the beginning of the N3A motif is predicted as intrinsically disordered.

was calculated from the crystal structure using FoXS (Schneidman-Duhovny et al., 2010; Schneidman-Duhovny et al., 2013) and the resulting pair-distance distribution function (P(r); **Fig. 2.4C**) was compared to the previously published P(r) determined from SAXS of the RIα homodimer (Vigil et al., 2004).

The from the crystal structure calculated data compares to the in-solution data with a $\chi^2 = 1.1$ (**Fig. 2.4B**) and despite the lack of electron density for the D/D domain, the P(r) from the crystal structure has a similar double-peak shape as obtained experimentally with SAXS for the full-length protein. The D_{max} value of the crystal structure is 95 Å rather than 110 Å as was determined from SAXS experiments and the R_g value of the crystal structure is also less than the SAXS of the full-length homodimer (Table 2.2). However, the smaller dimensions of the predicted SAXS of the crystal structure are consistent with the D/D domain and most of the linker not being represented in the dimer crystal structure. The double-peak shape of the P(r) curves of both the crystal structure and the experimental SAXS are indicative of a bilobal structure (**Fig. 2.4C**) where the first peak corresponds to interatomic distances within each lobe and the second peak corresponds to interatomic distances between the two lobes. The greater D_{max} seen in the P(r) of the full-length RIα SAXS is consistent with a Y-shaped structure where the D/D domain and linker form the stem of the Y and the CBDs form the arms or lobes of the Y (see **Fig. 2.4A** in Vigil et al., 2004). Indeed, the relative positions of the CBDs in the Y-shaped model presented by Vigil et al. (2004) are in very good agreement with the crystal structure. Considering the inherent resolution limitations of SAXS, combined with the fact that experimental

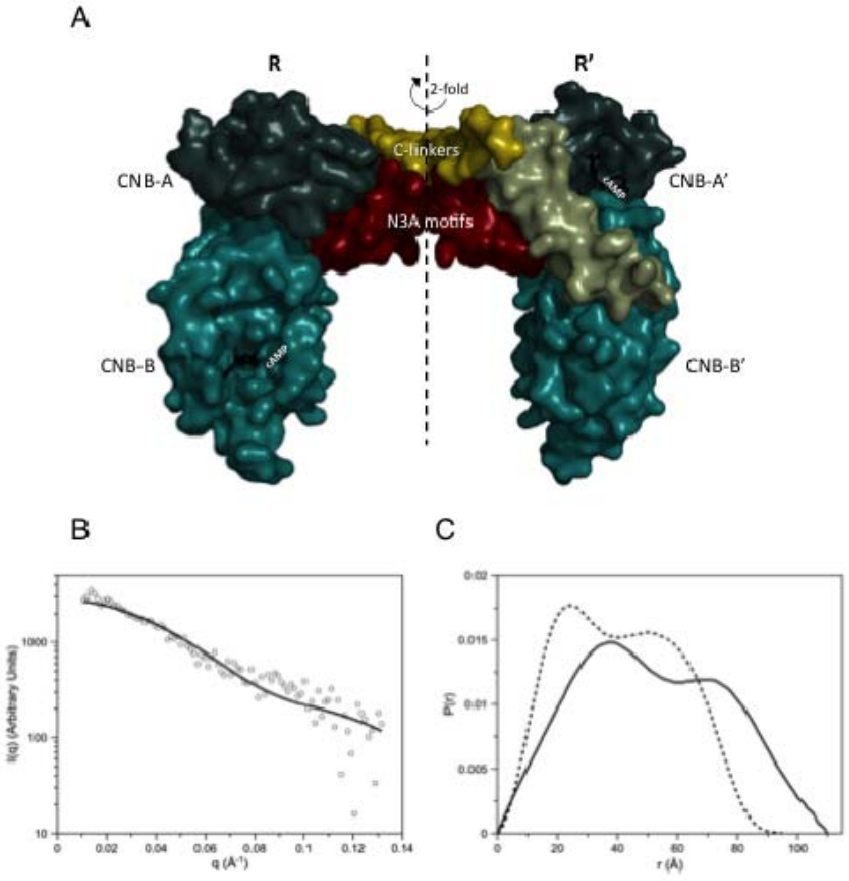

Figure 2.4. Overview of the RIα dimer molecular architecture. (A) A space filling depiction of the RIα homodimer crystal structure is shown. The CNB-A domains are in deep teal, the CNB-B domains in light teal. The PBC is colored purple, cAMP black, the linker gold, and the αB/C helix green. **(B)** Plot of the theoretical scattering profile of the RIα homodimer crystal structure as calculated with FoXS is shown as a solid black line in comparison to the experimental scattering profile (Vigil et al., 2004) shown as open black circles. **(C)** P(r) curve computed from the RIα homodimer crystal structure (dashed line) compared to the P(r) of RIα homodimer from SAXS (black line) (Vigil et al., 2004).

SAXS is the result of the time- and ensemble-average of all conformations of the protein, the published SAXS-based model nevertheless does validates the crystal structure and supports the idea that these contacts could readily form.

Conserved Features of the Dimer Architecture - At the vertex of the dimer, the two R subunits converge. Electron density is visible for the two RIα chains beginning with residue E^{105} (R) and A^{108} (R') respectively (**Fig. 2.5**), which are extended compared to the monomer cAMP bound structure (1rgs) that starts with residue 113 (Wu et al., 2004a). At the C-terminal ends, residues are visible up to S^{376} and each chain includes two bound cAMP molecules according to the F_o-F_c electron density maps (**Fig. 2.6**). The C-terminal portions of the linkers (C-linkers) that are resolved run antiparallel and are positioned on top of their respective helical α-subdomains (**Fig. 2.5**). This C-linker interaction between the two monomers seals an intermolecular interface below it. Docking of CNB-A and CNB-A' results in an interface, which will be described in detail later. The CNB-B domains are extended down and away from their CNB-A domains (**Fig. 2.5**). Structural features of previous cAMP-bound truncation monomers are conserved in the dimer structure as well. The CNB-A domains of the dimer compare to the 1rgs structure with an r.m.s.d. of 0.51 $Å^2$, whereas the CNB-B domains have an r.m.s.d. of 0.98 Å due to its highly dynamic nature (Cheng et al., 2009).

Furthermore, the interface created by R and R' in our dimer structure is also present in previous high-resolution RIα structures. All previous structures are of

Table 2.2. Effect of RIα mutations on SAXS

RIα Homodimer	R_g (Å)	D_{max} (Å)[b]
Wild-type RIα (experimental)[a]	39.8±1.2[a]	110[a]
Wild-type RIα (calculated from crystal structure)	32.1[b]±0.001	95
RIα Y120A	48.8±0.3[b]	150
RIα K121A	43.7±0.3[b]	130

[a]Data from Vigil et al. (2004)
[b]Calculated using GNOM

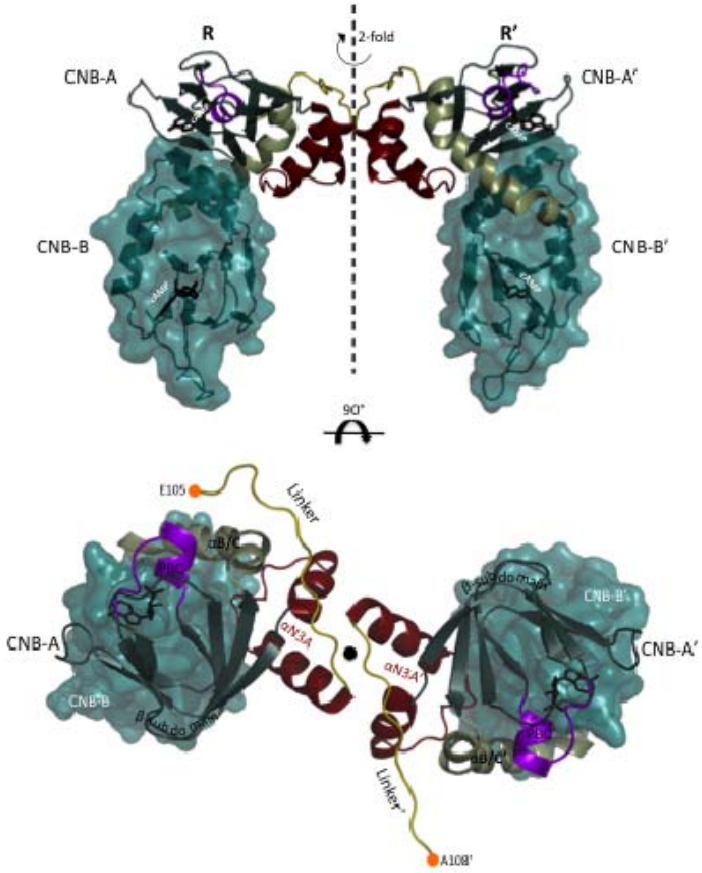

Figure 2.5. Crystal structure of the RIα homodimer complex. The CNB-A domains of R and R' dock into each other creating an upside down U-shape. The CNB-B domains are extended from the. The previously seen architecture within each R and R' monomer is conserved in this structure as well. On the bottom is shown a view from the top down the symmetry axis and thus the CNB-B domains are positioned underneath the CNB-A domains. The N-terminal Cα of the linkers are shown as orange circles.

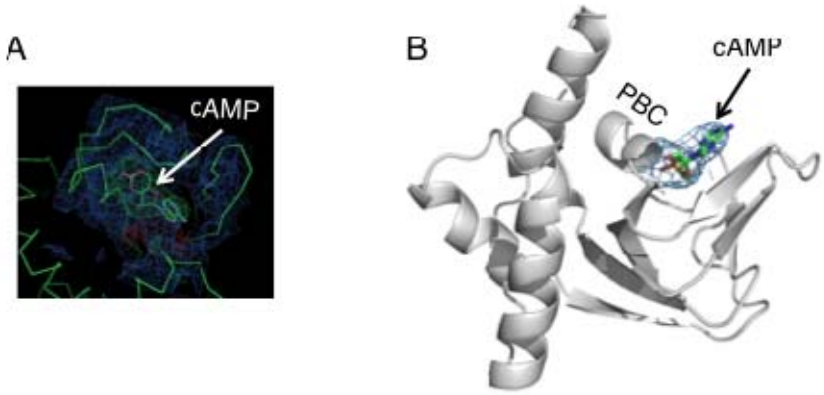

Figure 2.6. Electron density maps showing cAMP bound in CNB domains.
(**A**) The omit map of only the CNB-B is shown as countoured at 3σ and indicates cAMP to be bound in its binding pocket. Similar electron density is present in the other CNB domains. Figure was generated in Coot. (**B**) The $2F_o$-F_c electron density map at 1 σ shows cAMP bound in CNB-A. Figure was generated in PyMol.

deletion mutant monomer constructs that are missing at least the D/D and N-linker of RIα and include but are not limited to pdb accession codes 1rgs, 3iia, 1ne4, 1rl3 and 1ne6 (Badireddy et al., 2011; Su et al., 1995; Wu et al., 2004a; Wu et al., 2004b). Even in these previous crystal structures the monomers utilize the same interface as an interaction to pack in the crystals. Because the monomeric structures are missing the N-linker and D/D domain, the observed monomer contacts were interpreted as crystal packing only and thus not appreciated or analyzed as a functionally relevant interaction.

A Novel RIα-specific Homodimer Interface is Revealed - Each R monomer contains a previously described molecular architecture (Su et al., 1995), and we will use the same nomenclature here. The two linker segments from each monomer that immediately flank the N-terminal N3A motifs run antiparallel and are positioned just above their helical α-subdomains (**Fig 2.7, top**). The N3A and N3A' motifs of each protomer in CNB-A and CNB-A' are sandwiched between the two cAMP-binding β-subdomains (**Fig. 2.7, middle**). The adjacent N3A-motifs are thus wedged against each other creating hydrophobic interactions along the center of a helical-helical bundle (**Fig. 2.7, bottom**). The interface is symmetrical with each αA helix oriented nearly perpendicular against the opposing monomers' αN' helix. Clusters of residue interactions enable this docking of the αA helix against the αN' helix and αA' helix against the αN helix at opposite ends of the interface. Electron density for residue side chains positioned within the interface is visible in this homodimer.

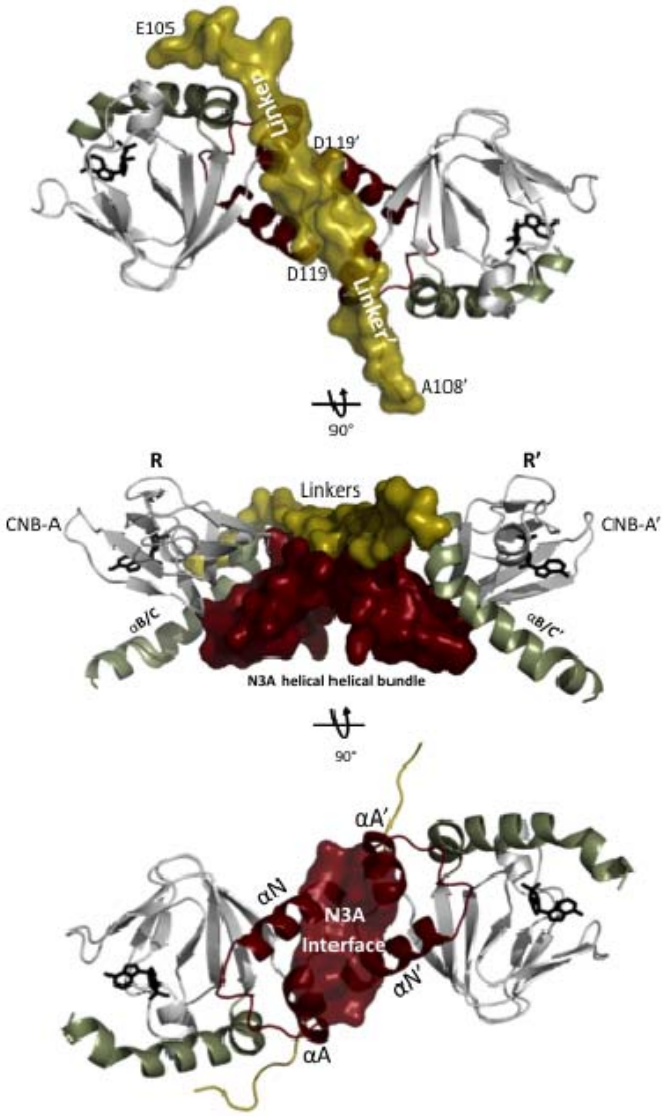

Figure 2.7. CNB-A domain docking creates a hydrophobic interface. The CNB-A domains only of each protomer are shown with the N3A motifs in red and the linkers in gold. Top: view down the symmetry axis to illustrate how the linkers are running antiparallel and sealing the hydrophobic interface below. Middle: shows docking of the CNB-A domains with their respective N3A motifs creating a helical-helical bundle. Bottom: the A helix of each N3A stacks against the N helix of the opposite N3A motif creating a hydrophobic interface between them.

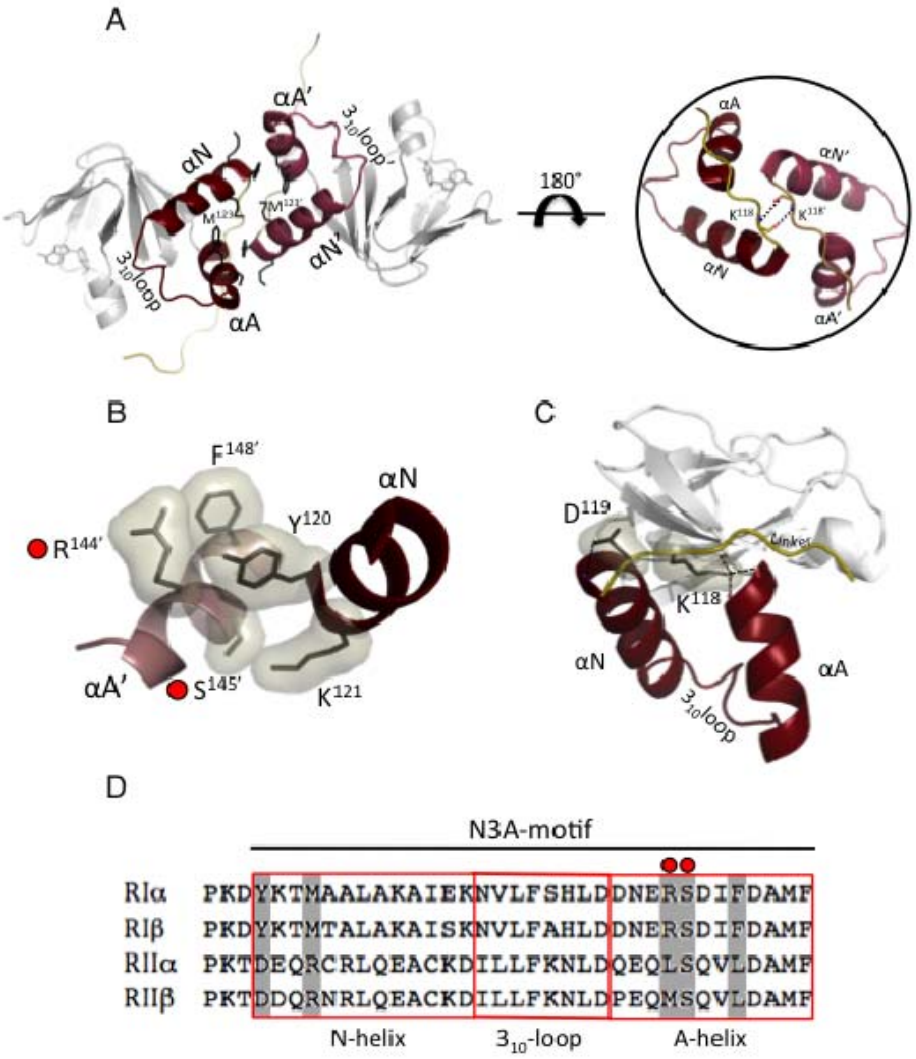

Figure 2.8. Isoform specific N3A motif residues support the RIα dimer interface. (**A**) Left: N3A helical-helical bundle creates H-bonding network on the interface. At the center the two opposing M123 from each protomer constitute a strong hydrophobic core. Right: a zoomed in view of the linker interactions between the protomers' K118 backbone nitrogens and oxygens. (**B**) Specific residue interaction present at opposite ends of the interface. Red circles denote CNC mutations. (**C**) The linkers are antiparallel to each other and cross over their own respective N3A motif. K118 H-bonds to backbone residues of the A helix thereby capping the A helix. (**D**) R subunit isoform sequence alignment of the N3A-motif. Boxed in grey are residues interacting on the interface of RIα. CNC mutations in RIα are marked with a red circle.

The orientation of the interface residues also compares well to that of the higher resolution monomeric structures. Each residue cluster is positioned such that they seal the hydrophobic interface resulting in a buried area of 485Å^2. The energy of desolvation is -6.2 kcal/mol making it an energetically favorable interaction (Krissinel and Henrick, 2007).

While the CNB-B domains are less well resolved, the CNB-A domains and the interface show electron density for several side chains (**Fig. 2.9**). A detailed look at the interface reveals that Phe^{148} of the αA helix pi stacks against Tyr$^{120'}$ in the opposing αN' helix. Tyr$^{120'}$ also hydrogen bonds to Arg^{144} of the αA helix (**Fig. 2.8**). Next to this Arg on the A-helix is Ser^{145} which, in turn, hydrogen bonds to Lys$^{121'}$ in the αN' helix of R'. This H-bonding cluster is present twice, at opposite ends of the interface, due to the 2-fold symmetry within the dimer. In the center of this elongated interface are two opposing methionines, Met^{123} from R and Met$^{123'}$ from R' (**Fig. 2.8**), which serve as a strong hydrophobic core by being 90% buried within the interface (Krissinel and Henrick, 2007)**.** Further stabilizing this conformation is Lys^{118} from each linker, which caps the corresponding A-helix by hydrogen bonding with the backbone oxygens of F^{148}, D^{149} and M^{151} (**Fig. 2.8C**). Lys^{118} and Lys$^{118'}$ are hydrogen bonding with each other's backbone oxygen and nitrogen atoms, thus stabilizing the protomers' linker interaction (**Fig. 2.8A**).

Previously published SAXS comparisons of the RI and RII subunits have demonstrated they have very different molecular shapes even though their sequences and domain organization are similar (Vigil et al., 2004). The published P(r) functions

for RIα and RIβ homodimers have a similar D_{max} of ~100 Å and are also predicted to have a similar bilobal shape (Ilouz et al., 2012). This prediction is supported by a comparison of their CNB-A N3A sequence, which shows high sequence similarity (**Fig. 2.8D**). In contrast, the SAXS P(r) functions for the RII homodimers are much more extended and suggest a different shape compared to the RI subunits (Vigil et al., 2004)**.** This could, in part, be due to the longer linker regions of the RII subunits. However, alignment of the CNB-A N3A-motif sequences of RIα, RIIα, and RIIβ reveal very different side chains at the key residues that form the intermolecular contacts that would presumably rule out a similar interface for the RII subunits. While the crucial Tyr120 of RIα is conserved in RIβ, in the corresponding position in the N-helix RIIα and β have an aspartate at this position. We predict that this aspartate (Asp137) of the N-helix in RIIβ would interfere with the interface formation since it is opposite Asp166 in the A-helix of the other RIIβ protomer. Lysine 121 of RIα, which also appears to be important, is replaced with either a Glu in RIIα or an Asp in RIIβ. Met123 in RIα forms the hydrophobic core of the interface and is an Arginine in both RII isoforms. These differences in sequence at key positions might largely explain the extended shape of the RII homodimers in solution since the crucial interface residues seen in the RIα homodimer structure are not conserved and would presumably prevent this same dimer interaction.

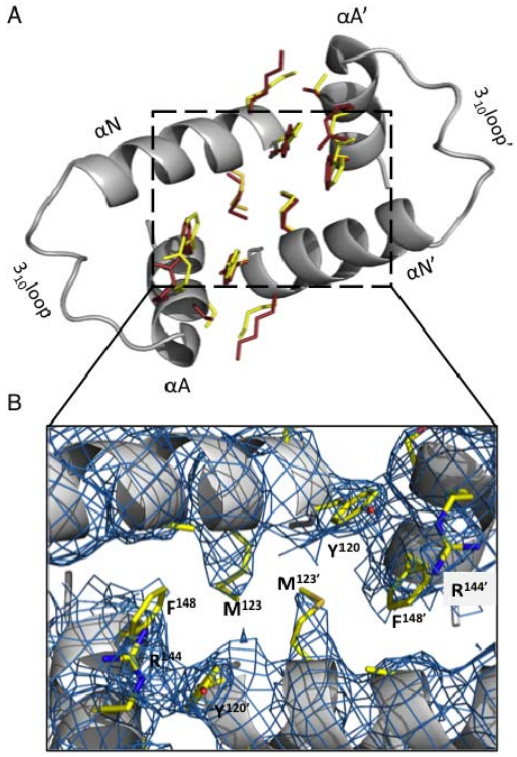

Figure 2.9. Comparison of N3A RIα dimer interface. (**A**) Alignment of RIα dimer structure from this study with 2 symmetry related molecules of 1RGS. The N3A motifs of the RIα dimer are shown in grey, the interface residues of the RIα dimer are shown in yellow and the interface residues located on the crystal packing interface of 1RGS are shown in red. (**B**) Electron density map at 1σ level showing interface residues.

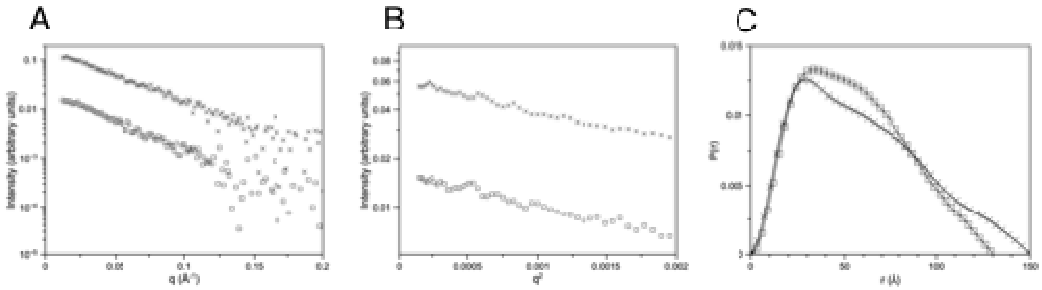

Figure 2.10. SAXS profiles of RIα Y120A and K121A mutants. (**A**) I(q) vs q, (**B**) Guinier plots, and (**C**) P(r) curves calculated from solution small-angle x-ray scattering data for RIα Y120A mutant (crosses) and K121A mutant (squares). Wild-type P(r) curve is from Vigil et al. (2004). P(r) curves have been normalized to area under the curve.

Mutational Analysis of the Interface Uncovers its Functional Significance - To study the homodimer interface in more detail, we mutated interface residues, namely Lys^{121} and Tyr^{120} to alanine. We characterized and evaluated changes in the mutant proteins by SAXS, catalytic subunit inhibition and holoenzyme activation assays. Since neither residue is part of the heterodimer R:C interface (Kim et al., 2007) or the R:cAMP binding interactions, changes in these residues would likely cause the R:R' interface to be perturbed. Comparison of the SAXS P(r) curves of the mutant proteins to the wild-type protein indicate the mutations cause significant structural changes in the RIα homodimer. While the predicted scattering of the crystal structure and the experimental SAXS data of the wild-type homodimer are indicative of compact structures (Table 2.2), the mutant homodimers are much more extended. The maximal distance (D_{max}) shifts from 110Å for the wild type R-subunit to 150Å and 130Å for the Tyr^{120} and Lys^{121} to Ala mutants, respectively (**Fig. 2.10**, Table 2.2). Moreover, the distinct double-peak shape of the P(r) becomes blurred which suggests that the lobes of the Y-shaped structure are more dynamic. These results indicate that the compact relatively rigid structural integrity of the RIα homodimer is lost when the interface is disrupted.

To establish if the interface plays a role in the activation of PKA, the mutant proteins Tyr^{120A} and Lys^{121A} were tested for their ability to regulate the catalytic subunit. Both mutants are able to form holoenzymes with the C subunit, however they show significant differences in their cAMP activation profiles. While the wild-type complex has an EC_{50} for cAMP of about 54 nM the mutant complexes require less

cAMP to release the catalytic subunit and have an EC_{50} values of around 35 nM (**Fig. 2.11A**). The mutants are thus more sensitive to cAMP and are more readily activated. In addition, the mutant holoenzymes show almost complete loss of cooperativity for cAMP activation with a shift in the Hill coefficient from 1.73 for wild type to ~1.0 for the mutants (**Fig. 2.11A**). These results suggest that the N3A interface is of functional as well as structural significance.

Carney Complex Disease Mutations are Localized at the Dimer Interface - Because our mutational analysis had a significant impact on RIα we searched for known disease mutations of RIα that could be linked to the interface. RIα is the only isoform that behaves as the tissue-specific extinguisher of cAMP-mediated gene expression (Boshart et al., 1991; Jones et al., 1991; Yin and Kirschner, 2009) and is linked to diseases such as systemic lupus erythematosus (Kammer, 2002; Kammer et al., 1996; Laxminarayana et al., 1999), Carney Complex disease (CNC), and breast cancer (Miller, 2002). Although most CNC mutations that escape nonsense-mediated mRNA decay (NMD), cluster around the cAMP binding site, we found three CNC mutations in the published literature that could be mapped to the interface of the homodimer structure including Arg^{144} to Ser, Ser^{145} to Gly as well as Ser^{145} to Asp (Horvath et al., 2010). While over 100 mutations of the RIα gene in humans have been identified, the majority are subject to NMD (Horvath et al., 2010; Kirschner et al., 2000). The CNC mutations located on the homodimer interface are residues that hydrogen bond to Tyr^{120} and Lys^{121}, mutations of which were analyzed structurally

and functionally in the previous section. Of great interest is also that these CNC mutations result in expressed altered protein and cause disease as a result of dysfunctional RIα. A publication by Green et al. in 2008 analyzed the Arg^{144} to Ser CNC mutation and found that it exhibited an increase in PKA-specific activation compared to wild-type (Greene et al., 2008). These data are consistent with the functional data for Tyr^{120} and Lys^{121} reported here.

To compare the affects of these CNC mutations with our study, we introduced the Carney Complex mutations Arg^{144} to Ser and Ser^{145} to Gly and Ser^{145} to Asp in the full-length RIα protein. While we saw changes in the SAXS scattering behavior and cAMP activation profile for Arg^{144} to Ser and Ser^{145} to Gly, the Ser^{145} to Asp mutation caused the protein to be insoluble during expression and we were thus unable to characterize this mutant. The Arg^{144} to Ser and Ser^{145} to Gly mutants also displayed an increase in sensitivity for cAMP in their activation of the corresponding holoenzymes (**Fig. 2.11B**), which is consistent with the analysis of their hydrogen bonding partners on the interface. Our previous structural knowledge could not explain the reason for the dysfunction of these RIα mutations, but this study can now link these Carney complex mutations to a specific structural feature. In addition, the Hill coefficient of the mutants is lowered to about 1.4, comparable to the Hill coefficient obtained for the heterodimer R:C complex (**Fig. 2.11B**).

A

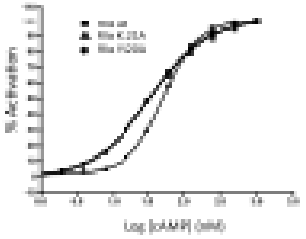

Holoenzyme	Hill Coefficient	EC_{50} (nM)
RIα wild type	1.73 ± 0.05	54.0 ± 0.5
RIα K121A	1.08 ± 0.07	34.0 ± 1.0
RIα Y120A	1.05 ± 0.04	35.0 ± 2.0

B

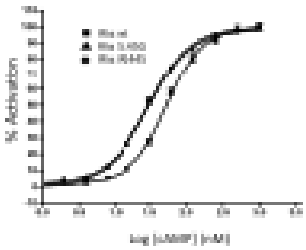

Holoenzyme	Hill Coefficient	EC_{50} (nM)
RIα wild type	1.79 ± 0.03	55.0 ± 1.0
RIα S145G	1.45 ± 0.02	30.0 ± 0.7
RIα R144S	1.49 ± 0.02	31.0 ± 0.7

Figure 2.11. cAMP-induced activation of holoenzymes. (**A**) Alanine mutations of interface residues were analyzed with a fluorescent polarization assay to monitor changes in the mutant compared to wild-type holoenzymes. Left: Activation profiles of holoenzymes formed with RIα wild type (squares), RIα K121A (triangles), RIα Y120A (circles). The curves for RIα K121A and Y120A are similar and lay on top of each other. Right: GraphPad Prism was used to fit binding curves and the standard error of the mean is shown with error bars. (**B**) CNC interface mutants were analyzed for their holoenzyme activation properties. Left: Activation profiles of holoenzymes formed with RIα wild type (squares), RIα S145G (triangles), RIα R144S (circles). The curves for RIα S145G and R144S are similar and lay on top of each other. Right: GraphPad Prism was used to fit binding curves and the standard error of the mean is shown with error bars.

2.4 Conclusion

The many previous structures of PKA served as a foundation for functional studies. Yet, the importance of integrating this structural information with PKA's biological functions has not subsided. On the contrary, the challenges have increased while attempting to solve the larger PKA macromolecular complexes. While the recently solved RIβ and RIIβ holoenzyme crystal structures represent a major milestone for PKA research, obtaining a regulatory subunit homodimer structure that lies at a lower level of complexity has been elusive (Ilouz et al., 2012; Zhang et al., 2012). We finally report here the structure of the PKA RIα homodimer and the discovery of a novel and functionally significant interface.

The compact homodimer structure of RIα is consistent with previous SAXS observations and the basis for this compact structure, a novel isoform-specific intermolecular interface, is revealed at the vertex of the two interacting monomers. This interface is conserved crystallographically, and is independent of the D/D domain as it is seen in many monomeric RIα structures, which further implies its significance. The interface is energetically favorable and interaction specific, and not a trivial artifact of crystal packing. Furthermore, we propose that the interface is isoform-specific and can account for the large differences in the solution structures of the type RI and RII homodimers observed by SAXS, where the RI homodimers are compact and the RII homodimers are extended (Vigil et al., 2004). Although the RII subunits contain longer linker regions, the large differences in the solution structures are most likely the result of interactions involving the R subunits' N3A-motif. Mutations on the

interface of RIα result in extended structures as analyzed by SAXS and now look more like the RII subunits in solution. Moreover, and in contrast to RI structures, monomeric deletion mutant structures of RIIα and RIIβ, that lack the D/D domain and the N-linker, do not have the N3A interface (Brown et al., 2009; Diller et al., 2001; Wu et al., 2007). The RIIβ holoenzyme likewise does not use this interface (Zhang et al., 2012). Thus the RII subunits do not utilize the N3A motif to create an interaction surface.

According to our results the D/D domain is structurally and spatially independent from the rest of the homodimer complex. Unfortunately, the flexibility of the linker segment apparently prevents the D/D domain from assuming a stable docked conformation in the crystal lattice, which results in the lack of electron density for this region. This may account in part for the low diffracting crystals. Yet, even at higher resolution, the RIIβ holoenzyme crystal structure published recently contains no electron density for the D/D domain nor the N-linker (Zhang et al., 2012). A requirement for the regulatory subunits to inhibit the catalytic subunits is that part of the linker and the inhibitor site (IS) must bind to and become immobilized within the active site cleft of the catalytic subunit (Kim et al., 2007; Kim et al., 2005). Thus, while limiting their crystallographic visualization, the flexibility of the linker region is intrinsic and necessary to allow the IS to search for the catalytic subunit to then become bound and finally form the holoenzyme complex.

While the N3A interface is the structural highlight in our dimer structure, it was not previously recognized as an integral or functional part of the RIα homodimer.

The D/D domain stably links the monomers at the N-terminus constraining the rest of the molecule into a close spatial proximity and thereby enhancing the dimer interface interaction. Yet, during crystallization, the interface is D/D domain-independent as it is also seen in the monomeric structures that lack the D/D domain sequence. In addition to its role as a docking site for A-Kinase Anchoring Proteins (AKAPs), the D/D domain functions as a covalently linked tether that increases the interaction of its CNB-A domains by increasing their effective concentration, independently of the local concentration of RIα. Furthermore, this allows the dimer interface to form and dissociate without compromising the global dynamics of the regulatory subunit, as would potentially be the case with a high affinity interaction. The D/D domain thus limits significant dissociation of the monomers and allows the regulatory subunit to sense its environment for binding partners such as the catalytic subunit and cAMP effectively.

Our dimer structure reveals a novel isoform-specific interaction site between the RIα monomers that allows the interpretation of previous cAMP binding studies. We show that there is long-range communication realized through the interface. Specifically, the interface limits access and dynamics of the CNB-A compared to CNB-B. An earlier study reported that when the cAMP-binding pocket of CNB-A is manipulated, solution structural changes are seen as reflected by the Stokes radius. Corresponding mutations in the CNB-B binding pocket on the other hand does not change the Stokes radius of RIα (Herberg et al., 1996). Thus, binding cAMP to the accessible CNB-B first is favorable over the more structurally constrained CNB-A and

results in a higher affinity site for CNB-B compared to CNB-A. Urea unfolding studies also support our structure in that the CNB-B unfolds first (Canaves et al., 2000; Leon et al., 2000). The CNB-A domain however, is much more stable and resistant to unfolding with urea. Contributing to this behavior could be that the CNB-A is positioned in the dimer such that it is protected and stably docked via the N3A interface. Finally, cooperative cAMP binding to the dimer is accomplished through the interface, where communication and sensing of the two monomers can be transmitted.

The realization that Carney Complex mutations are found on the dimer interface points to its functional importance for RIα. The *in vitro* studies presented in this work correlate well with previous analysis of CNC mutant proteins. It was shown that CNC mutant PKA is easier to activate and results in overactive catalytic subunits (Horvath et al., 2010). In CNC patients where haploinsufficiency of RIα is not the culprit, the increase in PKA activity is likely the result of disrupted C subunit inhibition by the mutant RIα. The holoenzyme activation of the CNC mutant proteins with interface residue changes shows this is due to a lower EC_{50} compared to wild type. These mutant holoenzymes display a lowered cooperativity with a Hill-Slope of 1.4. This is similar to the cooperativity seen with the heterodimeric holoenzyme, which is composed of just one RIα monomer and one catalytic subunit and suggests that disrupting the interface essentially uncouples the established communication between CBDs within the holoenzyme as well. A significant implication of our work is that cooperativity, while fine-tuning the response of PKA in the highly variable

cellular environment, is also a crucial component to PKA function that when disrupted can lead to disease.

In summary, this study reveals a novel and isoform-specific RIα homodimer interface that contributes to understanding RIα's *in vivo* function. With the knowledge gained from this structure it would be intriguing to test the Carney Complex interface mutants *in vivo* and explore if their cellular localization is affected. Support for a conformational equilibrium existing for PKA's R subunits is surfacing with recent studies utilizing NMR and MD analyzing the distribution of RIα in the H and B-forms (Akimoto et al., 2013). Accordingly, in the apo state RIα is toggling between and populating both the C subunit-bound and the cAMP-bound conformations. Addition of either binding partner pushes the equilibrium further to the corresponding conformation, suggesting that specific mutations could also alter the population of states within this equilibrium. While this study has filled a gap in the PKA structural library, the full RIα holoenzyme structure remains unsolved and is now a major target of our crystallographic efforts that will further aid in understanding the role the interface plays for PKA.

Chapter 2, in part, was published as PKA RI alpha homodimer structure reveals an intermolecular interface with implications for cooperative cAMP binding and Carney complex disease. Bruystens, J.G., Wu, J., Fortezzo, A., Kornev, A.P., Blumenthal, D.K., and Taylor, S.S. (2014). Structure *22*, 59-69. The dissertation author was the primary investigator and author of this work.

Chapter 3

Structural and Functional Characterization of the RI-specific smAKAP

3.1 Introduction

Many important cellular functions are regulated by signaling through parallel cAMP-dependent pathways (Mao et al., 2011). Amongst other targets, intracellular cAMP activates cAMP-dependent protein kinase (PKA). PKA contains a regulatory (R) subunit homodimer with the potential to bind one catalytic subunit (C) to each R monomer. Four genetically distinct R isoforms are expressed in mammalian systems, designated as RIα, RIβ, RIIα and RIIβ. Upon binding of cAMP to R, C is released and becomes active to subsequently phosphorylate Ser/Thr residues on protein substrates (Taylor et al., 2004). Due to PKA's importance and involvement in many parallel pathways, it needs additional levels of regulation in space and time. It achieves this through interaction with the protein scaffolding family of A-kinase anchoring proteins (AKAPs), which localize PKA, often together with many other signaling proteins (phosphatases, phosphodiesterases, other kinases, etc.) to a specific location in the cell (Scholten et al., 2008; Wong and Scott, 2004). At present, more than 30 mammalian AKAPs have been reported and experimentally verified (Scholten et al., 2008; Wong and Scott, 2004). Thus far, the majority of AKAPs identified bind preferentially to the PKA-RII isoforms and some are dual specific AKAPs, that can bind both RI and RII (dAKAP1(Huang et al., 1997b), dAKAP2(Huang et al., 1997a) and Opa1(Pidoux et al.)).

Initially, RIα was proposed to be mainly located in the cytosol and not anchored; however, recent chemical proteomics based studies discovered two novel AKAPs with exclusive specificity for RI: small membrane AKAP (smAKAP) was

(Burgers et al., 2012) and sphingosine kinase interacting protein (SKIP, SPHKAP)(Kovanich et al., 2010; Means et al., 2011). smAKAP has an unprecedented affinity for RIα (K_d = 6.7 nM) and RIβ (K_d = 6.9 nM) and localizes only these two isoforms to the plasma membrane using myristylation and palmitylation at Gly2 and Cys3, respectively. Its small size of only 11 kDa makes it the perfect model system to investigate the specific determinants of RI's interaction with its unique set of AKAPs.

Structural characterization showed that AKAPs bind to the N-terminal dimerization and docking (D/D) domain of the R dimer via their A-kinase binding (AKB) domain (Carr et al., 1991). This AKB-domain is an amphipathic helix of 3-4 turns long and its hydrophobic edge interacts with the hydrophobic face of the D/D domain. The drivers of R/AKAP specificity are only partially understood, although it is clear that both sides of the interaction have adopted specific structural determinants. The D/D domain structures of both RIα and RIIα demonstrated a tightly packed X-type bundle consisting of four helices (Banky et al., 2003; Newlon et al., 1999; Sarma et al., 2010). The monomers are positioned anti-parallel to one another and in the core there is a large hydrophobic surface to accommodate AKAP binding. The N-terminal helix (α0) shows isoform specific differences. Specifically, in RIα it contains cysteines, which lead to two identical inter-chain disulfide bridges between Cys16 and Cys37 (**Fig 3.1**). This connection reinforces the monomer-monomer interaction along the boundary and the anti-parallel alignment (Brennan et al., 2006). Also, the RIα D/D module presents a deeper cleft, allowing the presence of larger hydrophobic amino

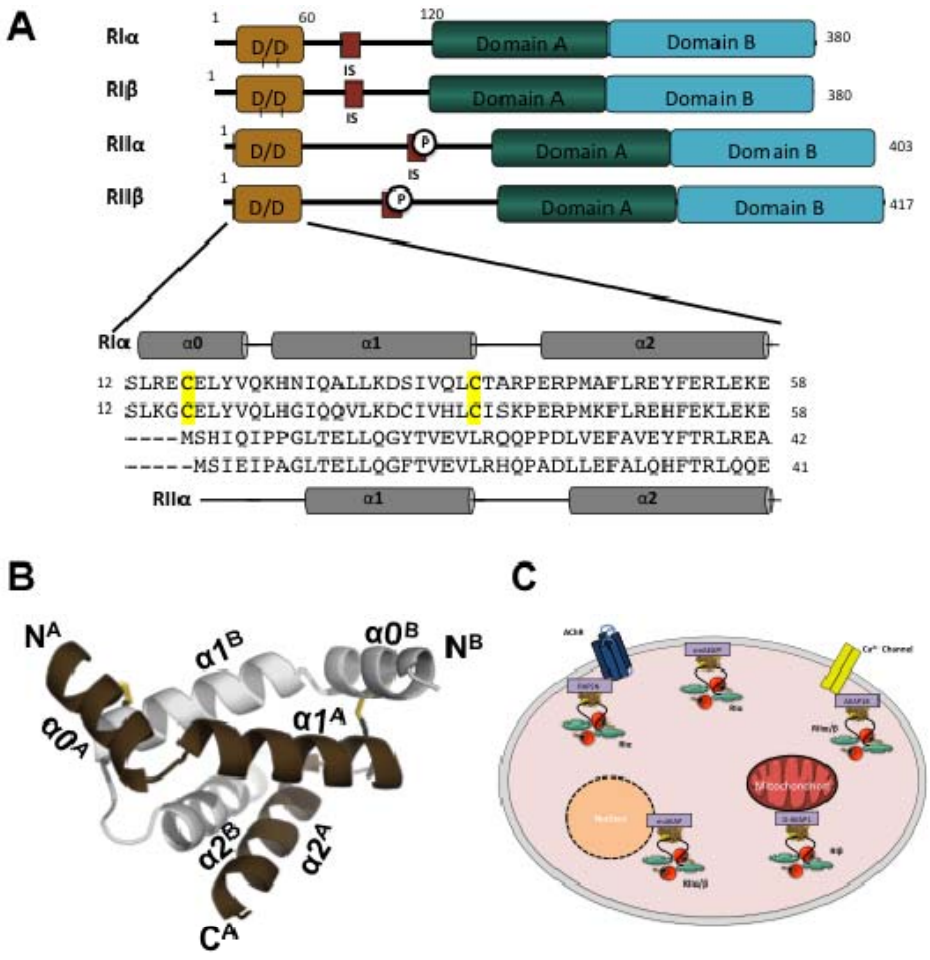

Figure 3.1. Overview of PKA R-subunit D/D domains. (**A**) Overall domain organization of the four R isoforms. The sequence alignment of the R-subunit isoforms D/D domains in the same order as the domain organization above. Cystines involved in disulfide-bonding are indicated in yellow. RIα's and RIIα'a secondary structure is shown with cylinders indicating α helices. (**B**) Structure of RIα D/D domain, pdb id 3IM3 (**C**) Model of AKAP's role for targeting PKA to subcellular sights.

acids in the AKB-domain(Banky et al., 2003). This was later confirmed by peptide screening (Burns-Hamuro et al., 2003; Carlson et al., 2006; Gold et al., 2006) and the presence of a phenylalanine residue in the AKB peptide of SPHKAP (Kovanich et al., 2010).

More recently, crystal structures revealing the interactions of RI and RII with the dual specific dAKAP2 (gene name AKAP10) provided a first glimpse into isoform specific interactions (Sarma et al., 2010) (Kinderman et al., 2006). First, the RII-dAKAP2 interaction is indeed characterized by a smaller interaction surface than the RI-dAKAP2 interaction. The former utilizes only two hydrophobic pockets of the AKB domain to interact, while in the latter, four hydrophobic contact sites were observed. The larger interaction surface is largely due to the above-mentioned disulfide bridges, which create a more stable domain at the end of the D/D helices (Banky et al., 2003). Since the RI-specific AKAPs have only recently been discovered (Burgers et al., 2012) (Kovanich et al., 2010), no detailed information on their structural determinants has been elucidated yet.

PKA is targeted close to its substrates at specific locations in the cell via AKAPs (**Fig. 3.1C**). PKA recognizes its substrates via a rather promiscuous phosphorylation motif: [R/K]-[R/K]-X-[S/T][noP](Neuberger et al., 2007; Tegge et al., 1995). PKA has been found to phosphorylate AKAPs, although only to a limited extent, suggesting that a regulatory mechanism controls AKAP complex composition, activity or perhaps localization. A few illustrative examples include PKA phosphorylation of AKAP-Lbc on Ser1565 to allow 14-3-3β/ε/ξ and binding at this

site to inhibit the Rho-GEF activity (Diviani et al., 2004). Similarly, AKAP79 has a number of PKA phosphorylation sites, which allow binding to phosphatidylinositol 4,5-bisphosphate (Dell'Acqua et al., 1998).

This chapter focuses on smAKAP and its putative PKA phosphorylation site within the AKB-domain. To investigate the structural basis for the tight binding to RI subunits we solved the crystal structure of the RIαD/D:smAKAP-AKB complex. This not only provided novel insights into what makes smAKAP specific towards PKA-RIα/β, but also led us to define the role of smAKAP phosphorylation in the AKB domain.

3.2 Experimental Procedures

Protein purification - Bovine full-length RIα (Wu et al., 2004b) (P00514) and RIα D/D (AA 12-61) (Sarma et al., 2010) were purified as previously described. His-smAKAP (and mutant) were expressed in *E. coli* (BL21 (DE3)) (Sarma et al., 2010). At OD_{600} the cell culture was induced with isopropyl β-D-thiogalactopyranoside and grown for another 6 h at 37 °C prior to harvesting at 6000 rpm. The cells were resuspended in lysis buffer (50 mM KH_2PO_4, 300 mM NaCl, 10 mM imidazole, 5% glycerol, 5 mM β-mercaptoethanol, pH 8.0) after which they were lysed using a Microfluidizer (Microfluidics, USA) at 18,000 p.s.i. The cells were then spun down for 75 min at 4 °C in a Beckman JA20 rotor. The supernatant was then run on a Profinia (Bio-Rad, USA) according to the native IMAC protocol. The eluent was dialysed in 20 mM tris, 100 mM NaCl, 5 mM DTT, pH 8.3). The resulting protein was

purified on an S75 column and concentrated to 30 mg/mL. The smAKAP-AKB peptide was dissolved into 0.5 M tris at pH 8.5 to a concentration of 5 mg/mL. The complex formed, consisting of RIαD/D and smAKAP-AKB peptide, had a final concentration of, respectively, 10 mg/mL and 2.52 mg/mL, and was used for crystallization.

Crystallography - Crystals of RIαD/D:smAKAP-AKB complex appeared approximately 2 months after being set with an Oryx8 protein crystallization robot at room temperature at a 2:3 ratio of protein solution:crystallizing in a sitting drop set-up (crystallizing solution: 0.1 M Citric acid pH 3.5, 28% w/v Polyethylene glycol 8,000). Data of the rod shaped crystals were collected on the synchrotron beamline 8.2.2 of the Advanced Light Source, Lawrence Berkeley National Labs (**Fig. 3.1**) (Berkeley, CA). The data were processed and scaled via HKL2000 (Otwinowski and Minor, 1997). For phasing the RIα D/D:dAKAP2-AKB structure (3IM4) was used for molecular replacement in CCP4 using Phaser (Krissinel and Henrick, 2007); (Sarma et al., 2010). This model was further refined using COOT and Refmac 5.2 (Emsley and Cowtan, 2004); (Murshudov et al., 1997). The refinement statistics are shown in Table 3.1.

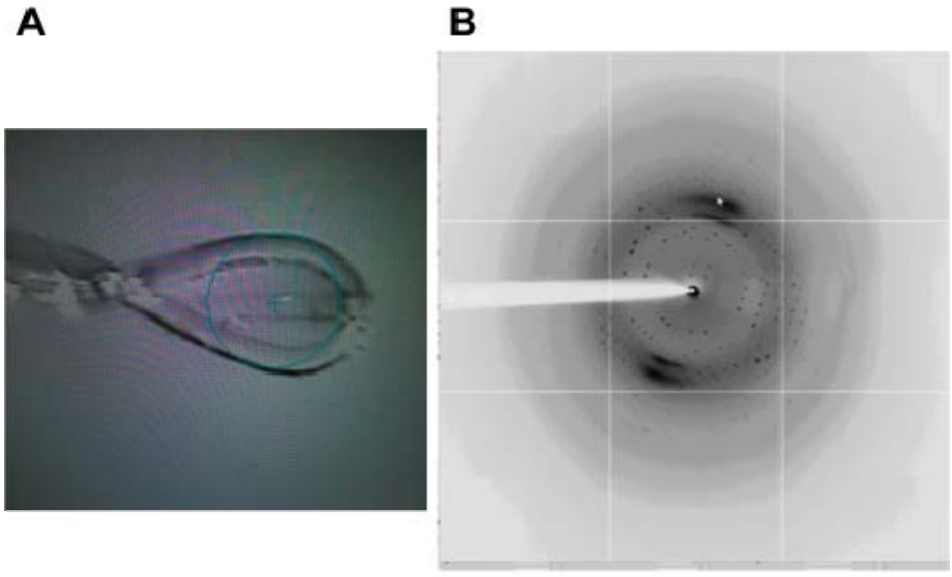

Figure 3.2. smAKAP crystallization and data collection. (**A**) Rod shaped crystals were harvested soaked in cryoprotectant, and flash frozen in liquid nitrogen. (**B**) Diffraction image collection was carried out remotely at the synchrotron beamline 8.2.2 of the Advanced Light Source, Lawrence Berkeley National Labs.

Table 3.1 Collection and refinement statistics of smAKAP:RIα.

	PKA-RIαD/D:smAKAP-AKB
Data collection	
Space group	$P2_12_12_1$
Cell dimensions (Å)	
a	37.5
b	55.7
c	57.3
No. of molecule per asymmetrical unit	1
Resolution (Å)	2.0
R_{merge} (%)	7.6 (46)
Completeness (%)	98.0 (100.0)
I/sigma	26.9 (4.0)
No. reflections	8480
Refinement	
Resolution (Å)	40.0-2.0
R_{work} / R_{free} (%)	21.0/24.1
R.m.s. deviations	
Bond lengths (Å)	0.024
Bond angles (°)	1.9
Ramachandran angles (%)	
most favored	90.9
disallowed	none

*Values in parentheses are for the highest-resolution shell: (2.00-2.05 Å)

Structure analysis - The final crystallography model was evaluated using MolProbity (Chen et al., 2010). Hydrogen-deuterium exchange mass spectrometry (HDX-MS): A 30-fold dilution with either 100% H_2O, pH 7 for the non-deuterated experiments or deuterium oxide (Sigma Aldrich, Germany), pH 7, for deuterated experiments was carried out for the following complexes: unbound smAKAP (60 pmol), smAKAP-excess RIα (60 pmol of smAKAP and 75 pmol of RIα), unbound RIα (60 pmol) and RIα-excess smAKAP (60 pmol of PKA-RIα and 75 pmol of smAKAP). Diluted samples were incubated at room temperature for time intervals of 0 min for the non-deuterated experiments and 10 sec, 1 min, 10 min, 60 min and 240 min for the deuterated experiments. The deuteration reaction was quenched by pH reduction to 2.5 with a 1:1 dilution using ice cold 4 M guanidine hydrochloride adjusted to pH 1.85. Quenched samples were immediately injected into a 50 µL injection loop on a nano-ACQUITY UPLC system with HDX technology (Waters, USA). Online digestion was performed using an in-house built immobilised pepsin column for 2 min in 0.05% formic acid in H_2O, (flow rate of 25 µL/min), held at a temperature of 15°C. Peptides were trapped and desalted online using an ACQUITY UPLC BEH C18 1.7 µm VanGuard Pre-column (Waters, USA) at 0°C, with subsequent elution onto an ACQUITY UPLC BEH C18 1.7 µm, 1 mm x 100 mm column (Waters) held at 0°C. Peptide separation was achieved using a 7 min linear acetonitrile gradient (5%-85%) in 0.1% formic acid (flow rate of 40 µL/min). The eluent was directed into a Xevo G2 instrument (Waters, USA) with electrospray ionisation and lock-mass correction (using Glu-fibrinogen peptide). Mass spectra were

acquired in MS^E mode over the *m/z* range 50-2000. Two blank injections were performed between each sample injection to prevent sample carry over. Peptides were identified prior to deuteration using ProteinLynx Global Server 2.5 software (Waters, USA).

Phosphorylation analyses - Human His-tagged smAKAP (*wt* and S66D) (10 μM) (Burgers et al., 2012)was taken up in a reaction buffer containing $MgCl_2$ (10 mM), ATP (200 μM), [^{32}P]ATP (500-1000cmp ρmol-1) and MOPS (50mM) (pH 7.5). Addition of recombinant Cα (20 nM)(Zheng et al., 1993) and/or PKG Iα (20 nM)(Alverdi et al., 2008). 10 μl of reaction volume was quenched with 90 μl of 30% acetic acid at the following time points: 0, 5, 10 and 15 min. The phosphorylation assays were also analyzed by LC-MS/MS to identify the exact phosphorylation site. An in-solution digestion of His-smAKAP using trypsin was performed as described previously (Aye et al., 2010). The sample was desalted with an HBL Oasis system (Waters, USA). The desalted sample was dried down and reconstituted in 10% formic acid. A vented-column setup was used for analyzing protein digests through an Agilent 1200-Series LC system coupled to an LTQ-Orbitrap XL mass spectrometer (Thermo Fisher Scientific, Germany) with conditions as described elsewhere (Meiring et al., 2002; Zoumaro-Djayoon et al., 2012).

Additionally, AKAP1-RRRAAFQIISQVISEATEQ, AKAP4-RRFYVNRLSSL VIQMAHKE, AKAP5-RRLIETASSLVKNAIQLSI, AKAP9-RRKVAAALVSQIQLE AVQE, AKAP10-RRELAWKIAKMIVSDVMQQ, AKAP18-RRAELVRLSKRLVEN

AVLK, and smAKAP-RRILEYAHRLSQDILCDAL, AKAP's AKB domains were synthesized (NKI, Netherlands) including a double arginine label at the N-terminus for efficient capture on phosphocellulose. These were incubated with six kinases according to protocol: PKB (NEB, USA), CKB1 (NEB, USA), MEK1 (SignalChem, Canada), MEK2 (SignalChem, Canada), Cα (Zheng et al., 1993) and PKG 1α (Alverdi et al., 2008). The reactions were spotted onto a phosphocellulose filter disk (Sigma-Aldrich, Netherlands). After four washes with 0.5% phosphoric acid the filter disks were rinsed with acetone, dried, and then analyzed on the ^{32}P channel in liquid scintillant.

Cell culture - HeLa and HEK293 cells were cultured and transfected with the plasmids (smAKAP-*wt*-GFP, PKA-RIα-mKO2, PKA-RIα-mKO2, PKA-C-HA and smAKAP-S66E-mGFP) as described previously (Burgers et al., 2012).

Fluorescence imaging - Cells were washed once with ice-cold PBS, fixed in 4% ice-cold formaldehyde in PBS and afterwards washed twice with PBS. Upon addition of Calyculin A and 8-CPT-cAMP live imaging was employed. The confocal images were obtained with a Zeiss LSM700 confocal system with a 63x oil objective lens.

Mutagenesis - The single site mutations (S66D and S66E) were introduced in the previously described smAKAP-GFP plasmid (Burgers et al., 2012) and pLICHIS

His_6-smAKAP plasmid via the QuikChange mutagenesis kit (Agilent Technologies, USA).

Circular Dichroism and Fluorescence Anisotropy - Four peptides: 1. IVILEYAHRL**S**QDILCDALQQWAC, 2. IVILEYAHRL**pS**QDILCDALQQWAC, 3. IVILEYAHRL**D**QDILCDALQQWAC and 4. IVIL**E**YAHRLEQDILCDALQQWAC (mutations in bold) were synthesized and purified (NKI, Netherlands). These were dissolved in a 0.1M Tris buffer at pH 8.5. CD measurements were carried out on a Jasco J-810 spectropolarimeter and analysed via the Jasco Spectra Manager. For fluorescence anisotropy measurements on the interaction between RIα and smAKAP, peptides 1 and 2 were N-terminally tagged with 5-TAMRA as described previously (Burgers et al., 2012). Measurements were also performed as described previously (Burgers et al., 2012).

Molecular dynamics - Molecular dynamics was performed with the program YASARA version 8.12.26 in an AMBER03 force field (Krieger et al., 2004). The simulations were run as described previously (Krieger et al., 2004; van Hell et al., 2010) with the exception of the following. In an aqueous continuous phase the smAKAP-AKB peptide from structure solved in this article was placed in a 50 Å x 50 Å x 50 Å box. Simulations were run for 25 ns, and coordinates were saved every 7.5 ps. The results were then analyzed using analysis programs written in our laboratory. The AKB-Phospho peptide was constructed using the FoldX package.

3.3 Results

Structure of the RIα-smAKAP complex - To understand the selectivity of smAKAP towards RI, we set out to determine the crystal structure of the complex consisting of the D/D-domain of RIα and the AKB-domain of smAKAP. As expected, the structure has an overall similar binding-mode to previously reported R D/D:AKB structures with the smAKAP's amphipathic α helix docking onto the RIα D/D helices (**Fig. 3.3A)** (Banky et al., 2003; Gold et al., 2006; Kinderman et al., 2006; Newlon et al., 2001; Sarma et al., 2010). The complex crystallized with one RIα-D/D helix-bundle containing two protomer chains (the monomer whose N-terminus is next to the N-terminus of smAKAP is named 'A' (AA12-58) whereas the other monomer is named 'B' (AA12-61)) bound to one smAKAP AKB-domain (AA 56-79), which is named 'C'. The majority of residues in the smAKAP peptide had clear electron density, however, $Trp77^{C}$ and $Cys79^{C}$ did not, therefore the sidechains of $Trp77^{C}$ and $Cys79^{C}$ have been omitted from the model. Similarly, most of the residues of both RIα D/D monomers are accounted for, except $Ser12^{B}$, $Leu13^{B}$, $Lys57^{A}$ and $Gly58^{A}$, of which the side chains have been omitted, and $Glu59^{A}$, $Ala60^{A}$ and $Lys61^{A}$ which have been omitted entirely.

The structure of the RIαD/D dimer helix-bundle consists of four anti-parallel helices. The smAKAP-AKB peptide lies diagonally across the hydrophobic interaction surface of the RIαD/D domain (**Fig. 3.3B**). The root mean square deviation (RMSD) between the PKA-RIαD/D of the dAKAP2 (Sarma et al., 2010) structure and the smAKAP complex presented here is 0.39 Å (Cα carbons), indicating that binding of

AKB peptides with different PKA-R specificity has little influence on the conformation of RI. The RMSD between the AKB domains is larger, 0.58 Å (Cα carbons), as expected due to the presence of several differences between the AKB domains of dual-specific and PKA-RI specific AKAPs.

There are four binding pockets in the D/D domain, each allowing two hydrophobic residues of the amphipathic helix to dock (**Fig. 3.3A**). The smAKAP-AKB domain has the hydrophobic amino acids fitting snugly in each binding pocket. What makes the smAKAP interaction different is that at each end of the domain there are additional hydrophobic interactions assisting in anchoring to the RIα D/D domain by burying the disulfide bonds into hydrophobic pockets. This creates a possible fifth and sixth pocket. In the fifth pocket, the disulfide bridge between $Cys16^{A}$ and $Cys36^{B}$ is surrounded by $Ile33^{B}$ and $Val34^{B}$ of helix αI, $Leu13^{A}$ of helix α0 and $Ile58^{C}$ and $Tyr61^{C}$ (of the amphipathic helix), creating an enhanced hydrophobic pocket (**Fig. 3.4A**). This creates a possible fifth and sixth pocket.

In the fifth pocket, the disulfide bridge between $Cys16^{A}$ and $Cys36^{B}$ is surrounded by $Ile33^{B}$ and $Val34^{B}$ of helix αI, $Leu13^{A}$ of helix α0 and $Ile58^{C}$ and $Tyr61^{C}$ (of the amphipathic helix), creating an enhanced hydrophobic pocket (**Fig. 3.4A**). In addition, there are hydrogen bonds between side-chains of both proteins, $Gln76^{C}$ and $Lys30^{A}$ in helix α1 and $Asp72^{C}$ and $Gln26^{A}$ in helix α1, which also help to stabilize the interaction due to many polar residues of RIα protruding from the edges of the interaction surface. All these factors lead to a very strong and specific interaction of smAKAP with RIα.

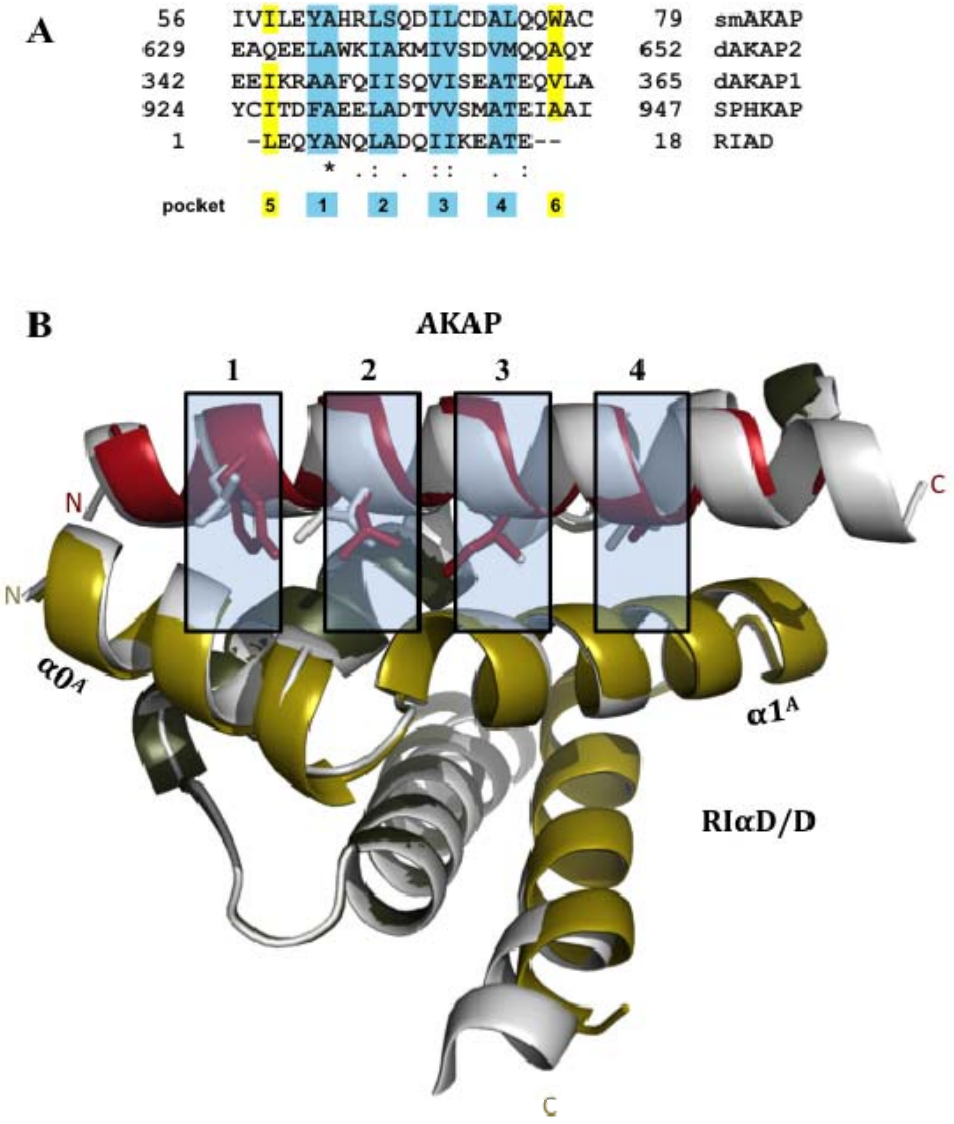

Figure 3.3. Crystal structure of the smAKAP-AKB/PKA-RIαD/D complex. (**A**) A sequence alignment of four AKAPs whose AKB domains each bind to PKA-RI with the established four binding pockets highlighted in blue. **(B)** A side view displaying the interaction surface between smAKAP-AKB (red) and PKA-RIαD/D (gold (A)/green (B)) with an overlay of dAKAP2:PKARIαD/D (silver).

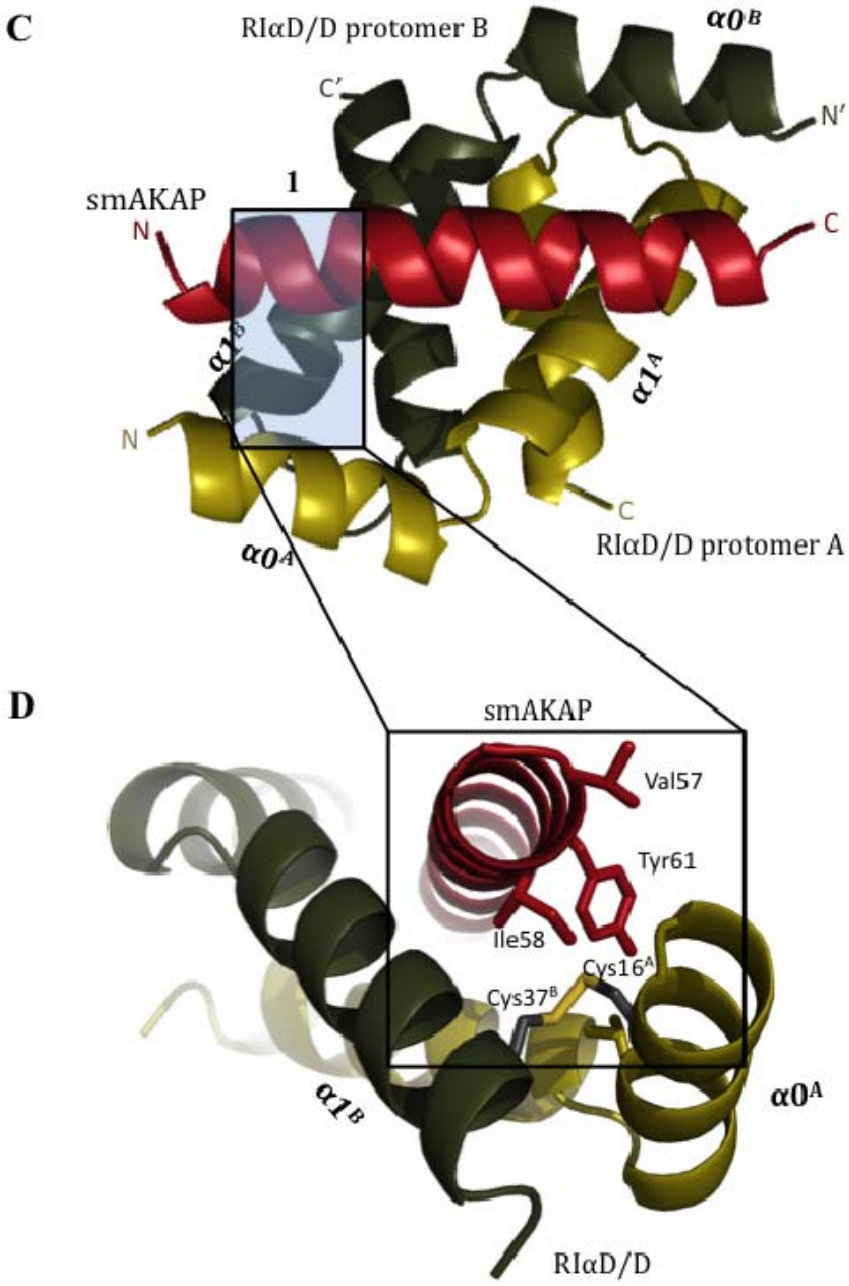

Figure 3.4. Crystal structure of the smAKAP-AKB/PKA-RIαD/D complex. (C) A top view of smAKAP overlaying PKA-RIαD/D. **(D)** The N-terminus of the AKB domain (red) establishes the fifth pocket. $Tyr61^{C}$ and $Ile58^{C}$ (highlighted in yellow in the sequence alignment of a)bury the disulfide bond $Cys16^{A}$-$Cys37^{B}$ into a hydrophobic pocket. $Leu13^{A}$ of α0-helix (gold) and $Ile33^{B}$ of α1-helix (green) also close up the hydrophobic pocket.

This is further illustrated by the conservation of Ile58^{C} throughout species and in SPHKAP (Kovanich et al., 2010) (Ile926), RIAD(Carlson et al., 2006) (Leu1) and dAKAP1(Huang et al., 1997a) (Ile344) but not in dAKAP2(Huang et al., 1997a) (Gln631) (**Fig. 3.3A**). Tyr61^{C} is also conserved in RIAD, whereas in SPHKAP another bulky hydrophobic amino acid resides at this site (Phe929). The bulky amino acid at this position has been proposed earlier as a PKA-RI specifier, as it would only fit in the deeper groove of the PKA-RI D/D domains (Burns-Hamuro et al., 2003; Sarma et al., 2010). It is likely that at the other end of the AKB domain, where the second disulfide bridge resides (Cys16^{B} and Cys36^{A}), a putative sixth pocket is formed in a similar way with Leu74^{C} and Trp77^{C}. Although the side chain of Trp77^{C} is not well resolved in the structure one could assume a function similar to the Ile58^{C} and Tyr61^{C} couple at the other end of the helix due to the internal symmetry present. However, the putative sixth pocket is much less defined and neither Leu74^{C} nor Trp77^{C} seem conserved in the other RI specific AKB domains of SPHKAP and RIAD (**Fig. 3.1A**)(Carlson et al., 2006; Kovanich et al., 2010).

The AKB-domain of smAKAP is phosphorylated by PKA - BLAST analysis and sequence alignment of smAKAP and its homologues revealed several well conserved serines and threonines (Burgers et al., 2012). One of them, Ser66, lies in the middle of the AKB domain and displays the phosphorylation motif H-R-L-S (**Fig. 3.5A**), a PKA substrate site proposed from peptide screens (Hennrich et al., 2013; Tegge et al., 1995). This PKA motif in smAKAP is conserved from zebrafish to

human with the positively charged residue (arginine or histidine) occupying either the -2 or -3 positions with respect to the serine (**Fig. 3.5A**). Even though serine to alanine mutations are very common in evolution, Ser66 in smAKAP remains stable across species. Interestingly, Ser66 seems to reside on the hydrophobic side of the amphipathic AKB domain helix (**Fig. 3.5B**), which could possibly induce steric and electrostatic hindrance for the hydrophobic based binding of smAKAP with PKA-RI.

An *in vitro* phosphorylation assay with purified His_6-smAKAP and the kinases PKA (catalytic subunit) and its closest homologue PKG Iα revealed that PKA phosphorylated smAKAP whereas PKG Iα did only marginally (**Fig. 3.5C**). Phosphorylation of smAKAP-*wt* had a V_{max} of 1.068±0.081 μM/sec and a K_m of 11.91±2.42 μM. The filter binding assay was repeated with Ser66 mutated to an aspartic acid (smAKAP-S66D), which showed no detectable levels of phosphorylation (**Fig. 3.5D**). To confirm further that Ser66 is indeed the substrate site of PKA, a digest of *in vitro* phosphorylated smAKAP was analyzed by LC-MS/MS analysis. The tandem MS-spectrum of the only observed phosphopeptide L**pS**QDILCDALQQWACNNIK (Mascot score 89) unambiguously identified Ser 66 as the phosphorylation target site of PKA (**Fig. 3.5E**).

Serine66 phosphorylation effectively abrogates binding of PKA-RI - We showed previously using a fluorescence polarization assay that smAKAP has a strong affinity ($K_d \approx 7$ nM) for PKA-RIα and RIβ (Burgers et al., 2012). Fluorescence

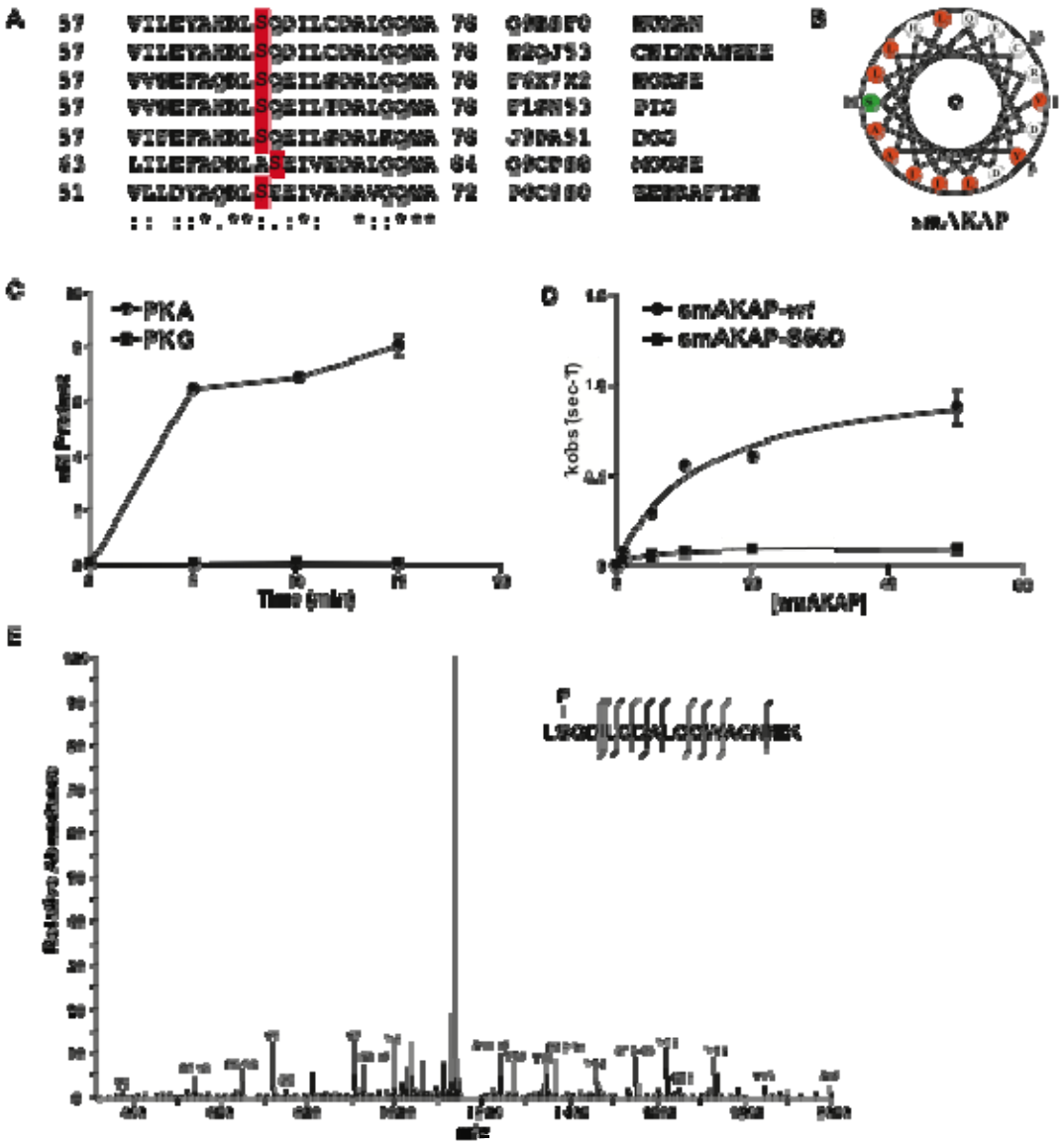

Figure 3.5. PKA phosphorylation of smAKAP at Ser66. (A) Sequence alignment of human smAKAP (AA 57-78) with various orthologues in other vertebrate species. Identity (*), similarity (:) and the serines highlighted in red. **(B)** Helical wheel alignment of the smAKAP's AKB domain reveals Ser66 (green) is on the hydrophobic surface (orange) of the amphipathic helix. **(C)** ^{32}P phosphorylation assay using PKA-Cα and PKG Iα as kinase and recombinant His$_6$-smAKAP as substrate. **(D)** ^{32}P phosphorylation assay using PKA-Cα on recombinant smAKAP-*wt* and smAKAP-S66D. **(E)** Annotated MS/MS spectrum of the peptide LpSQDILCDALQQWACNNIK with a phosphorylated serine at position 2, corresponding to Ser66 in smAKAP.

anisotropy measurements to determine the binding affinity (n=3, K_d ± standard deviation in nM) of the phosphorylated smAKAP AKB-domain peptide, tagged with 5-TAMRA (excitation at 535 nm and emission at 580 nm) with the full length regulatory subunit dimers: PKA-RIα and PKA-RIβ. The smAKAP *wt*, dAKAP2 and AKAP79 results were previously published(Burgers et al., 2012).

Executing this assay with the AKB peptide carrying a phosphorylated serine (IVILEYAHRL**pS**QDILCDALQQWAC), we noted a dramatic decrease in the binding affinity (K_d > 500 nM (**Table 3.2**)). HeLa cells transfected with smAKAP-*wt*-GFP and PKA-RIα-mCherry (Burgers et al., 2012) or PKA-RIβ-mKO2 (**Fig. 3.6A**), show strong co-localization along the plasma membrane. In order to deduce the impact of phosphorylated smAKAP in the cellular context, phosphomimetic mutants were created: smAKAP-S66E-GFP and smAKAP-S66D-GFP. Notably, when the HeLa cells were transfected with these mutants along with PKA-RIβ-mKO2 or PKA-RIα-mKO2 (**Fig. 3.6B**) smAKAP still localized at the plasma membrane, while both PKA-RI isoforms now predominantly resided in the cytoplasm, evidence that phosphorylation of Ser66 inhibits RI binding to smAKAP.

Table 3.2 Binding of the phophorylated smAKAP to RIα and RIβ.

	smAKAP *wt* (nM)	**smAKAP-P (nM)**	**dAKAP2 (nM)**	**AKAP79 (nM)**
RIα	6.7±0.7	>1000	50	nd
RIβ	6.9±0.6	>1000	-	nd

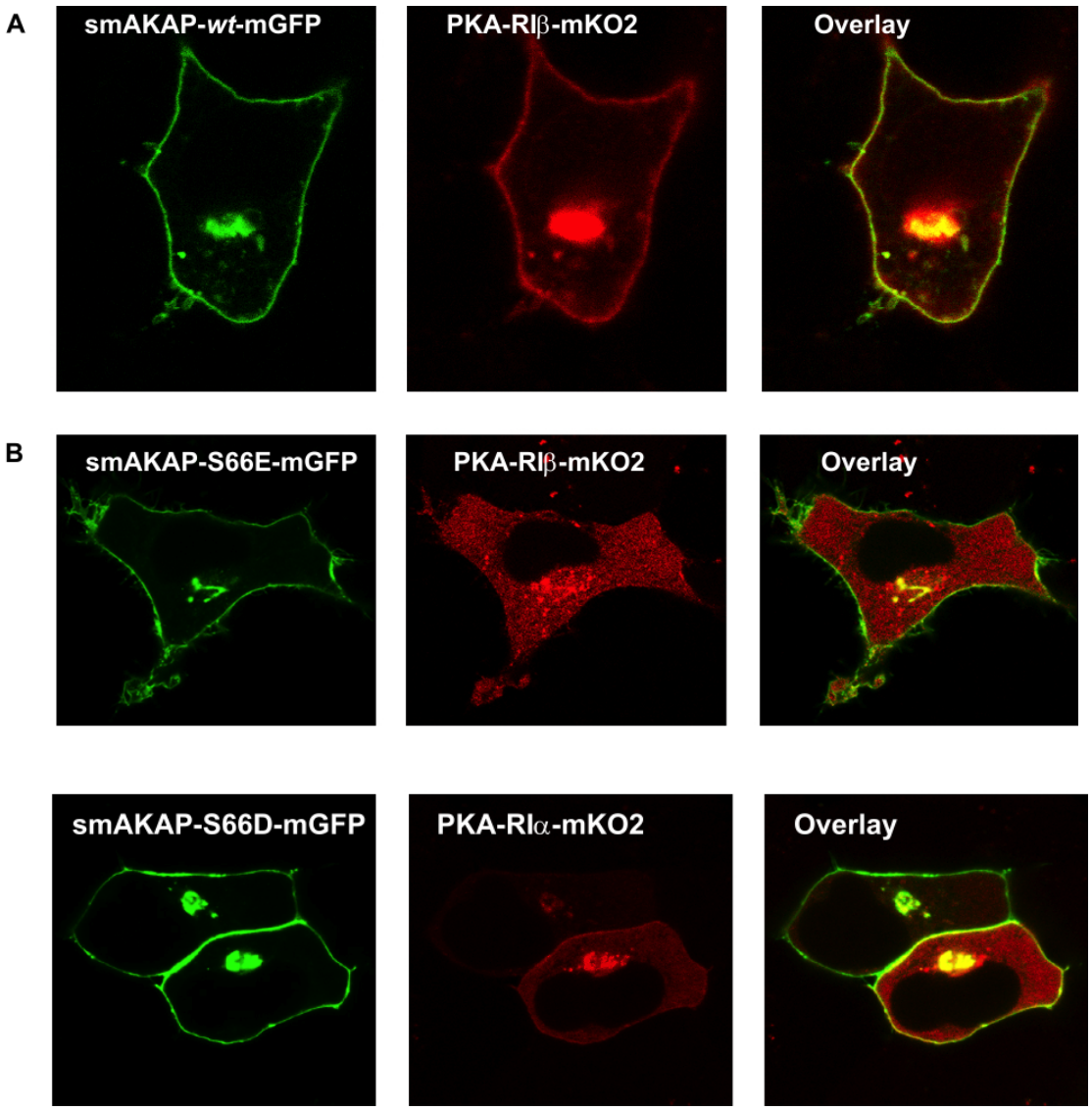

Figure 3.6. Phosphorylated smAKAP no longer localizes PKA-RI at the plasma membrane. (A) Transfection of HeLa cells with smAKAP-*wt*-mGFP and PKA-RIβ-mKO2 show co-localization at the plasma membrane. **(B)** In contrast, in the HeLa cells transfected with the phosphomimetic smAKAP-S66E-mGFP, PKA-RIβ-mKO2 (top row), PKA-RIβ-mKO2 (bottom row) less co-localization occurs.

Hydrogen deuterium exchange mass spectrometry - The fluorescence anisotropy binding affinity measurements suggests that smAKAP binds with low nanomolar affinity to RIα whereas the imaging data suggests that the helix is accessible for phosphorylation. To look at the native structural interaction dynamics between both proteins on a time-scale we used hydrogen/deuterium exchange (HDX) mass spectrometry with the full-length proteins. First, smAKAP, in the presence and absence of an excess of RIα, was incubated in deuterium oxide for various time points between 10 seconds and 4 hours. The reverse experiments, using an excess of smAKAP, were also conducted. For RIα with excess smAKAP, as expected, we observed a distinct difference in deuterium incorporation in different regions. For instance, peptide AA248-255 of RIα displayed no difference in deuterium uptake (**Fig. 3.7A**), whereas peptides in the N-terminal region such as AA19-37 revealed a substantial reduction in deuterium uptake (**Fig. 3.7B**).

Although we were able to cover large parts of the RIα sequence (77%), no other region displayed uptake differences. Similarly, focusing on smAKAP, we observed that only the peptides covering the region AA61-78, which is the AKB-domain, displayed a substantial decrease in deuterium uptake, whereas all other peptides, covering nearly the whole sequence of smAKAP (96%) displayed no substantial difference in deuterium uptake between presence and absence of RI (**Fig. 3.7 C, D**). In regards to the kinetics of deuterium uptake, in the protected regions we see RIα behaves very different than smAKAP. **Figure 3.7B** illustrates that the uptake of deuterium in the D/D domain of RIα is very slow with only detectible levels of

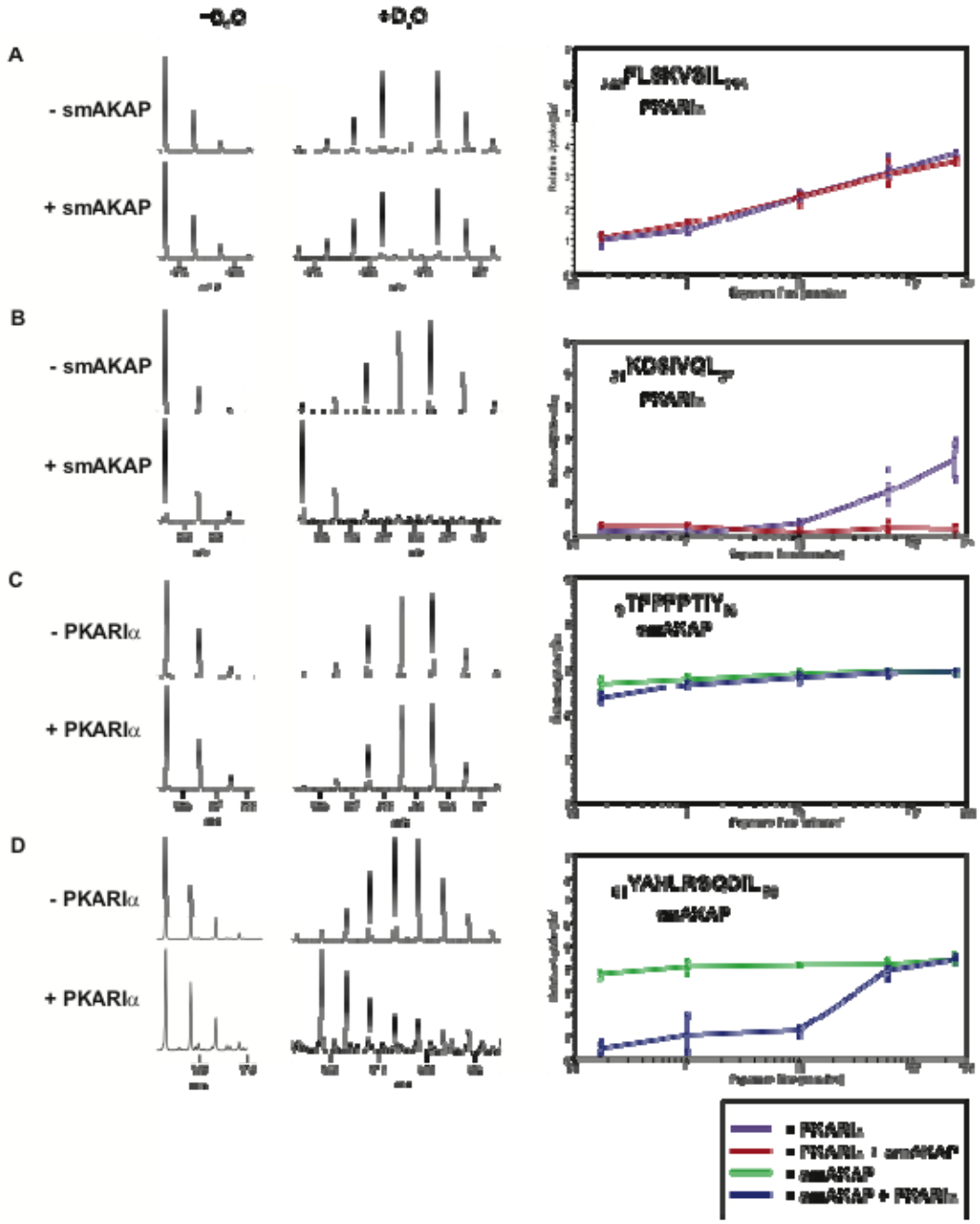

Figure 3.7. H/D exchange profiling of the interaction surface of full length smAKAP and PKA-RIα. (A) No difference in deuterium uptake was observed between PKARIα (purple) and PKARIα+smAKAP (red) for AA248-255 **(B)** whereas for AA31-37 there was an increasing difference in deuterium uptake starting after 10 minutes. **(C)** For AA9-16 of smAKAP there was no difference in deuterium incorporation between smAKAP (green) and smAKAP+PKARIα (blue) **(D)** whereas a large initial difference in uptake was noted for AA61-70.

incorporation after 60 min, indicating the hydrophobic groove is very protected in the absence of excess smAKAP. In contrast, kinetics on smAKAP are very fast (**Fig. 3.7D**). In the presence of excess RIα, smAKAP is initially withheld from incorporating deuterium, but already after one minute the incorporation is initiated and rises steep to reach full incorporation after 60 minutes. This suggests that smAKAP is able to dislodge from RIα, making its Ser66 residue available for phosphorylation by a nearby PKA C-subunit.

Initially, we hypothesized that electronegativity and steric clashing could inhibit binding of the phosphorylated AKB domain peptide (AKB-Phospho) to the hydrophobic RIα D/D. However, molecular modeling suggested that the phosphorylated wild type and the phosphomimetic mutants could bind at least as well to the D/D domain of PKA-RIα as the non-phosphorylated equivalent. These data indicated that a phosphorylated Ser66 can still fit within the hydrophobic groove and is able to extend its side-chain with the electronegative moiety out of the hydrophobic groove and create hydrogen bond interactions with $Lys30^{B}$ and $Gln26^{B}$ of PKA-RIα (**Fig. 3.8**). However, experimentally we observed disruption of binding upon phosphorylation, prompting us to investigate other putative modes of binding disruption.

Molecular mechanism of binding disruption - In molecular dynamic (MD) simulations on the AKB helices of AKB-*wt*, AKB-S66D, AKB-S66E and AKB-

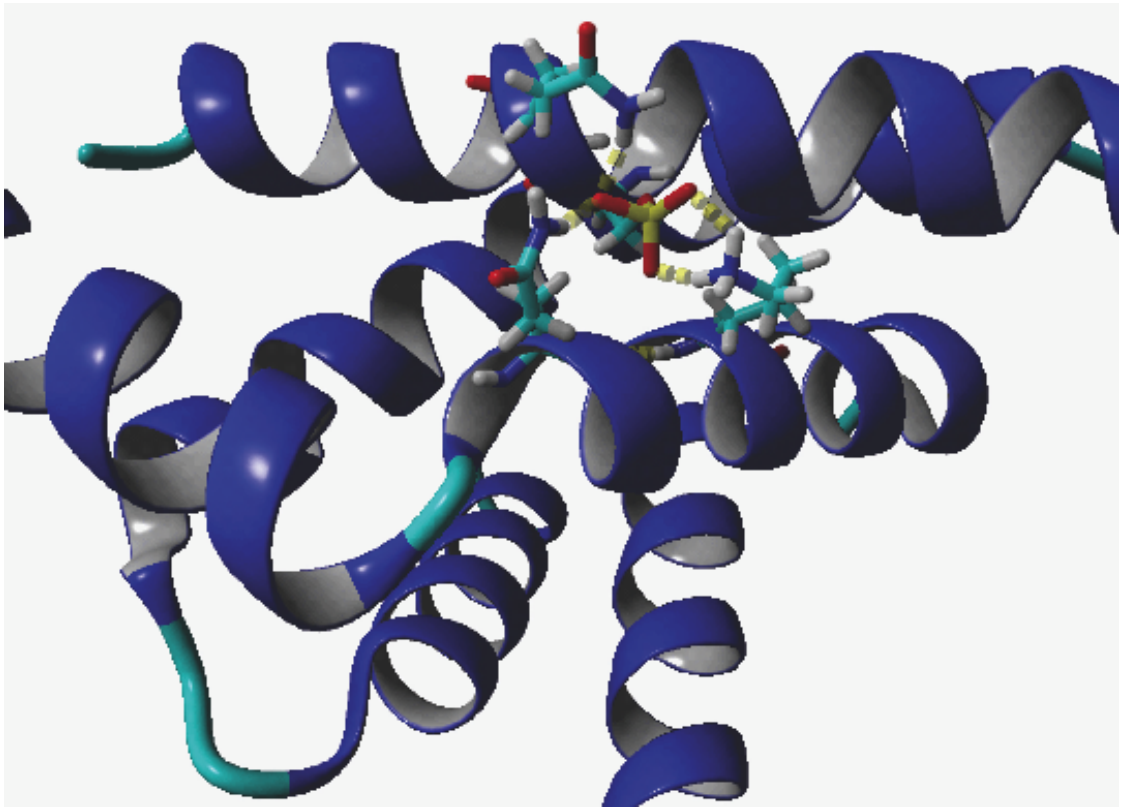

Figure 3.8. Model of smAKAP-AKB-Phospho:RIαD/D. Utilizing HADDOCK we modeled the smAKAP-AKB-Phospho:RIαD/D complex. Unexpectedly, this resulted in a much stronger interaction. As shown there is a larger interaction surface due to the phosphoserine sticking out of the hydrophobic domain which in turn allows hydrogen bonding with Gln26 and Lys 30 of RIα and Gln67 of smAKAP.

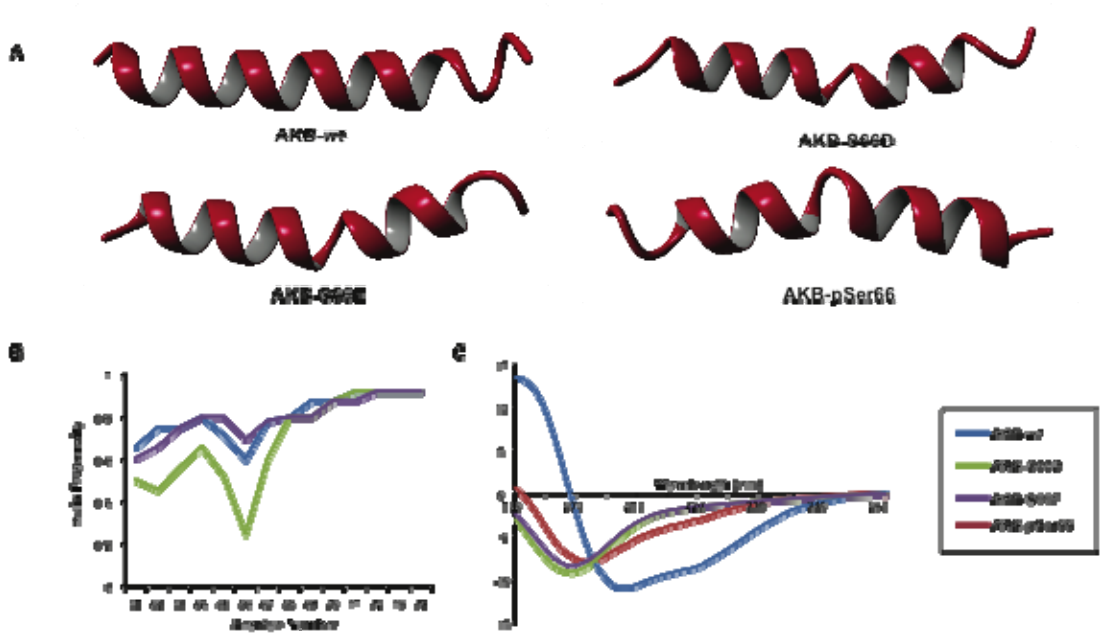

Figure 3.9. Loss of helical structure due to Ser66 phosphorylation. (A) 20 ns molecular dynamics simulations were run of the AKB-*wt* peptide in water. The peptide started to lose its helix from the N and C termini. In contrast, the AKB-S66D, AKB-S66E and AKB-pSer66 peptides already lost their secondary structure in the middle near the serine after 1ns. **(B)** Helix propensity prediction of AKB-*wt*, AKB-S66D and AKB-S66E were measured via NetSurfP 1.1. Upon the mutation of serine to aspartic acid there is a severe drop in helix propensity. NetSurfP 1.1 is unable to use phosphorylated serines. **(C)** CD measurements revealed a helix propensity of ~45% for the AKB-*wt* peptide. The AKB-S66D, AKB-S66E and AKB-pSer66 peptides showed no secondary structure.

pSer66, all peptides partially or even fully lost their secondary structure in 20 ns simulations. The AKB-*wt* helix started to lose its helicity relatively slowly at both termini of the peptide after ~1 ns. In contrast, the other three peptides quickly lost helicity next to the mutated serine after ~1 ns (**Fig. 3.9A**). This suggests that the phosphorylation causes a severe distortion in the helix, which could possibly lead to the entire amphipathic helix being lost. Using NetSurfP 1.1 (Petersen et al., 2009), the helical propensity was determined of the AKB-*wt*, AKB-S66D and AKB-S66E peptides (**Fig. 3.9B**). Mutation to an aspartic acid caused a severe drop in helical propensity, which led us to investigate this further using circular dichroism (CD). The four peptides used in the MD simulations (AKB-*wt*, AKB-S66D, AKB-S66E and AKB-pSer66) were synthesized and measured by CD. As suggested by the MD simulations, only the AKB-*wt* peptide displayed a strong α-helix propensity (~45%) whereas the phosphoserine and phospho-mimetic mutants showed no secondary structure (**Fig 3.9C**). This confirms the findings of the MD simulations and suggests that the formation of an amphipathic helix, required for PKA binding, is seriously hampered when Ser66 of smAKAP is phosphorylated.

3.4 Conclusion

Thus far, molecular understanding of the RI:AKAP interface has been limited to studying its interaction with the dual-specific dAKAP2 (Sarma et al., 2010) and the creation of RI specific peptide libraries (Carlson et al., 2006). Here we took advantage of the recent discovery of two RI-specific AKAPs, SPHKAP (Kovanich et al., 2010)

and smAKAP (Burgers et al., 2012), to extend our understanding of these specific interactions.

Comparison of dAKAP2 binding to either RI or RII revealed remarkable differences in the interaction surface (Kinderman et al., 2006; Sarma et al., 2010). The RIα:dAKAP2 interaction comprises contacts through four hydrophobic pockets on dAKAP2's amphipathic helix, whereas RII utilizes only two hydrophobic binding pockets, resulting in a much larger interaction surface for RIα:dAKAP2 (Sarma et al., 2010). In the structure of the RIαD/D:smAKAP-AKB complex solved here, we clearly see similar contacts via four binding pockets (**Fig 3.3B**). Another interesting difference between the D/D-domains of RIα and RIIα is the presence of two disulfide bridges between the protomers Cys16 and Cys37 (**Fig. 3.1B**) (Banky et al., 2003; Newlon et al., 2001). These reside at the edges of the AKAP interaction surface of the RIα-D/D-domain (Banky et al., 2003). It was suggested that these disulfide bridges could contribute to the interaction with dAKAP2, although in the crystal structure of Sarma et al. (Sarma et al., 2010), no direct interaction with any of dAKAP2's residues was observed. Interestingly, smAKAP did show these interactions as $Ile58^{C}$ and $Tyr61^{C}$ at the N-terminal end (**Fig. 3.4A**) and $Leu74^{C}$ (possibly in conjunction with Trp77) seal both disulfide bridges into the hydrophobic pockets. An additional interaction between $Ile58^{C}$ and $Leu13^{A}$ of RIα (helix α0) also assists. In dAKAP2, the locations of Gln631 and Met647 are identical to those of smAKAP's $Ile58^{C}$ and $Leu74^{C}$ respectively, however these are not able to accomplish the same task with respect to binding (Sarma et al., 2010).

These additional hydrophobic interactions could account for the much stronger binding affinity that RIα displays for smAKAP compared to dAKAP2 (Burgers et al., 2012; Burns-Hamuro et al., 2003). Three other RI binding sequences have an isoleucine or a leucine at the equivalent Ile58 position of smAKAP (**Fig. 3.3A**): dAKAP1 (dual specific, Ile344) SPHKAP (Kovanich et al., 2010) (RI-specific, Ile926) and RIAD (Carlson et al., 2006) (synthetic, Leu1). dAKAP2, does not have a hydrophobic residue at the Ile58 equivalent position but a glutamine (Gln631, **Fig. 3.3A**). A peptide substitution array performed on the AKB domain of dAKAP2 showed that phenylalanine, leucine, isoleucine or valine substitution of Gln631 increased the RIα binding affinity of dAKAP2 by 6-fold (Burns-Hamuro et al., 2003). These findings support the importance of creating an additional, fifth, hydrophobic pocket around $Ile58^{C}$ and the $Cys16^{A}$:$Cys37^{B}$ disulfide bridge to drive high affinity RIα binding. Our structure also suggests that $Tyr61^{C}$, located in pocket 1, is part of this extended hydrophobic interaction. This residue is likely not only important for affinity, but also for RI specificity. For instance, if the first amino acid in pocket dAKAP2 (Leu634) is mutated to an aromatic residue the PKA-RII binding affinity decreases approximately 40-fold. Additionally, when RIAD was generated (Carlson et al., 2006) it was observed that RI tolerates a bulky (aromatic) amino acid at that position (Tyr4 of RIAD), while PKA-RII did not, in line with the observation of Banky *et al.* that RIα contains a much deeper hydrophobic groove in the D/D-domain to accommodate this large side chain (Banky et al., 2003). This was confirmed by the

establishment of SPHKAP as the first PKA-RI specific AKAP (Phe929) (Kovanich et al., 2010).

In further support of the proposed sixth pocket at the C-terminal end of smAKAPs AKB domain, Burns-Hamuro *et al.* (Burns-Hamuro et al., 2003) also created a dAKAP2 AKB domain peptide in which both Gln631 and Met647 (equivalent to Ile58 and Leu74 of smAKAP) were substituted for phenylalanines. This resulted in an affinity increase for RIα of 24-fold, instead of 6-fold when substituting only Gln631 for phenylalanine. RII affinity was not affected, indicating that these interactions do not drive specificity, but rather affinity. The conservation of a hydrophobic amino acid at Trp77 (smAKAP, **Fig. 3.3A**) in the other RI-binding AKAPs suggests this could further assist binding in this region, however due to disorder of Trp77 in our crystal structure verification of this hypothesis awaits.

AKAPs accommodate spatial/temporal signaling of PKA. As such, AKAPs anchor PKA close to its substrates in a specific cellular compartment allowing it to respond instantly to local rises in cAMP levels. Phosphorylation of substrates may continue until halted via several feedback loops. The best described mechanism proceeds through nearby phosphodiesterases (PDEs), which degrade cAMP to AMP, thereby terminating PKA activity at the second messenger level (Maurice et al., 2003). Often, specific PDEs and PKA are sequestered by the same AKAP (Wong and Scott, 2004). An example of such a negative feedback mechanism is membrane bound PDE3A, which is activated by PKA phosphorylation (Maurice et al., 2003). Decreasing concentrations lead to dissociation of cAMP from R and subsequent re-

formation of the inactive PKA holoenzyme on the AKAP. Dephosphorylation of PDE3 by a nearby, or even AKAP-anchored, phosphatase then resets the system to respond to rises in cAMP again.

Direct disruption of the PKA:AKAP interaction, as suggested here, could be another potential mechanism to control localized cAMP signaling, however, thus far this has only been shown pharmacologically. For instance, the Ht31 peptide (Klussmann et al., 2001) and more recently the isoform specific peptides super-AKAP-IS (Gold et al., 2006) (PKA-RII) and RIAD (Carlson et al., 2006) (PKA-RI) have been proven to be useful tools in disrupting the PKA:AKAP interaction. FMP-API-1, a small molecule, was also shown to inhibit the binding of PKA to AKAPs, through an allosteric effect away from the D/D domain (Christian et al., 2011). Here we show an alternative negative feedback loop in which PKA inhibits its own anchoring to smAKAP by phosphorylating Ser66 in the AKB domain. Based on our findings we, at low cAMP concentrations smAKAP is bound to the inactive PKA $(R:C)_2$ holoenzyme. Once the cAMP concentration increases the C-subunt can be released and can phosphorylate smAKAP. This may be a mechanism used by other AKAPs as well that contain a Ser, Thr and Tyr residue, as for example found in at least 6 other human AKB domains, of which several (AKAP1 and AKAP4) are already annotated as sites of phosphorylation in online phosphoproteomics databases. Not all of these bear the typical PKA phosphorylation motif in the AKB domain, although AKAP4 and AKAP18 do. The physiological role of RI release from

smAKAP will require further studies and discussion. We speculate that release of the RI subunit induces a (temporary) signal termination by delocalizing PKA from the smAKAP site. In addition RI release may assist in more efficient capturing of the catalytic subunit when cAMP concentrations are dropping and PKA phosphorylation of smAKAP could play a role in the dynamics of degradation of this particular PKA signaling node. This should be particularly important in the light of the very strong interaction between smAKAP and RI.

In conclusion, we show here the first structure of RIα with one of its specific AKAPs, of which only 2 have been identified thus far (smAKAP and SPHKAP). The structure revealed several interesting points: (i) the interaction between RIα and smAKAP utilizes six hydrophobic contact sites, and extends over a much larger portion of the amphipathic helix, whereas RII interactions typically use less hydrophobic pockets; (ii), phosphorylation of smAKAP's AKB domain by PKA causes destabilization of the amphipathic helix which reduces smAKAP's affinity for RIα at least 1000-fold. Finally, other AKAPs have been shown to get phosphorylated in their AKB domains, suggesting this to be a potential general regulatory mechanism.

Chapter 3, in part, has been submitted for publication as PKA-induced phosphorylation inhibits its association to A-kinase anchoring proteins. Burgers, P.P.; Bruystens, J.G.; Rose, R.J.; Keshwani, M.M.; Wu, J.; Janssen, B.; Taylor, S.S.; Heck, A.J., and Scholten, A. The dissertation author was a secondary investigator and author of this work.

Chapter 4

Realizing the Allosteric Potential of the Tetrameric Protein Kinase A RIα Holoenzyme

4.1 Introduction

The regulatory (R) subunits of cAMP-dependent protein kinase (PKA) are modular and highly dynamic. In the absence of cAMP the R-subunit dimer is attached to two PKA catalytic (C) subunits and maintains the enzyme in an inactive tetramer. Each R-subunit contains a dimerization/docking (D/D) domain at the N-terminus that is joined by a flexible linker to two cyclic nucleotide binding domains at the C-terminus (CNB-A and CNB-B). The linker contains an inhibitor site (IS) that docks to the active site cleft in the C-subunit in the inactive holoenzyme but is disordered in the dissociated free R-subunits (Li et al., 2000). The linker, as summarized in Figure 1, can be divided into three segments, the consensus inhibitor site (P-3 to P+1), the N-Linker that joins the inhibitor site to the D/D domain, and the C-Linker that becomes ordered in the heterodimeric holoenzyme complex.

While much has been learned from the structures of the cAMP binding domains of the RIα and RIIβ subunits (Diller et al., 2001; Su et al., 1995), and the C-subunit has been crystallized in many different conformational states (Akamine et al., 2003; Knighton et al., 1991a; Madhusudan et al., 2002; Zheng et al., 1993), it was not until we solved structures of heterodimeric holoenzyme complexes that we could appreciate for the first time how the C-subunit was actually inhibited by the R-subunits, and how the complex was then activated by cAMP (Brown et al., 2009; Kim et al., 2007; Kim et al., 2005; Wu et al., 2007). The challenge now is to understand how the full length tetrameric holoenzymes are assembled as these represent the true physiological state of PKA. This is essential if we are to appreciate the full allosteric

potential of this key signaling enzyme. An additional goal is to determine how the N-Linker contributes to the assembly of the tetrameric holoenzyme.

Mammalian genomes typically code for four separate and functionally non-redundant R-subunit isoforms (RIα, RIβ, RIIα, and RIIβ). Although it has been difficult to crystallize full length R-subunits, presumably because the linkers are flexible, structures of the CNB domains and the D/D domains have been solved (Diller et al., 2001; Kinderman et al., 2006; Sarma et al., 2010; Su et al., 1995). To understand how the tetrameric holoenzymes are spatially organized, we initially used small angle X-ray and neutron scattering (SAXS/SANS). This revealed surprisingly that the shapes of the various R-subunits and holoenzymes are quite different (Heller et al., 2004; Vigil et al., 2004; Vigil et al., 2006). The RIα subunit and its corresponding holoenzyme are Y-shaped while the RII subunits are more rod-like and dumb-bell shaped. The RIIα holoenzyme remains extended while the RIIβ holoenzyme compacts into a globular protein (Vigil et al., 2006). These different architectures are due primarily to differences in the N-Linker regions (**Fig. 4.1**) and suggest that the allosteric signaling in each holoenzyme will be distinct. The Inhibitor Site and the C-Linker become organized upon association with the C-subunit; however, the role and ordering of the N-Linker, which contains many putative binding motifs, remains unknown.

It is known that cAMP activation of tetrameric holoenzyme is a cooperative process, that is reflected by the increased Hill coefficients (Herberg et al., 1994). Other evidence further supports the importance of the N-Linker and the tetrameric

configuration of the holoenzyme. Limited proteolysis of free RIa, for example, cleaves at Arg^{92} just before the inhibitor site whereas trypsin cleaves at Arg^{72} in the holoenzyme suggesting that at least part of the N-Linker is protected in the holoenzyme (Cheng et al., 2001). In addition, using cysteine mutagenesis coupled with fluorescence anisotropy, we explored the flexibility of residues that lie in different regions of RIα (Li et al., 2000). We found that residues that flank the D/D domain, Thr^{6} and Leu^{66}, were quite flexible independent of whether cAMP or catalytic subunit was bound. Other residues such as Ser^{99} were flexible in the dissociated R-subunit but immobilized in the holoenzyme. Two residues that lie in the N-Linker, Ser^{75} and Ser^{81}, were flexible in the free RIα subunit but became much less mobile in the holoenzyme suggesting that they might be interacting with another part of the protein and could possibly be contributing to forming the tetramer.

A final piece of evidence that supported the importance of the N-Linker for holoenzyme formation came from mutagenesis of two residues in the C-subunit that are predicted to lie on the surface where the N-Linker would bind (Cheng et al., 2001). Mutation of Arg^{133} selectively interfered with binding of RIIa whereas replacing Asp^{328} with Ala interfered with binding of RIa. These results led us to predict that the orientation of the N-Linker was not only important for formation of the tetrameric holoenzyme but also that the orientation of the N-Linker would be different in RI and RII (Cheng et al., 2001).

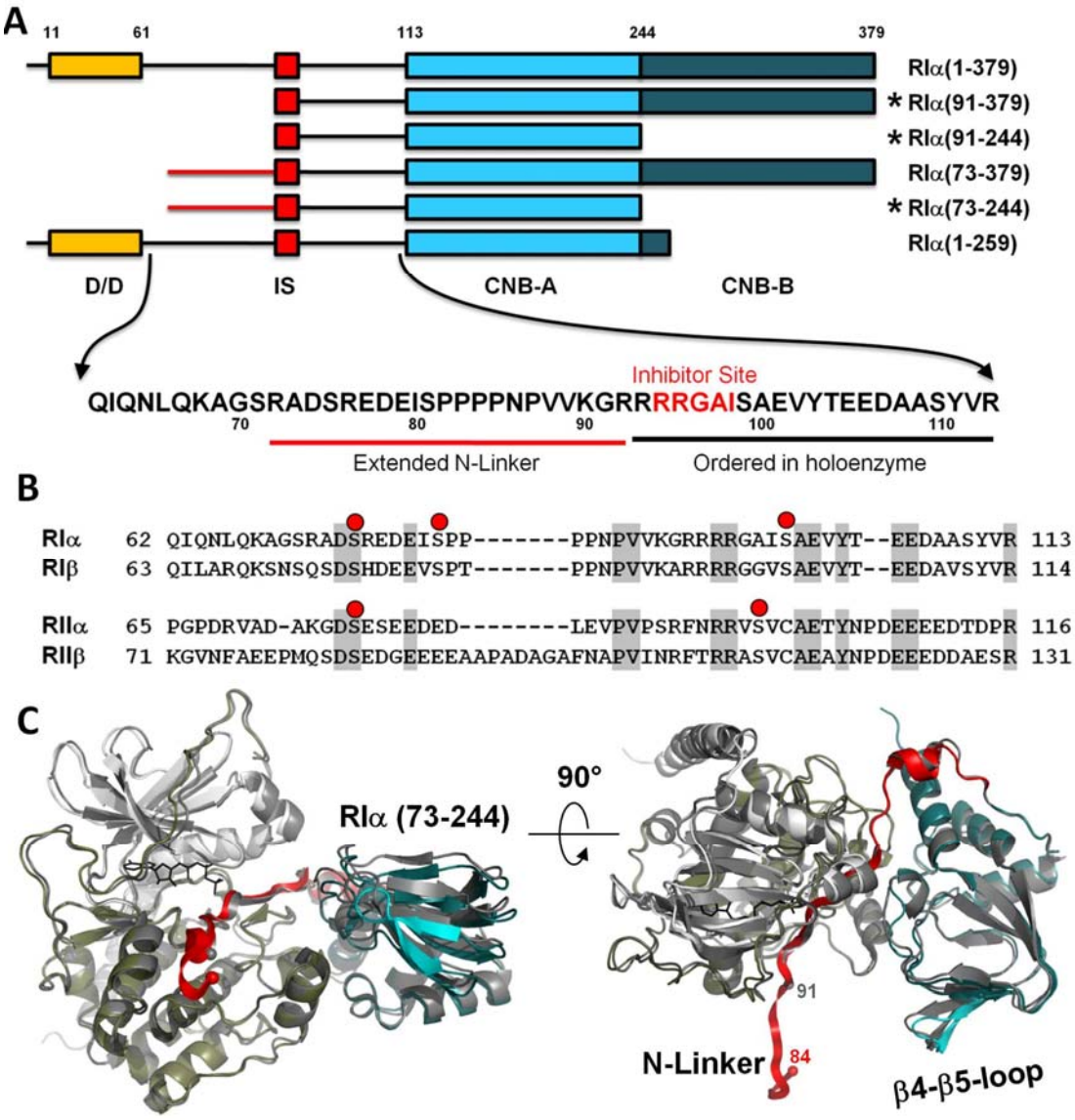

Figure 4.1. Extended N-Linker in RIα (73-244):C holoenzyme complex.
(A) Domain organization of different RIα constructs. Sequence of the linker between Dimerization Domain (D/D) and cAMP binding domain A (CNB-A) is shown. Constructs that were crystallized in holoenzyme complexes are marked with asterisks. **(B)** Sequence alignment of the linkers in different R-subunits. Possible sites of phosphorylation are shown as red dots. **(C)** RIα (73-244):C structure overlaid with the previously solved RIα (91-244):C (dark grey). Catalytic subunit is colored white (N-lobe) and tan (C-lobe). CNB-A is colored teal, the linker is colored red. N-terminal Ca atoms of the RIa constructs are shown as spheres.

The previous RIa monomers that were crystallized as a complex with the catalytic subunit began with the inhibitor site and contained no ordered residues from the N-Linker. To further explore the potential role of N-Linker residues and, in particular, to determine whether they contribute to formation of the tetramer, we engineered two longer constructs of RIα that contained 18 additional residues at the N-terminus compared to the constructs that had been crystallized previously as holoenzyme complexes (**Fig. 4.1**). We also engineered dimeric forms of RIa that lacked the second CNB Domain, RIa(1-259) and RIa(1-244). Although all of these constructs readily formed holoenzyme, only one, RIa(73-244), crystallized as a holoenzyme complex with crystal packing that was distinct from any of our previous structures.

The crystal structure of RIα(73-244) bound to catalytic subunit and Mn^{2+} AMP-PNP, a non-hydrolysable analog of ATP, was solved to a resolution of 3.3Å. Although not all of the additional linker was ordered, residues 84-92 could be easily traced. While the inhibitor site docked to the active site cleft of the catalytic subunit as expected, the extended linker interacted primarily with the β4-β5 loop of the symmetry-related dimer. In addition, this β4-β5 loop docked onto the hydrophobic pocket of the catalytic subunit that is created by the αF-αG loop in the symmetry-related dimer, a site that is also used in different ways as a docking site for both PKI and RIIβ. While these two heterodimers do not have a high tendency to form a tetramer when they are not tethered to one another by the dimerization/docking domain, there are many features of this holoenzyme complex that are consistent with

known features of the tetrameric holoenzyme. Forming the extended interface between the two heterodimers creates a highly allosteric surface that would explain the high Hill coefficient (1.6) that is associated with activation of the tetrameric holoenzyme compared to the heterodimer (Herberg et al., 1994). The two heterodimers are also oriented such that the linkers could be readily joined to the nearby D/D domain. From our previously solved structures, we are only missing 20 residues of the linker. Our model of the quaternary structure of the full-length tetramer, based on this structure, is also independently validated by our previous SAXS and SANS data where the C-subunits are well segregated from one another. To further validate this quaternary structure we also obtained SAXS data for an RIa(1-259):C complex, where the dimeric RIa is lacking the B-domain. This also is consistent with our model. Finally, we demonstrate that a mutation in the proposed interface between two heterodimers not only alters the cAMP induced activation of PKA but also reduces the Hill coefficient. This model allows us for the first time to appreciate the intricate ways in which the binding of a small messenger, cAMP, leads to the allosteric release of kinase inhibition.

4.2 Experimental Procedures

Protein Preparation - The catalytic subunit was expressed and purified as previously described (Gangal et al., 1998). The peak I of C-subunit which contains 4 phosphorylated residues (Ser^{10}, Ser^{139}, Thr^{197}, and Ser^{338}) was used for crystallography. Three regulatory subunit deletion mutants (RIa(73-379), RIa(73-

379:R333K), and RIa(73-244) were generated by Quikchange site-directed mutagenesis according to the Stratagene protocol. These mutants contained most of the linker residues compared to the previous structure of RIa (91-244). All mutants were expressed in E. coli BL21 (DE3) cells (Novagen) and purified as described previously (Saraswat et al., 1988) with slight modification. The cells were lysed and the spin supernatant was filtered with 0.22mm filter and loaded onto a Profinia protein purification system. The sample was run over a cartridge containing cAMP bound to resin, washed with lysis buffer containing 0.7M NaCl and then eluted with lysis buffer containing 35mM cGMP at pH 5.8. Eluted protein was then run on S75 gel filtration column.

Complex Formation - Each of the RIa mutants were mixed separately with the wild type C-subunit in a 1:1.2 molar ratio and dialyzed at 4°C in 10 mM MOPS (pH 7.0), 2 mM $MnCl_2$, 50 mM NaCl, 1 mM TCEP-HCl and 0.2 mM AMP-PNP.

Crystallization - The RIa(73-244):C complex was crystallized in 0.1M MES pH 6.0 and 12% PEG 20,000 by using a Douglas Instruments Oryx8 crystallography robot as 1:1 protein solution:crystallizing solution and incubated at room temperature. Crystals were flash frozen in a cryoprotectant solution (mother liquor containing 15% glycerol) and a data set was collected to 3.3Å on the Advanced Light Source beamline 8.2.1. Data was processed and scaled using HKL2000 (Table 1). The structure was solved using the RIa(91-244):C complex structure as the molecular replacement probe.

RIa(73-379):C complex was initially crystallized in 30% PEG 400, 0.1M HEPES pH 7.5, 0.2M NaCl using Douglas Instruments Oryx8 crystallography robot. Drops were set up under silicone oil as 1:1 protein solution:crystallizing solution. However, the crystals can only diffraction to 8Å. RIa(75-379:R333K) with a mutation in the essential arginine in the PBC of the cAMP-binding domain B did not purify well and had many contaminating proteins, so it was not set up for crystallization.

Phasing for the structure was made by molecular replacement in AMORE using 3FHI as a search model. Refinement was made by REFMAC and CNS 1.2 programs. The model was manually built based on the density maps using Coot. The final model was evaluated by PROCHECK and had good geometry.

cAMP-induced activation - A fluorescence polarization assay was used to monitor PKA activity as described earlier (Saldanha et al., 2006). C-subunit concentration was 10 nM. R-subunit was added in 1.3:1 molar ratio. Solution contained 1 mM ATP, 10 mM MgCl2 and 2 nM FAM-IP20.

Small angle scattering evaluation - Evaluation of the of X-ray solution scattering curves was made by CRYSOL program (Svergun et al., 1995). Previously published SAXS data (Heller et al., 2004) were used for the space filling model for Figure 7b by GASBOR program (Svergun et al., 2001).

Accession numbers - The atomic coordinates and structure factors have been deposited in the Protein Data Bank (accession code 3PVB).

Table 4.1. Data collection and refinement statistics RIα (91-365):C

	RIα(73-244):C
Data collection	
Space group	P 3_2 2 1
Cell dimensions	
a (Å)	116.7
b (Å)	116.7
c (Å)	140.1
γ (°)	120.0
No. of molecule per asymmetrical unit	1
Resolution (Å)	3.3
R_{merge}	0.088 (0.40)*
Completeness (%)	97.1 (93.7)
I/sigma	19.3 (3.4)
No. reflections	27860
Refinement	
Resolution (Å)	50.0-3.3
R_{work} / R_{free} (%)	24.2/29.0
No. of protein residues	522
No. of ligand/ion	3
No. of water	16
R.m.s. deviations	
Bond lengths (Å)	0.010
Bond angles (°)	1.6
Ramachandran angles (%)	
most favored (%)	81.5
disallowed	none

*Values in parentheses are for the highest-resolution shell (3.30-3.39 Å)

4.3 Results

Overall structure of RIα(73-244):C Complex - To understand how the RIα N-Linker region contributes to the holoenzyme structure, we extended the N-terminus of the previous construct of RIα(91-244) by 18 residues. We also engineered the extended form of RIα(91-379). Both proteins were very stable, and both readily formed a high affinity complex with the C-subunit that could be isolated on a gel filtration column; however, only the RIα(73-244) holoenzyme complex gave high resolution crystals. The crystal structure of RIα(73-244) in complex with the C-subunit, AMP-PNP and two Mn^{++} ions was solved at 3.3Å. Although the overall structure of the complex is very similar to that of the previously solved RIα(91-244):C complex (Kim et al., 2005) (**Fig. 4.1**), the crystal packing was different from other previous structures of free or complexed R- and C-subunits. The asymmetric unit contains a single heterodimer comprised of one R-subunit and one C-subunit. The C-subunit is generally unchanged and is in its closed conformation. The overall conformation of the R-subunit is also similar to what was seen in the RIα(91-244) complex although the β4-β5 loop is shifted about 2.5Å away from the C-subunit. All corresponding α-carbon atoms of the two complexes can be superimposed with an RMSD of 0.8Å (Maiti et al., 2004). In this structure, however, the electron density of the N-terminal linker region in RIα can now be clearly traced up to Pro^{84}, nine residues more than in the previous RIα(91-244):C complex. To understand how the N-Linker is ordered, one must look to the symmetry-related dimer. Specifically, it is the β4-β5 loop of the symmetry-related dimer that orders the N-Linker. The

consequences of this ordering creates a tetrameric configuration of the two heterodimers that not only orders the N-Linker of each dimer but also creates an allosteric symmetry-related interface that explains clearly and for the first time why the tetramer is essential for the highly cooperative activation of PKA by cAMP. The tetramer that is formed by the two symmetry mates is also consistent with our models of the full length tetrameric RIα holoenzyme based on small angle X-ray and neutron scattering (SAXS and SANS).

N-Linker is ordered by Inter-molecular interactions between symmetry-related holoenzymes - The Inhibitor Site is defined as residues P-3 to P+1 in the linker, and as RIα is a pseudosubstrate it has alanine in the P-site position (Ala^{97}). While this segment docks to active site of the C-subunit in more-or-less the same conformation as described previously in the PKI complex and in the RIα and RIIα holoenzyme complexes, in this structure we can now trace the N-terminal linker up to Pro^{84}. However, as seen in **Figure 4.1C**, most of this segment extruded out from the complex and did not make any interactions with its own R or C subunit. Analysis of the crystal packing showed that stabilization of this flexible linker is provided by a symmetry mate, designated here as R':C' (**Fig. 4.2**). The two symmetry-related dimers have an extensive interface area: 829Å^2 between the two R-subunits (R to R') and two 243Å^2 interfaces between C and R-subunits (C to R' and C' to R). The combined interface between C-R and C'-R', thus, was 1316Å^2 , and this is comparable to the interface between the C and R subunits within each holoenzyme dimer (1524Å^2). The

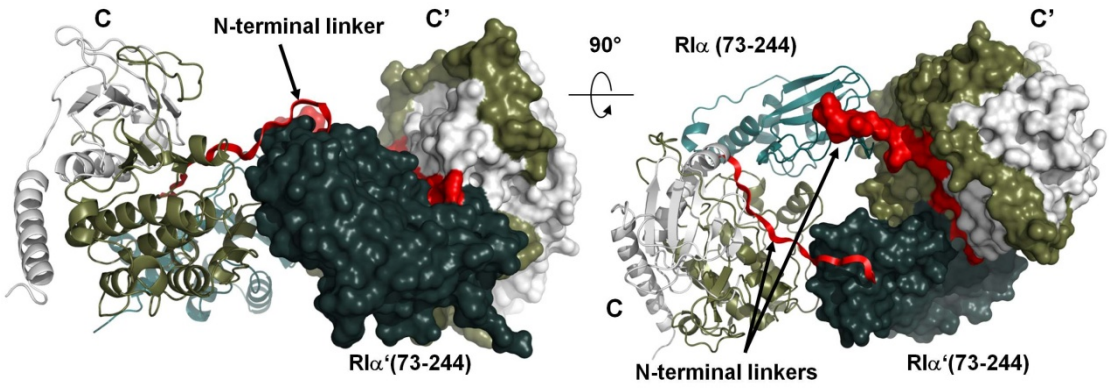

Figure 4.2. Crystal packing of the RIα (73-244):C holoenzyme. Color coding is the same as that used in Figure 4.1. Symmetry-related molecule is shown as surface.

interface was predominantly hydrophobic with desolvation energy estimated at -10.7 kcal/mol (Krissinel and Henrick, 2007).

The major element that interacted with the extended linker in the interface was the β4-β5 loop in the cyclic nucleotide-binding (CNB) A domain from the R'-subunit in the symmetry-related heterodimer. This loop (**Fig. 4.3**), which is highly conserved in an isoform-specific manner, is exposed to solvent in the absence of the N-Linker, but in the presence of the N-Linker, this loop from the symmetry-related dimer provides a mechanism for bridging the N-Linker and the C-subunit on the other dimer. Since the complex observed in the crystal had two-fold rotational symmetry, the β4-β5 loop in each R:C heterodimer was bound in exactly the same way to the symmetry-related heterodimer. We will consider first exactly how the β4-β5 loop from one dimer docks on the other dimer and then consider the consequences of this for creating a unique allosteric mechanism for activation of the tetrameric holoenzyme.

The N-Linker is ordered by the β4-β5 loop of the symmetry-related dimer - As shown in **Figure 4.3A**, the β4-β5 loop from the R' subunit interacts with the N-Linker from the symmetry-related R-subunit and in addition docks onto the hydrophobic pocket in the symmetry-related C-subunit that is formed by the αF-αG loop. Three residues, Tyr^{183}, Trp^{188} and Ser^{191}, contribute prominently to this interface that is created by the β4-β5 loop, and this interface can be divided into two distinct but overlapping segments. We will consider first the interactions of the β4-β5 loop with the neighboring N-Linker and then its interactions with the neighboring C-subunit.

The two hydrophobic residues, Tyr^{183} and Trp^{188}, are buttressed up against the N-Linker and provide the major interface with the N-Linker. In addition, two hydrogen bonds between Asn^{186} from the β4-β5 loop of the R'-subunit and backbone carbonyls of the N-terminal linker from the R-subunit (Pro^{87} and Val^{88}) were detected, and these anchor the proline-rich segment that is a characteristic feature of the N-Linker in RI-subunits.

As seen in **Figure 4.3** the β4-β5 loop also interacts with the αF-aG loop in the C-subunit of the symmetry-related dimer, and this site is known to be an important docking site for PKA and for other kinases as well. Specifically, Trp^{188} and Ser^{191} from the β4-β5 loop dock to the hydrophobic pocket on the C-subunit that is formed by Tyr^{235} and Phe^{239} from the aF-αG loop (**Fig. 4.4A**). Although solvent exposed residues of this pocket are different in different kinases, its backbone geometry is absolutely conserved and is defined by a set of hydrophobic interactions between highly conserved residues: Trp^{222}, Tyr^{229}, Pro^{237}, Phe^{238} and Ile^{250} (**Fig. 4a and b**). This site is anchored to the central F-helix that serves as a general scaffold for most of the important residues in protein kinases (Kornev et al., 2008). This pocket often serves as an important protein/protein docking site. It is this pocket that is used as a tethering site for the amphipathic helix of PKI which binds with high affinity to the C-

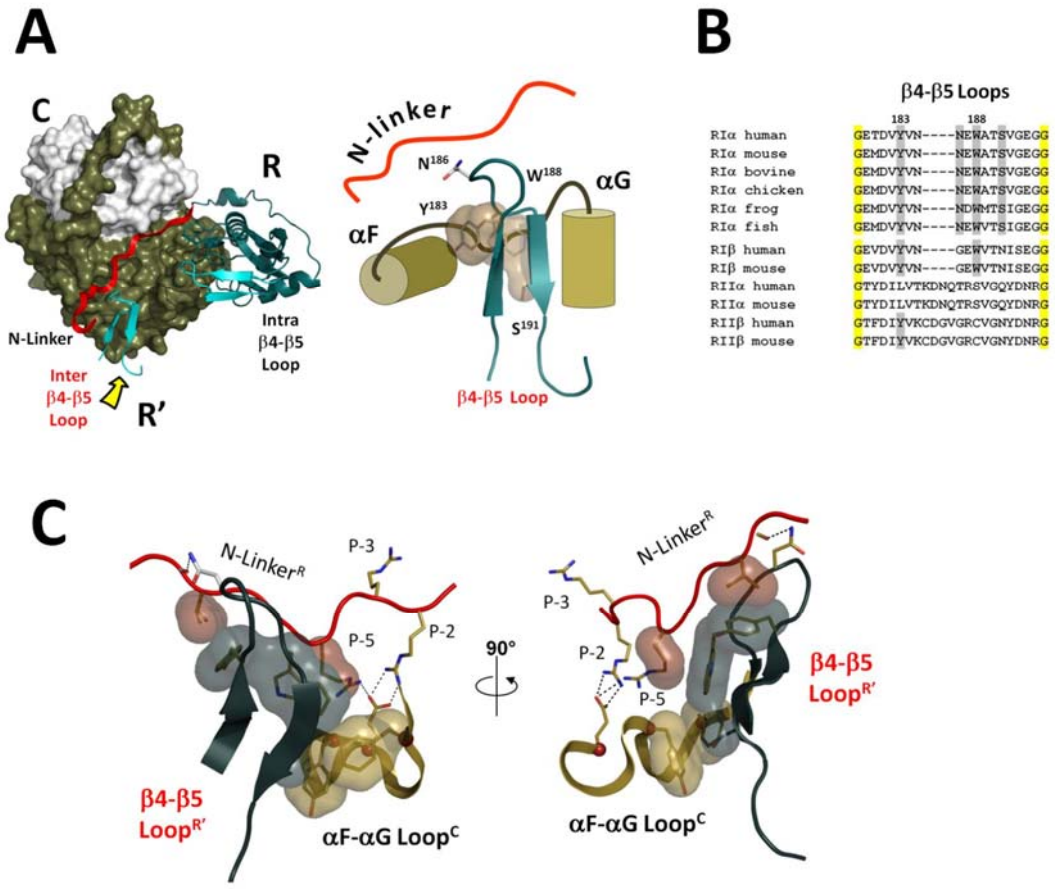

Figure 4.3. β4-β5 loop is a key element of the interface between symmetry-related heterodimers. (A) b4-b5 loop from the symmetry-related R'-subunit is marked by the yellow arrow. It docks to the aF-aG loop of the C-subunit and the extended N-Linker of the R-subunit. (**B**) Sequence alignment of b4-b5 loops from different R-subunits. Four residues from the b4-b5 docking interface are shaded grey, universally conserved glycines are shaded yellow. (**C**) A close-up view of the b4-b5 loop docking interface. Aliphatic parts of the interacting residues are shown as surfaces.

subunit (Knighton et al., 1991a). This pocket is also used in a very different way by the N-Linker of the RIIβ subunit when it is trapped in a complex with AMP-PNP (Brown et al., 2009) (**Fig. 4.4C**). The αF-aG loop also links residues in the core that interact with P-3 and P-2 residues in the inhibitor peptide and the P+1 loop which provides the docking site for the P+1 residue. Finally, this loop positions the G Helix which is a critical docking site for the regulatory subunits and for other tethered substrate proteins (**Fig. 4.4A**). This loop is thus a fundamental feature for peptide/protein recognition by every protein kinase.

In addition to Tyr^{235} and Phe^{239} from the αF-αG loop, the hydrophobic interface was formed by two additional residues from the N-terminal linker, Val^{89} (P-7) and Arg^{92} (P-5) (**Fig. 4.3C**). Arg^{92} in the P-5 position is strictly conserved in RIα subunits and is absent in RII subunits. Sequence alignment of the R subunits (**Fig. 4.1B and 4.3B**) indicates that the β4-β5 loop and the N-Linker are among the most isoform distinct sequences given the high homology of the RI and RII subunits. **Figure 4.3B** compares the sequence in the β4-β5 loop region in various RI and RII subunits. All four residues of the interface between two heterodimers are highly conserved in RIα, less conserved in RIβ, but are not conserved in RII subunits. In the RII subunits this segment is conserved differently suggesting that it will contribute in different ways to their holoenzyme structures, and this is consistent with our SAXS data (Vigil et al., 2004).

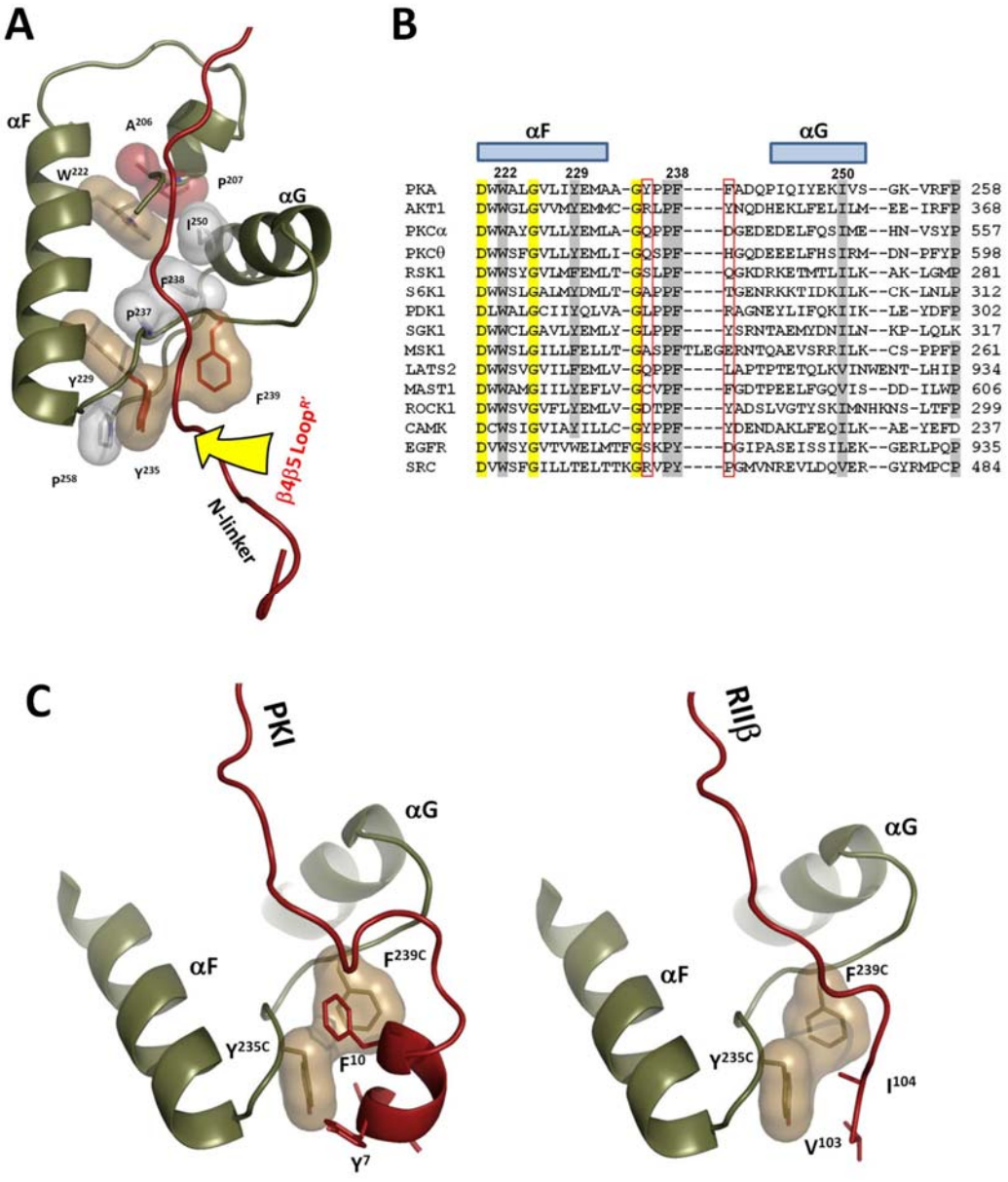

Figure 4.4. αF-αG loop is a universal docking site. (A) Geometry of the aF-aG loop is conserved through all protein kinases. It is defined by conserved hydrophobic interactions of Pro^{237} and F^{238} with aF(Trp^{222} and Y^{229}), aG(I^{250}), which are connected by the universal APE-motif (colored red). The b4-b5 loop docking site is indicated by the yellow arrow. (**B**) Structure based sequence alignment of aF-aG loops in different protein kinases. Universally conserved residues are shaded yellow. Residues that form hydrophobic interface are shaded grey. Two positions corresponding to Y^{235} and F^{239} which are exposed on the surface of the docking site are framed in red. **C**. Protein kinase A inhibitor PKI and N-terminal linker of RIIb dock to the same groove formed by the aF-aG loop.

N-linker contacts explain importance of Asp^{328} and Arg^{133} of the C-subunit for the holoenzyme formation - In the earlier work (Cheng et al., 2001) we demonstrated that sequence diversity in the N-linker of RIa and RIIb is functionally important. Mutagenesis of two C-subunit residues, Arg^{133} and Asp^{328}, showed that Arg^{133} is important for the formation of RIIb holoenzyme whereas Asp^{328} was more important for RIa subunit. In all previously solved structures Arg^{133} interacts with Glu^{230} from the F-helix, while Asp^{328},is solvent exposed (**Fig. 4.5a**). In this structure, however, the P-5 Arg^{92} binds to the Glu^{230} causing Arg^{133} to flip about 180° so that it is now contacting Asp^{328} (**Fig. 4.5b**). As we pointed out, Arg^{92} is a characteristic feature of RIa subunits, that require ATP and two Mg^{++} ions for the full length holoenzyme formation. The observed flip of Arg^{133} further locks the ATP-bound holoenzyme into a closed conformation where the N- and C-lobes together bury the ATP. Here we can see why loss of Asp^{328} is uniquely detrimental to the formation RIα holoenzymes. Mutation of Glu^{230} to Gln led to disruption of the Arg^{133}:Glu^{230} salt bridge and destabilization of the Arg^{133} side chain (1SYK (Wu et al., 2005)). The only other wild type PKA structure that did not have the Arg^{133}:Glu^{230} salt bridge was the apo C-subunit with its open active site cleft and partly unstructured C-terminal tail (1J3H (Akamine et al., 2003)). Here we present the first evidence to show that Arg^{133} can form a salt bridge with Asp^{328} from the C-tail. It was also shown previously that mutagenesis of Asp^{328} can decrease the catalytic efficiency of PKA, but it was not clear why (Batkin et al., 2000).

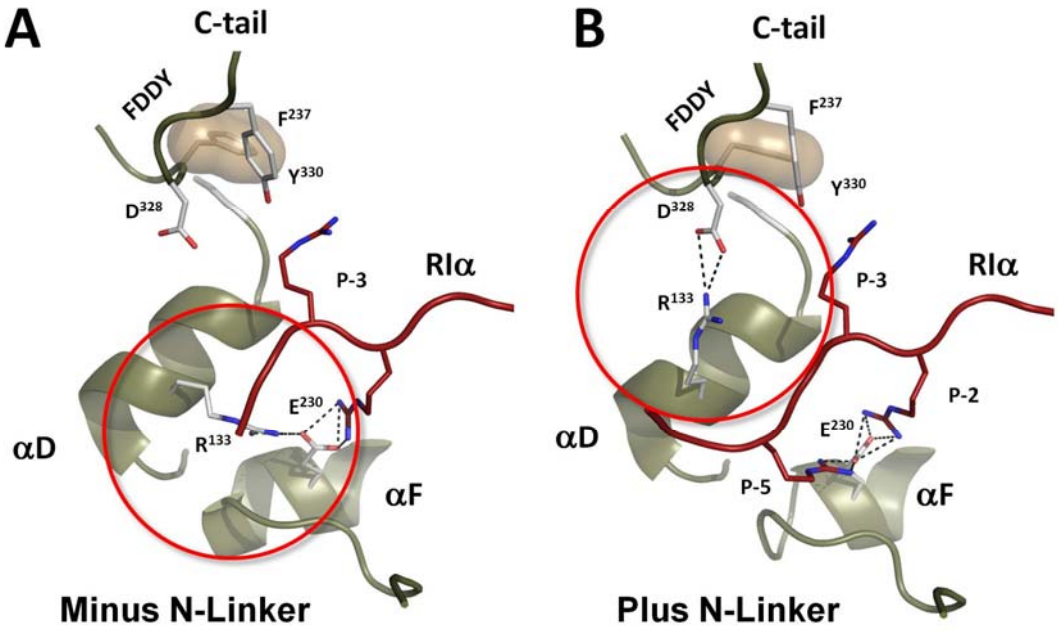

Figure 4.5. R^{133} flip in RIα (73-244):C holoenzyme. (A) In all previously known structures of PKA C-subunit R^{133} was bound to E^{230} from the aF-helix. (**B)** In the new holoenzyme structure it forms a salt bridge with D^{328} from the conserved FDDY motif in the C-terminal tail.

Allosteric Interface is created in the tetrameric complex - The detailed features showing how the N- and C-Linkers are anchored in the tetrameric holoenzyme that is made up of two symmetry-related dimers are indicated in **Figure 4.6**. What is revealed here for the first time is how binding of cAMP to one site can simultaneously influence both the R:C interface in its own R:C partner as we saw in earlier structures but also how it can influence positioning of the N-Linker from the symmetry-related dimer. Such influence is provided by the multiple direct contacts of the β4-β5 loop region of each CNB-A domain to the N-terminal linker of the opposite Regulatory subunit (**Fig. 4.3c**). This would explain for the first time why the Hill Coefficient is increased in the tetramer as compared to the dimer (Herberg et al., 1994). It also creates a unique symmetry that was never previously appreciated. This is the surface that faces towards the C-terminal surface of the helical D/D domain, and it remains to be determined whether there are additional interactions that are created between the D/D domain and the tetrameric configuration of the two dimers. In addition, as seen in **Figure 4.1**, there are two predicted phosphorylation sites in the missing 20 residues of the N-Linker, and these could significantly alter the configuration of the tetramer as well as the allosteric properties of the tetramer.

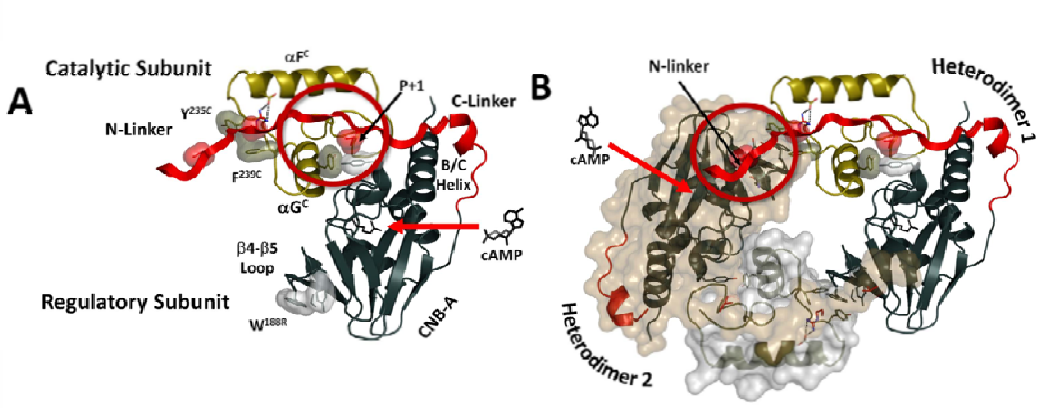

Figure 4.6. N-Linker mediates cross-talk between two heterodimers. (A) Binding cAMP molecule to CNB-A in a heterodimer (indicated by the red arrow) disrupts the R:C interface in the C-linker around the P+1 loop, aG-helix region (indicated by the red circle). (**B**) Binding of the second cAMP molecule to the symmetry related R'-subunit disrupts the R':C and R':R interface in the N-linker area.

Changes in the Phosphate Binding Cassette - The signature motif for cAMP binding is the Phosphate Binding Cassette (PBC), which is embedded within the β subdomain of the CNB. As shown previously, the PBC is distorted in the holoenzyme and assumes a conformation that has a low affinity for cAMP (Kim et al., 2005; Wu et al., 2007). **Figure 4.7** shows how the PBC is further distorted by the docking of the β4-β5 loop to the N-Linker of the symmetry-related dimer. In this figure the positions of the β4-β5 loop and PBC in the cAMP-bound conformation are compared with their conformation in the holoenzyme complexes that are formed with RIα(91-244) where the N-Linker is missing vs. RIα(73-244) where the N-Linker is included. From this alignment it is clear that the configuration of the β4-β5 loop is not significantly altered by its interactions with the symmetry-related dimer, although its position is slightly displaced. However, two changes are seen in the PBC. The tip of the PBC is different when the N-Linker is present and the region extending from Arg^{209} to Ala^{211} is moved slightly. This slight movement of Ala^{210} is significant, because this segment provides part of the hydrophobic packing for the nucleotide. This segment is referred to as the "Base Binding Region" (McNicholl et al., 2010; Rehmann et al., 2003). This distortion of the PBC:β4 interface causes the cAMP binding pocket to be occluded so that access of the nucleotide to the PBC is further restricted. This likely makes this complex even more resistant to activation by cAMP.

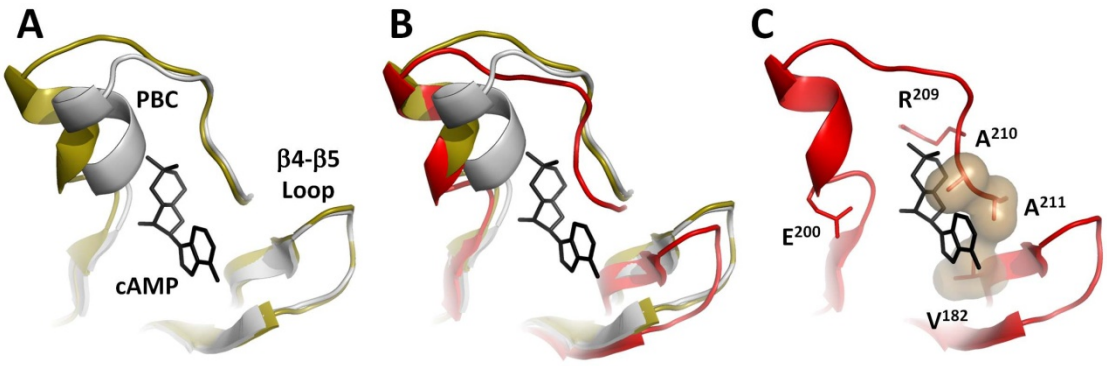

Figure 4.7. Structural changes in the Phosphate Binding Cassette (PBC) in RIα (73-244):C holoenzyme. (A) Overlay of PBCs in cAMP-bound RIa (1RGS) (white) and RIa(91-244):C holoenzyme (3FHI) (golden). (**B)** C-terminal part of the PBC in RIa(73-244):C holoenzyme (red) is distorted. The b4-b5 loop position in the new holoenzyme is also shifted. (**C)** V^{182} from the "Base Binding Region" interacts with the A^{210}-A^{211} region of the PBC, occluding cAMP binding. cAMP is modeled from the cAMP-bound RIa structure.

Model of the RIa tetrameric holoenzyme is consistent with SAXS/SANS data - Previously we assessed the general shape of PKA tetramers by using small angle X-ray and neutron scattering (SAXS/SANS) techniques (Heller et al., 2004; Vigil et al., 2006). Deuterium labeling of RIa subunits showed, in particular, that in the tetrameric holoenzyme they are in a close contact, while the two C-subunits are completely separated. To test if our present results are consistent with these data we created a model of the full length PKA tetramer based on the two symmetry-related dimers in our crystal (**Fig. 4.8A)**. To introduce the C-terminal CNB domain that was missing in the current RIα construct, we used structure of the C-subunit bound to the RIa(91-379) that also has an R333K mutation that prevents cAMP binding to the B-domain (2QCS (Kim et al., 2007)). Two copies of this heterodimer were positioned according to the packing depicted in **Figure 4.2**. As indicated earlier, the N-termini of the two RIα chains are positioned in a way that allows them to be readily linked to the D/D domain. Scattering data for this model were calculated by the CRYSOL program (Svergun et al., 1995) and fit to the experimental data for RIa holoenzyme with c^2=1.22 (**Fig. 4.8C)**. Ab intio reconstruction of the complex based on the previously reported SAXS data using the GASBOR program, gave us a butterfly shaped shell that also fits our model reasonably well (**Fig. 4.8B).** Analysis of the distance distribution functions P(r) for the R-subunits and C-subunits showed that they correspond well to the previously reported SANS results: R-subunits form a compact object, while C-subunits are widely separated (**Fig. 4.9a,b**).

Experimental validation of the model - To test this model of the tetramer, we used two approaches. One strategy was to characterize the tetrameric holoenzyme formed with RIα(1-259) (**Fig. 4.1A**) that is only 15 residues longer than the crystallized construct. This dimer expresses well and the holoenzyme formed readily. The Ka (cAMP) had a Hill coefficient of less than 1.0 as reported previously (Herberg et al., 1994) confirming the importance of the B domain for allostery. The SAXS intensity profile of the RIα(1-259):C complex was close to the theoretical curve predicted by our model (**Fig. 4.9c**).

To further validate the PKA holoenzyme model, we mutated Trp^{188} from the β4-β5 loop to Asp. As shown in **Figure 4.3b** the sequence of the β4-β5 loop is highly conserved in an isoform-specific manner. Nevertheless, there is no obvious role for this loop in either the cAMP bound structure or for the heterodimer with the C-subunit and the deletion mutant of RIa. In all of these earlier structures the β4-β5 is exposed to solvent. Previous studies of folding showed that the mutation of Trp^{188} had no effect on overall structure or unfolding of RIa (Leon et al., 2000). However, according to our model, Trp^{188} is one of the key contact residues in this loop. As seen in **Figure 4.8d**, the W188D mutation interfered with cAMP-induced activation of PKA increasing the EC_{50} from to 29 to 95 nM. In addition the Hill coefficient decreased from 2.1 to 1.7.

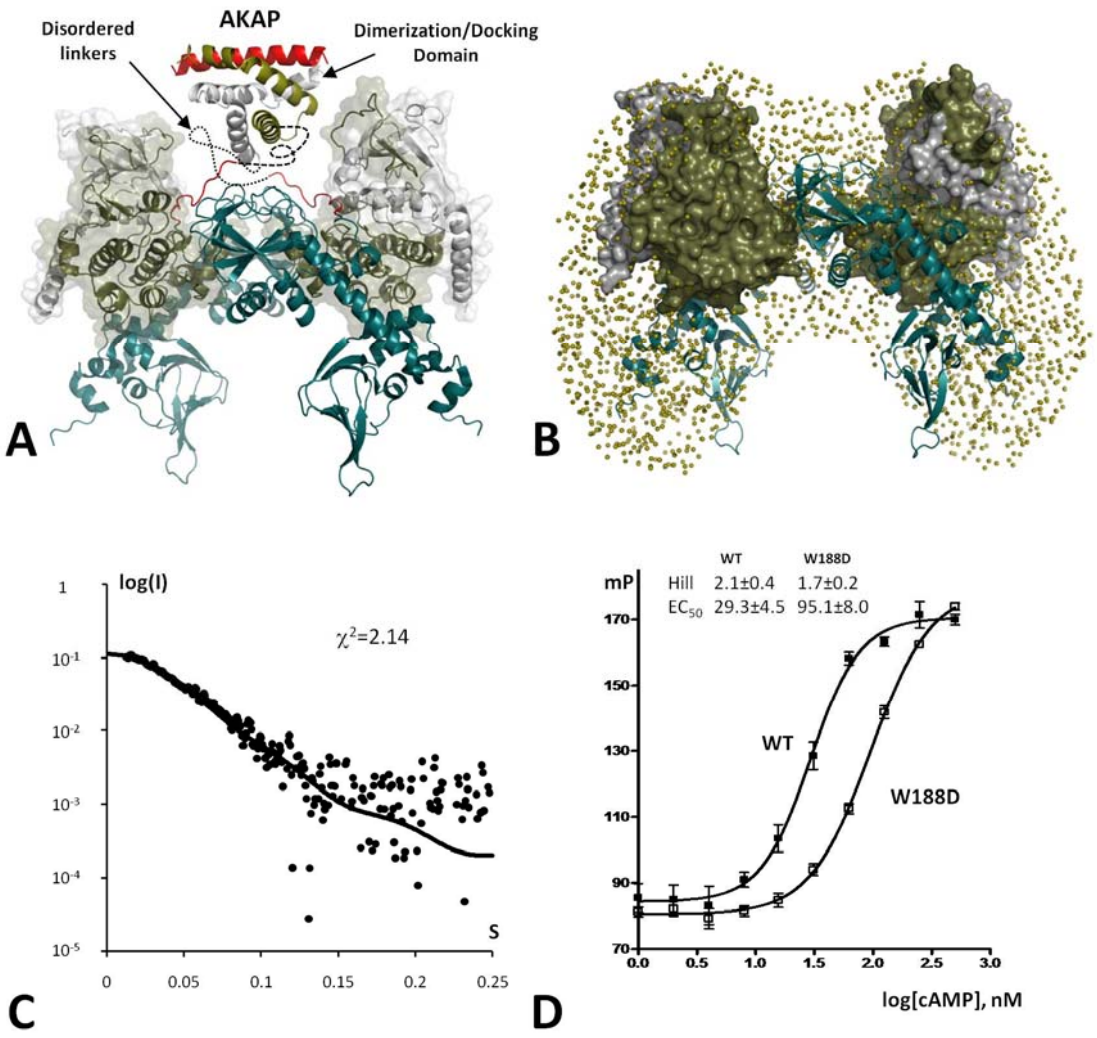

Figure 8. Model of the RIα tetrameric holoenzyme. (A) The proposed positions of two PKA heterodimers correspond to the observed packing (Figure 2). Possible position of the Dimerization/Docking domain bound to the AKAP helix is illustrated using 3IM4 structure. Still unknown linkers between the DD-domain and RIa CNB domains are shown as dashed lines. (**B**) Space filling model obtained from the previously reported SAXS data (Heller et al., 2004) (tan spheres) is overlaid with the proposed model. C-subunits are shown as tan colored surface. R-subunits are shown as tan cartoon. (**C**) Small Angle X-ray scattering curve computed from the RIa(73-244):C tetrameric complex showed on the Figure 2. Dots represent experimental data for RIa(1-259):C holoenzyme. (**D)** cAMP-induced activation of PKA monitored by FAP-IP20 binding.

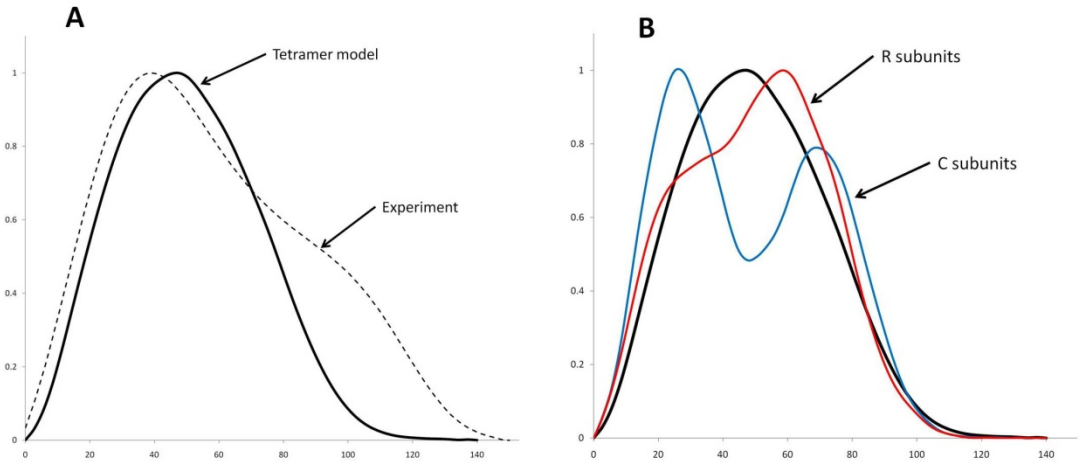

Figure 4.9. Distance distribution functions P(r) for the RIα holoenzyme model and its constituents. The tetramer model includes two C-subunits and two RIα (91-379) constructs (with R333K mutation) taken from the 2QCS structure bound to each other according to the interface shown on Figure 4.2. (**A**) Comparison of the tetramer model (solid line) to experimental P(r) function for the full length wild type of RIa holoenzyme reported earlier (dashed line) (Heller et al., 2004). (**B**) P(r) functions calculated separately for R-subunits (red line) and C-subunits (blue line) in the tetramer model.

4.4. Conclusion

To probe the function of the N-Linker in the RIα subunit of PKA and specifically to determine whether the N-Linker contributes to assembly of the tetrameric holoenzyme and to allostery, we engineered a monomeric form of RIα that contains most of the N-Linker, RIα(73-244), and crystallized a holoenzyme complex. In this holoenzyme the N-Linker is extended by 18 residues compared to our previous structures (Kim et al., 2007; Kim et al., 2005). Although nine N-terminal residues were not resolved, the coordinates for an additional nine N-Linker residues were resolved for the first time. Surprisingly, they were not bound to the C-subunit of their own heterodimer (**Fig. 4.1C)**. Instead, the linker was docked onto the R-subunit of the symmetry-related heterodimer (**Fig. 4.2)**. Specifically, the β4-β5 loop from one RIα subunit was docked onto the N-Linker of a symmetry-related dimer thus creating a novel tetrameric interface. Analysis of the interface between the two heterodimers showed that it is mostly hydrophobic and can be relatively stable in solution. This led us to the suggestion that this interface can in fact represent interactions between R and C subunits in the full length PKA tetrameric complex. This suggestion is supported by several observations including enhanced cooperativity in the tetramer (Herberg et al., 1994), protection of the N-Linker from proteolytic cleavage in the holoenzyme compared to free RIa, and isoform-specificity for docking of this portion of the N-Linker (Cheng et al., 2001). It was also shown that mutation of Arg^{133} in the C-subunit is important for RIIb holoenzyme formation, while mutation of Asp^{328} plays an

essential role in RIa holoenzyme. Our model for the first time can provide explanation of these results. According to the model the RIa-specific Arg^{92} in P-5 position

The structure also explains for the first time why the β4-β5 loop and the segment of the N-Linker that immediately precedes the Inhibitor Site are conserved in such a unique way in each isoform. The importance of the β4-β5 loop for activation of the tetrameric holoenzyme was also confirmed by mutagenesis. Finally, a model of the tetrameric holoenzyme, based on this structure, is quite consistent with our previous SAXS and SANS results (Heller et al., 2004; Vigil et al., 2004). To further confirm the model we carried out SAXS analysis of a mutant RIa tetramer that lacks the B domain.

Two methods, limited proteolysis (Cheng et al., 2001) and cys-scanning mutagenesis of linker residues coupled with fluorescence polarization (Li et al., 2000), indicated that the N-Linker is flexible in free RIα but ordered in the holoenzyme. It was shown that limited proteolysis of cAMP-bound RIα with trypsin cleaves at Arg^{92} whereas in the holoenzyme cleavage occurs at Arg^{72}. Cys scanning mutagenesis, on the other hand, allowed us to probe the flexibility of residues in this region (positions 75 and 81). These results also support the conclusion that the N-Linker is much more ordered in the holoenzyme. In this structure we begin to understand for the first time how the N-Linker can be ordered.

As summarized in **Figure 4.10**, direct docking of the linker region to the R-subunit of the symmetry-related heterodimer can explain the enhanced cooperativity of activation in the tetramer (Herberg et al., 1994). Although the entire linker region is disordered in the cAMP-bound RIα subunit, the Inhibitor Site through the C-Linker

becomes ordered at the R:C interface when the RIα subunit binds to the C-subunit (Kim et al., 2007; Kim et al., 2005). Of particular interest here, is the holoenzyme complex of RIα(92-244) where the RIα subunit begins with the Inhibitor Site. Extending the N-Linker segment by 18 residues causes the protein to crystallize in a completely different space group and an additional portion of the N-Linker can now be seen. **Figure 4.10,** in particular, shows how the N-Linker is ordered by the β4-β5 loop of the symmetry-related dimer and also shows how cAMP binding to one dimer will not only release its own associated C-subunit through previously described interactions with its own C-Linker; it will also unleash the adjacent heterodimer through its interactions with the N-Linker. In our model, binding of cAMP to one of the R-subunits in the tetramer will directly affect the linker of the other R-subunit, thus promoting dissociation of both C-subunits and contributing to the enhanced allostery that is characteristic of the tetrameric holoenzyme.

The interface between the two heterodimers in our model also highlights two regions that are highly conserved in RIa but are different in the RII subunits. This suggests that the observed interaction is not a result of random crystal packing but is biologically relevant. One such region is the b4-b5 loop, which is linked to a motif that is referred to as the "Base Binding Region" (McNicholl et al., 2010; Rehmann et al., 2003) because it makes a hydrophobic contact to the adenine ring (nucleobase) of cAMP. Specifically, Val^{182} in b4 together with Ala^{210} and Ala^{211} form one side of the hydrophobic cap that provide the docking site for the adenine ring of cAMP (**Fig. 4.7**).

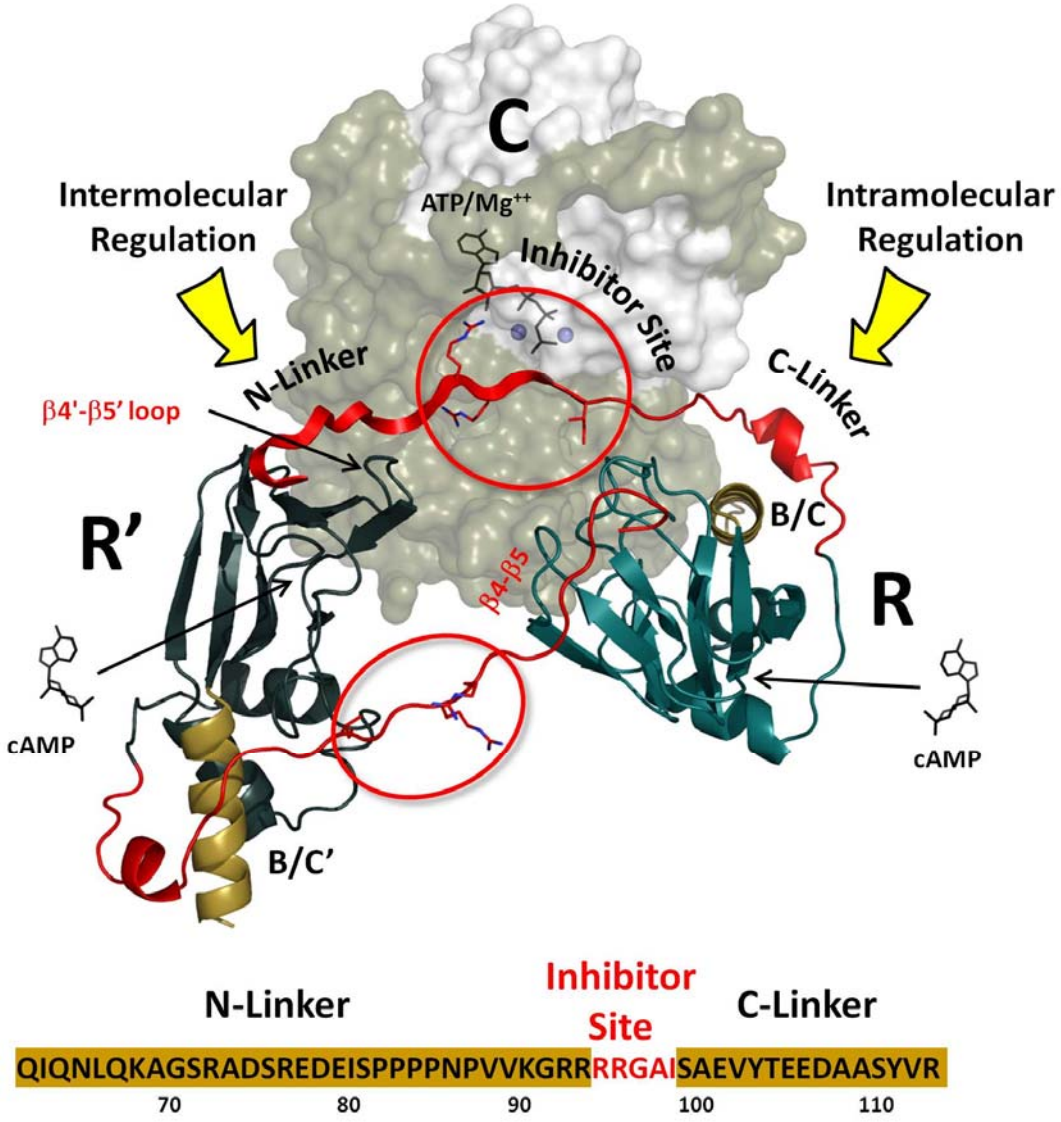

Figure 4.10. Proposed model of intra- and inter-molecular regulation of PKA by cAMP. C-linker of each R-subunits in the tetramer is controlled by its own CNB-A domain. N-linker is controlled by the symmetry related R'-subunit.

The adjacent loop itself is not conserved through different CNB domains but is highly conserved in RIα subunits (**Fig. 4.3B).** In all of our previous structures this loop is exposed to solvent. Here we see a molecular explanation for the conserved residues, as they bind to another RIa-specific region of the N-linker, the segment that precedes the Inhibitory Site (**Fig. 4.1**). It is the complementarily between these two sites that provides an explanation for their conservation.

Convincing evidence that this tetrameric configuration of the two RIα heterodimers reflects the general conformation of the full length tetrameric holoenzyme comes from our previous analyses of the RIα holoenzyme conformation in solution using SAXS and SANS. The proposed model of the tetrameric holoenzyme that we built here based on the RIa(73-244) crystal structure is consistent with low resolution models based on SAXS/SANS data reported earlier (Heller et al., 2004) and additional SAXS experiments of the RIα(1-259):C complex. Even more convincing is the substantial separation of the C-subunits in the complex. This was first detected by SANS experiments and is also reflected by our model. Additionally this model is supported by mutagenesis of the b4-b5 loop demonstrating that alteration of the predicted interface in the tetramer perturbs cAMP dependent activation of PKA (**Fig 4.8)**. While details of this model obviously need to be confirmed by further biochemical studies as well as by further structures, it provides for the first time a framework for understanding how the tetramer can be allosterically regulated, potentially in both positive and/or negative ways, that would not be possible in the simple heterodimer. It also emphasizes how important it is to obtain structures of

larger complexes that more accurately reflect full-length proteins if we are to appreciate the full allosteric potential of the highly dynamic signaling proteins.

Chapter 4, in its entirety, has been published as Realizing the allosteric potential of the tetrameric protein kinase A RIalpha holoenzyme. Boettcher, A.J., Wu, J., Kim, C., Yang, J., Bruystens, J., Cheung, N., Pennypacker, J.K., Blumenthal, D.A., Kornev, A.P., and Taylor, S.S. (2011). Structure *19*, 265-276. The dissertation author was a secondary author of this work.

Chapter 5

Structural and Functional Implications of RIα Acrodysostosis-1 Mutations

5.1 Introduction

In the absence of cAMP, protein kinase A (PKA) exists in an inactive complex composed of a regulatory (R) subunit dimer bound to two inhibited catalytic (C) subunits. Any mutation to the R subunit that either enhances or abrogates PKA activity results in aberrant signaling responsible for memory defects, cancer, and endocrine disorders. While there are four regulatory subunit isoforms (RIα, RIβ, RIIα, and RIIβ) of PKA that are expressed in mammals, their tissue distribution und functions are non-redundant. These isoforms share a general domain organization containing the N-terminal dimerization/docking domain (D/D), a linker with an inhibitor site, and two consecutive C-terminal cAMP binding domains (CNB-A, CNB-B); however, these isoforms are functionally non-redundant as their cAMP response profiles as well as their knock-out phenotypes in mice are different. Furthermore, soleley knock-out mice of RIα are embryonically lethal, thus indicating that RIα is pivotal and essential for survival (Boshart et al., 1991; Jones et al., 1991). As a result, RIα is the main regulatory subunit directly linked to cause human disease.

One such disease is Carney Complex (CNC) disease, which is an autosomal-dominant syndrome associated with mutations in the PRKAR1A gene, effectively disrupting RIα inhibition and leading to overactive catalytic (C) subunit. A majority of the approximately 120 mutations discovered so far to cause CNC disease are subject to nonsense mediated mRNA decay (NMD), which leads to haploinsufficiency of RIα protein levels in cells. The C subunits of PKA thus phosphorylate substrates in a cAMP-uncoupled signaling manner. Furthermore, in some patients the RIα mutant

proteins escape NMD and are expressed; these mutants are dysfunctional and therefore lead to CNC. The molecular causes for dysfunction of RIα are diverse but many mutations have been found localized to the N-terminus and CNB-A domain. Several mutations are located near the cAMP binding pocket and others are involved in the binding interactions with the C subunit, but residues with less understood roles have also been documented.

Contrary to CNC disease, hormone resistance and lowered PKA activity was observed in acrodysostosis (ACRDYS) patients and subsequently mutations in the PRKAR1A gene (ACRDYS1) and more recently in the PDE4D gene (ACRDYS2) were found (Linglart et al., 2011; Nagasaki et al., 2012). ACRDYS is a rare syndrome characterized by severe physical malformations due to skeletal dysplasia present already at birth of the patients. Short metacarpals and metatarsals of the hands and feet, cone-shaped epiphyses, midface hypoplasia, and overall short stature, are some of the reported physical characteristics of this disease (Ablow et al., 1977). In addition, developmental delay and intellectual disability accompanies the effected patients of this autosomal dominant genetic syndrome (Linglart et al., 2011; Nagasaki et al., 2012).

Reports suggested that the expressed mutant RIα associated with the acrodysostosis patients is likely linked to the disease symptoms (Linglart et al., 2011; Nagasaki et al., 2012). One particular mutation is found in several unrelated patients and results in a deletion of the C-terminus of RIα. Specifically, Arg366 becomes a stop codon leading to an expressed mutant protein that is missing the last 14 residues

(Δ366-379 RIα). Through structural and biochemical characterization, crucial elements in the CNB-B were revealed to contribute to the cAMP binding and activation properties of RIα. Particularly dramatic and relevant for this study are the perturbations caused by mutation of several residues in the C-terminus. These, together with the experiments carried out with the ACRDYS1 Δ366-379 RIα protein give insights for the hormone resistance observed in patients.

In an attempt to understand the molecular dysfunction at hand from a structural point of view, this study takes a closer look at ACRDYS1 mutations found in patients so far. First, we discuss the functional hot-spots responsible for causing dysregulated PKA in the ACRDYS1 mutations. Next, we use crystallography to investigate the acrodysostosis heterodimer [Δ1-91 + Δ366-379 RIα]:[C] complex to resolve the structural perturbations caused by this C-terminal deletion mutant. This structure shows that crucial C-terminal motifs of the CNB-B are nonfunctional beyond the Δ366-379 deletion alone and that this mutant PKA holoenyme is catalytically quenched.

The C-subunit has been shown to move through the catalytic cycle by adopting several conformations. Structures representative of some of these motions have provided an idea of the dynamic ensemble the C-subunit can traverse to carry out its enzymatic function. Accordingly, the C-subunit state is typically defined by the orientation of the C-lobe and N-lobe as either in an “open”, “closed”, or “intermediate” conformation. A compact C-subunit is usually observed with bound pseudo-substrate and ATP, which create a hydrogen bond network conducive of

closing the active site cleft by bringing the N- and C-lobes together (Zheng et al., 1993). The most distal separation of the N-lobe and C-lobe is seen at the other end of the conformational spectrum with the open C-subunit, found in the apo as well as the inhibitor peptide (IP20) bound enzyme (Akamine et al., 2003; Bastidas et al.; Knighton et al., 1991b). The C- and N-lobe must transition through intermediate steps to become separated, thereby opening the active site for ligand release (Narayana et al., 1997). The mutant RIα used in this heterodimer structure has enabled us to capture a pseudosubstrate R:C subunit complex with only ADP bound weakly in the active site, resulting in several changes near the active site compared to an ATP-bound complex.

While a wild-type holoenzyme crystal structure of RIα has remained elusive, utilizing this cAMP-desensitized ACRDYS-1 RIα we were able to crystallize and solve a low resolution structure of the Δ366-379 $RI\alpha_2$:C_2 complex. This holoenzyme reveals a conformation and molecular assembly of the dimer of heterodimers $(RI\alpha:C)_2$ that is compared with small angle X-ray scattering (SAXS) data. The non-canonical conformation seen in this structure is unusual most likely due to its more cAMP resistant characteristics.

5.2 Experimental Procedures

Protein Expression and Purification - Bovine full-length wild-type (1-379), deletion mutant Δ366-379, deletion mutant Δ371-379, and double deletion mutant Δ1-91 + Δ366-379 RIα proteins were purified as described previously (Su et al., 1995;

Wu et al., 2004b). The acrodysostosis mutation constructs Δ366-379, Δ371-379, Δ1-91 + Δ366-379 and were generated by QuickChange site-directed mutagenesis. Expression was carried at out at 16°C for 16-20 hours in *E.coli* BL21 (DE3) from Novagen suspended in YT Media. In summary, a combination of ammonium sulfate precipitation, affinity chromatography with cAMP-resin and size-exclusion chromatography were utilized to achieve >94% pure protein. Briefly, following expression cells were lysed with a Microfluidizer processor at 18,000 psi, centrifuged at 16,000 rpm, and the soluble fraction was then ammonium sulfate precipitated. The ammonium sulfate pellet was resuspended and batch bound over night to cAMP resin. After elution from the resin with 40mM cAMP the elution was applied to a Superdex™ 200 gel filtration column utilizing a buffer containing 50mM MES (pH 5.8), 200mM NaCl, 2mM EGTA, 2mM EDTA and 5mM DTT. Murine catalytic subunit of PKA was purified as documented previously (Gangal et al., 1998).

Holoenzyme Formation – Mutant and wild-type holoenzymes were formed by combining R and C subunits in a 1.2 to 1 molar ratio followed by two 24 hour dialysis in holoenzyme buffer (10 mM Mops pH 7, 50 mM NaCl, 2mM $MgCl_2$, 0.2 mM ATP, 1 mM TCEP-HCl). To isolate the complex the dialyzed protein was run over an S200 gel filtration column and resulted in a > 96% pure R:C preparation.

PKA Activation / IP-20 - The activation of wild-type and mutant RIα holoenzymes was investigated by a fluorescence polarization assay (Saldanha et al.,

2006). Holoenzymes were formed with molar ratio of 1.2 mol RIα to 1 mol C subunit and diluted in buffer containing 20 mM Hepes (pH 7), 75 mM KCl, 0.005% Triton X-100, 1 mM ATP, 1 mM DTT, and 10 mM $MgCl_2$. A 20-residue long PKA inhibitor peptide (IP-20) labeled with succinimidyl activated carboxyfluorescein (FAM-IP20) was added to RIα holoenzymes, followed by addition of cAMP to activate PKA. The working concentration of C subunit was 12nM, FAM-IP20 was 2nM, and 2-fold serial dilutions from 2000 - 0 nM cAMP were added to initiate holoenzyme dissociation and FAM-IP20 binding to the C subunit. Fluorescence polarization readings with excitation at 485 nm and emission at 535 nm were carried out with a GENios Pro micro-plate reader (Tecan) using black flat-bottom Costar® assay plates. Each protein was tested in quadruplicate and the data were analyzed with Prism 4.

Crystallization and Structure Determination of the Acrodysostosis Δ1-91 + Δ366-379 RIα:C Heterodimer - Purified RIα (92-365) was combined with purified C-subunit peak 1 to make the heterodimer complex as described above. The purified complex was concentrated to 10 mg/ml with a 30K MWCO concentrator and then centrifuged at 14,000 rpm for 10 minutes to remove particulate contamination. Crystallization trays were set up by hanging-drop vapor diffusion with various commercially available screens at 50% protein plus 50% screen buffer at 22°C. Several crystal hits were obtained with the best condition that yielded a 3.56Å structure being composed of 0.2 M Sodium thiocyanate and 20% PEG 3350 with the protein at a final concentration of 5 mg/ml in a 1.6 µl drop.

Rod-shaped crystals (**Fig. 5.1B**) were flash frozen in liquid nitrogen after soaking in a cryoprotectant composed of mother liquor supplemented with 15% Glycerol. X-ray diffraction data sets were collected at the Advanced Light Source, Berkeley California beamline 8.2.2 from one crystal and processed with HKL2000 (Otwinowski and Minor, 1997). This resulted in a P_1 space group and cell dimensions of a=60.1 Å, b=66.8 Å, and c=87.9 Å (Table 5.1). The best dataset resulted in a structure solution with final resolution of 3.56 Å. The acrodysostosis heterodimer crystals grew in a unique morphology and space group as compared to previous structures of RIα:C heterodimers (Boettcher et al., 2011; Kim et al., 2007; Kim et al., 2005). The structure was solved using the RIα:C (2qcs) heterodimer structure with pdb access code (2qcs) as a molecular replacement probe and the last 14 residues deleted (Su et al., 1995). Deletion of the N-terminus in the otherwise complete construct (92-379), containing both full-length CNB domains A and B as well as the C-terminal tail of RIα, presumably enabled the favorable packing interactions that ultimately aided in the crystallization and high resolution of that structure (pdb id 2qcs). Particularly notable is the insertion of the C-terminal tail of RIα into a pocket of the adjacent heterodimer. The C-tail docks into a space created by the C subunit and CNB-A of the corresponding R subunit (**Fig. 5.1A**). Packing of the ACRDYS1 RIα heterodimer within the crystal lattice is different from any of the previous structures (**Fig. 5.1C**), likely partially due to the C-terminus being truncated.

While set-up with ATP/Mg, the F_o-F_c density at 3-σ level is not complete for the entire ATP molecule in the active site of two C-subunit molecules in the ASU. In

addition, electron density for Mg ions cannot be located. The final model includes residues 1-357 for the R-subunit, residues 13 to 358 of the C-subunit and ADP with 80% occupancy. The R and R-free are 25 and 30 respectively, and the structure model has a good geometry as evaluated with PROCHECK (Laskowski R A, 1993)(**Table 5.1**).

Table 5.1. Data collection and refinement statistics

	RIα(91-365):C
Data collection	
Space group	P1
Cell dimensions□□ (Å)	
a	60.1
b	66.8
c	87.9
α□□□ (°)	101.8
β□□□ (°)	89.4
χ (°)	105.3
No. of molecule per asymmetrical unit	2
Resolution (Å)	3.56
R_{merge}	0.155 (0.49)
Completeness (%)	98.6 (98.2)
I/sigma	11.8 (4.1)
No. reflections	15767
Refinement	
Resolution (Å)	50.0-3.56
R_{work} / R_{free} (%)	26.6/32.2
R.m.s. deviations	
Bond lengths (Å)	0.009
Bond angles (°)	1.7
Ramachandran angles (%)	
most favored	93.9
disallowed	none

*Values in parentheses are for highest-resolution shell:(3.56-3.63Å)

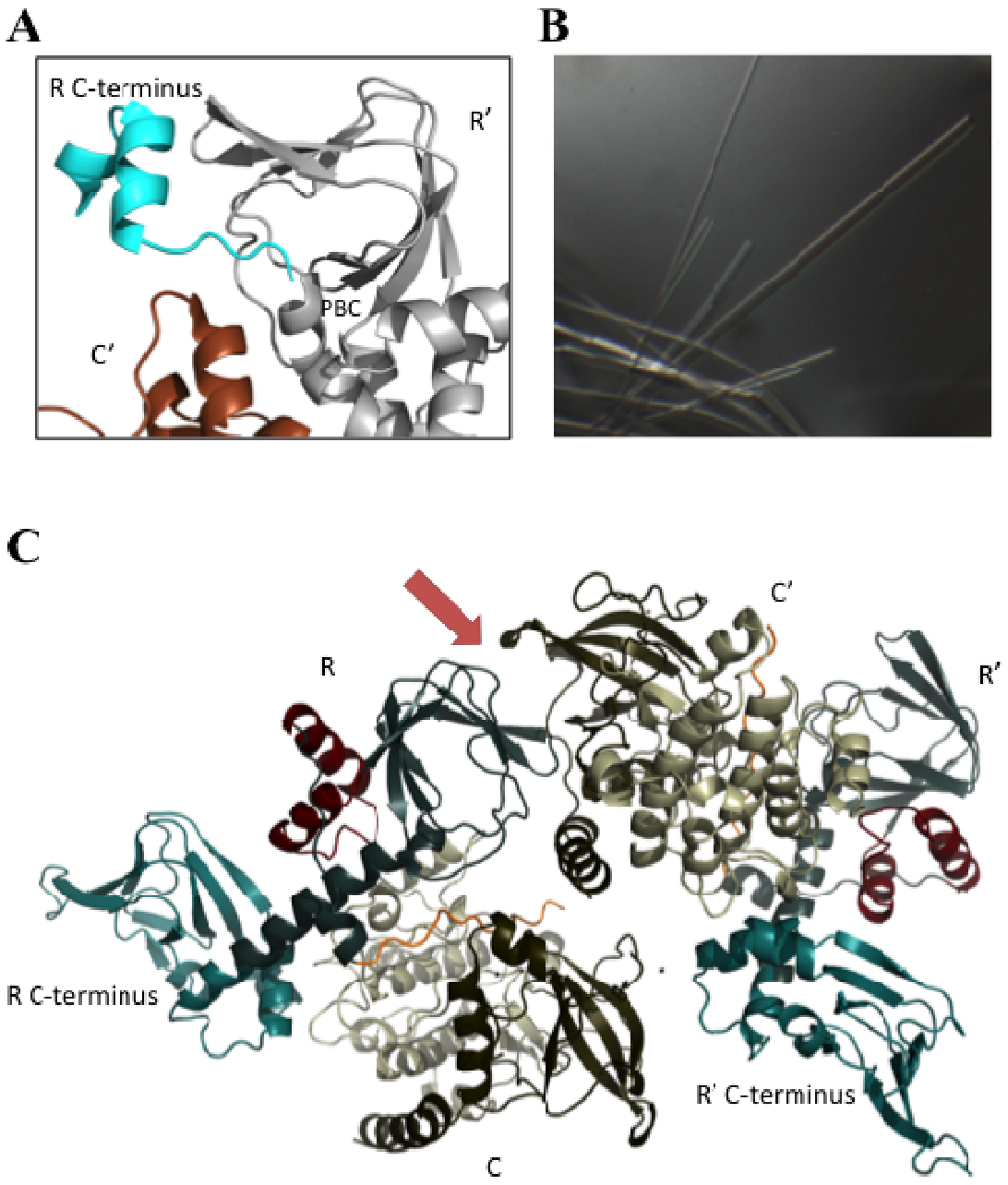

Figure 5.1. RIα heterodimer crystallization. (**A**)Packing in the full-length RIα:C structure (pdb id 2qcs).The C-terminus of one R-subunit (green) inserts in a pocket of the adjacent heterodimer R':C' (grey and brown respectively). (**B**) Rod-shaped crystals of the ACRDYS-1 RIα:C heterodimer complex. (**C**) Crystal–packing of two ACRDYS-1 RIα:C heterodimers in the asymmetric unit. Indicated with a red arrow is the main packing interaction between the CNB-A of one protomoer (R) and the N-lobe of the adjacent heterodimer C'-subunit.

Crystallization and Structure Determination of the Acrodysostosis Δ366-379 RIα$_2$:C$_2$ Holoenzyme - Purified RIα (1-365) and (1-370) holoenzymes were concentrated to 10 mg/ml with a 30K MWCO concentrator. Protein was then centrifuged at 14,000 rpm for 10 minutes to remove particulate contamination and was set up by hanging-drop vapor diffusion with various commercially available screens at 50% protein plus 50% screen buffer at 4°C and 22°C. Several crystal hits were obtained for the Δ366-379 RIα:C complex but no crystals grew for the Δ371-379 RIα:C complex. The best condition that yielded the 5Å structure was composed of .1 M Hepes pH7, 10% PEG 4000, 10% Isopropanol with the protein at a final concentration of 10mg/ml in a 1.6 µl drop. SDS gel analysis of the crystals confirmed the presence of non-proteolyzed R and C subunits.

Crystals were flash frozen in liquid nitrogen after soaking in a cryoprotectant composed of mother liquor supplemented with 20% Glycerol. X-ray diffraction data sets were collected at the Advanced Light Source, Berkeley California beamline 8.2.2 and processed with HKL2000 (Otwinowski and Minor, 1997). This resulted in a $C222_1$ space group and cell dimensions of a=83.1 Å, b=143.3 Å, and c=559.9 Å (Table 5.1). The best dataset resulted in a structure solution with final resolution of 5 Å. The acrodysostosis holoenzyme crystals grew in a unique morphology and space group as compared to previous holoenzyme structures and of RIα:C heterodimer structures. The structure was solved using the RIα:C (2qcs) heterodimer structure with pdb access code (2qcs) as a molecular replacement probe and deleting the last 14 residues from the RIα chains (Su et al., 1995). The positive F_o-F_c density at 3-σ level

is visible for each of the two ATP molecules in their binding pockets. The final model includes residues 92-357 for each chain of (R) (**Table 5.2**).

Table 5.2. Data collection statistics Δ366-379 RIα$_2$:C$_2$

	RIα(1-365)$_2$:C$_2$
Data collection	
Space group	$C222_1$
Cell dimensions (Å)	
a	83.1
b	143.3
c	559.9
No. of molecule per asymmetrical unit	1.5
Resolution (Å)	5.0
R_{merge}	0.124 (0.47)
Completeness (%)	90.5 (65.3)
I/sigma	8.0 (1.6)
No. reflections	13732

Small Angle X-ray Scattering – Holoenzymes were purified as described above and the final buffer composition was 10 mM Mops pH 7, 50 mM NaCl, 2 mM $MgCl_2$, 1 mM TCEP-HCl and 0.2 mM ATP. Immediately prior to the SAXS experiments purified holoenzyme complexes were concentrated to a final concentration of ~8-12 mg/ml using using 30,000 MWCO Millipore concentrators then filtered using 0.2 micron Z-spin microfuge filters. The SAXS data were collected for 90 min for the wild-type and mutant samples. SAXS data were acquired at 12 °C using the SAXSess (Anton Paar) line collimation (10 mm) instrument at the University of Utah. Data were collected using an image plate detector and normalized buffer subtraction and data reduction to I(q) versus q ($q = (4\pi\sin\theta)/\lambda$; 2θ is the scattering angle; $\lambda = 1.54$ Å CuK_α) was carried out using the program SAXSquant 2.0. P(r) functions for the experimental and theoretical scattering were calculated using GNOM (as implemented in ATSAS 2.5.0; (Svergun, 1992)). The experimental scattering data were corrected for smearing effects in GNOM using beam length profile parameters measured at the time of protein data collection. The theoretical scattering profile for the Δ366-379 $RI\alpha_2$:C_2 complex crystal structure was calculated using CRYSOL.

5.3 Results

Analysis of the ACRDYS1 mutations - Several mutations in the RIα gene have been found in patients with acrodysostosis-1 and most of them cluster around the cyclic nucleotide-binding domain B (CNB-B) (**Fig. 5.2**). The CNB-B domain has been called the gatekeeper CNB where cAMP is thought to bind first and initiate the C-subunit release. Beginning with residue 245, CNB-B contains several structural motifs that are conserved among cyclic nucleotide binding proteins and major conformational changes occur in a correlated fashion from the C-subunit bound to the cAMP-bound state (Kornev et al., 2008). The importance of several amino acids located within the CNB-B has been analyzed by mutational studies and published (Bubis et al., 1988a; Herberg et al., 1996; Kim et al., 2007).

The crucial role for several of the CNB-B residues are now further validated by the discovery that when mutated they can cause disease in humans. Mutations so far found in patients with acrodysostosis-1 cluster mainly around the PBC (residues 323-335) and C-terminus of CNB-B, indicating that perturbations in these areas have substantial effects on the activation potential of RIα PKA to the extent of causing physiological effects and thereby disease (**Fig. 5.2**). Five residues associated with ACRDYS1 are either structurally close to the PBC (Gln283Arg and Gly287Glu) or part of the PBC (Iso325Thr , Ala326Val and Arg333Leu/Pro/Cys) in the CNB-B (Lee et al., 2012; Linglart et al., 2012; Muhn et al., 2013). Gln283 and Gly287 are in the β2-β3 loop, which is stacked on top of the PBC. Gln283Arg and Gly287Glu mutations have been found in patients. Surprisingly, mutating Gly287 to Trp causes

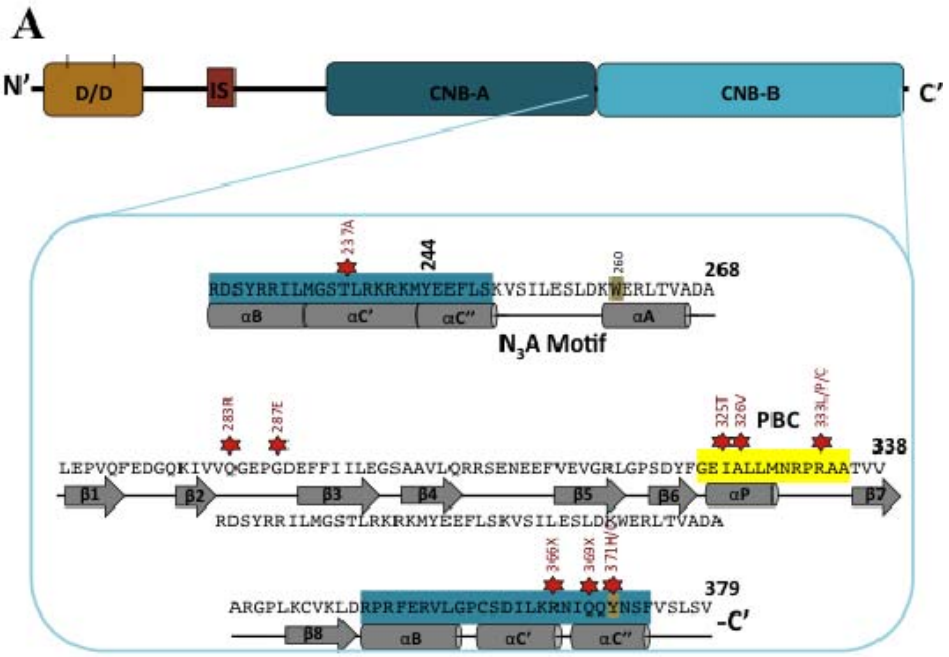

B

RIα Residue	Position	Protein change
Ala 211	PBC CNB-A	Ala➔Thr
Thr 237	αB-αC helix	Thr➔ Ala
Gln 283	β2-β3 loop CNB-B	Gln➔ Arg
Gly 287	β2-β3 loop CNB-B	Gly➔ Glu
Iso 325	PBC CNB-B	Iso➔ Thr
Ala 326	PBC CNB-B	Ala➔ Val
Arg 333	PBC CNB-B	Arg➔Leu/Pro/Cys
Arg 366	αB-αC helix	Arg➔ stop
Gln 369	αB-αC helix	Gln➔ stop
Tyr 371	αB-αC helix	Tyr➔ His/Cys

Figure 5.2. Location of ACRDYS1 mutations. (**A**) Shows the domain organization of RIα with the CNB-B sequence and the locations of ACRDYS1 mutations (**B**) List of the known PRKAR1A mutations to cause acrodysostosis-1. Mutations are sorted by their position along the gene.

causes a decrease in cAMP binding and an increase in PKA activity (Greene et al., 2008). Gln283 and Gly287 are also in close proximity to the essential PBC Arg333.

An Arg333Lys mutation was originally discovered in S49 mouse lymphoma cells and later shown to cause cAMP resistance of the associated R:C holoenzyme (Murphy and Steinberg, 1985; Steinberg et al., 1987). Artificially mutating this arginine to a lysine enabled the crystallization of the RIα:C heterodimer complex (Kim et al., 2007) as it stabilized complex formation by rendering this RIα mutant cAMP resistant. It was subsequently shown with SAXS that the Arg333Lys mutant caused the R:C dimer to be more compact compared to the wild-type complex (Cheng et al., 2009). Three separate amino acid changes have been detected in patients solely for Arg333 as it has been found mutated to a Leu, Pro, or Cys. Arg333 is important for high affinity binding of cAMP to CNB-B as it binds directly to the phosphate of cAMP and mutations in this area are likely to interfere with this crucial interaction. Furthermore, the mutations Iso325Thr and Ala326Val are located on the small α helix that is part of the PBC of CNB-B, thereby likely destabilizing cAMP binding and PKA activation (Lee et al., 2012; Linglart et al., 2012).

Early studies already hinted at the importance of Tyr371 for cAMP binding and this has been confirmed with structural studies (Bubis et al., 1988b; Kapphahn and Shabb, 1997). Tyr371 was shown by Kim et al 2007 to play a crucial role structurally and biochemically (Kim et al., 2007). The cAMP-bound structure of RIα revealed Tyr371's capping function as it is seen stacked above the adenine ring of cAMP (Su et al., 1995)

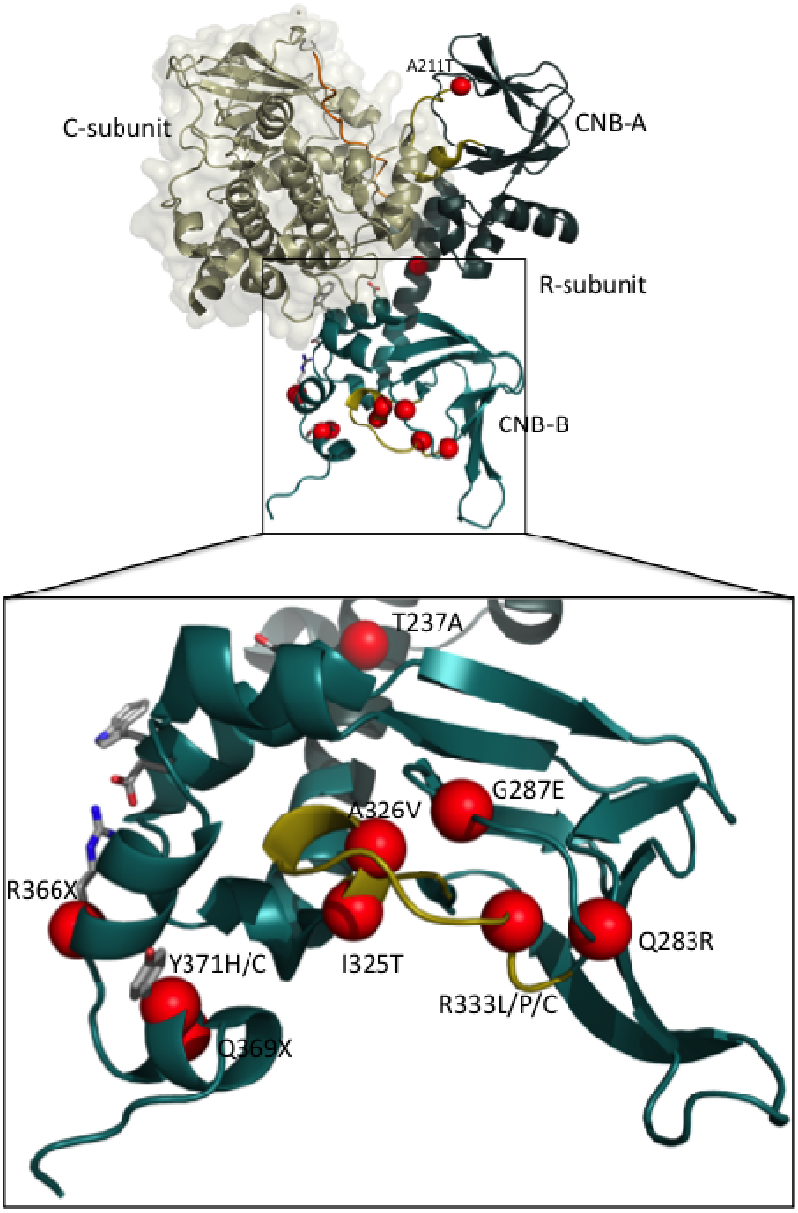

Figure 5.3. RIα acrodysostosis mutations mapped onto the C-subunit bound structure (pdb 2qcs). (**C**) The thus far known acrodysostosis-1 mutations have been mapped onto the RIα structure in the C-bound conformation (pdb 2qcs). A majority of the point mutations in addition to the C-terminal deletion mutants are located near the C-terminal CNB-B domain

This tyrosine has been found mutated to histidine and cysteine by exome sequencing in acrodysostosis patients and may lead to dysfunctional PKA activation by eliminating the capping mechanism required for a stably bound cAMP ligand (Michot et al.) (Muhn et al.).

Two positions within the RIα gene cause truncation of the C-terminus. The longer truncation published mutation represents the most frequently identified mutation linked to ACRDYS1. It causes a heterozygous cytosine-to-thymidine substitution at position c.1101 in exon 11. This recurrent mutation thus results in the conversion of the conserved Arg366 to a stop codon and deletion of the C-terminal 14 residues (Linglart et al., 2011). Expression of the mutant messenger RNA and protein was detected in the patients and suggests that the presence of a heterozygous pool of wt and this functionally impared R-subunit can lead to physiological effects. According to the structures solved thus far the fragment of residues missing are not part of an R-subunit to C-subunit interface but play roles mostly for the cAMP binding events. The capping residue Tyr371 is missing and thus even if cAMP can bind in the PBC it is not stable enough without the hydrophobic cap. Furthermore, Arg366 is part of a salt bridge with Glu261 that was previously studied with mutational analysis that caused a dramatic decrease in the EC_{50} for cAMP activation (Kim et al., 2007). While this implies the importance of this salt bridge for RIα function, in combination with the other residues missing in the ACRDYS1 deletion mutant, the overall effect is inhibitory and likely increases the requirement for cAMP activation. This is because it

was shown that this protein makes a holoenzyme that is more resistant to cAMP activation as monitored by BRET in cells (Linglart et al., 2011).

Only two mutations were found upstream of the CNB-B. The missense mutation Thr237 to Ala is located on the αB/C helix and potentially interferes with the crucial conformational switch from the contiguous helix in the C-subunit bound to the kinked helix in the cAMP-bound state (Nagasaki et al., 2012). Furthermore, Thr237 is located in a previously proven functional hot-spot as it sits adjacent to Arg241 which makes a salt-bridge with Asp267 and when mutated lowers cAMP binding and disrupts the cooperative coupling between domain A and B (Kim et al., 2007; Symcox et al., 1994). Also in the vicinity is Met234, which was analyzed for its role in the cAMP induced activation pathway(Sjoberg et al.). Gly235 is located at one of the two hinge points of the αB/C helix where a kink is introduced upon cAMP binding. In summary, these mutations support the αB/C helix is emerging as a major transducer of the cAMP signal from CNB-B to CNB-A. Surprisingly, mutations of A211 have been identified in patients with carney comlex and ACRDYS1, where Ala211 to Thr results in ACRDYS1 and Ala211 to Asp causes CNC. This alanine is in the PBC of CNB-A and is conserved among all the PKA R-subunits and thus likely prone to interfere with or enhance cAMP binding affinity of the R-subunit depending on the chemical properties of the amino acid mutation it is replaced with.

To further discern the structural and functional effects ACRDYS1 mutations have and how they contribute to cause disease we crystallized the recurrent C-terminal

deletion (R366 stop) mutant that was found in several ACRDYS1 patients (Linglart et al., 2011; Michot et al., 2012; Muhn et al., 2013).

Overall structure of the acrodysostosis R:C heterodimer complex - To investigate structural perturbations caused by acrodysostosis-1, a crystal structure was solved by forming a heterodimer complex with an N-terminal deletion construct (Δ 1-91) of the recurrent ACRDYS1 mutant (Δ365-379) and full-length C-subunit. This complex, which contains an N-terminal deletion construct (Δ 1-91) to produce the monomeric R-subunit of the acrodysostosis mutant protein, was solved to 3.5 Å resolution (**Table 5.1**). This structure is not representative of the physiological tetrameric R_2C_2 holoenzyme but a basic functional unit of PKA. Structures of N-terminal deletion mutants of RIα provided fundamental information of how the regulatory subunit interacts and inhibits the catalytic subunit (Kim et al., 2007; Kim et al., 2005). Comparing previous RIα structures to our ACRDYS1 complex reveals similarities and distinctions. The rod-shaped crystals show a different packing arrangement of the R:C heterdimer in the crystal lattice, with the RIα CNB-A β4β5 loop docking against the N-terminal tail loop that follows the A-helix (residues 13-30) in the C-subunit (**Fig. 5.1C**).

While the ACRDYS1 construct used for crystallization has the C-terminal amino acids 366-379 truncated, additional residues are missing in the structure with electron density going only up to Leu357 (**Fig. 5.4B**). This indicates that the 366-379 deletion affects additional residues immediately upstream, which become disordered

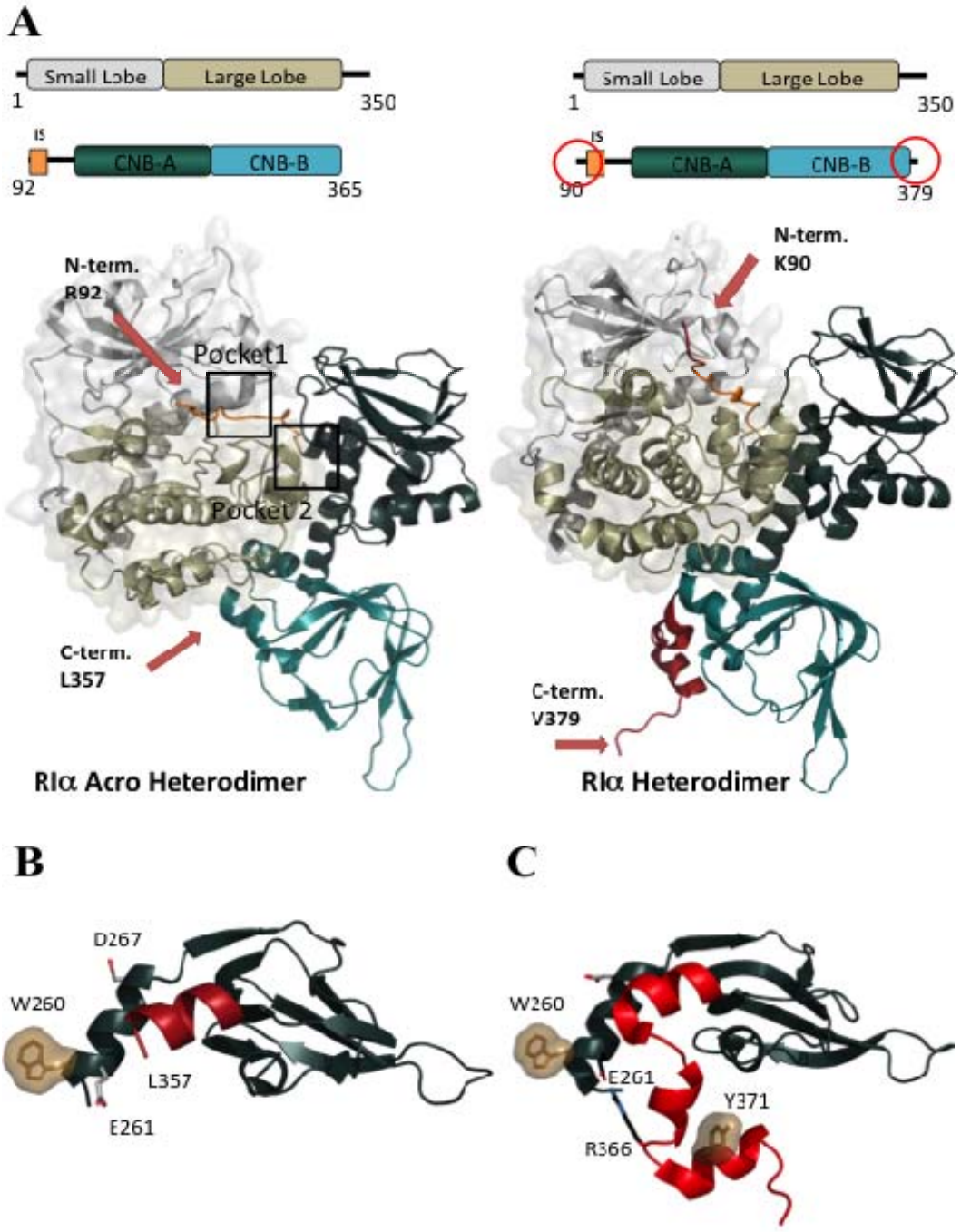

Figure 5.4. RIα acrodysostosis heterodimer structure. (**A**) Overall comparison of the acrodysostosis mutant RIα (left) and the previously published heterodimer (right, pdb 2qcs). (**B**) In the ACRDYS1 Arg366 stop mutant structure residues beyond Leu357 are disordered. (**C**) The full-length RIα C-terminus (shown in the holoenzyme conformation) contains several crucial residues including Arg366 and Tyr371.

and potentially unable to serve their structural and activation functions within the activation pathway. Crucial residues such as Arg366 which is part of the holoenzyme-specific salt-bridge and Tyr371 which is responsible for capping cAMP when bound in the CNB-B, are missing and potentially contribute to the dysfunctional regulatory behavior of this acrodysostosis protein (**Fig. 5.4B&C**). Furthermore, truncation beyond Arg366 also induces residues upstream to be disordered such that the αC following Leu357 cannot stably form. As previous structural and mutational experiments suggested, the CNB-B domain of RIα serves as the gatekeeper for binding cAMP to CNB-A and the ACRDYS-1 mutations interfering with this function effectively disable the progressive cAMP binding to CNB-B and the conformational rearrangements induced thereby.

While the bulk of interactions previously described are conserved in this structure, due to the C-terminal deletion of this mutant crucial binding interactions between the R and C-subunit are perturbed. The inhibitor site bound in the active site of the C-subunit is termed pocket one and shows several noteworthy differences discussed in the next section. Pocket two and three comprise major interactions and result in a large buried surface area between the subunits. Residues 198-205 make up the substrate-binding loop of the C-subunit, also called P+1 loop, and together with the G helix is responsible for the pocket two H-bonding network. Pocket three involves mainly the activation loop of the C-subunit and residues from the αB/C helix and N_3A motif of the R-subunit (**Fig. 5.4B**). The phosphorylated T197 on the C-

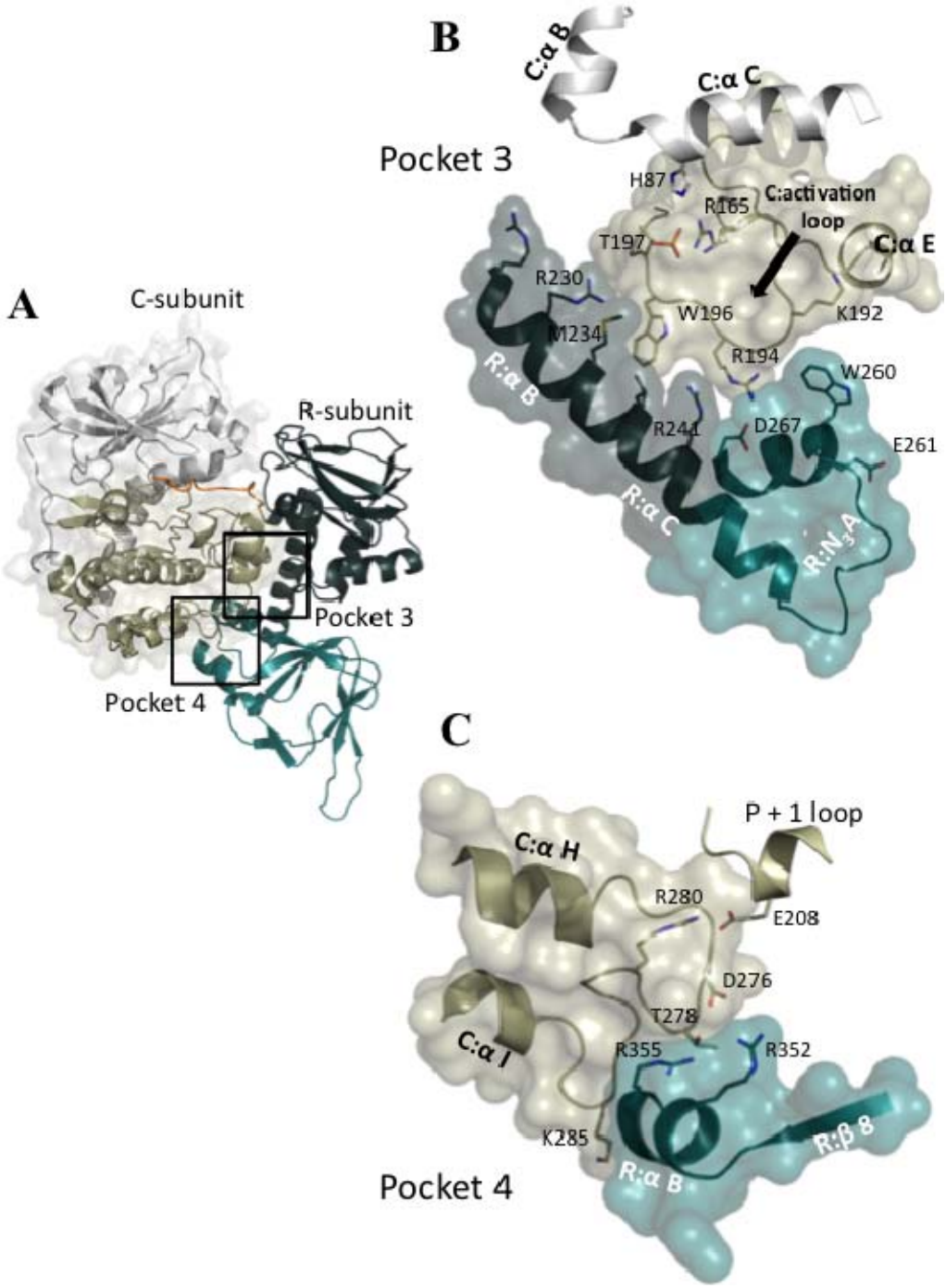

Figure 5.5. ACRDYS-1 R:C-subunit interactions. (**A**) Structure of the RIα:C heterodimer with the C-subunit N-lobe colored in white and the C-lobe colored in olive. The R-subunit linker is colored in orange, the CNB-A is colored in dark teal, and the CNB-B is colored in light teal. (**B**) Zoom of the R:C interaction pocket 3. C-subunit residues are colored in olive and white. R-subunit residues are colored in dark and light tan. (**C**) Zoom of the R:C interaction pocket 4.

subunit activation loop is positioned within a H-bonding network with H87, R165, K189, T195, and Y215. Even though the CNB-B αBαC of the R-subunit is incomplete with the last residue of the αB helix L357, some crucial interactions with the C-subunit are conserved. The two αB helix residues Arg 355 and 352 are taking part in the pocket 4 cluster together with αHαI loop residues D276 and T278 of the C-subunit (**Fig. 5.5C**).

Figure 5.5 demonstrates the impaired cAMP-induced activation in the acrodysostosis R366stop mutant holoenzyme. For the wild-type R:C complex, rearrangement of the αBC helix in CNB-B allows for stable docking of the cAMP molecule to the PBC. An important contributor is Tyr371 as it caps the nucleotide. The αC helix creates a hydrophobic gate and protects the PBC/cAMP pocket from solvent. This results in the movement of the αBC helix inward and the N3A motif upward and breaks the R366-E261 salt-bridge that connected these two motifs in the C-subunit bound conformation. Furthermore, the αBC helix inward-shift toward the PBC also causes release of the important electrostatic cluster between the R-subunit residues Arg355 and Arg352 on the αB helix with C-subunit residues T278 and D276 (**Fig. 5.6 top**). It is these first moments of cAMP binding that the ACRDYS-1 mutant is dysfunctional. While the PBC pocket is solvent accessible in the R:C complex, cAMP cannot stably dock as it is not locket in by the αC helix and is not capped by Tyr371. The by cAMP-docking induced αBC helix rearrangements are dysfunctional and result in inefficient propagation of the following steps, such as breaking the electrostatic cluster between the R-subunit αB helix residues and C-subunit residues of

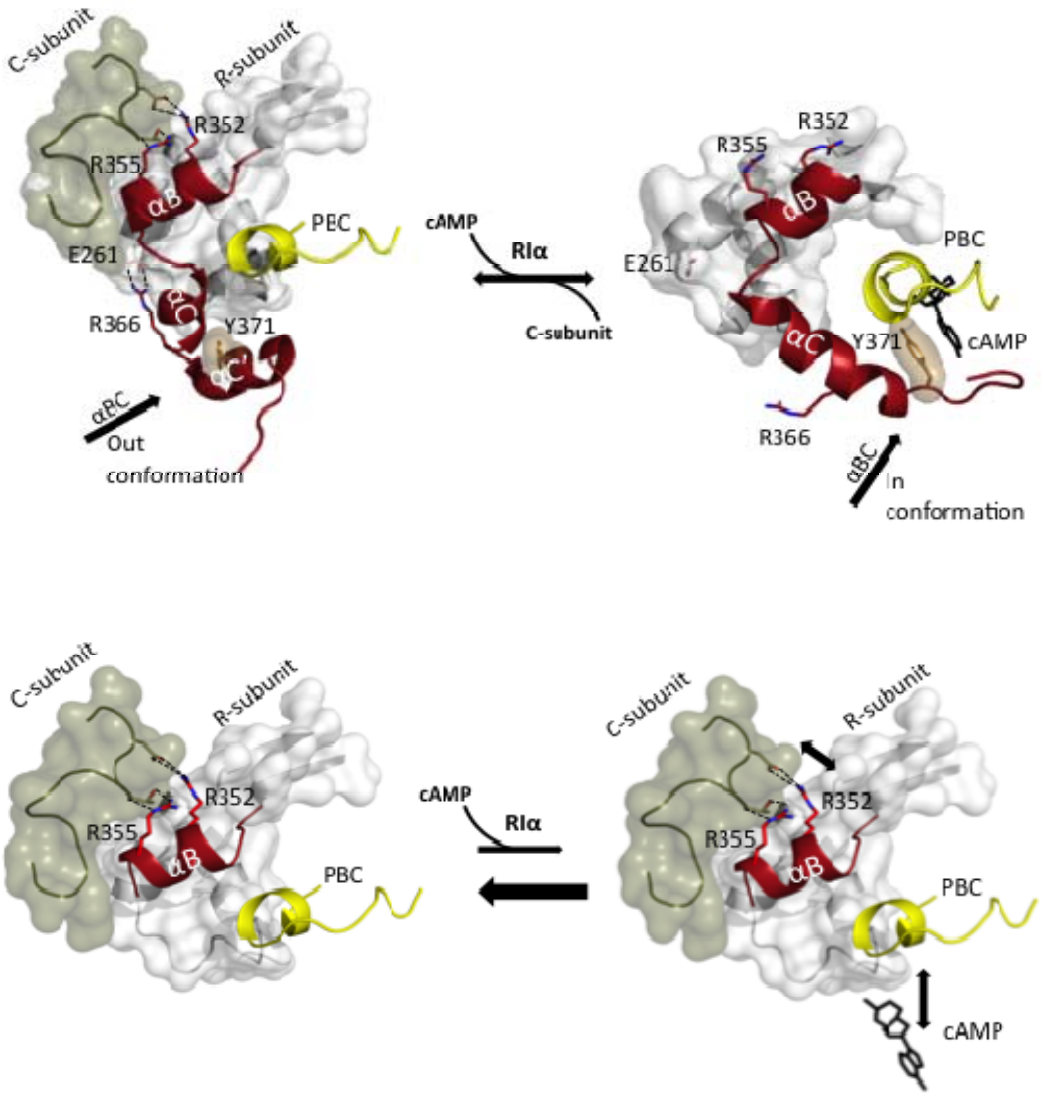

Figure 5.6. cAMP-binding to CNB-B initiates the PKA activation pathway. The top figure illustrates binding of cAMP to the CNB-B domain of the C-bound R-subunit, which causes rearrangement of the N3A motif (white), the αBC helix (red), and the PBC (yellow). To stabilize cAMP in CNB-B the αBC helix moves in towards the PBC to allow the Tyr371 capping interaction. The bottom figure shows the impaired cAMP binding aspects in the recurrent ACRDYS-1 R-subunit. While important R:C-subunit interactions are conserved (bottom left), due to the missing αC helix cAMP cannot stably bind to CNB-B. Thus it cannot initiate the activation-specific rearrangements for propagation of the message to the rest of the complex that would otherwise lead to C-subunit release.

(pocket 4). Disruption of these initial steps thus perturbs the downstream release of the C-subunit, leaving the mutant PKA complex cAMP resistant (**Fig. 5.6**).

Pseudosubstrate C-subunit complex contains ADP - Surprisingly, our R:C complex also enabled the capture of an unusual conformational state of PKA. Structures of RI-bound C-subunits thus far showed the linker and inhibitor site snuggly positioned in the active site (**Fig. 5.7)**. In the structure presented here the RIα linker is more dynamic and density of the whole ATP is not clear. One explanation for this could be that while the purified complex contained ATP, during the crystallization process the γ-phosphate may have hydrolyzed. When ATP was used initially for molecular replacement, strong negative electron density appeared around the γ-phosphate. Also, the omit map at 3σ shows density for ADP.

There is no electron density in the active site for the two magnesium ions that are usually bound together with nucleotide. Once again, when we initially included them in the structure, strong negative electron density appeared and refinement parameters (R-factors) worsened. When ADP and no Mg^{+2} ions are used a decrease in the R factors are seen during refinement. This might be the result of them not being bound consistently in their usual positions in the active site. There are two molecules (two R:C heterodimers) in the ASU and both show similar electron density for the nucleotide and no density for either of the Mg^{+2} ions (**Fig. 5.8**). This suggests that the

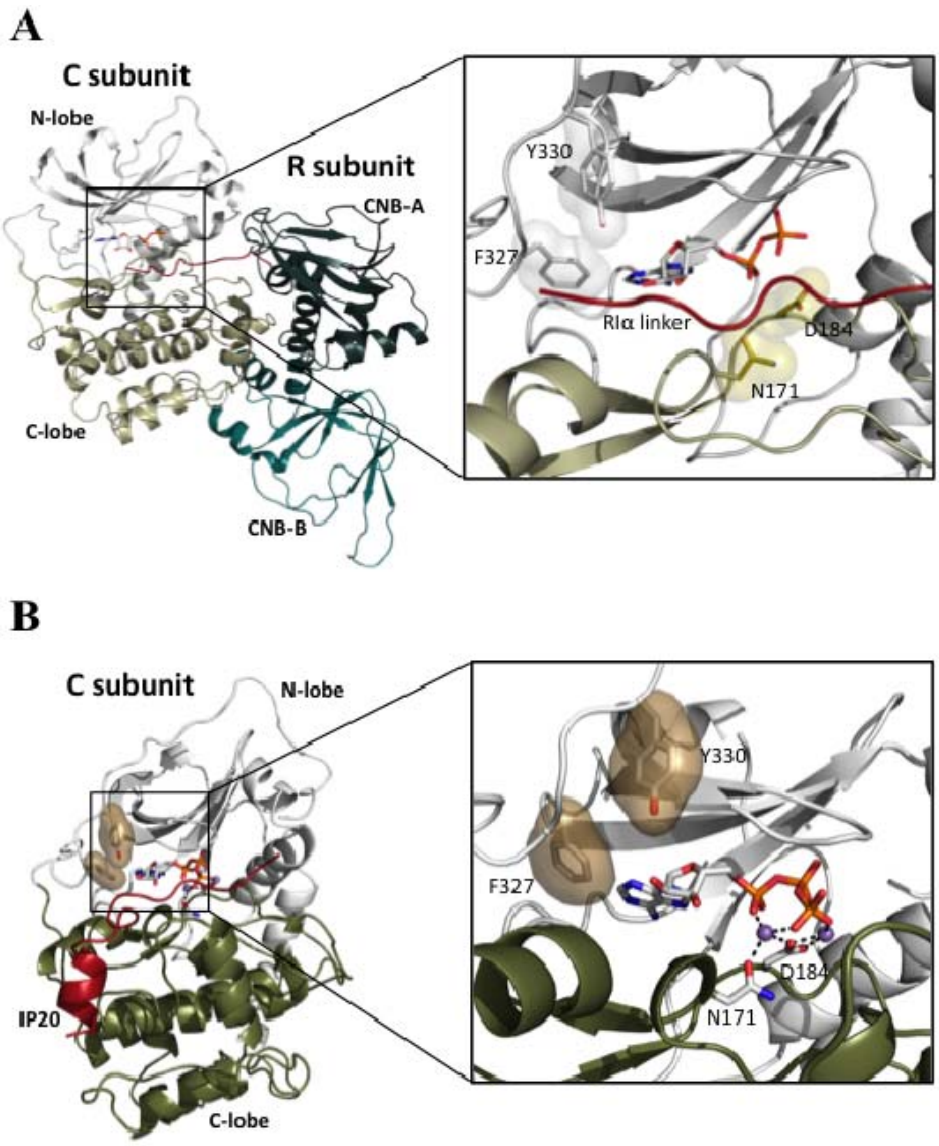

Figure 5.7. C-sununit active-site comparison. Residues with known function for ligand-binding are shown in stick representation and colored by element. (**A**) The overall ACRDYS1 heterodimer structure (left) is shown with a focus on the active site of the C-subunit (right). The C-lobe is colored in light olive and the N-lobe is colored in white. ADP is shown in stick representation and colored by element. The RIα linker is colored in red. (**B**) The overall ternary C-subunit structure (left, pdb 1ATP) is shown with a focus on the active site of the C-subunit (right). The C-lobe is colored in dark olive and the N-lobe is colored in white. The PKI derived IP20 peptide is shown in red. ATP is shown in stick representation and colored by element. Two Mg ions are bound and shown as purple spheres.

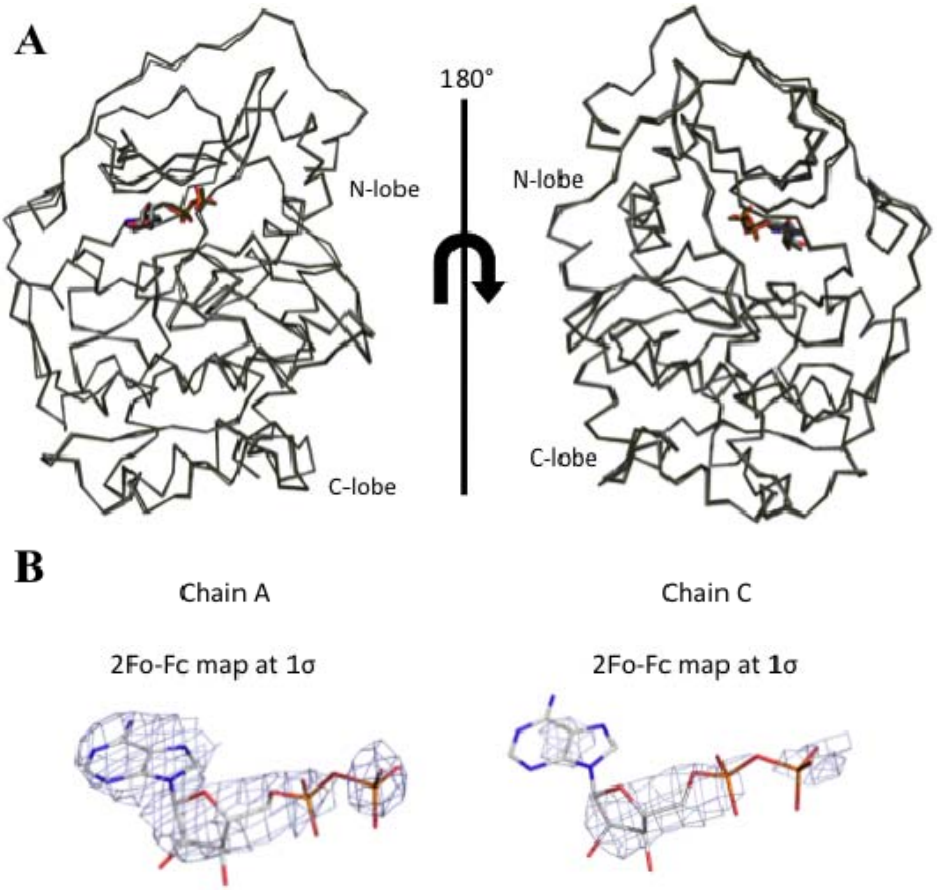

Figure 5.8. The two ADP-bound C-subunit molecules in the ASU. (**A**) The two molecules of the C-subunit within the ASU are shown in ribbon representation and were aligned with each other with chain A shown in grey and chain C shown in olive. ADP is colored by element and is displayed in stick representation. (**B**) Electron density maps for ADP of the two C-subunit chains in the ASU. For chain A (left), and for chain C (right) the 2Fo-Fc maps are shown and were contoured at 1σ.

Mg^{+2} ions may be present but not bound consistently within the active site. Alignment of the two C-subunit molecules found in the ASU (chain A and chain C) results in a root-mean-square deviation of 0.37 Å and indicates that they are overall very similar to each other. Both molecules in the ASU show positive electron density for nucleotide, but density is less strong in chain C compared to chain A. Refinement suggests the occupancy of each ADP molecule in chain A and chain C is 80 % and 60 % respecitively.

Activation of acrodysostosis holoenzymes require more cAMP - Next, we assessed the cAMP requirements for activation of the ACRDYS1 holoenmzymes. This shows a significant increase of the EC_{50} compared to the wild-type holoenzyme. A fluorescence polarization assay was carried out utilizing physiologically relevant holoenzymes that contain the N-terminal D/D domain and thus the dimeric RIα protein bound to two C-subunits. Pre-formed wild-type and mutant holoenzymes are then tested for their ability to bind cAMP for the subsequent release of the R-subunits and binding of the fluorescently labeled 20 residue PKA inhibitor peptide (IP-20) to the active site of the C-subunit (Saldanha et al., 2006). Published studies included biochemical, mutational, and structural experimental data and lead to the widely accepted cAMP-induced PKA activation model (Kim et al., 2007; Ogreid and Doskeland, 1981a, b).

In-line with the PKA activation model and other published proposals of the molecular origin of ACRDYS1 we found that the recurrent RIα C-terminal deletion mutant proteins are cAMP desensitized. While both mutants tested (**Fig. 5.9**, construct

1-365 or Acro1, construct 1-370 or Acro2) show a notable increase in the EC_{50} values for cAMP induced activation, with a ~ 5-fold increase the larger C-terminal deletion of Δ366-379 resulted in a more pronounced effect. This is also the mutant that has been termed the recurrent ACRDYS1 mutant due to its relative high frequency of having been identified in patients. The slightly longer mutant construct of RIα 1-370 (unpublished) also shows an increase in cAMP requirement for activation with an EC_{50} of 169 nM compared to the wild-type EC_{50} of 47 nM (**Fig. 5.9**).

The cooperative pathway for cAMP has been the focus of many studies and lead to the proposal of a highly coordinated pathway of nucleotide binding and conformational rearrangements. This is reflected in the Hill coefficient, where a value of 1 indicates independent binding and a value of above one indicates positive cooperativity. The cooperativity of PKA activation is conserved in the ACRDYS1 mutants that were studied here. The wild-type full-length RIα holoenzyme has a Hill coefficient of 1.8 and the mutant proteins show only slight deviations with 1.6 and 1.9 for RIα 1-365 and RIα 1-370 respectively. Thus, the deletions of the C-terminus of RIα assessed in this study presumably only interferes with the first binding event of cAMP to CNB-B, but once cAMP bound to CNB-B the activation pathway could be initiated and the mutant proteins were not sufficiently interrupting the communication pathway of cAMP binding for PKA activation. Additionally, removing access for cAMP and dynamics of CNB-B allows more flexibility at the N-terminal region of RIα.

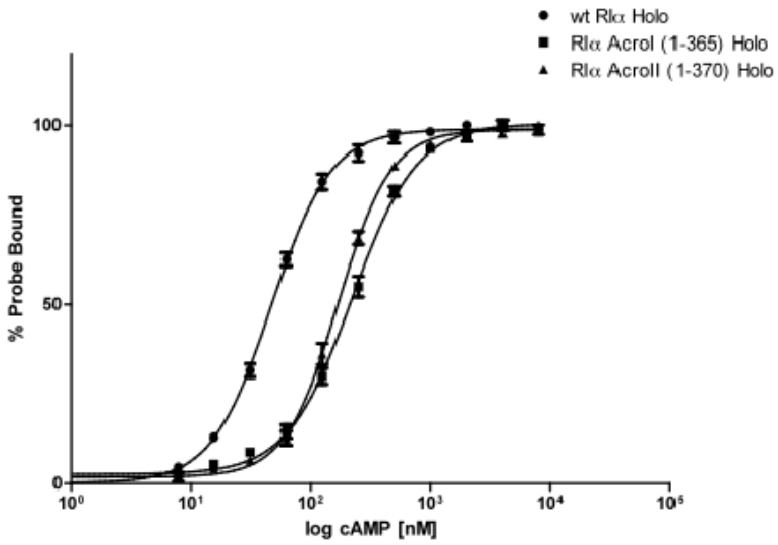

Holoenzyme	EC50 [nM]	Hill Slope
Wild type	47	1.8
Acrol (1-365)	221	1.6
AcroII (1-370)	169	1.9

Figure 5.9. cAMP-induced activation of ACRDYS1 C-terminal deletion mutant holoenzymes. C-terminal deletion mutations of ACRDYS1 were analyzed with a fluorescent polarization assay to monitor changes in the mutant compared to wild-type holoenzymes. Activation profiles of holoenzyme formed with RIα wild type (circles), RIα 1-365 (squares) and RIα 1-370 (triangles) are shown. The curves for ACRDYS1 mutants are similar and show increased EC_{50} values compared to wild-type. GraphPad Prism was used to fit binding curves and the standard error of the mean is shown with error bars.

SAXS analysis of acrodysostosis holoenzymes - To assess possible structural effects of the C-terminal ACRDYS1 mutations in solution, SAXS data was collected for the corresponding holoenzyme complexes formed with RIα 1-365 and full-length Cα subunits. The resulting scattering plots of *I(q) versus q*, Guinier plots and pair-distance distribution functions (P(r)) were compared to the SAXS data for the wild-type full-length RIα holoenzyme published previously (Heller et al., 2004). As judged by the *I(q) versus q* and the linear Guinier plots the samples were free of non-specific aggregation (**Fig. 5.10)**. The overall shape of the mutants is comparable to that of the wild-type holoenzyme but the slightly longer (Q370stop) ACRDYS1 protein appears to show an increase in the bilobal character. The wild-type and R365stop mutant have a major peak at ~40 Å and a shoulder at around 110 Å, which is consistent with previous published characterization for the wild-type holoenzyme (Heller et al., 2004). The Q370stop mutant holoenzyme, while also having a bilobal shape shows a much more pronounced shoulder that is shifted to ~100 Å.

Both mutants show a 10 Å reduction in their D_{max} value to 130 Å compared to the wild-type value of 140 Å. The R_g values for these mutant holoenzyme complexes are also smaller with 43.8 and 45.4 Å for Q370stop and R365stop, respectively, compared to 47.1 Å for the wild-type protein. Due to the C-termini being truncated by 14 and 10 residues respectively a reduction in the maximum linear dimension might be expected but the reductions in R_g and D_{max} we observed were surprisingly large and

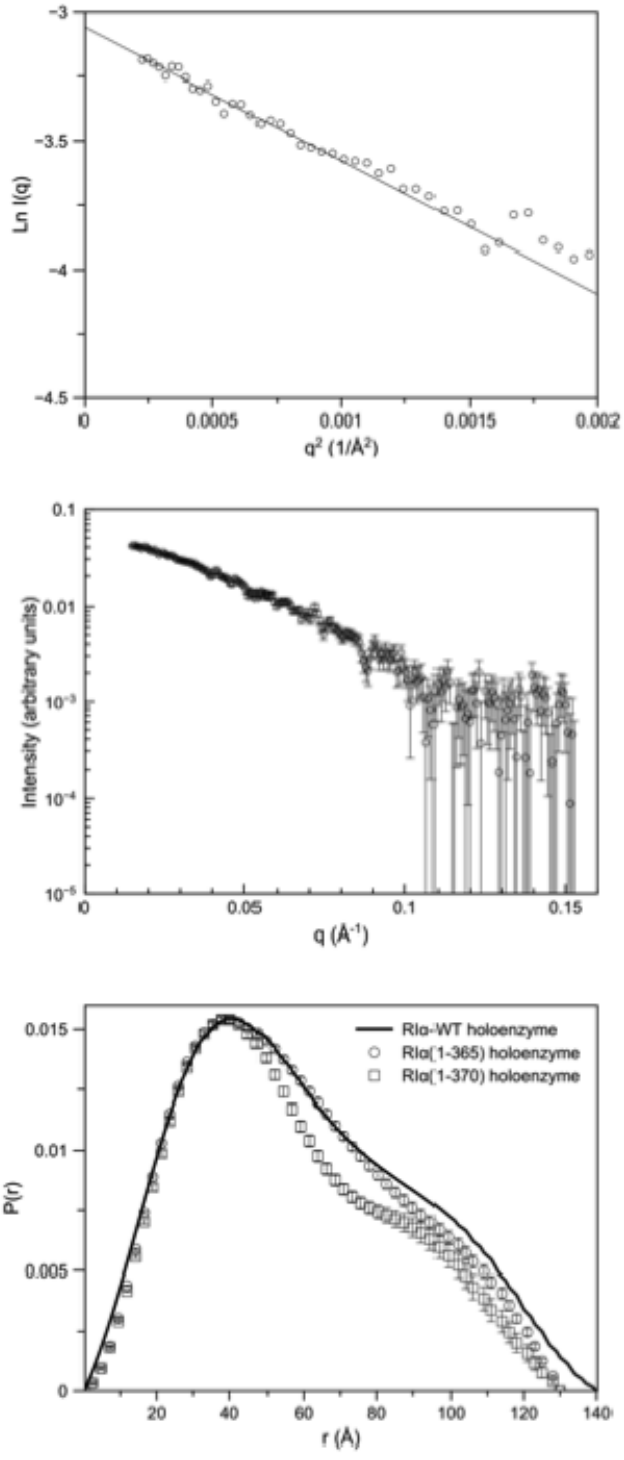

Figure 5.10. SAXS profiles of ACRDYS1 mutants. (Top) Guinier plot, (middle) I(q) vs q, and (bottom) P(r) curves calculated from solution small-angle x-ray scattering data for RIα (1-365) mutant (circles) and RIα (1-370) mutant (squares). Wild-type P(r) curve is from Vigil et al. (2004). P(r) curves have been normalized to area under the curve.

indicative of significant compaction of the mutant holoenzymes molecule in solution compared to the wild-type holoenzyme. These data, together with gel filtration observations prompted us to set-up crystallization trials of the ACRDYS1 RIα 1-365 mutant in complex with the C-subunit since it appears this holoenzyme complex is more compact and would more likely crystallize while maintaining a very similar overall molecular architecture as the wild-type PKA holoenzyme.

Structure of the recurrent ACRDYS1 holoenzyme - The observation that the C-terminal deletion mutants of ACRDYS1 holoenzymes are more compact in-solution and resistant to cAMP-induced dissociation led us to attempt crystallization of the RIα 1-365:C complex. With an intact N-terminus and the D/D domain present, this is the dimer of heterodimers $(RI\alpha:C)_2$ of the PKA holoenzyme and the physiologically relevant state of this mutant RIα. After extensive screening and optimization of the original crystal hit we obtained a 5 Å resolution structure from the diamond shaped crystals (**Fig. 5.11A&B**). The same ACRDYS-1 C-terminal mutant construct that was used for the heterodimer crystals described in the previous sections had the additional N-terminal 1-91 residues truncated, which made that C-bound complex a heterdimer in solution. That construct consistently produced rod-shaped crystals in all of the crystallization conditions discovered (**Fig. 5.11B**). Since RIα is prone to degredation we carried out SDS gel analysis of the $(RI\alpha:C)_2$ diamond shaped crystals and confirmed the presence of full-length ACRDYS-1 RIα (1-365) and C-subunit protein (**Fig. 5.11.B**). While optimization is still being carried out to obtain

higher resolution details, this current structure provides interesting new information. This low-resolution structure is the first holoenzyme crystal structure of the RIα isoform and reveals the architectural arrangement of its subunits.

SAXS had provided the initial clues on the different quaternary structures of the PKA holoenzyme isoforms (Heller et al., 2004; Vigil et al., 2006). The ACRDYS-1 holoenzyme complex crystallized with a unique molecular arrangement within the unit cell and space group ($C222_1$) compared to previous RI and RII structures. The D/D domain and N-terminal linker are not resolved. Lack of the D/D domain and linker electron density was also observed in previous structural studies such as the 2.3 Å resolution RIIβ holoenzyme structure (Zhang et al., 2012) and the 3.8 Å resolution RIα homodimer structure (Bruystens et al., 2014). The R-subunit linkers are predicted to be intrinsically disordered regions and their flexibility was observed already at the early stages of studying PKA (Erlichman et al., 1973; Rannels and Corbin, 1980). Site-directed labeling experiments previously showed that these linkers are highly flexible (Li et al., 2000).

The holoenzyme structure presented here shows a new architectural arrangement of the heterodimers and thus differs from our proposed holoenzyme model (Boettcher et al., 2011). For the holoenzyme model the molecular arrangement of a deletion mutant construct of RIα (74-244) bound to the C-subunit resulted in packing interactions of two heterodimers that were interpreted to be a possible holoenzyme

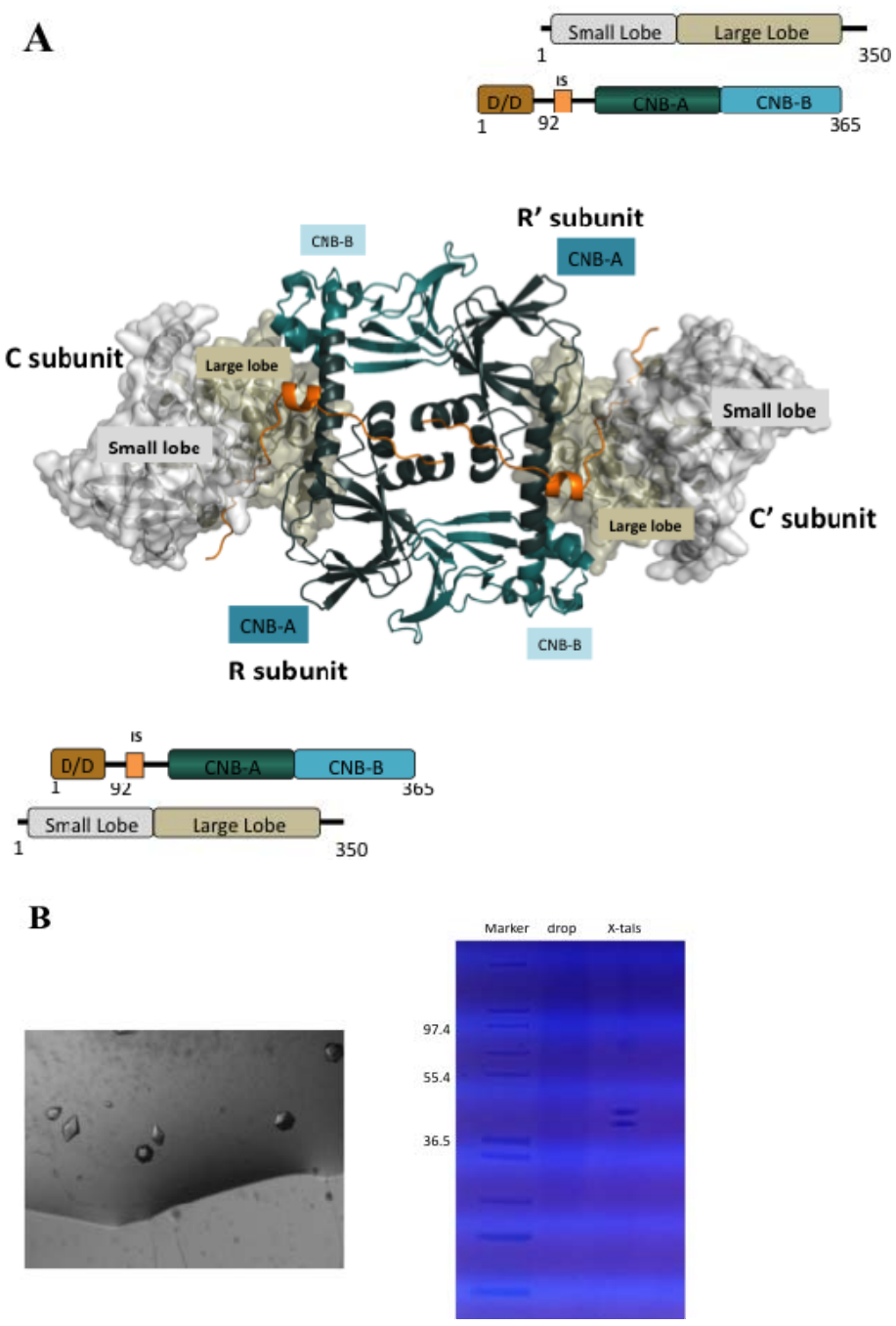

Figure 5.11. ACRDYS-1 RIα$_2$:C$_2$ crystal structure. (**A**) Type I alpha holoenzyme structure consists of a dimer of RIα:C heterodimers. Two ACRDYS-1 RIα (1-365) subunits are positioned in the center with their corresponding C-subunits bound on either side. The R-subunit's CNB-A is colored in dark teal, the CNB-B is colored in light teal, and the linker is colored in orange. The C-subunit large lobe is colored in olive and the small lobe is colored white. (**B**) The left figure shows the holoenzyme crystals. The right figure shows an SDS gel of the crystals and crystallization drop.

configuration. Even though the N-terminal linker was extended in this construct (RIα 73-244) from previously presented heterodimer structures (RIα 92-379), the D/D domain, part of the linker and the CNB-B were not present. Thus the complex was a minimal R:C heterodimer in solution and was purified for crystallization as such.

The R-subunit is in the characteristic C-subunit bound holoenzyme conformation (H-form) and residues Lys90 to Leu357 are present for each RIα chain, confirming a similar structural perturbation of the ACRDYS-1 mutant C-terminus. Residues upstream of the deletion at R366 are thus missing. Residues E13 to V337 for each C-subunit are resolved and because ion-exchange elution peak 1 was used for the crystals, phosphorylation of residues Ser139, Thr197, and Ser338 is present. The complex was set up for crystallization in a buffer containing ATP/$MgCl_2$ and despite the low resolution, electron density indicates that the nucleotide and metals are present in the active site together with the inhibitor site (residue 94-98) of the RIα linker. The presence of ATP/$MgCl_2$ was also confirmed with alternate molecular replacement strategies and when omitted, the positive density is clearly visible. Presence of the D/D domain did not hinder the arrangement of each R:C heterodimer in a similar way as has been published previously and includes an extensive interface between the R-subunit and C-subunit, mediated mainly by contacts with the CNB-A but including crucial contacts with CNB-B as well (Kim et al., 2007; Kim et al., 2005).

The heterodimer structure discussed in the previous sections has shown that the C-terminal deletion of the protein does not perturb the binding interactions between

the R and C-subunit and this is confirmed with this structure as well. Interaction clusters termed pockets 1-4 as described in Figures 5.3 and 5.4. are conserved for each of the two R:C dimers here as well. Furthermore, presence of the D/D domain and with that the R-dimer does not change the contacts within each R:C heterodimer. However, the covalent linkage present in this structure with the D/D domain, now reveals the inter-heterodimer R:C/R':C' organization to build a holoenzyme complex for this mutant RIα (**Fig. 5.12A**). The corresponding heterodimer structure of this mutant and fluorescent polarization assays indicated that this ACRDYS-1 holoenzyme is a cAMP-desensitized, over-inhibited mutant enzyme. The SAXS and gel filtration data further suggest that this dysfunctional holoenzyme complex and its structure represent an acutely inhibited state of PKA. Yet, proteins are dynamic molecules present in the cell in an ensemble of conformational states, which exist in equilibrium with each other. Thus the most populated conformational state of PKA depends on the cellular environment, with the holoenzyme $(RI\alpha:C)_2$ structure presented here illustrating a state that has been pushed toward strong inhibition.

In the structure presented here, the quaternary arrangement of R:C/R':C' is mediated by the R-subunits and results in an overall compact shape. The experimental wild-type and ACRDYS-1 (1-365) SAXS profiles indicate consistent shape parameters. The small-angle scattering function calculated from the ACRDYS-1 holoenzyme structure and the resulting pair-distance distribution function (P(r); **Figure 5.12A**) agrees well with the in-solution profiles. Thus, the longest distance of

Table 5.3 RIα holoenzyme SAXS data

RIα Holoenzyme	R_g (Å)	D_{max}(Å)
Wild-type SAXS	47.1±0.5	140
1-365 SAXS	45.4±0.3	130
RIα (1-370)	43.8±0.7	130
1-365 structure	42.8	130

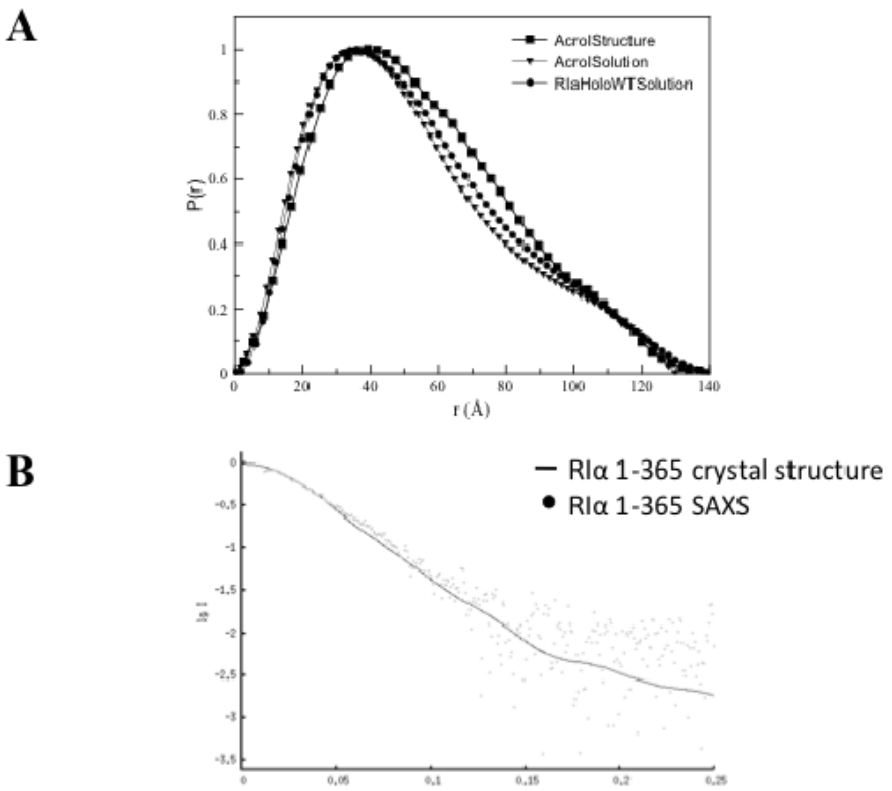

Figure 5.12. RIα 1-365 holoenzyme SAXS comparison. (**A**) P(r) curve computed from the RIα 1-365 holoenzyme crystal structure (squares) compared to the P(r) of the RIα 1-365 holoenzyme SAXS (triangles) and the RIα wt holoenzyme from SAXS (circles) (Vigil et al., 2004). (**B**) Plot of the theoretical scattering profile of the RIα 1-365 holoenzyme crystal structure as calculated with FoXS is shown as a solid black line in comparison to the experimental scattering profile (Vigil et al., 2004) shown as black circles.

the molecule in the structure also compares well with the in-solution D_{max} of ~130 Å. Furthermore, the theoretical R_g (42.8 Å) from the back-calculated intensity scattering data of the structure is close to the experimentally determined in-solution R_g (45.4 Å) (Table 5.3). The smaller R_g derived for the structure is consistent with the notion that the packing process of proteins during crystallization removes some dynamics and can influence overall size. Considering the inherent resolution limitations of SAXS, combined with the fact that experimental SAXS is the result of the time- and ensemble-average of all conformations of the protein, the SAXS-based data validates the crystal structure. As expected, the crystal structure derived scattering data results in a P(r) curve that shows some deviation compared to the in-solution data that is due to the missing D/D domain and N-terminal linker electron densities in the crystal structure (**Fig. 5.12A**).

According to our structure, the C-subunits are far apart as was predicted with SANS studies (Heller et al., 2004). It was published that the inter-atomic distances between the two C-subunits within the holoenzyme were predicted to be ~112 Å and the ACRDYS1 structure presented here agrees well with that prediction. The centers of the C-subunits in the structure are separated by ~110Å. Also consistent with SAXS and SANS data is the extension of the RIα dimer upon C-subunit binding (**Fig. 5.13**). This extension is achieved as the R-subunit releases cAMP and binds the C-subunit, shifting the αB/C helix from the kinked to the continuous conformation (Bruystens et al., 2014). Conserved in this holoenzyme complex and seen also in the R-dimer is an interaction between the R protomers utilizing their N3A motifs. However, due to

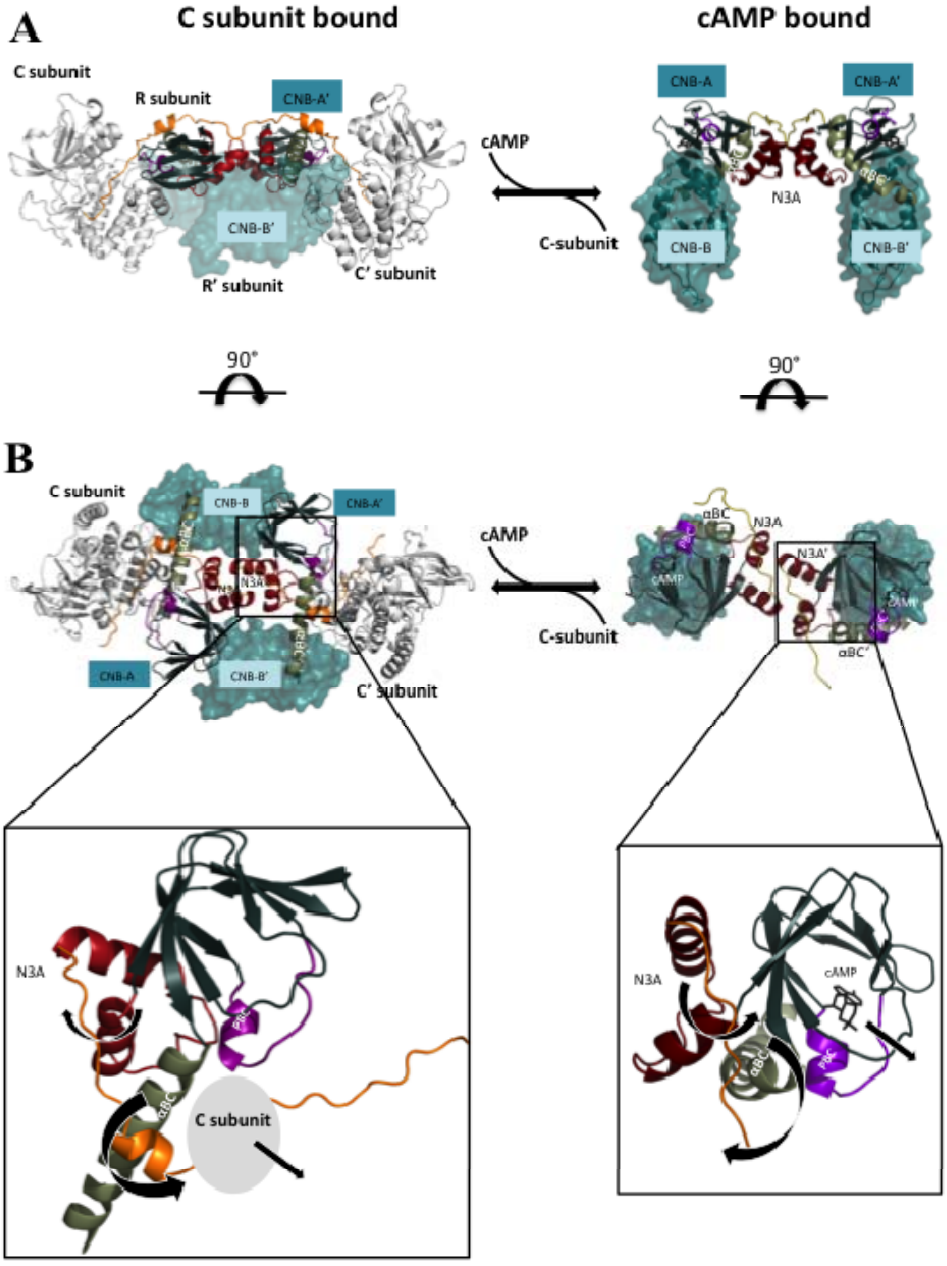

Figure 5.13. ACRDYS-1 RIα$_2$:C$_2$ crystal structure shows central role for N3A motif. The R-subunit's CNB-A is in dark teal, the CNB-B is in light teal, and the linker is in orange. Highlighted in red is the CNB-A N3A motif, the αBC helix in olive, and in purple the PBC. The C-subunit is colored white. (**A**) Side view of the C-bound holoenzyme structure (left) and the cAMP-bound RIα dimer (pdb id: 4mx3). cAMP bound RIα has a kinked αBC helix which causes the CNB-B domain to reposition underneath CNB-A (**B**) Top-view illustrating the C-subunit bound state (left). When cAMP is bound (right) the αBC helix is kinked, forcing the N3A upward and away from the PBC.

the rearrangement of the αB/C helix and PBC of CNB-A upon binding the C-subunit the N3A motif is shifted down to allow the H-form specific contacts (**Fig. 5.13)**. This down-shift allows the 3_{10} -loop of the N3A motif to make contacts with the PBC and the large lobe of the C-subunit. cAMP binding results in a kinked αBC helix, reorienting the CNB-B below CNB-A (**Fig. 5.13A**). In this conformation the αBC helix interferes with the PBC:N3A interaction and the N3A motif is forced upward and away from the PBC (**Fig. 5.13B**).

Evidence for a possible role of the N3A motif was seen previously when residues in this region were mutated and resulted in the perturbation of cAMP-induced activation. Not only did the in-vitro analysis of these interface-mutants reveal a lowering of the EC_{50} for cAMP but also a significant effect on the cooperativity of activation(Bruystens et al., 2014). Further proof of the role of the N3A motif for RIα function is the discovery of several carney complex mutations in this region that cause overactive PKA activity in patients (Horvath et al., 2010). Thus our structure taken together with previously published data suggest a crucial role for the N3A interface between the RIα protomers for the cooperative activation of PKA.

5.4 Conclusion

The cAMP signaling pathway plays essential roles for healthy cells by binding to and effecting PKA, exchange protein activated by cAMP (Epac), and cyclic nucleotide –gated channels. Almost all mutations of PKA regulatory subunits that play a causative role in disease have been found in the RIα isoform. Only recently, a mutation was found in the D/D domain of RIβ in the patients of one family that suffers

from a unique hereditary neurodegenerative disorder. Interference of the AKAP interactions necessary for proper localization of PKA within the cell is suggested to cause the disease (Wong et al., 2014). While differential expression of the four R-subunit isoforms in organisms has been studied extensively and suggests tissue-specific fine-tuned cAMP responses, particular focus is demanded for the RIα isoform due to its most frequent involvement in disease. Mutations of PRKAR1A have been found along the entire coding sequence and in the study presented here we focus on mutations that were identified in ACRDYS patients. Our findings describe the relationship between the functional domains of the PKA RIα subunit and corresponding mutation "hot-spots" to enhance our understanding of the molecular dysfunction that causes ACRDYS disease.

Our understanding of cAMP-induced activation of PKA has made major strides over the last decade and this study is an effort in utilizing this knowledge to decipher possible molecular causes of acrodysostosis. Previous studies have shown that CNB-B serves as the gatekeeper for CNB-A. cAMP thus binds to CNB-B first to initiate the cooperative pathway that leads to PKA activation. The C-terminal tails of the R-subunits thus play a crucial role in the activation of PKA. Comparison of the R-subunit C-tail sequence shows conservation of the cAMP capping Tyr for CNB-B and the crucial Arg that is involved a C-bound specific salt bridge. Conformational rearrangements of the C-tails are similar for all R-subunits and highlight the importance and mechanism of the initial cAMP-binding event to the PKA holoenzymes (**Fig. 5.14**). However, the RIα isoform is essential for survival as seen

with RIα knockout mice being embryonically lethal and RIα has been called the tissue-specific extinguisher, which acts to down regulate the expression of genes in the liver (Boshart et al., 1991; Jones et al., 1991). Thus, the clustering of mutations found at the C-terminus highlighted here implicates the underlying molecular perturbations of the ACRDYS-1 symptoms.

Comparison of ACRDYS-1 mutations to CNC mutations is reflective of the contrasting hypotheses for the molecular causes of the two diseases. CNC is an autosomal-dominant syndrome associated with mutations in the PRKAR1A gene resulting in decreased RIα expression by about 50% in CNC patients which results in disrupting RIα inhibition and leading to overactive C-subunit. This is due to the majority of the approximately 120 mutations discovered so far being subject to nonsense mediated mRNA decay (NMD) as most of the mutations result in a premature stop codon. The C subunits of PKA thus phosphorylate substrates in a cAMP-uncoupled signaling manner. Furthermore, in some patients the RIα mutant proteins escape NMD and are expressed, yet dysfunctional in their regulatory roles and nevertheless lead to CNC. In contrast to ACRDYS-1 mutations, the mutations of the expressed CNC mutations are localized to the N-terminus and CNB-A domain and result in decreased inhibition of the C-subunit. Several mutations are located near the cAMP-binding pocket and others are involved in the binding interactions with the C

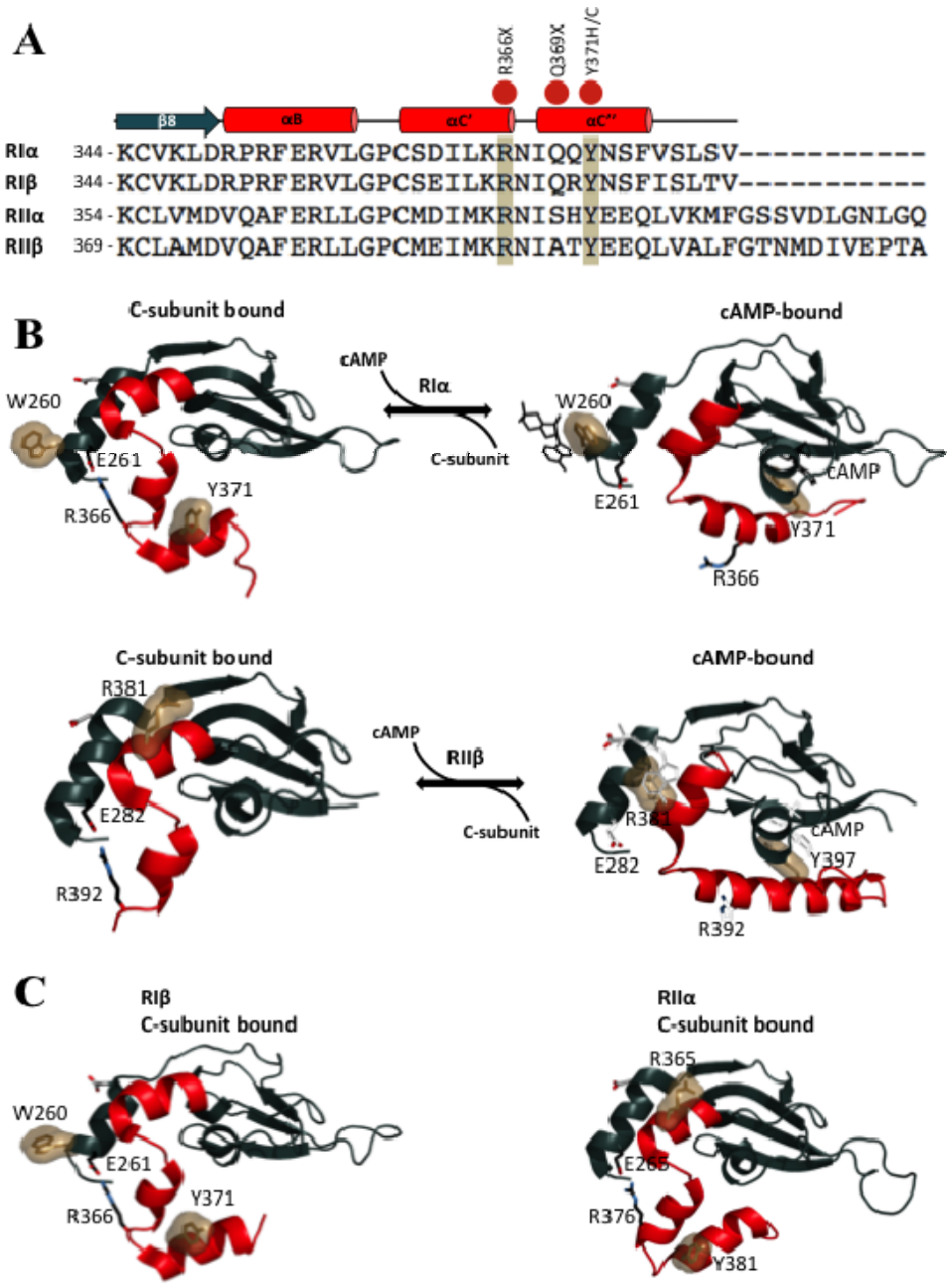

Figure 5.14. Comparison of C-terminal tail sequences and conformations of PKA R-subunit isoforms. (A) Sequence alignment of PKA R-subunits C-terminal tails with the conserved Tyr cAMP capping residue and conserved salt-bridge Arg highlighted in brown. The secondary structures are indicated with red cylinders for α helices and green arrows for β sheets above the sequences. ACRDYS-1 mutations of RIα are denoted with red circles. **(B)** Comparison of the C-tail structures of RIα and RIIβ in their C-subunit bound (left) and cAMP-bound (right) conformations. **(C)** C-subunit bound conformation of the RIβ (left) and RIIα (right) C-terminal tails.

subunit, but residues with less understood roles have also been documented (**Fig. 5.15 & Fig.5.16**).

Two motifs of the CNB-B known to be crucial for R-subunit function harbor the majority of mutations found so far among ACRDYS1 patients. The PBC in CNB-B represents one of the two mutational hot-spots with the mutations concentrated around Arg333 (**Fig. 5.15 & Fig.16**). This arginine is essential for high-affinity binding of cAMP to CNB-B and was replaced with a lysine to obtain the R:C heterodimer structure (Kim et al., 2007). SAXS experiments showed that this mutant makes for a more compact R:C complex compared to the extended wild-type R:C complex and likely aided in the crystallization (Cheng et al., 2009). Structures of the R-subunits show increased b-factors and often times lack electron density of the C-tail and/or the C-tail side chains. The evidence thus suggests that the CNB-B domain is more dynamic than the cAMP-binding domain A, which is also required for the activation mechanism. First insights into the crucial role of the CNB-B were seen by early studies of the CNB-B active site mutant (R333K) and laid some of the groundwork for the cooperative activation mechanism of cAMP binding first to CNB-B to allow access of a second cAMP molecule to bind to CNB-A(Herberg et al., 1996; Ogreid and Doskeland, 1981a, b). Considering the increased stability obtained by removal of the CNB-B dynamics in the ACRDYS-1 recurrent mutant can in-part explain the capture of an ADP-bound RIα:C complex when utilizing the mutants protein for crystallization.

RIα is a nonphosphorylatable pseudosubstrate and contrary to the Ser residue present in the RII subunits' inhibitor site contains an alanine instead. Therefore the capture of an ADP-bound RIα heterodimer was surprising. Previous studies had shown that RIα:C complex formation requires ATP and Mg^{+2} ions. Therefore, to obtain the high-resolution crystal structures of RIα bound to the C-subunit the non-hydrolyzable ATP analog AMP-PNP and manganese has typically been utilized to enable tight complex formation and crystallization (Boettcher et al., 2011; Kim et al., 2007; Kim et al., 2005). Manganese in addition to nucleotide was previously shown to result in maximum stability of the complex compared to other divalent metals tested (Herberg et al., 1999). To assess the effect of ADP on RIα holoenzyme formation in detail, surface plasmon resonance experiments revealed the ADP-sensitivity for the RI holoenzymes. This suggests that the ATP/ADP ratios can affect PKA and may thus enable PKA to sense the cellular energy environment.

Earlier published studies showed that PKA does have some intrinsic ATPase activity (Mendelow et al., 1993; Yang et al., 2004). In situ ATP hydrolysis in our structure was likely made possible by stabilizing the C-terminus with the deletion mutant and thus allowing the N-terminus and active site to be more dynamic, allowing water into the structure for the hydrolysis reaction without dissociating the complex. Preliminary experiments currently in progress suggest that the recurrent ACRDYS-1 mutant can form a stable holoenzyme with the C-subunit even when subjected to gel filtration chromatography (data not shown). Also consistent with our structure is the recently published ADP-bound C-subunit structure that gave insights into the

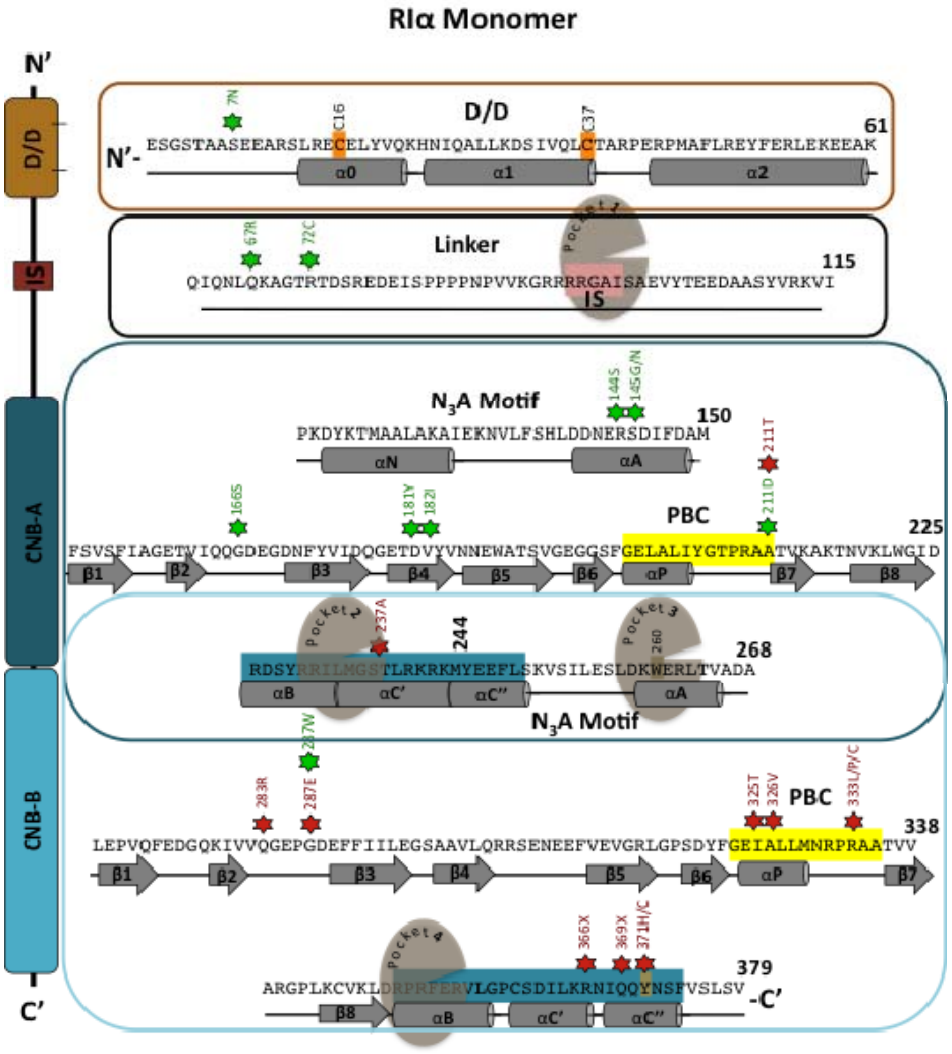

Figure 5.15. Sequence and domain organization of human PKA RIα. The human RIα sequence is shown to the right of the overall domain organization of the R-subunits. Red stars denote ACRDYS1 mutations and green stars denote CNC mutations. Secondary structural elements are shown under the sequence with solid grey arrows representing residues involved in β sheets and solid grey cylinders representing residues involved in α helices. D/D domain disulfide bond residues are highlighted in orange, the inhibitor site is highlighted in pink, the PBCs are highlighted in yellow and the αBαC helices are highlighted in teal. C-subunit interaction site pockets 1-4 ((Kim et al., 2007; Kim et al., 2005)are shown with labeled grey ovals.

intermediate conformations the catalytic subunit can adopt in the reaction progression (Bastidas et al., 2014).

Another ACRDYS-1 mutational hot-spot within CNB-B is the C-terminal tail (**Fig. 5.15 & Fig.16**). Two truncation mutants and two point mutations have been discovered so far. Due to the recurrence of the 14 residue C-terminal deletion mutant we focused our structural studies on this mutant. Mutations of Tyr371 and the salt bridge gave a glimpse of the steps involved in activation of RIa PKA. Urea denaturization studies also showed early on that the CNB-B domain is more accessible and will unfold first (Canaves et al., 2000; Leon et al., 2000). While the CNB-A domain is necessary for high affinity binding to the C-subunit, the CNB-A domain provides regulation and access of cAMP to CNB-A. Our data suggests that it is this initial step and thus the principle cAMP access that is perturbed in the mutant cAMP binding and PKA activation (Lee et al., 2012; Linglart et al., 2012).

It is astonishing how disease causing PKA mutations can be so clearly linked with previous and independently collected data thus providing cross-validation between the observations. Previous and recent studies have provided a general understanding of PKA as a physiological macromolecular signaling complex where activation is mediated by allosteric binding of cAMP to the R2C2 holoenzyme. In addition, current computational analysis of this process supports a model where cAMP docks initially to the CNB-B domain which initiates the process of unleashing the catalytic activity. It not only supports a conformational selection model for allostery

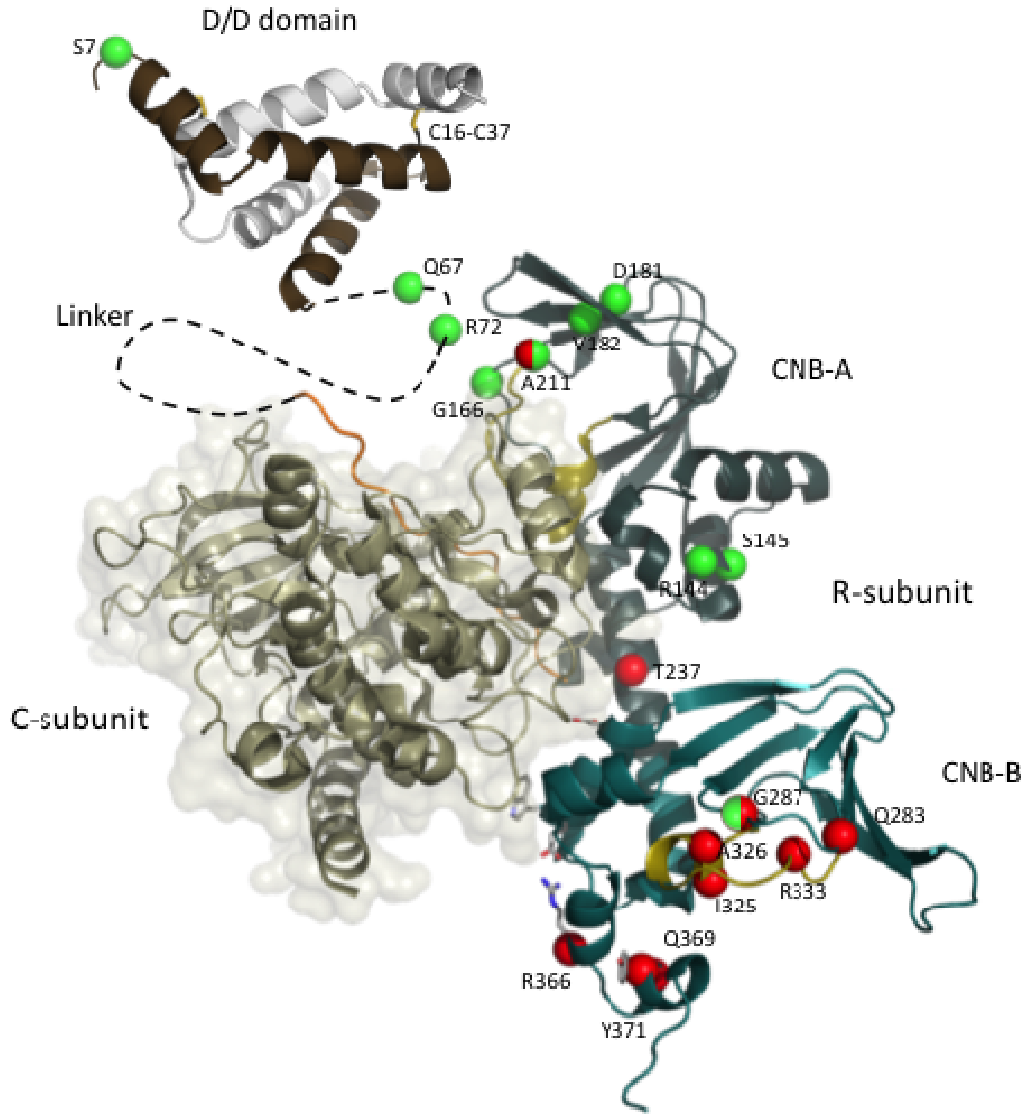

Figure 5.16. Acrodysostosis-1 and carney complex mutations mapped onto the RIα:C heterodimer structure. The thus far known expressed carney complex mutations are shown with green spheres and the expressed acrodysostosis-1 mutations are shown as red spheres. Spheres that are half green and half red represent residues for which both an ACRDYS1 and a carney complex mutation have been found. Shown is RIα in the C-bound conformation (pdb 2qcs) with the CNB-A in dark teal, CNB-B in light teal, and the linker in orange. The C-subunit is shown in olive. The D/D domain structure (pdb 3im3) relative position was modeled with the linker (dashed black line). One protomer of the D/D domain in colored brown, the other protomer is shown in white, and the disulfide bonds between them is shown in yellow.

but also helps to explain why ACRDYS1 mutations that hinder cAMP binding to the CNB-B domain are inhibitory and have such severe clinical consequences.

Chapter 5, in part, is being prepared for publication as Structural and functional implications of RIα acrodysostosis-1 mutations. Bruystens, J.G.; Wu, J.; and Taylor, S.S. The dissertation author was the primary investigator and author of this work.

Chapter 6

Non-canonical PKA scaffolding interaction of RI subunits with P-Rex1

6.1 Introduction

cAMP-dependent protein kinase (PKA) is highly conserved from fungi to humans and plays essential roles in cellular signaling pathways such as cell differentiation, regulation of metabolism, and cell growth (Krebs and Beavo, 1979). Cellular mechanisms have been implemented to control the promiscuous phosphorylation by PKA. In the inhibited state, PKA is composed of a regulatory (R) dimer bound to two catalytic (C) subunits and there are four isoforms that can inhibit the C-subunit. cAMP-binding to RIα, RIβ, RIIα, and RIIβ nucleated holoenzymes permits the C-subunits to phosphorylate a serine or threonine in its downstream targets. PKA is part of macromolecular signaling complexes that must be targeted by scaffolding proteins to specific sites in the cell. Compelling data by the Vazquez-Prado group at the CINESTAV-IPN, Mexico stimulated this project. According to their studies, an interaction of PKA with phosphatidylinositol-3,4,5-trisphosphate-dependent Rac exchange factor 1 (P-Rex1) was revealed by yeast two-hybrid experiments. The guanine nucleotide exchange factor P-Rex1 is one of the many known substrates of PKA(Mayeenuddin and Garrison, 2006) but the functional and molecular details for this signaling node have not been resolved.

Small GTPases hydrolyze guanosine triphosphate (GTP) into guanosine diphosphate (GDP) and play crucial roles in many cellular functions including cell proliferation, migration, and differentiation (Coisy-Quivy et al., 2006; Parri and Chiarugi, 2010). The Rho family of small GTPases can be organized into the following 6 classes: Rho, Rac, Cdc42, RhoBTB, RhoT, and Rnd. Two major

regulators of their activity are guanine nucleotide exchange factors (GEFs), which facilitate GTP loading, and GTPase activating proteins (GAPs), which facilitate GTP hydrolysis. Although some GEFs will regulate several small GTPases, P-Rex1 facilitates nucleotide exchange specifically for Rac GTPases(Bustelo et al., 2007). P-Rex1 itself is activated through binding PIP and the Gβγ subunit of heterotrimeric G proteins, though phosphorylation by PKA can inhibit this (Mayeenuddin and Garrison, 2006).

P-Rex1 has been implicated in multiple forms of cancer, including breast, skin, and prostate (Lindsay et al.; Qin et al., 2009; Wertheimer et al., 2012). It is dramatically overexpressed in breast cancer where it functions as a mediator of ErbB receptor signaling, commonly hyperactivated in breast cancer. Notably, its involvement in different types of breast cancer varies, evidenced by its overexpression in luminal tumors but virtual absence in basal-type breast tumors (Sosa et al., 2010). Furthermore, in a murine model it has been demonstrated that P-Rex1 is required for melanoblast migration during development and metastasis of melanoma. Its involvement in many cellular functions makes it an ideal candidate for investigation and its role in cancer further underscores its importance. P-Rex1 contains 28 putative PKA phosphorylation sites (Wertheimer et al., 2012) with one confirmed site as an actual target. Our understanding of P-Rex1 involvement in breast and skin cancer and its regulation by PKA phosphorylation is still in its initial stages.

The P-Rex1 protein family comprises P-Rex1, P-Rex2a, and P-Rex2b. Each member consists of at least a DH, PH, two DEP, and two PDZ domains. P-Rex1 also

includes a C-terminal region with significant similarity to inositol polyphosphate 4-phosphatase (IP4P), although phosphatase activity has not been observed(Welch et al., 2002). In addition to differing at their C-termini, P-Rex1 and P-Rex2 exhibit different tissue distributions. P-Rex1 is abundant in brain, whereas P-Rex2a is found in skeletal muscle, heart, kidney, placenta and lung (Donald et al., 2004). P-Rex2b, on the other hand, is predominantly found in cardiac tissue (Rosenfeldt et al., 2004). Figure 6.1A illustrates various functional domains in P-Rrex1 and their relative locations. Point mutations and deletion mutant experiments demonstrated the DH domain is necessary for Gβγ-dependent activation of GEF activity and the PH domain is required for PIP-dependent activation of GEF activity. Interestingly, the absence of the PH domain results in a 10-fold increase in P-Rex1 GEF activity, suggesting the PH domain exerts inhibitory action on the catalytic DH domain (Hill et al., 2005).

P-Rex1 in heregulin β1 (HRG)-stimulated breast cancer cells translocates to the plasma membrane. The DH-PH region is necessary for translocation, which is PI3Kγ-dependent (Sosa et al., 2010). In addition to translocation, HRG-stimulated breast cancer cells exhibit altered phosphorylation states. HRG causes Ser313/Ser319 dephosphorylation and Ser605/Ser1169 phosphorylation. Therefore, it was proposed by Sosa *et al.* that Ser313/Ser319 phosphorylation prevents Rac1 activation while Ser605/Ser1169 phosphorylation promotes it (Montero et al., 2011). The abundance of potential PKA phosphorylation sites in P-Rex1, their altered states in cancer cells, and documented PRex1 inhibition by PKA indicates a link between the PKA and P-Rex1/Rac signaling pathways. Initial data from yeast two hybrid experiments by the

Vazquez-Prado group at the CINESTAV-IPN, Mexico showed the RIα C-terminus as prey obtained utilizing the P-Rex1 PDZ1-PDZ2 as bait (unpublished). This chapter discusses the studies carried out to define the underlying molecular mechanism of the PKA:P-Rex1 pathway.

The C-terminus of the type I regulatory (R) subunits of PKA bear a class II PDZ binding motif (bovine sequence residues 377-379). Here we present evidence for a PKA:P-Rex1 interaction. Pull-down experiments from HEK293 cells reveal P-Rex1 to be a possible binder with its PDZ domains to the RI subunits. We tested several disease and deletion construct mutants of RIα to decipher the interaction requirements. Further we present peptide arrays to define the binding motifs. While the N-terminal dimerization docking (D/D) domains of the R-subunits are well established binding modules for A-kinase anchoring proteins that serve to nucleate PKA containing macromolecular signaling complexes and target these to sub-cellular sites, the C-terminus of the R-subunits potential as a scaffolding module has been much less understood. Based on our experiments we propose a binding model for the PDZ domains of P-Rex1 to the RIα CNB-B domain.

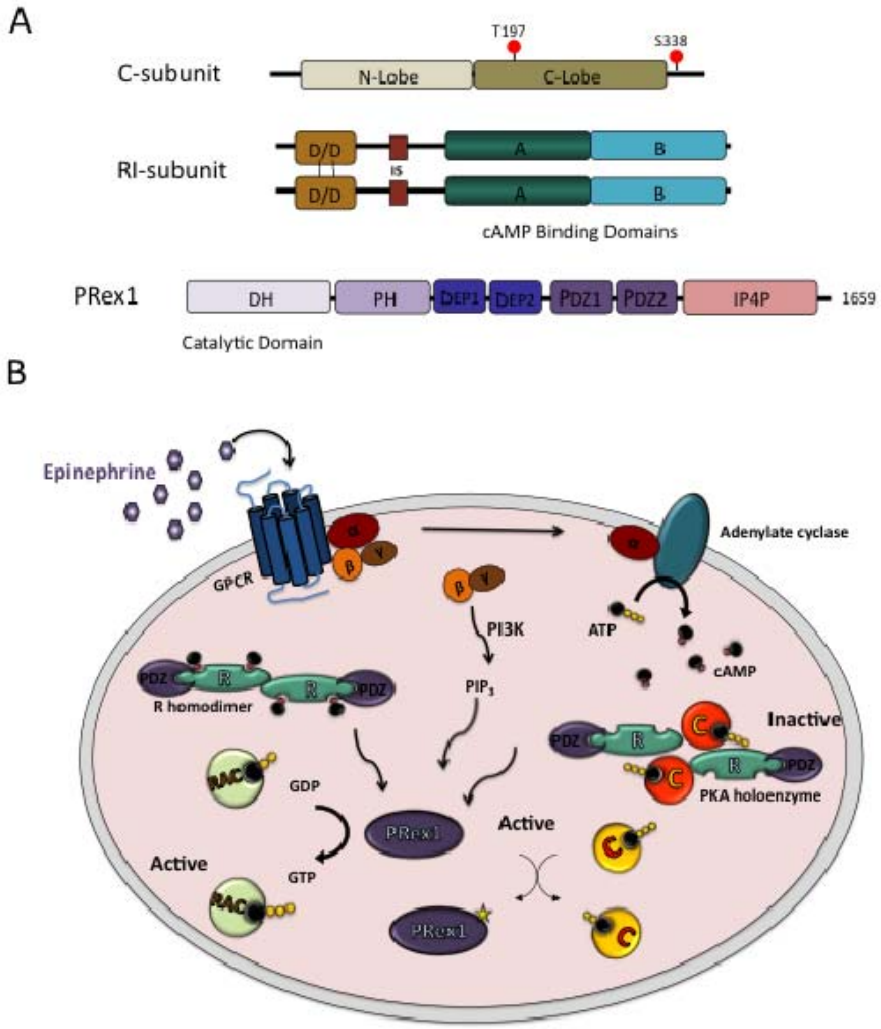

Figure 6.1. PKA and P-Rex1/Rac signaling overview. (**A**) Domain organization of PKA-C, PKA-RI, and P-Rex1. (**B**) Schematic of signaling pathway convergence of PKA with P-Rex1/Rac.

6.2 Experimental Procedures

Protein Expression and Purification - Bovine full-length (1-379) wild type and deletion mutant RIα proteins were purified as described previously (Su et al., 1995; Wu et al., 2004b). Expression was carried at out 16C for 16-20 hours in *E.coli* BL21 (DE3) from Novagen® suspended in YT Media. In summary, a combination of ammonium sulfate precipitation, affinity chromatography with cAMP-resin and size-exclusion chromatography were utilized to achieve >94% pure protein. Briefly, following expression cells were lysed with a Microfluidizer® processor at 18,000 psi, centrifuged at 16,000 rpm, and the soluble fraction was then ammonium sulfate precipitated. The ammonium sulfate pellet was resuspended and batch bound over night to cAMP resin. After elution from the resin with 40mM cAMP the elution was applied to a Superdex™ 200 gel filtration column utilizing a buffer containing 50mM MES (pH 5.8), 200mM NaCl, 2mM EGTA, 2mM EDTA and 5mM DTT.

Human P-Rex1 PDZ1-PDZ2 (residues 607-783) and P-Rex1 PDZ1 (residues 607-706) were cloned as His-tagged proteins in pET28 vector from (Novagen). Protein expression was carried out in *E.coli* BL21 (DE3) cells in LB media containing 100 μg/ml ampicillin. At OD_{600}=.8 – 1 overnight protein expression was induced with 1mM IPTG and the temperature was lowered to 15°C. Next, the cells were lysed using a Microfluidizer® processor at 18,000 psi. The lysis buffer contained 50 mM Tris-HCl pH 7.5, 500 mM NaCl, 5 % glycerol, 5 mM imidazole, and a protease inhibitor cocktail (Sigma). After one hour of centrifugation at 16,000 rpm the supernatant was collected and mixed with Probond Ni-NTA resin overnight at 4°C. After washing with

a buffer containing 50 mM Tris-HCl pH 7.5, 500mM NaCl, 5 % glycerol, and 5mM immidazole protein was eluted with a buffer containing 50 mM Tris-HCl pH7.5, 500mM NaCl, 5 % glycerol, and 200mM imidazole. The elution was dialyzed into 50 mM Tris-HCl pH7.5, 500mM NaCl, and 5 % glycerol and then subjected to a S75 gel filtration column equilibrated with 50 mM Tris-HCl pH 7.5, 500mM NaCl, and 5 % glycerol.

GST fusion protein pull-down assay – HEK293 cells were transfected with GST only, GST-tagged P-Rex1 PDZ1PDZ2, various human and bovine RIα constructs, human RIβ, and human Cα, as indicated in the figures. Transfected cells were lysed in buffer A (50mM Tris, pH 7.4, 150mM NaCl, 1 mm EDTA, 1 mm dithiothreitol, plus complete proteinase inhibitor cocktail, Roche) with sonication for 5 seconds at 36J. The soluble cell lysates were incubated with glutathione-Sepharose on a rolling wheel in the presence of 0.5% Triton X-100 and 1% BSA for 2 hrs at 4°C. The beads were washed twice with buffer B (50mM Tris, pH 7.4, 150mM NaCl, 1 mm EDTA, and 1 mm dithiothreitol), and once with buffer B without dithiothreitol. The proteins bound to the glutathione-Sepharose beads were separated with SDS-PAGE and analyzed with western blot using chemiluminescence.

Peptide blots – P-Rex1 overlay of the Regulatory (RI) subunits CNB-B domain of PKA. The CNB-B domain of RIα and RIβ was divided into 15-amino-acid peptides, with a 3 amino-acid shift and 1 amino-acid shift, and synthesized using the

INTAVIS MultiPep peptide synthesizer (INTAVIS Bioanalytical Instruments AG, Koeln, Germany), which spotted the peptides onto an AC-S01 type amino-PEGylated membrane (INTAVIS AG). Following activation with ethanol, the membrane was blocked, washed with PBS-T, and incubated overnight with purified 100 nM human P-Rex1 PDZ domain 1 (residues 606-706) protein or double PDZ1-PDZ2 (residues 606-781) protein. This His-tagged protein was generated as documented above. After incubation with PDZ1 or double PDZ1-PDZ2, the peptide array was analyzed by western blot analysis with polyclonal rabbit His-tag antibody.

PKA RIα/β overlay of the PDZ1PDZ2 double domain of P-Rex1. The PDZ1PDZ2 double domain of P-Rex1 was divided into 15-amino-acid peptides, with a 3 amino-acid shift, and synthesized using the INTAVIS MultiPep peptide synthesizer (INTAVIS Bioanalytical Instruments AG, Koeln, Germany), which spotted the peptides onto an AC-S01 type amino-PEGylated membrane (INTAVIS AG). Following activation with ethanol, the membrane was blocked, washed with PBS-T, and incubated overnight with 100 nM bovine RIα or human RIβ protein. RIα was generated as documented above and RIβ was purified as described previously (Ilouz et al., 2012). After incubation with the proteins, the peptide arrays were analyzed by western blot analysis with polyclonal rabbit RIα or RIβ antibodies.

P-rex1 PDZ1:RIα:C complex model - Docking was performed by ZDOCK server (Petersen et al., 2009) without restrictions on predicted interface. The target structure was CNB-B domain of PKA-RIa PDBID: 2QCS residues 245-375. The last

four residues (377-380) were removed. The ligand structure was PDZ domain PDBID:2VSP residues 375-456. The predicted structure represents six out of ten top predictions clustered tightly around the cAMP-binding site of the target protein.

6.3 Results

Pull-down assays from HEK293 cells - Our first attempts of confirming the interaction of P-Rex1 with the RI-subunits were carried out with pull-down assays from HEK293 cells. Co-transfection of either HA-RIα or HA-RIβ alone with P-rex1 GST-PDZ1-PDZ2 and in combination with co-tranfected PKA Cα is shown in **Figure 6.2**. Following incubation of cell lysates with GST-resin, the pull-downs were run on SDS gels and analyzed by western blotting. Transfection with GST alone does not result in detection of C-subunit, RIα-subunit or RIβ-subunit and shows that PKA does not pull-down with the GST tag (lane 1 and 3, **Fig. 6.2 A&B**). When the GST-tagged PDZ domains of P-Rex1 are used and co-transfected with RIα or RIβ, the R-subunits are pulled-down as seen in lane 4 of **Figure 6.2 A & B**. Triple transfection with P-Rex1, PKA-Cα, and PKA-RIα or PKA-RIβ also successfully pulls-down both the C- and R-subunit with the PDZ domains. Thus P-Rex1 PDZ domains are capable of pulling-down both the R-subunits alone and the C-bound R-subunits. Noteworthy is however the fact that even the cells where no C-subunit was added by transfection, none-the-less do contain some endogenous C but were not detected in the lanes 4, likely due to its relatively low abundance.

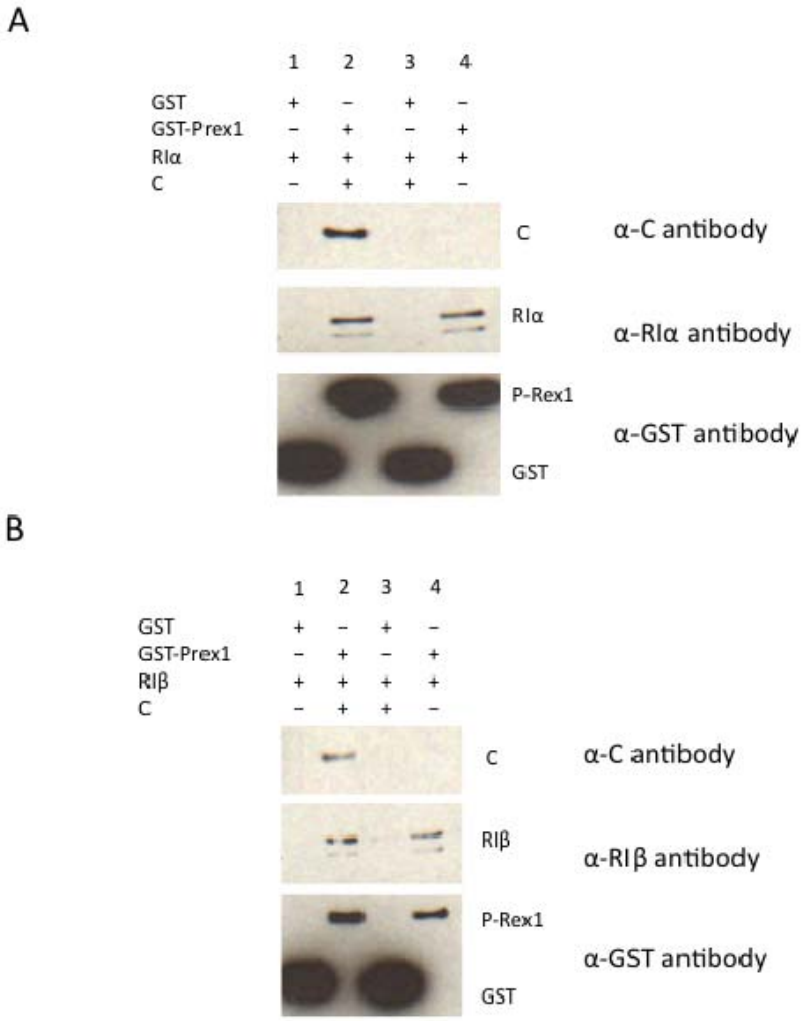

Figure 6.2. Initial pull-downs of PKA C- and RIα/β-subunits with P-Rex1 PDZ1-PDZ2. (**A**) Pull-down of RIα and RIα:C with P-Rex1 PDZ domains (1&2). (**B**) Pull-down of RIβ and RIβ:C with P-Rex1 PDZ domains (1&2).

After optimizing the conditions we repeated and extended the pull-downs (**Fig. 6.3, 6.4**). These have been repeated at least twice more with getting similar results. Again, wild-type RIα (**Fig. 6.3B,**; **Fig. 6.4**) and RIβ (not shown) subunits pull-down with P-Rex1 alone (lane 2) and in the triple transfection experiment with the C-subunit (lane 6 and 8 respectively). Additionally, we tested the Carney Complex disease mutant R74C, the cAMP-binding deficient G325E, and the acrodysostosis-1 (ACRDYS1) Δ365-379 disease mutant. This recurrent ACRDYS1 disease mutant was found in humans to make a holoenzyme with the C-subunit that is cAMP-resistant and causes a severe phenotype (Linglart et al., 2011). We also tested the essential for cAMP bindng arginine mutant R335K (Bubis et al., 1988a; Herberg et al., 1996) and the PDZ-motif deletion mutant RIα 1-378, as well as the D/D domain deletion construct that results in a monomeric RIα (92-381).

The RIα 92-381 protein is the only one that does not pull-down alone or in combination with transfected C-subunit (**Fig. 6.4 lane 3 & 9**). While there is a faint C band present, this is likely due to endogenous RIα and RIβ pulling it down. The other constructs used showed varying results. The weakest signal results from PKA CNC R74C mutant without C-transfection (**Fig. 6.3B, lane 1; 6.3B, lane 1**), yet when the PKA C-subunit is co-transfected with this mutant, the pull-down signal increases (**Fig. 6.3B, lane 5; 6.3B, lane 7**). This might be reflecting the increased turn-over of the CNC mutant protein, compared to wild-type RIα protein and that addition of C-subunit by transfection stabilizes the mutant that is now bound to the C-subunit. The fact that RIα is more stable and has an extended 4-5 fold longer half-life through

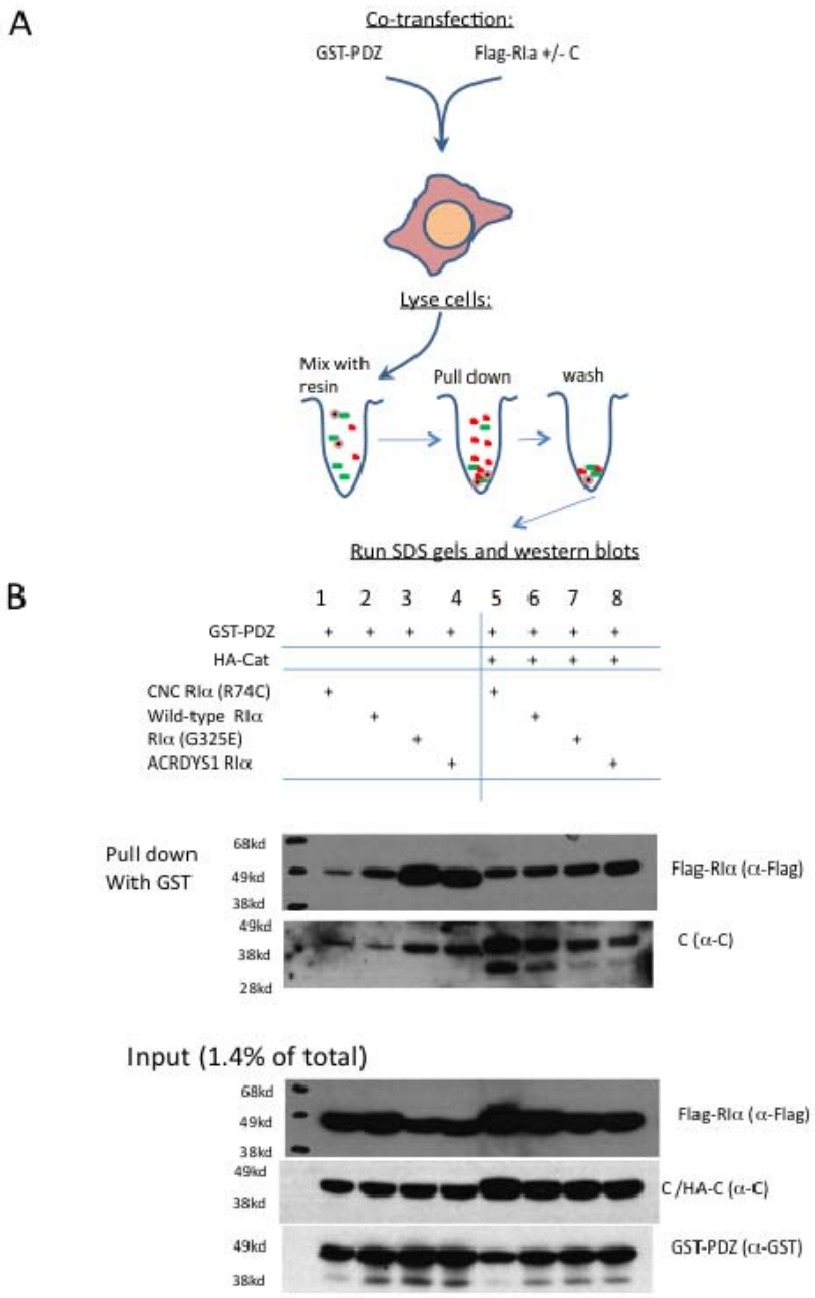

Figure 6.3. Pull-downs of PKA C- and RIα/β-subunits with PRex1 double PDZ1-PDZ2. (**A**) Schematic of pull-down procedure with GST-PDZ domains of PRex1 and Flag-RIα+/-C. (**B**) Pull-down of various constructs of RIα with PRex1 PDZ domains. Lane1: Carney Complex R74C, Lane 2: wild-type RIα, Lane 3: G325E RIα, Lane 4: ACRDYS1 RIα. Lanes 5 – 8 are the same as 1-4 but with Cα added by transfection.

holoenzyme formation was previously observed and published (Amieux et al., 1997). Thus, while this CNC cysteine mutant likely has stability issues and get degraded faster than the wild-type RIα, addition of the C-subunit can counteract the degradation. This is supported by the increased amount of the mutant protein present in the load sample when C-subunit was co-transfected (**Fig. 6.4 lane 7**; **Fig. 6.3 lane 5**) compared to when no C-subunit if transfected (**Fig. 6.4 lane 1;Fig. 6.3 lane 1**). The R333K mutant pulls down weaker compared to wt RIα and that is true also for the C-subunit co-tranfection (**Fig. 6.4 lane 4 &10**). Even PDZ-motif deletion still results in that mutant (RIα 1-378) to be pulled-down in a to wt RIα comparable level (**Fig. 6.4 lane 5 &11**). The ACRDYS1 mutant protein (**Fig. 6.4 lane 6&12;Fig. 6.3 lane 4&8**) and G325E (**Fig. 6.3 lane 3&7**) both give the best signals with or without co-transfection of the C-subunit.

Peptide blots reveal binding to RI CNB-B motifs – In order to define the motif's capable of binding to the P-Rex1 PDZ domains we initially generated peptide arrays of RIα and RIβ containing 15 amino acid long peptides, starting with residue 244 and shifted by 3 residues from there along the CNB-B domain sequences (**Fig. 6.5**). The peptides that were thereby tested are listed in **Figure 6.6A** for RIα. The arrays were then probed with purified P-Rex1 PDZ1. For both RIα and RIβ three areas are binding to PDZ1 of P-Rex1 and correspond to the β4β5 loop, the PBC, and

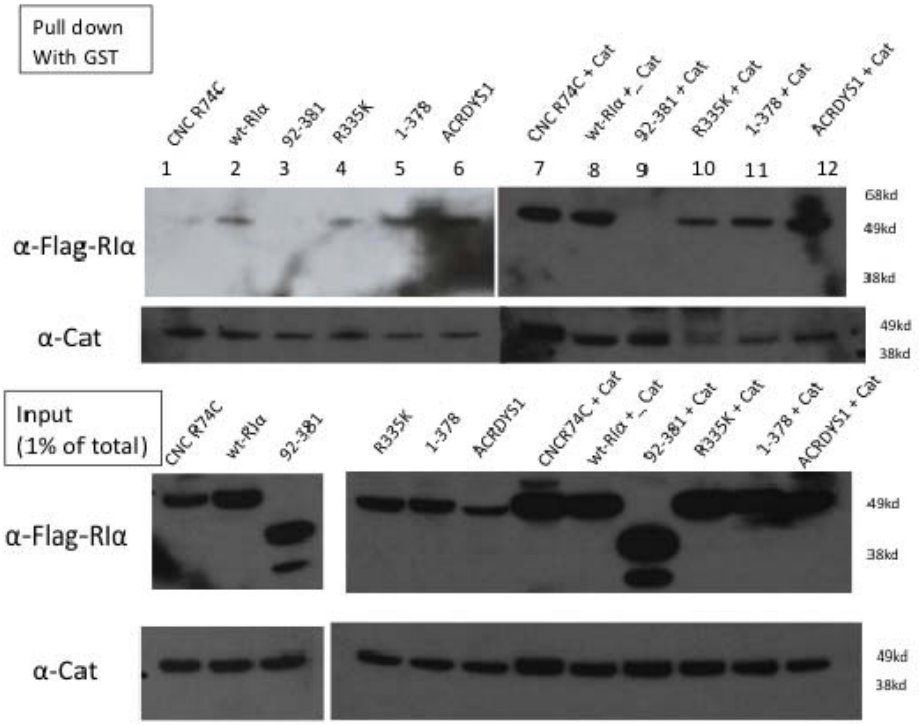

Figure 6.4. Pull-downs of PKA C- and RIα-subunit with PRex1 double PDZ1-PDZ2. Pull-down of various constructs of RIα with PRex1 PDZ domains. Lane1: Carney Complex R74C, Lane 2: wild-type RIα, Lane 3: 92-381 RIα, Lane 4: , Lane 5: , Lane 6: ACRDYS1 RIα. Lanes 7 – 12 are the same as 1-6 but with Cα added by transfection.

the αBαC helix but there are some significant differences (**Fig. 6.6B**). While there was better binding to the β4β5 loop and the PBC peptides of RIβ, there are more peptides binding to the αBαC helix of RIα (**Fig. 6.5**). The arrays were repeated and gave similar results (not shown). When the same peptide arrays are probed with the double PDZ domains of P-Rex1 similar trends of binding are seen (**Fig. 6.7**). However, binding to the αBαC helical region of RIβ is now improved but the equivalent peptides are bound to RIα already with PDZ domain 1 and bind one additional peptide when the double PDZ domain protein is used to.

In order to define the molecular determinants for P-Rex1 PDZ domain binding in more detail we generated 15mer peptides with single residue shifts along the RI sequences that we saw good binding for in the previous array. In addition we conducted alanine substitutions for the peptides that showed good binding. The results are summarized in **Figure 6.10A**. Thus, three peptides near the PBC, 8 peptides of the αB helix, and 10 peptides of the αC helix were capable of binging PDZ1. According to the Ala mutations along the peptides, the Ala mutation causes abolishment of binding of any (but Lys347) residues from Cys345 to Glu354 on the αC helix. In addition the Arg356Ala, Asp362Ala, Leu364Ala, Lys365Ala, and Arg366Ala mutations prevented PDZ1 binding to the peptides. The sequences of the corresponding motifs are located close to each other on the folded CNB-B of RIα (**Fig. 6.9).** From structures of the C-bound and cAMP-bound RIα subunit it would seem P-Rex1 would be able to bind either one of the two conformations.

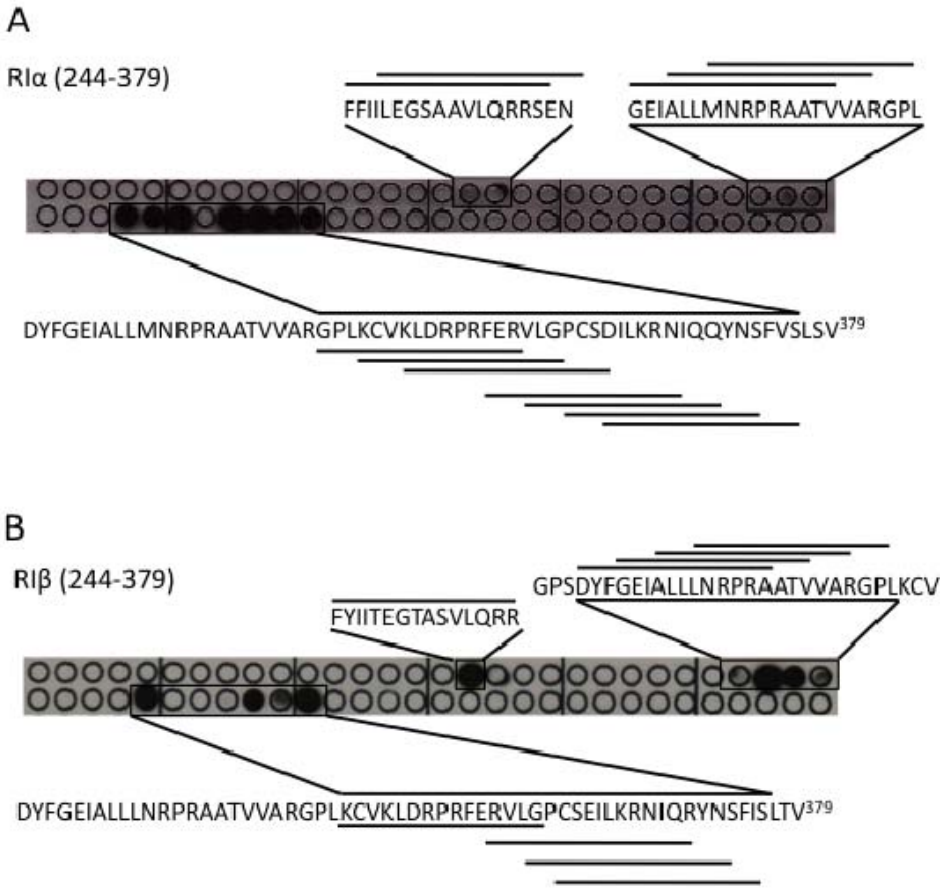

Figure 6.5. Peptide arrays of PKA RI-subunits probed with PRex1 PDZ domain 1. (**A**) Peptide array of residues 244-379 of RIα. 15mer peptides with a 3 residue shift along the sequence were immobilized on the membrane. (**B**) Peptide array of residues 244-379 of RIβ. 15mer peptides with a 3 residue shift along the sequence were immobilized on the membrane.

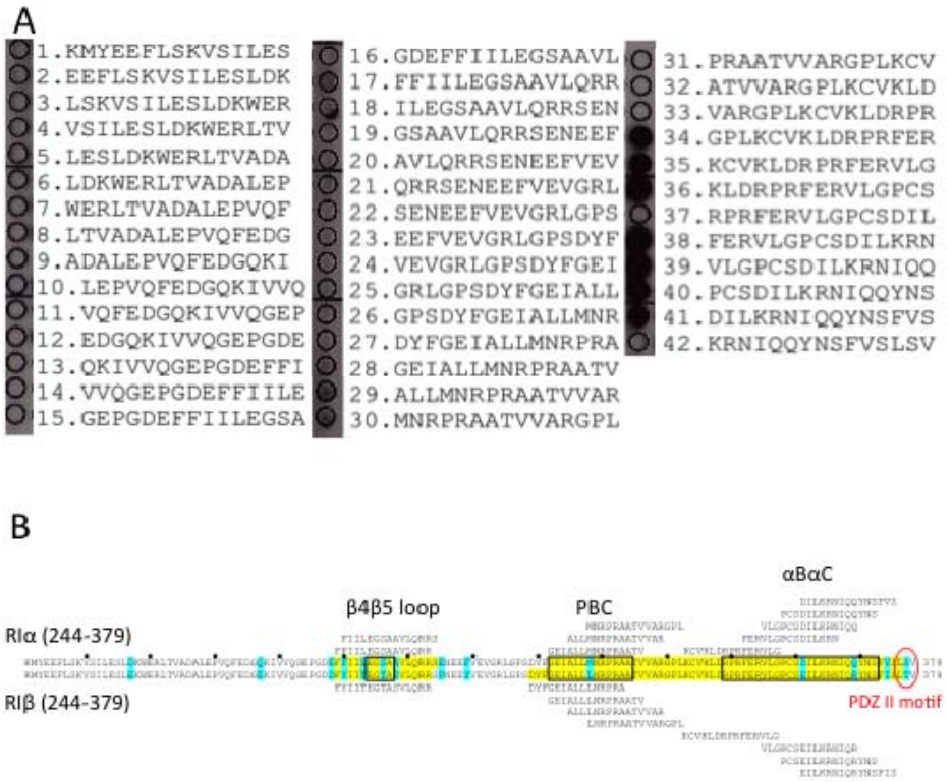

Figure 6.6. Peptides of PKA RI-subunits. (**A**) Peptide array 15mer sequences of RIα from 244-379 (**B**) Sequence and peptide comparison between RIα (top sequence) and RIβ (bottom sequence). Every tenth residue is indicated with a dot. Motifs are boxed in black and differences in sequences are highlighted in blue.

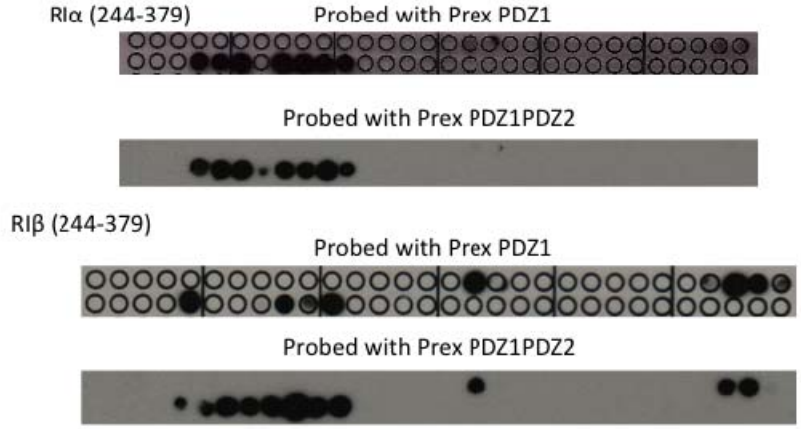

Figure 6.7. Peptide arrays of PKA RI-subunits probed with double PRex1 PDZ1-PDZ2. The identical peptide array scheme as in figure 6.5 but probed with the tandem PDZ domains of P-Rex1.

Docking model of a PDZ domain to the RIα C-bound structure – PDZ domains are compact globular scaffolding modules typically containing about 90 amino acids. The structure of the first of two PDZ domains of P-Rex1 displays the typical PDZ fold of six β-strands (βA-βF) and two α-helices (αA and αB) (**Fig. 6.8**). The published P-Rex1 structure also includes an extra N-terminal α helix (α1) that is not part of the PDZ fold and connects PDZ1 to the preceding DEP2 domain. The canonical PDZ binding mechanism is achieved by β-stand addition. For this usually the PDZ motif (3 terminal residues) of the target protein will insert in the pocket between αB and βB (**Fig. 6.8B**). According to our peptides blots, additional interactions are made between PDZ1 and the RI subunits (**Fig. 6.9**). We thus attempted to dock the PDZ domain structure onto the CNB-B domain of the C-bound RIα structure (pdb id 2qcs) utilizing the ZDOCK server(Petersen et al., 2009). The resulting model represents six out of ten top predictions and shows a nice interface at the bottom of the CNB-B domain. Accroding to the model, the PDZ domain can cluster tightly near the cAMP-binding site and αBαC helix of the target RIα and the model is thus consistent with our peptide blots.

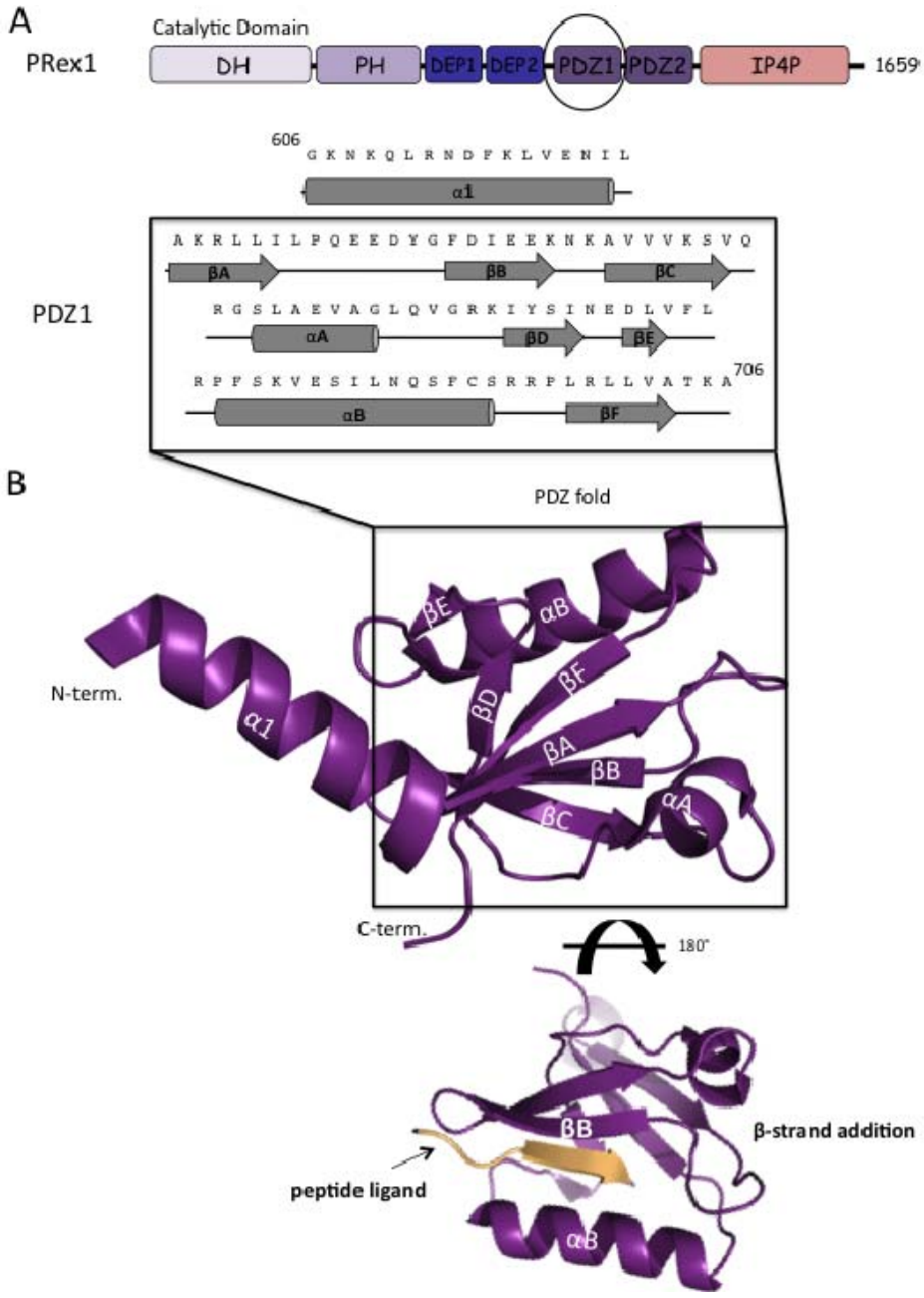

Figure 6.8. Sequence and structure of PRex1 PDZ domain 1. (**A**) The sequence of the structure and first PDZ domain of PRex1 is shown with barrels representing α helices and arrows indicating β sheet. (**B**) Structure of PRex1-PDZ1 shown as ribbon diagram in purple (pdb id 3QIK) with the PDZ fold boxed. Bottom figure is a model of the typical peptide ligand binding mode of β-strand addition would look like.

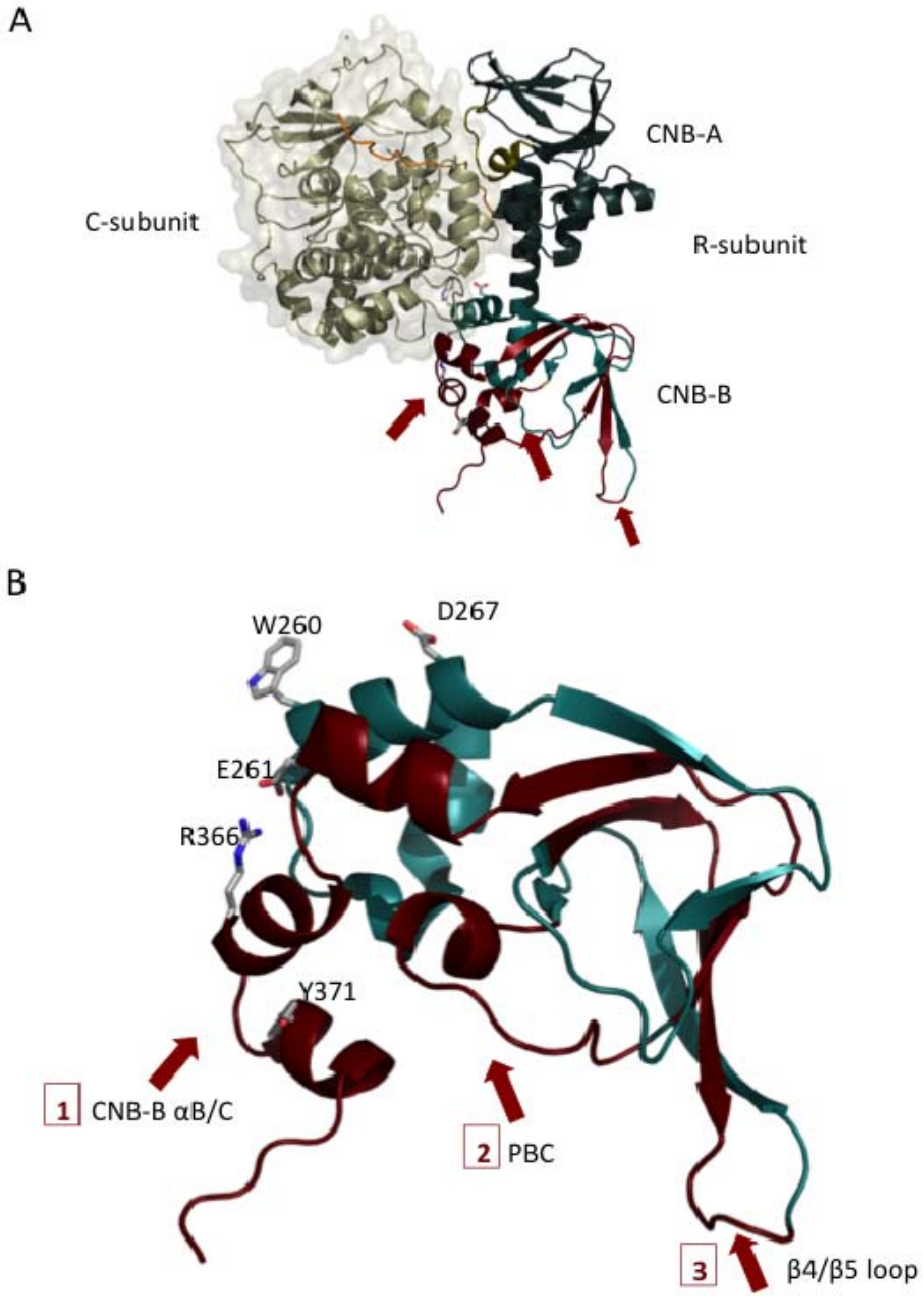

Figure 6.9. CNB-B domain of C-bound RIα. Red arrows point to the three binding areas observed in the peptide blots.(**A**) Structure of the C-bound RIα (pdb id 2qcs) with the C-subunit in olive and RIα in teal and red. (**B**) Zoom of the CNB-B of RIα in the heterodimer structure with the PDZ1 binding motifs colored red.

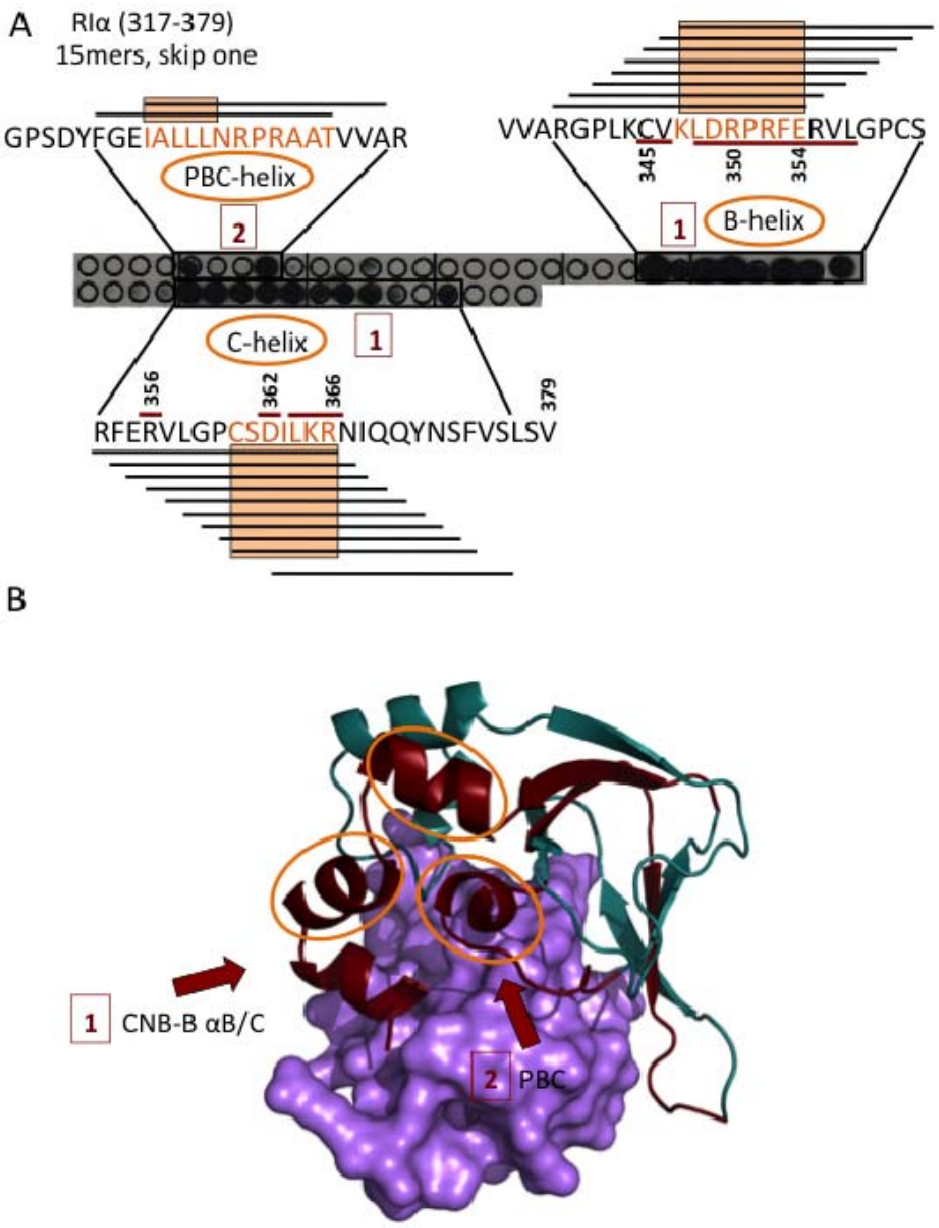

Figure 6.10. PRex1 PDZ1/RIα binding model. (**A**) Single skip 15mer peptide blots of C-term. of RIα with detrimental Ala substitutions underligned in red. (**B**) Docking with ZDOCK of 2qcs with PDZ pdb id 2vsp.

7.4 Conclusion

Melanoma is the second most common form of cancer in American women ages 20-35 and the leading cause of cancer deaths in American women ages 25-30. P-Rex1 involvement in cell migration has previously been described to occur via mammalian Target of Rapamycin (mTOR) interaction with P-Rex1 DEP domains. It can also be activated through interactions with mTOR complex 2, initiating Rac activation and cell migration (Hernandez-Negrete et al., 2007). As cell motility is a major contributing factor to metastasis, a role for P-Rex1 and PKA in cancer progression is plausible.

PDZ domains are well known molecular scaffolding folds found in many proteins with targeting their protein interaction partners to sub-cellular sites. The interaction between P-Rex1 PDZ domains, according to our results, indicate binding of P-Rex1 to the C-terminus of RIα and RIβ. While the canonical binding mode would lead to insertion of the C-terminal residues of the RI subunits into the PDZ grove between βB and αB, we present evidence for an unusual binding interaction. The interaction is accomplished with the PBC, β4β5 loop, and αBαC helix of the CNB-domain. While the pull-downs were carried out with the GST-tagged tandem PDZ1-PDZ2 protein, peptide blots indicate that one PDZ is able to bind as well. However, the interaction of the tandem PDZ-domain protein does increase the peptide hits. An important role for the PBC in the interaction is also indicated by the fact that the R333K mutation in the RI subunits significantly interferes with the pull-down. In

addition we show that binding to RIα versus RIβ is different according to the peptide arrays.

While both, transfection of R-subunit only and the co-transfections of R-subunit with C-subunit, successfully pulled-down various RI protein constructs, addition of the C-subunit increased the pull-down efficiency. This indicates that binding to the C-bound R conformaiton is preferred by P-Rex1 (**Fig. 6.3 & 6.4**). This could also explain why the G325E and ACRDYS1 RIα mutants were the best P-Rex1 binders in the pull-downs. The R subunits adopt characteristic conformations in the cAMP-bound and the C-subunit bound state (**Fig. 6.11B**). Major molecular motions are carried out by the PBC and αCαB helix. The ACRDYS1 mutant protein lacks the C-terminal helix and was shown to cause a more inhibited R:C complex (Linglart et al., 2011). A similar effect is accomplished by the G325E mutant of RIα, leaving the corresponding holoenzyme cAMP-resistant. Even without ligands present, the R-subunit toggles between the cAMP-bound conformation and the C-bound conformation (Akimoto et al., 2013). Thus, we believe that these mutants are pushing the conformational equilibrium of the R-subunits towards the C-bound state and are then pulled-down better with the P-Rex1 PDZ domain. Modeling the structure of RIα with the PDZ domain shows convincing docking sites that are consistent with our peptide blots and pull-downs (**Fig. 6.10B**).

Our work is now focusing on expanding this study and solve a crystal structure of the P-Rex1 PDZ domains bound to RIα to decipher the exact interactions involved. For this in vitro pull-downs are being conducted. We are also developing the P-Rex1

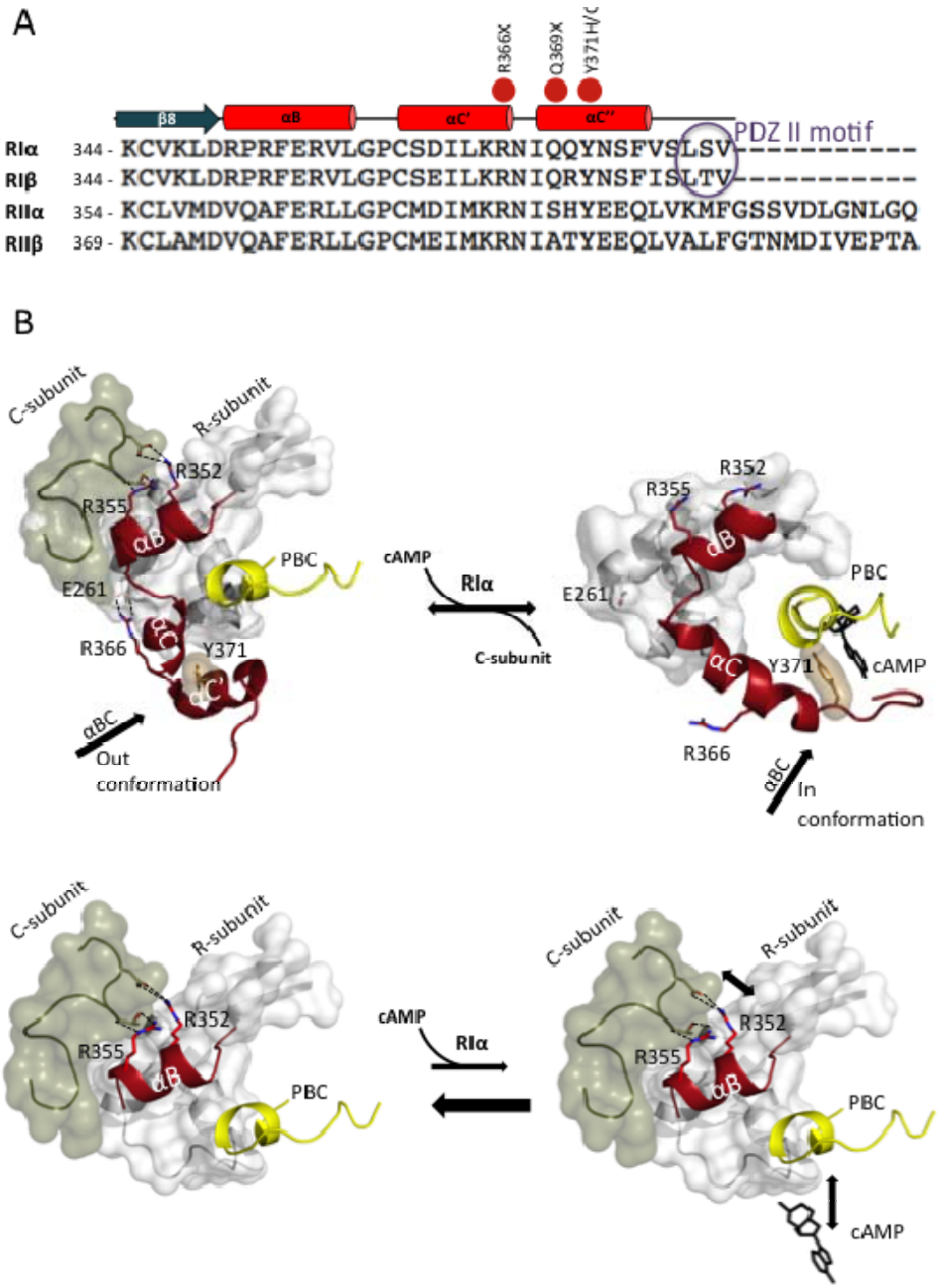

Figure 6.11. RIα conformational states. (**A**) Sequence alignment of the R-subunits C-tails. Mutations that cause ACRDYS1 are indicated with a red circle. The PDZ motif of RI is circled. (**B**) Conformational rearrangements of the RIα subunit's C-tail is shown. The top figure shows the wild-type protein and the bottom shows the ACRDYS1 protein that is missing the C-terminal 14 residues which pushes the conformational equilibrium to the left (C-bound state).

tandem PDZ peptide arrays by probing with the RIα and RIβ subunits. It would be interesting to design and test RIα C-terminal based peptides that can be used to test the binding to the PDZ domains as well as for their disruption capabilities in cells.

Chapter 6, in part, will be submitted for publication as Non-canonical PKA scaffolding interaction of RI subunits with P-Rex1. Bruystens, J.H.; Moody, I.S.; Ma, Y.; Sastri, M; Kornev, A; and Taylor, S.S. The dissertation author was the primary investigator and author of this work.

Chapter 7

Conclusions

cAMP-dependent protein kinase (PKA) is a highly conserved and promiscuous kinase that has served as a prototype for the entire kinase family. The R-subunit isoforms are responsible for inhibiting catalytic activity as well as assembling PKA in a cell-type specific and cell localization-specific mannor. Dispite the wealth of PKA structures published since the first PKA C-subunit structure, we have only recently begun to understand the complexity of the physiologically relevant macromolecular signaling assemblies, as we have begun to utilize the full-length proteins in our studies. Because RIα is the main isoform associated with disease and the only isoform that is embrionically lethal the underlying theme of this dissertation has been to investigate PKA RIα nucleated signaling assemblies by studying the full-length proteins and focusing on RIα'a scaffolding regions. This is reflected in the sub aims and chapters contained in this work. Thus, we focused on studying the RIα homodimer, the smAKAP:D/D domain interaction, and the RIα holoenzyme structures. In addition, we investigated how disease causing RIα mutant proteins cause molecular dysfunction and finally characterized the novel interaction of PKA with PRex1, allowing us to build new dimensions of complexity into PKA signaling by RIα.

While the challenges increase with attempting to solve the larger PKA complexes, the insights gained are crucial for deciphering PKA fucntion. The first objective was thus to solve the structure of the PKA RIα homodimer complex. This however, required the use of the full-length RIα construct that includes the flexible linker and dimerization docking (D/D) domain, which couples the two protomer

chains and results in dimer formation. Previous site-directed labeling experiments showed that these linkers are highly flexible (Li et al., 2000). In fact, the flexibility of the linker region and its resulting inherent instability was observed already at the early stages of studying PKA (Erlichman et al., 1973; Rannels and Corbin, 1980). Moreover, the linkers are predicted to be intrinsically disordered regions (Romero et al., 2001) and the recently published RIIβ holoenzyme structure could not locate density for the D/D domain (Zhang et al., 2012). Thus, crystallization of the dynamic RIα dimer complex came with pre-conceived challenges and it was not surprising that the final structure model lacked electron density for the D/D domain. Our RIα dimer structure further supports the idea that the D/D domain is structurally and spatially independent from the rest of the homodimer complex. Unfortunately, the flexibility of the linker segment most likely prevents the D/D domain from assuming a stable docked conformation in the crystal lattice and may account in part for the low diffracting crystals. However, to inhibit the C-subunit part of the linker and the inhibitor site (IS) must bind to and become immobilized within the active site cleft of the catalytic subunit thus the flexibility of the linker region is intrinsic and necessary to allow the IS to search for the catalytic subunit to then become bound and finally form the holoenzyme complex.

The homodimer structure of RIα presented in this study is consistent with previous SAXS observations and the basis for the compact arrangement of the cyclic nucleotide binding (CNB) domains is a novel intermolecular interface at the vertex of the two interacting monomers. We propose that the interface is isoform-specific and

can account for the large differences in the solution structures of the type RI and RII homodimers observed by SAXS, where the RII homodimers are much more extended (Vigil et al., 2004). Although the RII subunits contain longer linker regions, the large differences in the solution structures are most likely the result of interactions involving the R subunits' N3A-motif. Mutations on the interface of RIα resulted in extended structures as analyzed by SAXS and now look more like the RII subunits in solution. Moreover, and in contrast to RI structures, monomeric deletion mutant structures of RIIα and RIIβ, that lack the D/D domain and the N-linker, do not have the N3A interface (Brown et al., 2009; Diller et al., 2001; Wu et al., 2007).

The N3A interface revealed by the dimer structure represents a novel functional module for RIα. The D/D domain stably links the monomers at the N-terminus constraining the rest of the molecule into a close spatial proximity and thereby enhancing the dimer interface interaction. In addition to its role as a docking site for A-Kinase Anchoring Proteins (AKAPs), the D/D domain functions as a covalently linked tether that increases the interaction of its CNB-A domains by increasing their effective concentration, independently of the local concentration of RIα. Furthermore, this allows the dimer interface to form and dissociate without compromising the global dynamics of the regulatory subunit, as would potentially be the case with a high affinity interaction between the two CNB-A domains. The D/D domain thus limits significant dissociation of the monomers and allows the regulatory subunit to sense its environment for binding partners such as the catalytic subunit and cAMP effectively. A significant implication of our work is that cooperativity, while

fine-tuning the response of PKA in the highly variable cellular environment, is also a crucial component of PKA function that when disrupted can lead to disease as seen with Carney Complex mutations located on the interface.

For years it was thought that only the RII holoenzymes are localized within the cell to specific organelles by A kinase anchoring proteins (AKAPs) and that the RI holoenzymes are delocalized and present in the cytosol (Feliciello et al., 2001). This general notion has been increasingly challenged by the discovery of dual specific AKAPs that are capable of binding both RII and RI (Huang et al., 1997a, b) and when reports were published that saw RIα localized to the neuromuscular junction in fetal skeletal muscle (Imaizumi-Scherrer et al., 1996). Evidence further supporting the RIα sub-cellular targeting potential was the discovery of the small novel membrane-bound RI-specific A Kinase Anchoring Protein (smAKAP) that docks to the N-terminal D/D domain of RIα (Burgers et al., 2012). Presented in this thesis is the crystal structure of smAKAP's A-kinase binding domain (smAKAP-AKB) in complex with the dimerization/docking domain of PKA-RIα (PKA-RIαD/D) revealing a unique interaction surface with a large number of contact residues to drive smAKAP's affinity and specificity.

Comparing the RIα versus RII interactions that are made with dAKAP2, RI utilized four hydrophobic pockets whereas RII only shows two hydrophobic pockets (Sarma et al., 2010). Our smAKAP-bound RIα D/D complex highlights the four-pocket interaction clusters with important amino acid contributions from smAKAP's sequence compared to dAKAP's sequence that results in the increased smAKAP

affinity as well as specificity for RI-subunits. Significant differences are seen near the disulfide cysteincs responsible for stabilizing the D/D domain formation. Cys 16 from each protomer D/D forms a bridge to the opposite Cys 37 due to the antiparallel positioning of the protomer chains. smAKAP uniquely shows stabilization of these disulfide bonds via creating hydrophobic seals at each end of the smAKAP AKB domain. Furthermore, we show smAKAP's potential to be a substrate target of PKA by its Ser66 phosphorylation and present compelling evidence for this to be a regulatory mechanism to control smAKAP-mediated RI localized cAMP signaling in the cell.

Crystal structures of the RIβ and RIIβ holoenzymes were solved recently and detailed the unique assemblies of two heterodimers (R:C) into the dimer of heterodimers $(R:C)_2$ for the physiological holoenzyme complexes present in cells (Ilouz et al., 2012; Zhang et al., 2012). The RIIβ holoenzyme structure showed a compact architecture of two C-subunits and the RIIβ dimer complex. This doughnut-shaped, 2.3 Å structure revealed the holoenzyme-specific packing interaction of the R-subunits' CNB-A β4-β5 loop with the opposite C-subunit's C-terminal tail (residues 320-339). In contrast, in the RIβ holoenzyme the R-subunits are far apart and the RIβ heterodimer interface involves the two C-subunits' C-tails. While a crystal structure of the RIα holoenzyme remained elusive we proposed a model based on the packing interactions observed in a crystal structure of two heterodimers that contained an extended N-terminus compared to previous heterodimer structures of RIα. Extending the N-Linker segment by 18 residues caused an additional portion of the N-Linker to

be visualized as it makes contacts with the symmetry related heterodimer. In particular, the N-Linker becomes ordered by the β4-β5 loop of the symmetry-related dimer, which is highly conserved in RIα subunits. This suggests that the observed interaction is not a result of random crystal packing but might be biologically relevant.

Almost exclusively, mutations in the PKA regulatory subunits that play a causative role in disease have been found in the RIα isoform. This dissertation focused mainly on Carney Complex (CNC) disease and Acrodysostosis-1 (ACRDYS1). When comparing their locations, the contrasting molecular dysfunctions found as the culprit of the two diseases can be explained. Our findings describe the relationship between the functional domains of the PKA RIα subunit and corresponding mutation "hot-spots" to enhance our understanding of the molecular dysfunction that causes ACRDYS1 and CNC. Thus, CNC mutations occur mainly at the N-terminus and CNB-A domain and result in disruption of C-subunit inhibition and the clinical features caused by overactive catalytic activity.

ACRDYS-1 mutations, on the other hand, are localized mainly to the CNB-B and C-terminal tail of RIα, causing cAMP resistant complexes and more inhibited C-subunit. Two motifs of the CNB-B known to be crucial for R-subunit functions for the cAMP activation of PKA harbor the majority of mutations found so far among ACRDYS-1 patients. The PBC in CNB-B represents one mutational hot-spot and the C-terminal tail is another. We obtained two structures containing a C-terminal deletion mutation frequently found in ACRDYS-1 patients. First we solved the corresponding heterodimer structure and show why this mutant leads to the severe cAMP-resistant C-

bound complex. We also obtained a low resolution holoenzyme structure by utilizing this recurrent ACRDYS-1 mutant and reveal a possible quaternary arrangement of the two RIα:C heterodimers. While this structure differs from the proposed holoenzyme model described earlier, it likely represents another possible conformation for RIα in cells as an overly inhibited cAMP-desensitized holoenzyme.

Finally we set out to improve our knowledge of RIα's potential to serve as a scaffold with its C-terminal PDZ motif. We present in this thesis the progress with our structural and functional analysis of P-Rex1, an important Rac guanine nucleotide exchange factor (GEF) that binds through its PDZ domains to the C-terminus of RIα. PRex1 is one of the many known substrates of PKA and convergence of the PRex1 and PKA signaling pathways could provide a regulatory mechanism whereby phosphorylation of P-Rex1 acts to inhibit its GEG activity. P-Rex1 is upregulated in cancers and linked to proliferation, emphasizing the importance to decipher PKA's role in PRex1 regulation. We show in this work that both RIα and RIβ can be pulled down with the PDZ domains of P-Rex1 and that the C-subunit appears to enhance this interaction. In addition we used several RI mutants to decipher the binding preferences of P-Rex1. Furthermore, peptide blots and a compelling model of a P-Rex1 PDZ1 bound RIα:C complex are presented to shed light onto the possible interactions at hand.

Future work:

This dissertation presented the first full-length R-subunit dimer structure and revealed an isoform-specific interface that contributes to understanding RIα's *in vivo* function. With the knowledge gained from this structure it would be intriguing to test the Carney Complex interface mutants *in vivo* and explore if their cellular localization is affected. Support for a conformational equilibrium existing for PKA's R subunits is surfacing with recent studies utilizing NMR and MD analyzing the distribution of RIα in the H and B-forms (Akimoto et al., 2013). Accordingly, in the apo state RIα is toggling between and populating both the C subunit-bound and the cAMP-bound conformations. Addition of either binding partner pushes the equilibrium further to the corresponding conformation, suggesting that specific mutations could also alter the population of states within this equilibrium.

AKAPs have evolved as frequent therapeutic targets over the years because they are responsible for the crucial targeting of PKA phosphorylation to specific sites in the cell. Having contributed to this area with the elucidation of the RI-specific smAKAP bound to the RIα D/D domain the next step should be to test if smAKAP or other AKAP's effect the function and conformation of the full-length R-subunit complexes, especially since evidence presented thus far speaks for a structurally uncoupled role of the D/D domain with the rest of the R-subunits.

Important information regarding a non-canonical PKA scaffolding interaction of the RI subunits with the PDZ domains of R-Rex1 was presented and leads to many new questions. The most detailed molecular information on this interaction will most

likely be revealed by a crystal structure and our efforts are moving forward to accomplish this. Additional pull-downs and peptide blots will be conducted to tease apart the best candidates for crystallographic trials but also to gain a better understanding on the role of this signaling node. While this study has filled in a few gaps in the PKA structural library, obtaining a high-resolution full-length RIα holoenzyme structure will require future efforts and for this, several of the ACRDYS-1 mutations we have analyzed might prove as useful.

References

Ablow, R.C., Hsia, Y.E., and Brandt, I.K. (1977). Acrodysostosis coinciding with pseudohypoparathyroidism and pseudo-pseudohypoparathyroidism. AJR Am J Roentgenol *128*, 95-99.

Akamine, P., Madhusudan, Wu, J., Xuong, N.H., Ten Eyck, L.F., and Taylor, S.S. (2003). Dynamic features of cAMP-dependent protein kinase revealed by apoenzyme crystal structure. J Mol Biol *327*, 159-171.

Akimoto, M., Selvaratnam, R., McNicholl, E.T., Verma, G., Taylor, S.S., and Melacini, G. (2013). Signaling through dynamic linkers as revealed by PKA. Proc Natl Acad Sci U S A *110*, 14231-14236.

Alverdi, V., Mazon, H., Versluis, C., Hemrika, W., Esposito, G., van den Heuvel, R., Scholten, A., and Heck, A.J. (2008). cGMP-binding prepares PKG for substrate binding by disclosing the C-terminal domain. J Mol Biol *375*, 1380-1393.

Amieux, P.S., Cummings, D.E., Motamed, K., Brandon, E.P., Wailes, L.A., Le, K., Idzerda, R.L., and McKnight, G.S. (1997). Compensatory regulation of RIalpha protein levels in protein kinase A mutant mice. J Biol Chem *272*, 3993-3998.

Amieux, P.S., and McKnight, G.S. (2002). The essential role of RI alpha in the maintenance of regulated PKA activity. Ann N Y Acad Sci *968*, 75-95.

Aye, T.T., Scholten, A., Taouatas, N., Varro, A., Van Veen, T.A., Vos, M.A., and Heck, A.J. (2010). Proteome-wide protein concentrations in the human heart. Mol Biosyst *6*, 1917-1927.

Badireddy, S., Yunfeng, G., Ritchie, M., Akamine, P., Wu, J., Kim, C.W., Taylor, S.S., Qingsong, L., Swaminathan, K., and Anand, G.S. (2011). Cyclic AMP analog blocks kinase activation by stabilizing inactive conformation: conformational selection highlights a new concept in allosteric inhibitor design. Mol Cell Proteomics *10*, M110 004390.

Bang, M.L., Centner, T., Fornoff, F., Geach, A.J., Gotthardt, M., McNabb, M., Witt, C.C., Labeit, D., Gregorio, C.C., Granzier, H., Labeit, S. (2001). The complete gene sequence of titin, expression of an unusual approximately 700-kDa titin isoform, and its interaction with obscurin identify a novel Z-line to I-band linking system. Circ Res *89*, 1065-1072.

Banky, P., Huang, L.J., and Taylor, S.S. (1998). Dimerization/docking domain of the type Ialpha regulatory subunit of cAMP-dependent protein kinase. Requirements for dimerization and docking are distinct but overlapping. J Biol Chem *273*, 35048-35055.

Banky, P., Roy, M., Newlon, M.G., Morikis, D., Haste, N.M., Taylor, S.S., and Jennings, P.A. (2003). Related protein-protein interaction modules present drastically different surface topographies despite a conserved helical platform. J Mol Biol *330*, 1117-1129.

Bastidas, A.C., Deal, M.S., Steichen, J.M., Keshwani, M.M., Guo, Y., and Taylor, S.S. (2012). Role of N-Terminal Myristylation in the Structure and Regulation of cAMP-Dependent Protein Kinase. J Mol Biol *422*, 215-229.

Bastidas, A.C., Wu, J., and Taylor, S.S. (2014). Molecular Features of Product Release for the PKA Catalytic Cycle. Biochemistry.

Batkin, M., Schvartz, I., and Shaltiel, S. (2000). Snapping of the carboxyl terminal tail of the catalytic subunit of PKA onto its core: characterization of the sites by mutagenesis. Biochemistry *39*, 5366-5373.

Beebe, S.J., Oyen, O., Sandberg, M., Froysa, A., Hansson, V., and Jahnsen, T. (1990). Molecular cloning of a tissue-specific protein kinase (C gamma) from human testis--representing a third isoform for the catalytic subunit of cAMP-dependent protein kinase. Mol Endocrinol *4*, 465-475.

Beebe, S.J., Salomonsky, P., Jahnsen, T., and Li, Y. (1992). The C gamma subunit is a unique isozyme of the cAMP-dependent protein kinase. J Biol Chem *267*, 25505-25512.

Boettcher, A.J., Wu, J., Kim, C., Yang, J., Bruystens, J., Cheung, N., Pennypacker, J.K., Blumenthal, D.A., Kornev, A.P., and Taylor, S.S. (2011). Realizing the allosteric potential of the tetrameric protein kinase A RIalpha holoenzyme. Structure *19*, 265-276.

Boshart, M., Weih, F., Nichols, M., and Schutz, G. (1991). The tissue-specific extinguisher locus TSE1 encodes a regulatory subunit of cAMP-dependent protein kinase. Cell *66*, 849-859

Brennan, J.P., Bardswell, S.C., Burgoyne, J.R., Fuller, W., Schroder, E., Wait, R., Begum, S., Kentish, J.C., and Eaton, P. (2006). Oxidant-induced activation of type I protein kinase A is mediated by RI subunit interprotein disulfide bond formation. J Biol Chem *281*, 21827-21836.

Brown, S.H., Wu, J., Kim, C., Alberto, K., and Taylor, S.S. (2009). Novel isoform-specific interfaces revealed by PKA RIIbeta holoenzyme structures. J Mol Biol *393*, 1070-1082.

Bruystens, J.G., Wu, J., Fortezzo, A., Kornev, A.P., Blumenthal, D.K., and Taylor, S.S. (2014). PKA RIalpha homodimer structure reveals an intermolecular interface with implications for cooperative cAMP binding and Carney complex disease. Structure *22*, 59-69.

Bubis, J., Neitzel, J.J., Saraswat, L.D., and Taylor, S.S. (1988a). A point mutation abolishes binding of cAMP to site A in the regulatory subunit of cAMP-dependent protein kinase. J Biol Chem *263*, 9668-9673.

Bubis, J., Saraswat, L.D., and Taylor, S.S. (1988b). Tyrosine-371 contributes to the positive cooperativity between the two cAMP binding sites in the regulatory subunit of cAMP-dependent protein kinase I. Biochemistry *27*, 1570-1576.

Burgers, P.P., Ma, Y., Margarucci, L., Mackey, M., van der Heyden, M.A., Ellisman, M., Scholten, A., Taylor, S.S., and Heck, A.J. (2012). A small novel A-kinase anchoring protein (AKAP) that localizes specifically protein kinase A-regulatory subunit I (PKA-RI) to the plasma membrane. J Biol Chem *287*, 43789-43797.

Burns-Hamuro, L.L., Ma, Y., Kammerer, S., Reineke, U., Self, C., Cook, C., Olson, G.L., Cantor, C.R., Braun, A., and Taylor, S.S. (2003). Designing isoform-specific peptide disruptors of protein kinase A localization. Proc Natl Acad Sci U S A *100*, 4072-4077.

Bustelo, X.R., Sauzeau, V., and Berenjeno, I.M. (2007). GTP-binding proteins of the Rho/Rac family: regulation, effectors and functions in vivo. Bioessays *29*, 356-370.

Cadd, G., and McKnight, G.S. (1989). Distinct patterns of cAMP-dependent protein kinase gene expression in mouse brain. Neuron *3*, 71-79.

Canaves, J.M., Leon, D.A., and Taylor, S.S. (2000). Consequences of cAMP-binding site mutations on the structural stability of the type I regulatory subunit of cAMP-dependent protein kinase. Biochemistry *39*, 15022-15031.

Carlson, C.R., Lygren, B., Berge, T., Hoshi, N., Wong, W., Tasken, K., and Scott, J.D. (2006). Delineation of type I protein kinase A-selective signaling events using an RI anchoring disruptor. J Biol Chem *281*, 21535-21545.

Carr, D.W., Stofko-Hahn, R.E., Fraser, I.D., Bishop, S.M., Acott, T.S., Brennan, R.G., and Scott, J.D. (1991). Interaction of the regulatory subunit (RII) of cAMP-dependent protein kinase with RII-anchoring proteins occurs through an amphipathic helix binding motif. J Biol Chem *266*, 14188-14192.

Chen, V.B., Arendall, W.B., 3rd, Headd, J.J., Keedy, D.A., Immormino, R.M., Kapral, G.J., Murray, L.W., Richardson, J.S., and Richardson, D.C. (2010). MolProbity: all-atom structure validation for macromolecular crystallography. Acta Crystallogr D Biol Crystallogr *66*, 12-21.

Cheng, C.Y., Yang, J., Taylor, S.S., and Blumenthal, D.K. (2009). Sensing domain dynamics in protein kinase A-I{alpha} complexes by solution X-ray scattering. J Biol Chem *284*, 35916-35925.

Cheng, X., Phelps, C., and Taylor, S.S. (2001). Differential binding of cAMP-dependent protein kinase regulatory subunit isoforms Ialpha and IIbeta to the catalytic subunit. J Biol Chem *276*, 4102-4108.

Christian, F., Szaszak, M., Friedl, S., Drewianka, S., Lorenz, D., Goncalves, A., Furkert, J., Vargas, C., Schmieder, P., Gotz, F., Zuhlke, K., Moutty, M., Gottert, H., Joshi, M., Reif, B., Haase, H., Morano, I., Grossman S., Klukovits, A., Verli, J., Gaspar, R., Noack, C., Bergmann, M., Kass, R., Hampel, K., Kashin, D., Genieser, HG., Hergberg, FW., Willoughby, D., Cooper, DM., Baillie, GS., Houslay, MD., von Kries, JP., Zimmermann, B., Rosenthal, W., Klussmann, E. (2011). Small molecule AKAP-protein kinase A (PKA) interaction disruptors that activate PKA interfere with compartmentalized cAMP signaling in cardiac myocytes. J Biol Chem *286*, 9079-9096.

Coisy-Quivy, M., Sanguesa-Ferrer, J., Weill, M., Johnson, D.S., Donnay, J.M., Hipskind, R., Fort, P., and Philips, A. (2006). Identification of Rho GTPases implicated in terminal differentiation of muscle cells in ascidia. Biol Cell *98*, 577-588.

Dell'Acqua, M.L., Faux, M.C., Thorburn, J., Thorburn, A., and Scott, J.D. (1998). Membrane-targeting sequences on AKAP79 bind phosphatidylinositol-4, 5-bisphosphate. EMBO J *17*, 2246-2260.

Desseyn, J.L., Burton, K.A., and McKnight, G.S. (2000). Expression of a nonmyristylated variant of the catalytic subunit of protein kinase A during male germ-cell development. Proc Natl Acad Sci U S A *97*, 6433-6438.

Diller, T.C., Madhusudan, Xuong, N.H., and Taylor, S.S. (2001). Molecular basis for regulatory subunit diversity in cAMP-dependent protein kinase: crystal structure of the type II beta regulatory subunit. Structure *9*, 73-82.

Diviani, D., Abuin, L., Cotecchia, S., and Pansier, L. (2004). Anchoring of both PKA and 14-3-3 inhibits the Rho-GEF activity of the AKAP-Lbc signaling complex. EMBO J *23*, 2811-2820.

Donald, S., Hill, K., Lecureuil, C., Barnouin, R., Krugmann, S., John Coadwell, W., Andrews, S.R., Walker, S.A., Hawkins, P.T., Stephens, L.R., Welch, HC. (2004). P-Rex2, a new guanine-nucleotide exchange factor for Rac. FEBS Lett *572*, 172-176.

Emsley, P., and Cowtan, K. (2004). Coot: model-building tools for molecular graphics. Acta Crystallogr D Biol Crystallogr *60*, 2126-2132.

Erlichman, J., Rubin, C.S., and Rosen, O.M. (1973). Physical properties of a purified cyclic adenosine 3':5'-monophosphate-dependent protein kinase from bovine heart muscle. J Biol Chem *248*, 7607-7609.

Fantozzi, D.A., Harootunian, A.T., Wen, W., Taylor, S.S., Feramisco, J.R., Tsien, R.Y., and Meinkoth, J.L. (1994). Thermostable inhibitor of cAMP-dependent protein kinase enhances the rate of export of the kinase catalytic subunit from the nucleus. J Biol Chem *269*, 2676-2686.

Feliciello, A., Gottesman, M.E., and Avvedimento, E.V. (2001). The biological functions of A-kinase anchor proteins. J Mol Biol *308*, 99-114.

Gangal, M., Cox, S., Lew, J., Clifford, T., Garrod, S.M., Aschbaher, M., Taylor, S.S., and Johnson, D.A. (1998). Backbone flexibility of five sites on the catalytic subunit of cAMP-dependent protein kinase in the open and closed conformations. Biochemistry *37*, 13728-13735.

Gold, M.G., Lygren, B., Dokurno, P., Hoshi, N., McConnachie, G., Tasken, K., Carlson, C.R., Scott, J.D., and Barford, D. (2006). Molecular basis of AKAP specificity for PKA regulatory subunits. Mol Cell *24*, 383-395.

Greene, E.L., Horvath, A.D., Nesterova, M., Giatzakis, C., Bossis, I., and Stratakis, C.A. (2008). In vitro functional studies of naturally occurring pathogenic PRKAR1A mutations that are not subject to nonsense mRNA decay. Hum Mutat *29*, 633-639.

Guthrie, C.R., Skalhegg, B.S., and McKnight, G.S. (1997). Two novel brain-specific splice variants of the murine Cbeta gene of cAMP-dependent protein kinase. J Biol Chem *272*, 29560-29565.

Heller, W.T., Vigil, D., Brown, S., Blumenthal, D.K., Taylor, S.S., and Trewhella, J. (2004). C subunits binding to the protein kinase A RI alpha dimer induce a large conformational change. J Biol Chem *279*, 19084-19090.

Hennrich, M.L., Marino, F., Groenewold, V., Kops, G.J., Mohammed, S., and Heck, A.J. (2013). Universal quantitative kinase assay based on diagonal SCX chromatography and stable isotope dimethyl labeling provides high-definition kinase consensus motifs for PKA and human Mps1. J Proteome Res *12*, 2214-2224.

Herberg, F.W., Dostmann, W.R., Zorn, M., Davis, S.J., and Taylor, S.S. (1994). Crosstalk between domains in the regulatory subunit of cAMP-dependent protein kinase: influence of amino terminus on cAMP binding and holoenzyme formation. Biochemistry *33*, 7485-7494.

Herberg, F.W., Doyle, M.L., Cox, S., and Taylor, S.S. (1999). Dissection of the nucleotide and metal-phosphate binding sites in cAMP-dependent protein kinase. Biochemistry *38*, 6352-6360.

Herberg, F.W., Taylor, S.S., and Dostmann, W.R. (1996). Active site mutations define the pathway for the cooperative activation of cAMP-dependent protein kinase. Biochemistry *35*, 2934-2942.

Hernandez-Negrete, I., Carretero-Ortega, J., Rosenfeldt, H., Hernandez-Garcia, R., Calderon-Salinas, J.V., Reyes-Cruz, G., Gutkind, J.S., and Vazquez-Prado, J. (2007). P-Rex1 links mammalian target of rapamycin signaling to Rac activation and cell migration. J Biol Chem *282*, 23708-23715.

Hill, K., Krugmann, S., Andrews, S.R., Coadwell, W.J., Finan, P., Welch, H.C., Hawkins, P.T., and Stephens, L.R. (2005). Regulation of P-Rex1 by phosphatidylinositol (3,4,5)-trisphosphate and Gbetagamma subunits. J Biol Chem *280*, 4166-4173.

Horowitz, J.F. (2003). Fatty acid mobilization from adipose tissue during exercise. Trends Endocrinol Metab *14*, 386-392.

Horvath, A., Bertherat, J., Groussin, L., Guillaud-Bataille, M., Tsang, K., Cazabat, L., Libe, R., Remmers, E., Rene-Corail, F., Faucz, F.R., Clauser, E., Calender, A., Bertagna, X., Carney, JA., Stratakis, CA. (2010). Mutations and polymorphisms in the gene encoding regulatory subunit type 1-alpha of protein kinase A (PRKAR1A): an update. Hum Mutat *31*, 369-379.

Huang, L.J., Durick, K., Weiner, J.A., Chun, J., and Taylor, S.S. (1997a). D-AKAP2, a novel protein kinase A anchoring protein with a putative RGS domain. Proc Natl Acad Sci U S A *94*, 11184-11189.

Huang, L.J., Durick, K., Weiner, J.A., Chun, J., and Taylor, S.S. (1997b). Identification of a novel protein kinase A anchoring protein that binds both type I and type II regulatory subunits. J Biol Chem *272*, 8057-8064.

Ilouz, R., Bubis, J., Wu, J., Yim, Y.Y., Deal, M.S., Kornev, A.P., Ma, Y., Blumenthal, D.K., and Taylor, S.S. (2012). Localization and quaternary structure of the PKA RIbeta holoenzyme. Proc Natl Acad Sci U S A *109*, 12443-12448.

Imaizumi-Scherrer, T., Faust, D.M., Benichou, J.C., Hellio, R., and Weiss, M.C. (1996). Accumulation in fetal muscle and localization to the neuromuscular junction of cAMP-dependent protein kinase A regulatory and catalytic subunits RI alpha and C alpha. J Cell Biol *134*, 1241-1254.

Jones, K.W., Shapero, M.H., Chevrette, M., and Fournier, R.E. (1991). Subtractive hybridization cloning of a tissue-specific extinguisher: TSE1 encodes a regulatory subunit of protein kinase A. Cell *66*, 861-872.

Kammer, G.M. (2002). Deficient protein kinase a in systemic lupus erythematosus: a disorder of T lymphocyte signal transduction. Ann N Y Acad Sci *968*, 96-105.

Kammer, G.M., Khan, I.U., Kammer, J.A., Olorenshaw, I., and Mathis, D. (1996). Deficient type I protein kinase A isozyme activity in systemic lupus erythematosus T lymphocytes: II. Abnormal isozyme kinetics. J Immunol *157*, 2690-2698.

Kammer, G.M., Laxminarayana, D., and Khan, I.U. (2004). Mechanisms of deficient type I protein kinase A activity in lupus T lymphocytes. Int Rev Immunol *23*, 225-244.

Kannan, N., Haste, N., Taylor, S.S., and Neuwald, A.F. (2007). The hallmark of AGC kinase functional divergence is its C-terminal tail, a cis-acting regulatory module. Proc Natl Acad Sci U S A *104*, 1272-1277.

Kapphahn, M.A., and Shabb, J.B. (1997). Contribution of the carboxyl-terminal regional of the cAMP-dependent protein kinase type I alpha regulatory subunit to cyclic nucleotide interactions. Arch Biochem Biophys *348*, 347-356.

Keshwani, M.M., Klammt, C., von Daake, S., Ma, Y., Kornev, A.P., Choe, S., Insel, P.A., and Taylor, S.S. (2012). Cotranslational cis-phosphorylation of the COOH-terminal tail is a key priming step in the maturation of cAMP-dependent protein kinase. Proc Natl Acad Sci U S A *109*, E1221-1229.

Kim, C., Cheng, C.Y., Saldanha, S.A., and Taylor, S.S. (2007). PKA-I holoenzyme structure reveals a mechanism for cAMP-dependent activation. Cell *130*, 1032-1043.

Kim, C., Xuong, N.H., and Taylor, S.S. (2005). Crystal structure of a complex between the catalytic and regulatory (RIalpha) subunits of PKA. Science *307*, 690-696.

Kinderman, F.S., Kim, C., von Daake, S., Ma, Y., Pham, B.Q., Spraggon, G., Xuong, N.H., Jennings, P.A., and Taylor, S.S. (2006). A dynamic mechanism for AKAP binding to RII isoforms of cAMP-dependent protein kinase. Mol Cell *24*, 397-408.

Kirschner, L.S. (2014). Medicine. A unified cause for adrenal Cushing's syndrome. Science *344*, 804-805.

Kirschner, L.S., Carney, J.A., Pack, S.D., Taymans, S.E., Giatzakis, C., Cho, Y.S., Cho-Chung, Y.S., and Stratakis, C.A. (2000). Mutations of the gene encoding the protein kinase A type I-alpha regulatory subunit in patients with the Carney complex. Nat Genet *26*, 89-92.

Klussmann, E., Edemir, B., Pepperle, B., Tamma, G., Henn, V., Klauschenz, E., Hundsrucker, C., Maric, K., and Rosenthal, W. (2001). Ht31: the first protein kinase A anchoring protein to integrate protein kinase A and Rho signaling. FEBS Lett *507*, 264-268.

Knighton, D.R., Zheng, J.H., Ten Eyck, L.F., Ashford, V.A., Xuong, N.H., Taylor, S.S., and Sowadski, J.M. (1991a). Crystal structure of the catalytic subunit of cyclic adenosine monophosphate-dependent protein kinase. Science *253*, 407-414.

Knighton, D.R., Zheng, J.H., Ten Eyck, L.F., Xuong, N.H., Taylor, S.S., and Sowadski, J.M. (1991b). Structure of a peptide inhibitor bound to the catalytic subunit of cyclic adenosine monophosphate-dependent protein kinase. Science *253*, 414-420.

Kornev, A.P., Taylor, S.S., and Ten Eyck, L.F. (2008). A generalized allosteric mechanism for cis-regulated cyclic nucleotide binding domains. PLoS Comput Biol *4*, e1000056.

Kovanich, D., van der Heyden, M.A., Aye, T.T., van Veen, T.A., Heck, A.J., and Scholten, A. (2010). Sphingosine kinase interacting protein is an A-kinase anchoring protein specific for type I cAMP-dependent protein kinase. Chembiochem *11*, 963-971.

Krebs, E.G., and Beavo, J.A. (1979). Phosphorylation-dephosphorylation of enzymes. Annu Rev Biochem *48*, 923-959.

Krieger, E., Darden, T., Nabuurs, S.B., Finkelstein, A., and Vriend, G. (2004). Making optimal use of empirical energy functions: force-field parameterization in crystal space. Proteins *57*, 678-683.

Krissinel, E., and Henrick, K. (2007). Inference of macromolecular assemblies from crystalline state. J Mol Biol *372*, 774-797.

Kuo, J.F., and Greengard, P. (1969). An adenosine 3',5'-monophosphate-dependent protein kinase from Escherichia coli. J Biol Chem *244*, 3417-3419.
Laskowski R A, M.M.W., Moss D S, Thornton J M (1993). PROCHECK - a program to check the stereochemical quality of protein structures. J App Cryst *26*, 283-291.

Laxminarayana, D., Khan, I.U., Mishra, N., Olorenshaw, I., Tasken, K., and Kammer, G.M. (1999). Diminished levels of protein kinase A RI alpha and RI beta transcripts and proteins in systemic lupus erythematosus T lymphocytes. J Immunol *162*, 5639-5648.

Lee, H., Graham, J.M., Jr., Rimoin, D.L., Lachman, R.S., Krejci, P., Tompson, S.W., Nelson, S.F., Krakow, D., and Cohn, D.H. (2012). Exome sequencing identifies PDE4D mutations in acrodysostosis. Am J Hum Genet *90*, 746-751.

Leon, D.A., Canaves, J.M., and Taylor, S.S. (2000). Probing the multidomain structure of the type I regulatory subunit of cAMP-dependent protein kinase using mutational analysis: role and environment of endogenous tryptophans. Biochemistry *39*, 5662-5671.

Li, F., Gangal, M., Jones, J.M., Deich, J., Lovett, K.E., Taylor, S.S., and Johnson, D.A. (2000). Consequences of cAMP and catalytic-subunit binding on the flexibility of the A-kinase regulatory subunit. Biochemistry *39*, 15626-15632.

Lindsay, C.R., Lawn, S., Campbell, A.D., Faller, W.J., Rambow, F., Mort, R.L., Timpson, P., Li, A., Cammareri, P., Ridgway, R.A., Morton, JP., Doyle, B., Hegarty, S., Rafferty, M., Murphy, IG., McDermott, EW., Sheahan, K., Pedone, K., Finn, AJ., Groben, PA., Thomas, NE., Hao, H., Carson, C., Norman, JC., Machesky, LM., Gallagher, WM., Jackson, IJ., Van Kempen, L., Beermann, F., Der, C., Larue, L., Welch, HC., Ozanne, BW., Sansom, OJ. (2011). P-Rex1 is required for efficient melanoblast migration and melanoma metastasis. Nat Commun *2*, 555.

Linglart, A., Fryssira, H., Hiort, O., Holterhus, P.M., Perez de Nanclares, G., Argente, J., Heinrichs, C., Kuechler, A., Mantovani, G., Leheup, B., Wicart, P., Chassot, V., Schmidt, D., Rublio-Cabezas, O., Richter-Unruh, A., Berrade, S., Pereda, A., Boros, E., Munoz-Calvo, MT., Castori, M., Gunes, Y., Bertrand, G., Boughneres, P., Clauser, E., Silve, C. (2012). PRKAR1A and PDE4D mutations cause acrodysostosis but two distinct syndromes with or without GPCR-signaling hormone resistance. J Clin Endocrinol Metab *97*, E2328-2338.

Linglart, A., Menguy, C., Couvineau, A., Auzan, C., Gunes, Y., Cancel, M., Motte, E., Pinto, G., Chanson, P., Bougneres, P., Clauser, E., Silve, C. (2011). Recurrent

PRKAR1A mutation in acrodysostosis with hormone resistance. N Engl J Med *364*, 2218-2226.

Madhusudan, Akamine, P., Xuong, N.H., and Taylor, S.S. (2002). Crystal structure of a transition state mimic of the catalytic subunit of cAMP-dependent protein kinase. Nat Struct Biol *9*, 273-277.

Maiti, R., Van Domselaar, G.H., Zhang, H., and Wishart, D.S. (2004). SuperPose: a simple server for sophisticated structural superposition. Nucleic Acids Res *32*, W590-594.

Manning, G. (2005). Genomic overview of protein kinases. WormBook, 1-19.
Manning, G., Whyte, D.B., Martinez, R., Hunter, T., and Sudarsanam, S. (2002). The protein kinase complement of the human genome. Science *298*, 1912-1934.

Mao, T., Shao, M., Qiu, Y., Huang, J., Zhang, Y., Song, B., Wang, Q., Jiang, L., Liu, Y., Han, J.D., Cao, P., Li, J., Gao, X., Rui, L., Qi, L., Li, W., Liu, Y. (2011). PKA phosphorylation couples hepatic inositol-requiring enzyme 1alpha to glucagon signaling in glucose metabolism. Proc Natl Acad Sci U S A *108*, 15852-15857.

Maurice, D.H., Palmer, D., Tilley, D.G., Dunkerley, H.A., Netherton, S.J., Raymond, D.R., Elbatarny, H.S., and Jimmo, S.L. (2003). Cyclic nucleotide phosphodiesterase activity, expression, and targeting in cells of the cardiovascular system. Mol Pharmacol *64*, 533-546.

Mayeenuddin, L.H., and Garrison, J.C. (2006). Phosphorylation of P-Rex1 by the cyclic AMP-dependent protein kinase inhibits the phosphatidylinositiol (3,4,5)-trisphosphate and Gbetagamma-mediated regulation of its activity. J Biol Chem *281*, 1921-1928.

McNicholl, E.T., Das, R., Sildas, S., Taylor, S.S., and Melacini, G. (2010). Communication between tandem cAMP-binding domains in the regulatory subunit of protein kinase A (PKA)-I{alpha} as revealed by domain-silencing mutations. J Biol Chem.

Means, C.K., Lygren, B., Langeberg, L.K., Jain, A., Dixon, R.E., Vega, A.L., Gold, M.G., Petrosyan, S., Taylor, S.S., Murphy, A.N., Ha, T., Santana, LF., Tasken, K., Scott, JD. (2011). An entirely specific type I A-kinase anchoring protein that can sequester two molecules of protein kinase A at mitochondria. Proc Natl Acad Sci U S A *108*, E1227-1235.

Meinkoth, J.L., Ji, Y., Taylor, S.S., and Feramisco, J.R. (1990). Dynamics of the distribution of cyclic AMP-dependent protein kinase in living cells. Proc Natl Acad Sci U S A *87*, 9595-9599.

Meiring, H.D., van der Heeft, E., ten Hove, G.J., and de Jong, A.P.J.M. (2002). Nanoscale LC-MS(n): technical design and applications to peptide and protein analysis. . Journal of Seperation Science *25*, 557-568.

Mendelow, M., Prorok, M., Salerno, A., and Lawrence, D.S. (1993). ATPase-promoting dead end inhibitors of the cAMP-dependent protein kinase. J Biol Chem *268*, 12289-12296.

Michot, C., Le Goff, C., Goldenberg, A., Abhyankar, A., Klein, C., Kinning, E., Guerrot, A.M., Flahaut, P., Duncombe, A., Baujat, G., Lyonnet, S., Thalassinos, C., Nitschke, P., Casanova, JL., Le Merrer, M., Munnich, A., Cormier-Daire, V. (2012). Exome sequencing identifies PDE4D mutations as another cause of acrodysostosis. Am J Hum Genet *90*, 740-745.

Miller, W.R. (2002). Regulatory subunits of PKA and breast cancer. Ann N Y Acad Sci *968*, 37-48.

Montero, J.C., Seoane, S., Ocana, A., and Pandiella, A. (2011). P-Rex1 participates in Neuregulin-ErbB signal transduction and its expression correlates with patient outcome in breast cancer. Oncogene *30*, 1059-1071.

Muhn, F., Klopocki, E., Graul-Neumann, L., Uhrig, S., Colley, A., Castori, M., Lankes, E., Henn, W., Gruber-Sedlmayr, U., Seifert, W., Horn, D. (2013). Novel mutations of the PRKAR1A gene in patients with acrodysostosis. Clin Genet *84*, 531-538.

Murphy, C.S., and Steinberg, R.A. (1985). Hotspots for spontaneous and mutagen-induced lesions in regulatory subunit of cyclic AMP-dependent protein kinase in S49 mouse lymphoma cells. Somat Cell Mol Genet *11*, 605-615.

Murshudov, G.N., Vagin, A.A., and Dodson, E.J. (1997). Refinement of macromolecular structures by the maximum-likelihood method. Acta Crystallogr D Biol Crystallogr *53*, 240-255.

Murshudov, G.N., Vagin, A.A., Lebedev, A., Wilson, K.S., and Dodson, E.J. (1999). Efficient anisotropic refinement of macromolecular structures using FFT. Acta Crystallogr D Biol Crystallogr *55*, 247-255.

Nagasaki, K., Iida, T., Sato, H., Ogawa, Y., Kikuchi, T., Saitoh, A., Ogata, T., and Fukami, M. (2012). PRKAR1A mutation affecting cAMP-mediated G protein-coupled receptor signaling in a patient with acrodysostosis and hormone resistance. J Clin Endocrinol Metab *97*, E1808-1813.

Narayana, N., Cox, S., Nguyen-huu, X., Ten Eyck, L.F., and Taylor, S.S. (1997). A binary complex of the catalytic subunit of cAMP-dependent protein kinase and adenosine further defines conformational flexibility. Structure *5*, 921-935.

Neuberger, G., Schneider, G., and Eisenhaber, F. (2007). pkaPS: prediction of protein kinase A phosphorylation sites with the simplified kinase-substrate binding model. Biol Direct *2*, 1.

Newlon, M.G., Roy, M., Morikis, D., Carr, D.W., Westphal, R., Scott, J.D., and Jennings, P.A. (2001). A novel mechanism of PKA anchoring revealed by solution structures of anchoring complexes. EMBO J *20*, 1651-1662.

Newlon, M.G., Roy, M., Morikis, D., Hausken, Z.E., Coghlan, V., Scott, J.D., and Jennings, P.A. (1999). The molecular basis for protein kinase A anchoring revealed by solution NMR. Nat Struct Biol *6*, 222-227.

Ogreid, D., and Doskeland, S.O. (1981a). The kinetics of association of cyclic AMP to the two types of binding sites associated with protein kinase II from bovine myocardium. FEBS Lett *129*, 287-292.

Ogreid, D., and Doskeland, S.O. (1981b). The kinetics of the interaction between cyclic AMP and the regulatory moiety of protein kinase II. Evidence for interaction between the binding sites for cyclic AMP. FEBS Lett *129*, 282-286.

Otwinowski, Z., and Minor, W. (1997). Processing of X-ray diffraction data collection in oscillation mode. Macromolecular Crystallography *276*, 307-326.

Papin, J.A., Hunter, T., Palsson, B.O., and Subramaniam, S. (2005). Reconstruction of cellular signalling networks and analysis of their properties. Nat Rev Mol Cell Biol *6*, 99-111.

Parri, M., and Chiarugi, P. (2010). Rac and Rho GTPases in cancer cell motility control. Cell Commun Signal *8*, 23.

Pawson, T., and Scott, J.D. (2005). Protein phosphorylation in signaling--50 years and counting. Trends Biochem Sci *30*, 286-290.

Petersen, B., Petersen, T.N., Andersen, P., Nielsen, M., and Lundegaard, C. (2009). A generic method for assignment of reliability scores applied to solvent accessibility predictions. . BMC Structural Biology.

Pidoux, G., Witczak, O., Jarnaess, E., Myrvold, L., Urlaub, H., Stokka, A.J., Kuntziger, T., and Tasken, K. (2011). Optic atrophy 1 is an A-kinase anchoring protein on lipid droplets that mediates adrenergic control of lipolysis. EMBO J *30*, 4371-4386.

Potter, R.L., and Taylor, S.S. (1979). Relationships between structural domains and function in the regulatory subunit of cAMP-dependent protein kinases I and II from porcine skeletal muscle. J Biol Chem *254*, 2413-2418.

Qin, J., Xie, Y., Wang, B., Hoshino, M., Wolff, D.W., Zhao, J., Scofield, M.A., Dowd, F.J., Lin, M.F., and Tu, Y. (2009). Upregulation of PIP3-dependent Rac exchanger 1 (P-Rex1) promotes prostate cancer metastasis. Oncogene *28*, 1853-1863.

Rannels, S.R., and Corbin, J.D. (1980). Studies of functional domains of the regulatory subunit from cAMP-dependent protein kinase isozyme I. J Cyclic Nucleotide Res *6*, 201-215.

Rehmann, H., Prakash, B., Wolf, E., Rueppel, A., de Rooij, J., Bos, J.L., and Wittinghofer, A. (2003). Structure and regulation of the cAMP-binding domains of Epac2. Nature Structural Biology *10*, 26-32.

Reinton, N., Haugen, T.B., Orstavik, S., Skalhegg, B.S., Hansson, V., Jahnsen, T., and Tasken, K. (1998). The gene encoding the C gamma catalytic subunit of cAMP-dependent protein kinase is a transcribed retroposon. Genomics *49*, 290-297.

Romero, P., Obradovic, Z., Li, X., Garner, E.C., Brown, C.J., and Dunker, A.K. (2001). Sequence complexity of disordered protein. Proteins *42*, 38-48.

Rosenfeldt, H., Vazquez-Prado, J., and Gutkind, J.S. (2004). P-REX2, a novel PI-3-kinase sensitive Rac exchange factor. FEBS Lett *572*, 167-171.

Rubin, C.S. (1979). Characterization and comparison of membrane-associated and cytosolic cAMP-dependent protein kinases. Studies on human erythrocyte protein kinases. J Biol Chem *254*, 12439-12449.

Saldanha, S.A., Kaler, G., Cottam, H.B., Abagyan, R., and Taylor, S.S. (2006). Assay principle for modulators of protein-protein interactions and its application to non-ATP-competitive ligands targeting protein kinase A. Anal Chem *78*, 8265-8272.

Saraswat, L.D., Filutowics, M., and Taylor, S. (1988). Expression and mutagenesis of the regulatory subunit of cAMP-dependent protein kinase in Escherichia coli. Methods Enzymol *159*, 325-336.

Sarma, G.N., Kinderman, F.S., Kim, C., von Daake, S., Chen, L., Wang, B.C., and Taylor, S.S. (2010). Structure of D-AKAP2:PKA RI complex: insights into AKAP specificity and selectivity. Structure *18*, 155-166.

Sastri, M., Barraclough, D.M., Carmichael, P.T., and Taylor, S.S. (2005). A-kinase-interacting protein localizes protein kinase A in the nucleus. Proc Natl Acad Sci U S A *102*, 349-354.

Schneidman-Duhovny, D., Hammel, M., and Sali, A. (2010). FoXS: a web server for rapid computation and fitting of SAXS profiles. Nucleic Acids Res *38*, W540-544.

Schneidman-Duhovny, D., Hammel, M., Tainer, J.A., and Sali, A. (2013). Accurate SAXS Profile Computation and its Assessment by Contrast Variation Experiments. Biophys J *105*, 962-974.

Scholten, A., Aye, T.T., and Heck, A.J. (2008). A multi-angular mass spectrometric view at cyclic nucleotide dependent protein kinases: in vivo characterization and structure/function relationships. Mass Spectrom Rev *27*, 331-353.

Schroder, G.F., Levitt, M., and Brunger, A.T. (2010). Super-resolution biomolecular crystallography with low-resolution data. Nature *464*, 1218-1222.

Sjoberg, T.J., Kornev, A.P., and Taylor, S.S. Dissecting the cAMP-inducible allosteric switch in protein kinase A RIalpha. Protein Sci *19*, 1213-1221.

Sosa, M.S., Lopez-Haber, C., Yang, C., Wang, H., Lemmon, M.A., Busillo, J.M., Luo, J., Benovic, J.L., Klein-Szanto, A., Yagi, H., Gutkind, JS., Parsons, RE., Kazanietz, MG. (2010). Identification of the Rac-GEF P-Rex1 as an essential mediator of ErbB signaling in breast cancer. Mol Cell *40*, 877-892.

Steinberg, R.A., Russell, J.L., Murphy, C.S., and Yphantis, D.A. (1987). Activation of type I cyclic AMP-dependent protein kinases with defective cyclic AMP-binding sites. J Biol Chem *262*, 2664-2671.

Su, Y., Dostmann, W.R., Herberg, F.W., Durick, K., Xuong, N.H., Ten Eyck, L., Taylor, S.S., and Varughese, K.I. (1995). Regulatory subunit of protein kinase A: structure of deletion mutant with cAMP binding domains. Science *269*, 807-813.

Svergun, D., Barberato, C., and Koch, M.H. (1995). CRYSOL- a Program to Evaluate X-ray Solution Scattering of Biological Macromolecules from Atomic Coordinates. Journal of Applied Crystallography *28*, 768-773.

Svergun, D.I. (1992). Determination of the regularization parameter in indirect-transform methods using perceptual criteria. J Appl Crystallogr *25*, 495-503.

Svergun, D.I., Petoukhov, M.V., and Koch, M.H. (2001). Determination of domain structure of proteins from X-ray solution scattering. Biophys J *80*, 2946-2953.

Symcox, M.M., Cauthron, R.D., Ogreid, D., and Steinberg, R.A. (1994). Arg-242 is necessary for allosteric coupling of cyclic AMP-binding sites A and B of RI subunit of cyclic AMP-dependent protein kinase. J Biol Chem *269*, 23025-23031.

Taylor, S.S., Keshwani, M.M., Steichen, J.M., and Kornev, A.P. (2012). Evolution of the eukaryotic protein kinases as dynamic molecular switches. Philos Trans R Soc Lond B Biol Sci *367*, 2517-2528.

Taylor, S.S., Kim, C., Cheng, C.Y., Brown, S.H., Wu, J., and Kannan, N. (2008). Signaling through cAMP and cAMP-dependent protein kinase: diverse strategies for drug design. Biochim Biophys Acta *1784*, 16-26.

Taylor, S.S., and Kornev, A.P. (2011). Protein kinases: evolution of dynamic regulatory proteins. Trends Biochem Sci *36*, 65-77.

Taylor, S.S., Yang, J., Wu, J., Haste, N.M., Radzio-Andzelm, E., and Anand, G. (2004). PKA: a portrait of protein kinase dynamics. Biochim Biophys Acta *1697*, 259-269.

Tegge, W., Frank, R., Hofmann, F., and Dostmann, W.R. (1995). Determination of cyclic nucleotide-dependent protein kinase substrate specificity by the use of peptide libraries on cellulose paper. Biochemistry *34*, 10569-10577.

Temmerman, K., Simon, B., and Wilmanns, M. Structural and functional diversity in the activity and regulation of DAPK-related protein kinases. FEBS J *280*, 5533-5550.
Thullner, S., Gesellchen, F., Wiemann, S., Pyerin, W., Kinzel, V., and Bossemeyer, D. (2000). The protein kinase A catalytic subunit Cbeta2: molecular characterization and distribution of the splice variant. Biochem J *351*, 123-132.

van Hell, A.J., Klymchenko, A., Burgers, P.P., Moret, E.E., Jiskoot, W., Hennink, W.E., Crommelin, D.J., and Mastrobattista, E. (2010). Conformation and intermolecular interactions of SA2 peptides self-assembled into vesicles. J Phys Chem B *114*, 11046-11052.

Veugelers, M., Wilkes, D., Burton, K., McDermott, D.A., Song, Y., Goldstein, M.M., La Perle, K., Vaughan, C.J., O'Hagan, A., Bennett, K.R., Meyer, BJ., Legius, E., Karttunen, M., Norio, R., Kaariainen, H., Lavyne, M., Neau, JP., Richter, G., Kirali, K., Farnsworth, A., Stapleton, K., Morelli, P., Takanashi, Y., Bamforth, JS., Eitelberger, F., Noszian, I., Manfoi, W., Powers, J., Mochizuki, Y., Imai, T., Ko, GT., Driscoll, DA., Goldmuntz, E., Edelberg, JM., Collins, A., Eccies, D., Irvine, AD., McKnight, GS., Basson, CT. (2004). Comparative PRKAR1A genotype-phenotype analyses in humans with Carney complex and prkar1a haploinsufficient mice. Proc Natl Acad Sci U S A *101*, 14222-14227.

Vigil, D., Blumenthal, D.K., Heller, W.T., Brown, S., Canaves, J.M., Taylor, S.S., and Trewhella, J. (2004). Conformational differences among solution structures of the type Ialpha, IIalpha and IIbeta protein kinase A regulatory subunit homodimers: role of the linker regions. J Mol Biol *337*, 1183-1194.

Vigil, D., Blumenthal, D.K., Taylor, S.S., and Trewhella, J. (2006). Solution scattering reveals large differences in the global structures of type II protein kinase A isoforms. J Mol Biol *357*, 880-889.

Walsh, D.A., Perkins, J.P., and Krebs, E.G. (1968). An adenosine 3',5'-monophosphate-dependant protein kinase from rabbit skeletal muscle. J Biol Chem *243*, 3763-3765.

Wang, Y., Ho, T.G., Bertinetti, D., Neddermann, M., Franz, E., Mo, G.C., Schendowich, L.P., Sukhu, A., Spelts, R.C., Zhang, J., Herberg, FW., Kennedy, EJ. (2014). Isoform-selective disruption of AKAP-localized PKA using hydrocarbon stapled peptides. ACS Chem Biol *9*, 635-642.

Welch, H.C., Coadwell, W.J., Ellson, C.D., Ferguson, G.J., Andrews, S.R., Erdjument-Bromage, H., Tempst, P., Hawkins, P.T., and Stephens, L.R. (2002). P-Rex1, a PtdIns(3,4,5)P3- and Gbetagamma-regulated guanine-nucleotide exchange factor for Rac. Cell *108*, 809-821.

Wertheimer, E., Gutierrez-Uzquiza, A., Rosemblit, C., Lopez-Haber, C., Sosa, M.S., and Kazanietz, M.G. (2012). Rac signaling in breast cancer: a tale of GEFs and GAPs. Cell Signal *24*, 353-362.

Wong, T.H., Chiu, W.Z., Breedveld, G.J., Li, K.W., Verkerk, A.J., Hondius, D., Hukema, R.K., Seelaar, H., Frick, P., Severijnen, L.A., Lammers, JG., Lebbink, JHG., van Duinen, S., Kamphorst, W., Rezemuller, AJ., Netherlands Brain Bank, Bakker, EB., The International Parkinsonism Genetics Network, Neumann, M., Willemsen, R., Bnifati, V., Smit, AB., van Swieten, J. (2014). PRKAR1B mutation associated with a new neurodegenerative disorder with unique pathology. Brain *137*, 1361-1373.

Wong, W., and Scott, J.D. (2004). AKAP signalling complexes: focal points in space and time. Nat Rev Mol Cell Biol *5*, 959-970.

Wu, J., Brown, S., Xuong, N.H., and Taylor, S.S. (2004a). RIalpha subunit of PKA: a cAMP-free structure reveals a hydrophobic capping mechanism for docking cAMP into site B. Structure *12*, 1057-1065.

Wu, J., Brown, S.H., von Daake, S., and Taylor, S.S. (2007). PKA type IIalpha holoenzyme reveals a combinatorial strategy for isoform diversity. Science *318*, 274-279.

Wu, J., Jones, J.M., Nguyen-Huu, X., Ten Eyck, L.F., and Taylor, S.S. (2004b). Crystal structures of RIalpha subunit of cyclic adenosine 5'-monophosphate (cAMP)-dependent protein kinase complexed with (Rp)-adenosine 3',5'-cyclic monophosphothioate and (Sp)-adenosine 3',5'-cyclic monophosphothioate, the phosphothioate analogues of cAMP. Biochemistry *43*, 6620-6629.

Wu, J., Yang, J., Kannan, N., Madhusudan, Xuong, N.H., Ten Eyck, L.F., and Taylor, S.S. (2005). Crystal structure of the E230Q mutant of cAMP-dependent protein kinase reveals an unexpected apoenzyme conformation and an extended N-terminal A helix. Protein Sci *14*, 2871-2879.

Yang, J., Ten Eyck, L.F., Xuong, N.H., and Taylor, S.S. (2004). Crystal structure of a cAMP-dependent protein kinase mutant at 1.26A: new insights into the catalytic mechanism. J Mol Biol *336*, 473-487.

Yin, Z., and Kirschner, L.S. (2009). The Carney complex gene PRKAR1A plays an essential role in cardiac development and myxomagenesis. Trends Cardiovasc Med *19*, 44-49.

Zhang, J., Yang, P.L., and Gray, N.S. (2009). Targeting cancer with small molecule kinase inhibitors. Nat Rev Cancer *9*, 28-39.

Zhang, P., Smith-Nguyen, E.V., Keshwani, M.M., Deal, M.S., Kornev, A.P., and Taylor, S.S. (2012). Structure and allostery of the PKA RIIbeta tetrameric holoenzyme. Science *335*, 712-716.

Zheng, J., Knighton, D.R., Xuong, N.H., Taylor, S.S., Sowadski, J.M., and Ten Eyck, L.F. (1993). Crystal structures of the myristylated catalytic subunit of cAMP-dependent protein kinase reveal open and closed conformations. Protein Sci *2*, 1559-1573.

Zoller, M.J., Kerlavage, A.R., and Taylor, S.S. (1979). Structural comparisons of cAMP-dependent protein kinases I and II from porcine skeletal muscle. J Biol Chem *254*, 2408-2412.

Zoumaro-Djayoon, A.D., Heck, A.J., and Munoz, J. (2012). Targeted analysis of tyrosine phosphorylation by immuno-affinity enrichment of tyrosine phosphorylated peptides prior to mass spectrometric analysis. Methods *56*, 268-274.